LOW NOx COMBUSTION UTILISING A COANDA EJECTOR BURNER

By

Phillip O'Nions

Department of Chemical and Process Engineering

University of Sheffield

1997

FRONTISPIECE

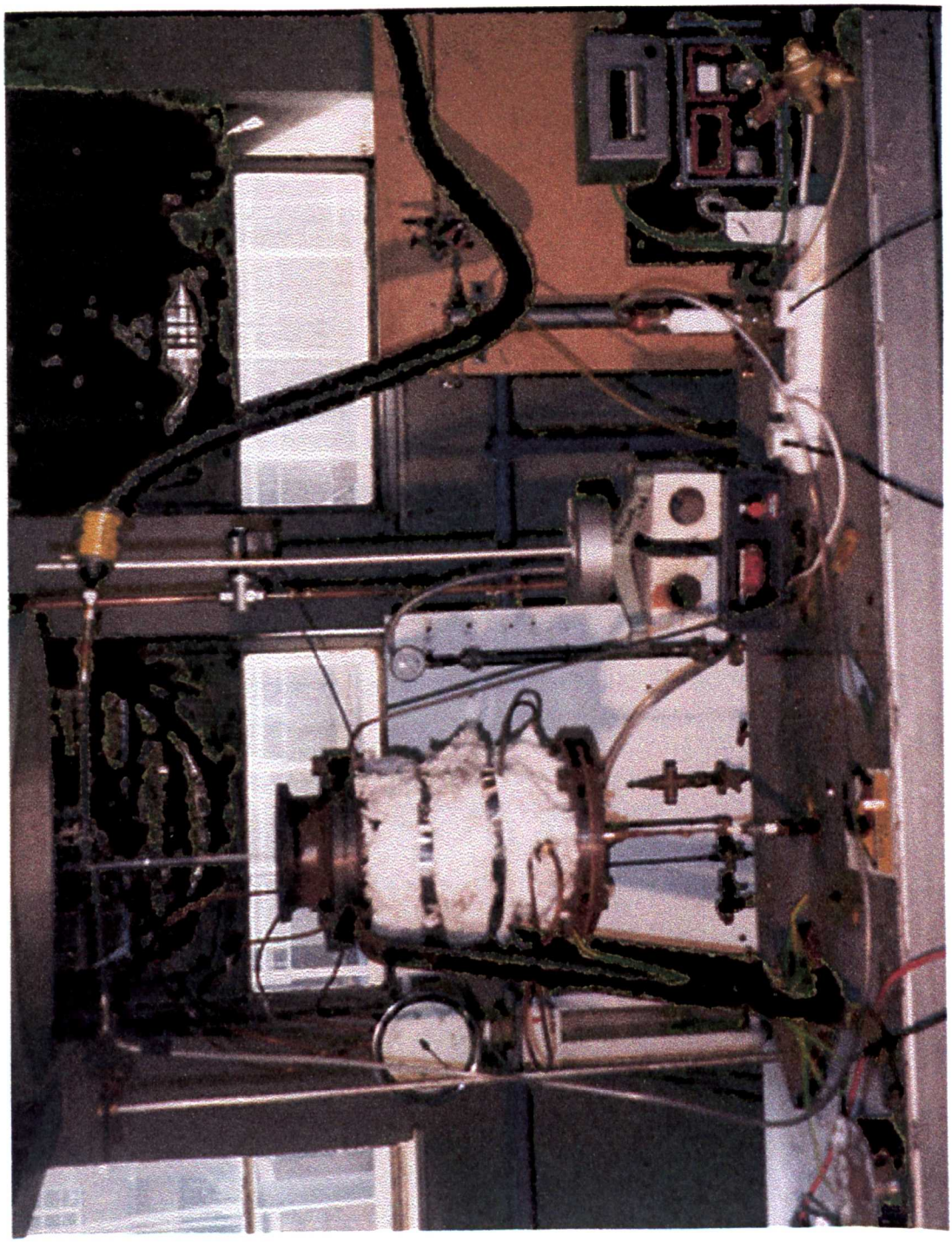

The Coanda ejector burner

SUMMARY

Current and future pollutant emission legislation calls for decreased NOx emissions from combustion systems. A review of techniques used for NOx abatement led to the choice of combustor redesign to be the most cost effective method available. This led to the design, construction and development of a combustion system that utilised a Coanda ejector to generate recirculation of the exiting high temperature combustion products to mix with the air supply. Cooling of the burner was integrated into the design through the use of the air and fuel supplies.

Computational fluid dynamics was used to model and aid development of the design. The model was used to predict NOx and CO emissions and the fuel-air mixing pattern. This, along with an analysis of experimental results and observations led to an understanding of the burner operation with respect to pollutant emissions and stability.

NOx emissions from the Coanda burner were found to be lowest when using a 0.2 mm Coanda gap width, resulting in 16 ppm NOx being emitted at an air to fuel ratio of 1.5. However, the use of a 0.2 mm Coanda gap width required an air supply pressure of up to 4 bar. The use of a 0.5 mm Coanda gap width enabled burner operation at lower air supply pressures. The resulting NOx emissions were measured as 23 ppm at an air to fuel ratio of 1.1, with a corresponding exit gas temperature of 2200 K.

Flue gas recirculation quantity, flame stability, flame stabiliser shape and operational limits proved to be inter-linked in the reduction of NOx emissions. It was found that fuel-air mixing was controlled by the entrainment properties of the Coanda ejector and the flame stabiliser. The average oxygen concentration entering the combustion chamber when using a 0.2 mm and 0.5 mm Coanda gap width was 13.7 % and 16.6 %, respectively. Due to the position of the fuel injector, a fuel rich region formed behind the flame stabiliser. With a suitable flame stabiliser geometry and the use of 'fingers', low NOx combustion and flame stability was achieved near stoichiometric conditions.

It was shown that the design of the burner enabled very low pollutant emissions near stoichiometric conditions, resulting in high exit gas temperatures. Conceivable applications of this type of burner could lie in small and intermediate furnaces where low NOx emissions are required. Additionally, very high temperature applications, such as glass furnaces could benefit in both cost and pollutant emissions from such a burner.

ACKNOWLEDGMENTS

I would especially like to thank Dr. M. M. Vahdati for her support, guidance and supervision of this research project, and to acknowledge the funding of the Coanda burner project by the EPSRC.

I wish to thank Mr. M. Jackson for the construction of the experimental rig, and all the staff and technicians in the department for their expert advice and help with the maintenance and operation of the Coanda burner.

TABLE OF CONTENTS

LIST OF TABLES

LIST OF FIGURES

NOMENCLATURE

A = Area
a = Constant
A_k = Pre-exponential factor
C = Molar concentration
C_m = Empirical constant
C_p = Specific heat capacity at constant pressure
C_v = Specific heat capacity at constant volume
D = Diameter
E_k = Activation energy
F = External body forces
G_φ = Angular momentum
G_x = Axial momentum
g = Gravitational acceleration
h = Enthalpy
h_c = convective heat transfer coefficient
I = Total hemispherical intensity
J = Diffusive mass flux
K = Equilibrium constant
k = Thermal conductivity; rate constants (section 2); turbulent kinetic energy (section 3.4.7)
L = Coanda gap width
m = Mass
$\dot{m}$ = Mass flow rate
M = Molecular weight
Nu = Nusselt number
Pr = Prandtl number
p = Pressure
R = Gas constant
Re = Reynolds number
R_i = Reaction of species
r = Radius
S = Source term
Sw = Swirl number
t = Time
T = Temperature
U = Velocity
X = Mole fraction

Greek

α = Vane angle
α_{abs} = Absorption coefficient
αs = Scattering coefficient
βk = Temperature exponent
δ = emmisivity
ε = Dissipation rate of k

ϕ = Scalar quantity
$\gamma = C_p/C_v$
φ = Mass entrainment ratio
λ = Skewness factor
μ = Viscosity
ρ = Density
σ = Stefan Boltzman constant = 5.672E-8 W/m^2K^2
τ = Stress tensor

Subscripts

1 = Constant
2 = Constant
3 = Constant
air = Air supply
amb = ambient conditions
eq = Equilibrium
fuel = Fuel supply
i = Ejector plane inlet; direction (section 3.4)
gas = Flue gas
h = Hub
j = Ejector nozzle area; direction (section 3.4)
k = Direction
m = Mass
o = Ejector plane outlet
recirc = Recirculated
TC = Thermocouple temperature
0 = Stagnation condition

1. INTRODUCTION

1.1 **NOx in the environment**

Pollutants generated from combustion systems have detrimental effects on plants and animals. The severity of these effects will depend upon the pollutant concentration and the time of exposure. Photochemical smog which refers to the complex mixture of pollutants formed through the interaction of sunlight with NO and hydrocarbons, was first noticed as a problem in Los Angeles in 1943, and has been noticed in many other cities around the world since then.

Classical smog was first noticed as detrimental to health in London during 1952. The use of coal as fuel for most heating purposes produced large quantities of sulphur dioxide and smoke particles near to ground level in highly populated areas. In the local atmosphere, sulphuric acid was formed along with nitric acid through the oxidation and hydrolisation of SO_2 and NO, the reactions being catalysed on carbon particles and trace metallic elements. Together, these pollutants caused chronic bronchitis, emphysema and asthmatic attacks, contributing to a large increase in pollution related deaths.

Oxides of nitrogen rank second to sulphur compounds in their contribution to acid rain, accounting for up to 30% of acidity in precipitation [1].

1.2 **Pollutant emissions and legislation since 1956**

Following the serious effects to health and the environment, the 1956 Clean Air Act was introduced. This required the emissions from combustion systems to be controlled through the best practical means available. A revision of this act, the 1968 Clean Air Act, imposed quantitative limits on emissions. The Environmental Protection Act of 1990 consolidated previous proposals into the system of integrated pollution control (IPC) [2]. IPC is a system whereby a single enforcing authority is responsible for all aspects of IPC. In England and

Wales, this authority is Her Majesty's Inspectorate of Pollution (HMIP). The enforcing authority ensures that the best available technique not entailing excessive cost (BATNEEC) is used.

As with many other countries, the United Kingdom has set a national plan for the reduction of pollutant emissions. With respect to NOx and large combustion plants, the aim is that by 1998, NOx emissions are reduced to 70% of the 1980 emissions. The current legislation for boilers and furnaces with a net thermal rating of between 20 MW to 50 MW, burning natural gas is 200 mg/Nm^3, expressed as NO_2 at 3% oxygen. Consequently, almost all combustion systems, including domestic heating appliances are being targeted for NOx reduction [3].

1.3 **Development of low NOx burners**

Due to environmental legislation, technologies for low NOx combustion were first implemented into utility coal and oil fired burners. The design of low NOx burners was such that the fuel and air were introduced in a manner that inhibited NOx formation. This was accomplished through decreasing the intensity of mixing and combustion. This inherently resulted in poor flame stability and increased emissions of unburnt fuel unless the burners were designed and operated well. Additional processes, such as flue gas recirculation, were used to limit the availability of oxygen and decrease the temperature of the flame. For coal and heavy fuel oil combustion without NOx abatement technology, over 500 ppm NOx can be emitted in the flue gas. However, if the technology is implemented, NOx emissions can be reduced to approximately 200 ppm [4].

Stringent NOx emission legislation, cost of implementation and capital expenditure has led to the widespread use of gaseous fuels, which emit considerably less NOx than solid and liquid fuels. However, NOx reduction systems are also required of gaseous fuelled systems to meet the legislative

requirements. These gaseous fuelled combustion systems have used similar NOx reduction techniques as those developed for solid and liquid fuel combustion systems, such as air and fuel staging, swirl and flue gas recirculation.

1.4 **Applications of low NOx combustion technology in industrial systems**

High temperature combustion gases are advantageous for increasing the efficiency of thermodynamic cycles. In many cases, such as glass furnaces and cement kilns, high temperature combustion gases are a primary requirement.

For smaller scale furnaces, the option to switch the furnace off or operate at part load may be a cost effective option. For such an application, easy lighting from cold start-up conditions and a wide turndown ratio are essential. An added requirement for such furnaces and other high temperature applications is the need for a NOx reduction capability. For low NOx burners to meet the above criteria for furnace operation, increased burner complexity and ancillary equipment are required.

Post combustion NOx control systems can be used as an alternative to low NOx burners. However, such systems require high capital investment and an annual operating cost. In addition to the cost, space is required for the additional equipment needed for such control systems.

Clearly, there is a need for a low NOx burner that has very low pollutant emissions, is simple in design and operates in a purely aerodynamic way. The use of a Coanda ejector can provide a design for such a burner.

The Coanda effect was discovered in 1910 and has been incorporated into ejector systems, as well as aircraft flaps and fluidic switches. Coanda ejectors have been used in burners and flarestacks but have suffered from poor cold start-up and the release of high emissions.

In this work, a Coanda ejector has been used to recirculate large quantities of hot, fully burnt combustion products near the burner exit. The entrained combustion gases and air supplied through the ejector are mixed before entering the combustion chamber. The fuel is then injected in such a way that a fuel rich region is formed, resulting in low NOx combustion.

The use of the Coanda ejector enabled low NOx combustion with high exit gas temperatures through a purely aerodynamic process.

2. LITERATURE REVIEW

2.1 Nitrogen chemistry in the atmosphere

2.1.1 Introduction

The role of nitrogen in the biosphere is extremely important as it both contributes 79% by volume to the atmosphere, and is a vital element in nutrients for plant life. The term NOx is used to combine the various oxides of nitrogen, these include NO, NO_2, N_2O, N_2O_3, N_2O_4 and N_2O_5. The natural sources of NOx production are mainly from microbial activity, lightning and biomass burning. Man made NOx comes from both combustion systems and industrial processes. An overview of NOx sources from both man made and natural sources is given in table 1.

Source	NOx (10^9 kgN/yr)	%	N_2O (10^9 kgN/yr)	%
Human Sources				
Fossil fuel combustion				
Stationary sources	13	24	0.35 (0.1 - 0.5)	3
Mobile sources	8	15		
	21 (14 - 28)	39	0.35 (0.1 - 0.5)	3
Biomass burning	12 (4 - 24)	22	<1 (0.02 - 1)	<8
Agriculture	5 (1 - 10)	9	<1 (0.01 - 1)	<8
Sub-total	**38 (19 - 62)**	**70**	**2.3 (0.1 - 2.5)**	**19**
Natural sources				
Soils	8 (4 - 16)	15	5 (2.9 - 5.2)	41
Oceans	<1		2 (1.4 - 2.6)	16
Lightning	8 (2 - 20)	15		
Other	0.5		3 (0.2 - 6.3)	24
Sub-total	**17 (6 - 37)**	**30**	**10 (4.5 - 14)**	**81**
Total	55 (25 - 100)	100	12.3 (5 - 17)	100

Table 1. Estimated global sources of NOx and N_2O [5].

2.1.2 NO_2 and ozone formation

When considering fossil fuel combustion sources, the main contributor to NOx is NO which typically accounts for 90 to 95% of emissions [6]. As soon as the NO leaves the combustion system and enters the atmosphere, it is quickly oxidised to NO_2. The time required for this conversion may vary from between minutes to several days. The reaction concerned for this oxidation is given by equation (1).

$$2NO + O_2 \Rightarrow NO_2 \qquad (1)$$

In the stratosphere, man made sources of NO are derived from either high flying aircraft or through the transportation of NO near ground level to the high altitudes. The concentration of oxygen in the stratosphere is low, and oxidation to NO_2 is through reaction with ozone, as given in equation (2). This reaction contributes to the depletion of the Earth's ozone layer.

$$NO + O_3 \Rightarrow NO_2 + O_2 \qquad (2)$$

In the troposphere, the presence of NO_2 is brought about by equation (1). However, NO_2 can be reconverted to NO through photolysis which liberates a free oxygen radical, as given by equation (3). This O radical rapidly reacts with oxygen to form ozone, through equation (4).

$$NO_2 \overset{light}{\Rightarrow} NO + O \qquad (3)$$

$$O + O_2 \Rightarrow O_3 \qquad (4)$$

Ozone produced in the troposphere acts as a pollutant. It is a toxic gas to humans, contributes to the greenhouse effect, and the formation of photochemical smog in conjunction with hydrocarbon pollutants.

2.1.3 N_2O chemistry in the environment

As can be seen from table 1, the majority of N_2O is formed through natural processes, especially from microbial activity in soils. Very little N_2O production is attributed to fossil fuel combustion.

N_2O is a strong infra-red absorber and has a long atmospheric lifetime, typically over a century [5]. It is a stable compound but can be decomposed through photolysis in the stratosphere through equation (5).

$$N_2O \overset{light}{\Rightarrow} N_2 + O \qquad (5)$$

The free oxygen radical is then able to react with N_2O to produce NO through equation (6).

$$N_2O + O \Rightarrow 2NO \qquad (6)$$

The reaction given in equation (6) is the main source of NO in the stratosphere. The NO formed then reacts with ozone through equation (2). N_2O therefore acts indirectly towards the depletion of the ozone layer.

2.1.4 NO_2 chemistry in the environment

The removal of NO_2 from the atmosphere can be accomplished through either wet or dry deposition over the land and sea. The reaction of NO_2 and the hydroxyl radical can produce nitric acid through equation (7).

$$NO_2 + OH \Rightarrow HNO_3 \qquad (7)$$

Reactions between NO_2 and water droplets can result in the formation of both nitric and nitrous acids through equations (8) and (9). This contributes towards acidification of rainwater.

$$2NO_2 + H_2O \Rightarrow HNO_3 + HNO_2 \quad (8)$$

$$NO_2 + NO + H_2O \Rightarrow 2HNO_2 \quad (9)$$

NO_2 may also be removed from the atmosphere to form peroxyacyl nitrate (PAN) [5]. Where hydrocarbon pollutants are in the air, such as urban areas, PAN is formed through equation (10), where M is a third molecular species,

$$CH_3COO_2 + NO_2 + M \Rightarrow CH_3COO_2NO_2 + M \quad (10)$$

PAN is insoluble in water and its stability decreases with increasing temperature. This means that the compound cannot be locally rained out of the atmosphere and may be transported over greater distances before decomposition, forming NO_2.

The overall cycle of nitrogen in the atmosphere is displayed in figure (1).

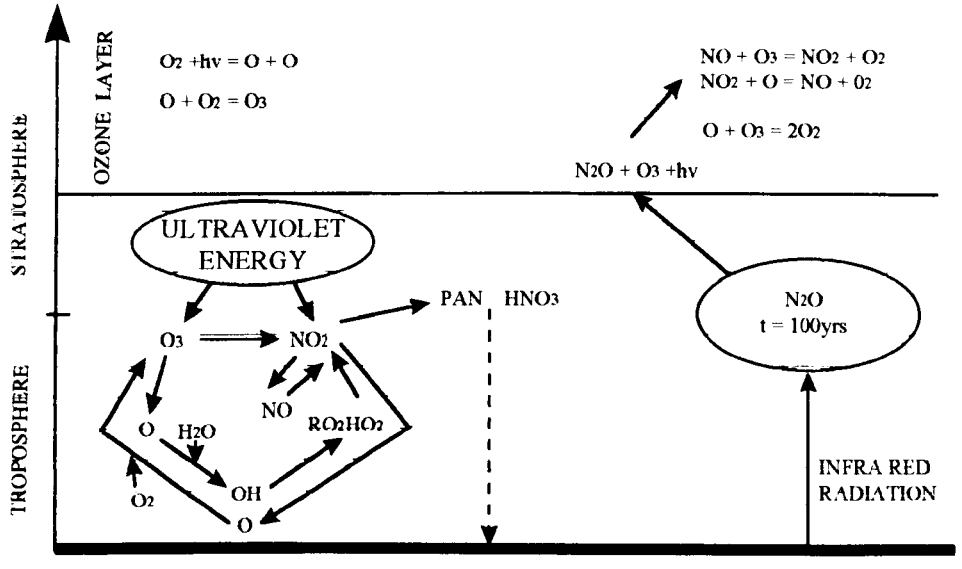

Figure 1. The atmospheric nitrogen cycle [5].

2.2 NOx FORMATION MECHANISMS

2.2.1 Introduction

It has been found that there are three NOx formation mechanisms in combustion systems, termed thermal NOx, prompt NOx and fuel NOx. When combustion occurs, it is possible that none, some or all of these mechanisms will contribute towards NOx formation. The mechanisms that lead to NOx formation are dependent upon temperature, fuel type and the chemical composition of the oxidising environment.

2.2.2 Thermal NOx

Nitric oxide, formed through the thermal NOx mechanism, is the primary constituent of NOx emitted from most combustion systems [7]. The Zeldovich mechanism [8] is now the accepted NO formation process in non chemical equilibrium situations. In regions of chemical equilibrium, the NO formed is termed 'thermal NOx'. The mechanism of thermal NO formation comprises of three reactions. The first, reaction (11), involves the attack of a nitrogen molecule by an oxygen atom. Due to the nitrogen molecules triple bond, a high dissociation energy of 941 $kJmol^{-1}$ is required to initiate reaction (11). This dissociation energy requirement causes reaction (11) to be the rate determining step in the formation of thermal NOx [9]. Under most conditions, reaction (12) follows. However, reaction (13) becomes important in fuel rich flames where there is a high concentration of water vapour [10]. The thermal NO formation rate is much slower than the combustion rate, and in general, in systems where NO emission levels are significant, most of the NO is formed after completion of combustion [7, 11]. To calculate the maximum formation rate of NO through the above reactions, a steady state approximation for nitrogen and oxygen atom concentrations may be calculated from equilibrium considerations [12]. Equation (14) can then be used to determine the formation rate of NO.

$$O + N_2 \underset{k-1}{\overset{k1}{\leftrightarrow}} NO + N \tag{11}$$

$$N + O_2 \underset{k-2}{\overset{k2}{\leftrightarrow}} NO + O \tag{12}$$

$$N + OH \underset{k-3}{\overset{k3}{\leftrightarrow}} NO + H \tag{13}$$

$$\frac{d[NO]_T}{dt} = 2k_1[O_2][N_2]\left\{\frac{1-[NO]^2/K[O_2][N_2]}{1+k_{-1}[NO]/k_2 + k_3[OH]}\right\} \tag{14}$$

where K is the equilibrium constant ($k_1k_2/k_{-1}k_{-2}$).

When incorporating temperature into equation (14), the NO formation rate is expressed as an exponential term [11], as given in equation (14a).

$$\frac{d[NO]}{dt} = 6*10^{16} T_{eq}^{1/2} \exp\left[\frac{-69060}{T_{eq}}\right][O_2]_{eq}^{1/2}[N_2]_{eq} mol/cm^3 s \tag{14a}$$

It is evident from equation (15) that the formation of thermal NO is strongly dependent on temperature but is also dependent upon oxygen and nitrogen concentrations at equilibrium conditions. Elevated temperatures and high oxygen concentrations in the post combustion gases result in relatively high NO formation rates.

2.2.3 **Prompt NOx**

Prompt NOx is formed in regions near the flame zone. In these flame regions, turbulent combustion causes the gas temperature, supra-equilibrium concentrations of radicals and concentrations of short lived species to fluctuate

randomly. Attempts to sample the gases and determine the contribution of prompt NOx in hot lean flames can lead to errors in excess of 100% [9].

The overall formation of prompt NOx is still not fully understood, mainly due to the number of conditions that may exist in a flame, the number of possible reactions and the difficulty in measuring the species. It was found by Fenimore [10] that the rate of production of NOx through the Zeldovich mechanism could not account for the very rapid production of NO at the flame front in fuel rich hydrocarbon flames, even if super equilibrated concentrations of O and OH were used. This phenomenon of rapid NOx formation was termed prompt NOx. Experimentally, this was determined through sampling axially backwards through a flame to the burner head [9]. Using H_2 - O_2 flames, the NOx formation rate measured along the axis to the burner head was in accordance with the Zeldovich mechanism, however when small quantities of hydrocarbon fuel was added to the mixture, prompt NOx was encountered. The quantity of prompt NOx formed was proportional to the quantity of fuel added and the relative number of carbon atoms contained within the fuel. From this, Fenimore postulated that prompt NO is formed through the attack of a hydrocarbon fragment, such as C, CH and C_2 on a nitrogen molecule as given by reactions (15) to (17). Evidence to support this theory was found through sampling at the combustion zone. This revealed the production of HCN and CN in small quantities. The nitrogen atom produced results in the formation of NO through reactions (12) or (13), depending on the flame conditions.

$$CH + N_2 \Rightarrow HCN + N \tag{15}$$

$$C_2 + N_2 \Rightarrow 2CN \tag{16}$$

$$C + N_2 \Rightarrow CN + N \tag{17}$$

The reactions concerned for prompt NOx are much faster than those of thermal NOx production [9, 11]. It was found that prompt NO formation was weakly dependent on temperature and varied with the square root of the pressure [9].

2.2.4 **Fuel NO**

Fuel NO is produced when nitrogen contained within the fuel is oxidised. The quantity of NO formed in this way is proportional to the concentration of nitrogen chemically bound to the fuel. Coals and heavy fuel oils have a relatively high nitrogen content, typically 0.65 to 2% by weight [13]. It was also found that oxidation of the nitrogen containing compound was on a time scale comparable to that of the combustion reaction. This contributed to a large portion of total NOx and was influenced little by temperature. However, another researcher [5] found the conversion of organic nitrogen compounds to NO to be strongly dependent on both air - fuel ratio and temperature. Gaseous hydrocarbon fuels have a typically low fuel bound nitrogen content and the contribution of this to total NOx emissions can be considered to be negligible.

The chemical reaction scheme for fuel NO is highly complex and will not be considered in great detail. The final product of the fuel based nitrogen is dependent upon the flame stoichiometry, and is displayed in a simplified version in figure (2). Under fuel rich, reducing conditions, conversion to ammonia and molecular nitrogen will occur. When oxygen is present, the oxidation to NO will occur and will contribute to the total NOx produced.

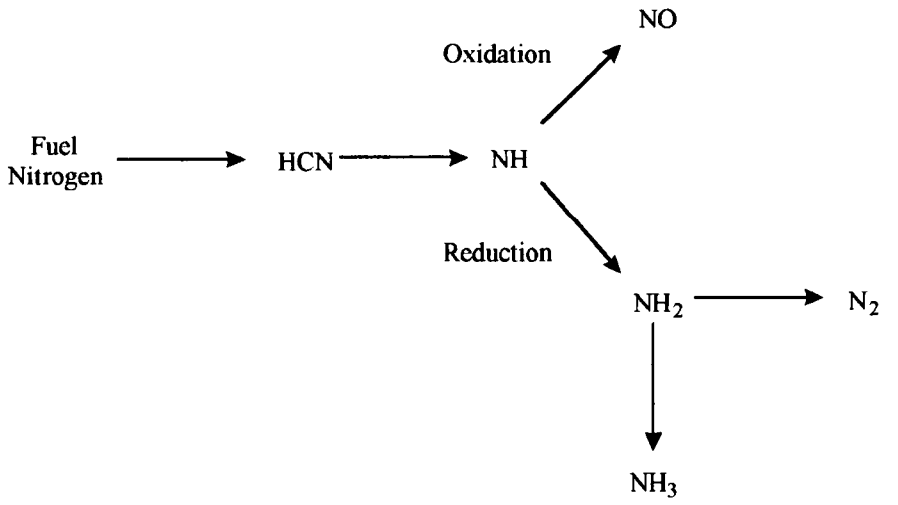

Figure 2. Basic route for the conversion of fuel nitrogen to either nitrogen or NOx.

2.3 **NOx ABATEMENT**

2.3.1 **Introduction**

The introduction of stringent air pollution legislation in many countries around the world has led to the requirement of NOx abatement technologies for most combustion systems. To decrease NOx emissions into the environment, the process of NOx abatement can be tackled at two points in the combustion system. Firstly, modifications to the burner design and hence the combustion process can be made to limit the production of NOx. Secondly, post combustion treatment of flue gases can be included after the combustion chamber to reduce the quantity of NOx emitted into the atmosphere.

2.3.2 **Modifications to the burner and combustion process**

2.3.2.1 **Flue gas recirculation**

Flue gas recirculation involves the recycling of combustion products, normally from the flue gas exit point. The recirculated flue gas is mixed with the incoming air supply, decreasing the average oxygen concentration [14]. The

recycled flue gas also has a high concentration of CO_2 and H_2O. Both of these molecules have a high specific heat capacity, resulting in a decrease in the peak flame temperature. Flue gas recirculation can be accomplished in a variety of combustion systems, large or small, and for a variety of fuel types.

A number of methods are used to determine the mass ratio of recycled combustion products,

$$\varphi = \frac{\dot{m}_{recirc}}{\dot{m}_{air}} * 100 \qquad (18)$$

$$\varphi = \frac{\dot{m}_{recirc}}{\dot{m}_{fuel} + \dot{m}_{air}} * 100 \qquad (19)$$

$$\varphi = \frac{\dot{m}_{recirc}}{\dot{m}_{fuel} + \dot{m}_{air} + \dot{m}_{recirc}} * 100 \qquad (20)$$

equations (18) and (19) are very similar, basing the recycled quantity on the incoming reactants [15, 16]. However, equation (19) will take account of changes in fuel type and stoichiometry. Equation (20) gives the mass recirculation ratio of combustion products to the total mass of gases present in the combustion system, and therefore cannot increase beyond 100% recirculation [17].

The recirculation of combustion gases has the potential disadvantage of increased CO and unburnt hydrocarbons [14]. Flame colour transitions are commonly associated with flue gas recirculation. Using equation (18), Cooper et al [15] found colour transitions from smoky yellow flames to clean blue flames as the quantity of recirculation was increased above 50%.

Flue gas recirculation may be categorised into either cold flue gas recirculation or hot flue gas recirculation.

2.3.2.2 **Cold flue gas recirculation**

This is the most common type of flue gas recirculation used in industrial combustion systems. It can be expected that cold flue gas recirculation alone can account for up to an 80% reduction in NOx for gaseous combustion systems [18, 19]. It has been used most commonly in large utility systems where the recycled combustion gases are drawn after the economiser, and mixed with the incoming combustion air, as displayed in figure (3).

The cooled combustion gases, containing large quantities of CO_2 and H_2O absorb a greater quantity of heat from the combustion zone due to their high specific heat capacities. This high specific heat capacity and increased oxygen deficient gas flowing into the combustion zone has the effect of reducing the peak temperatures, and hence reducing the thermal NOx produced. Baltasar et al [14] used cold flue gas recirculation with a gas swirl burner burning propane. The quantity of flue gas recirculated was varied between 0 and 32%, resulting in a NOx reduction from 43 to 2 ppm. Further increases in flue gas recirculation resulted in CO, particulates and unstable combustion. Dupont et al [12] investigated a domestic central heating boiler with up to 15% flue gas recirculation. After passing over a cold water heat exchanger, the exiting flue gas was entrained into the combustion air supply. This resulted in up to a 50% decrease in NOx emissions. However, further increases in flue gas recirculation resulted in significant quantities of methane to be emitted.

Higher quantities of flue gas recirculation (variable up to 70%) were used in a highly swirling flame burning either light fuel oil or methane [20]. It was found that NOx emissions decreased from 90 to 15 ppm, and that the colour of the flame and its stability altered with the recirculation quantity and air to fuel

ratio. The effect of flue gas recirculation on flame stability is further discussed in section 2.5.

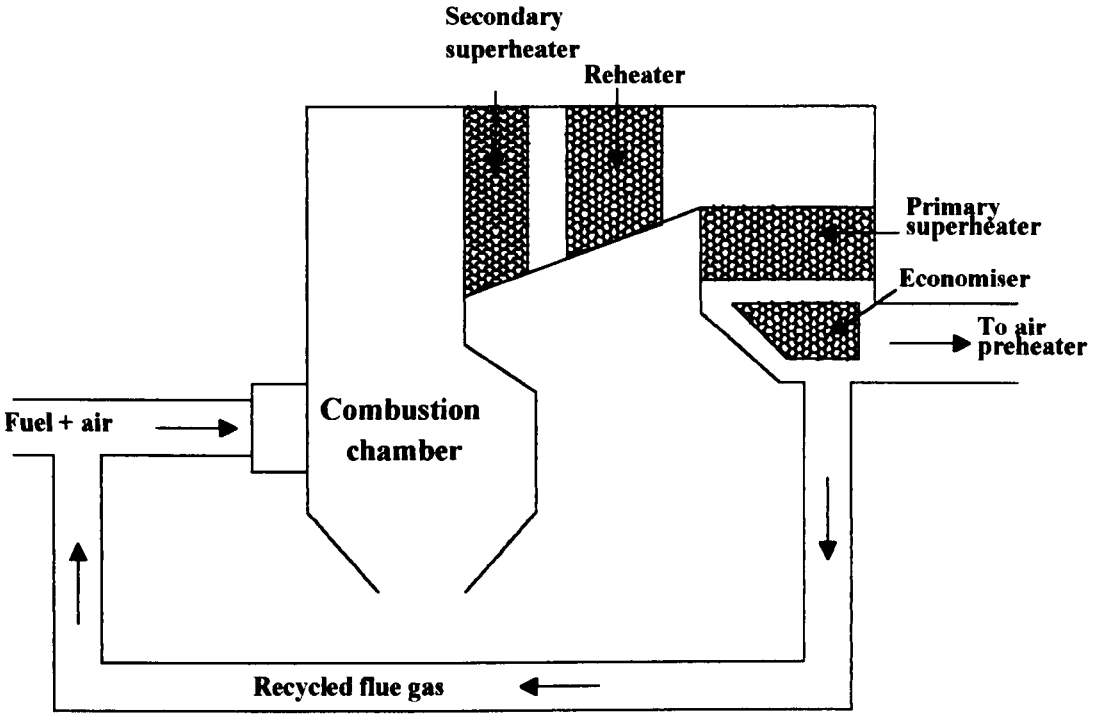

Figure 3. Diagram of cold flue gas being recycled after the economiser.

2.3.2.3 **Hot flue gas recirculation**

The principle of hot flue gas recirculation is similar to that of cold flue gas recirculation except that the recycled combustion gases are at higher temperatures, often near combustor outlet temperatures. As no heat is removed from the recycled gases, the outlet temperature of the combustion device does not decrease.

Hot flue gas recirculation has been successfully utilised in combustion systems. Recirculation of up to 63% at a temperature of 700°C was found to reduce NOx from 400 to below 20 ppm [21]. The recirculation of hot flue gas has been found to increase the flame stability [22]. A flameless burner was

developed by Wuenning [23] that utilised entrainment of furnace gases to reduce NOx production. The quantity of recirculated flue gas was found to affect burner stability. Three regions were found which were dependent upon the furnace temperature and the mass of recirculated flue gas. The flame was found to be stable at all furnace temperatures when the mass recirculation ratio of flue gas to air was less than 1.0. However, increasing the flue gas mass recirculation ratio produced an unstable flame. Only when the recirculation ratio was increased above 3.0, and at furnace temperatures above 900°C was the flame stable.

It is clear that significantly more hot flue gas can be recycled than cold flue gas, typically more than 500% (as calculated through equation (19)). By increasing the quantity of recycled flue gas, the local oxygen concentration is reduced to low levels and thus reduces thermal NOx formation.

2.3.2.4 **Control of air/fuel stoichiometry**

The control of air-fuel stoichiometry can be used in both premixed and non premixed combustion systems. The control of stoichiometry can lead to an environment in the combustion zone that does not favour NOx formation.

Premixed air-fuel mixtures can operate under fuel lean conditions [3]. This produces a dilution effect in the combustion zone, decreasing the flame temperature and hence the thermal NOx formation. NOx emissions of below 20 ppm have been measured for such systems operating with 80% excess air.

For non premixed combustion systems, fuel-air staging can be employed. Staged combustion involves the staged introduction of fuel and air into the combustion system to create successive fuel rich and fuel lean conditions, thereby avoiding stoichiometric conditions which produce high levels of NOx. The most common technique involves operating the bulk of the flame zone under fuel rich conditions, producing high concentrations of carbon monoxide,

followed by a fuel lean zone to complete the burnout of the fuel. It has been found that staged combustion is highly effective in the control of NOx [24], with the ability to reduce the emissions of NOx by a factor of 4.3. Air staging has also found to be highly effective when burning fuel oil which has a high fuel bound nitrogen content [25]. The use of air staging decreased the NOx emissions from 390 to 109 ppm. However, Drearden et al [26] found that air staging significantly increases the formation of prompt NO and it was computationally modelled that prompt NO increased from 29 to 113 ppm.

The use of two stage combustion in the form of over-fire air has been demonstrated with the use of low NOx burners for coal combustion [6]. With the use of low NOx burners alone, NOx emissions decreased by 42.8% as compared to conventional burners. The introduction of two-stage combustion increased the NOx reduction to 57%. The total cost of implementing low NOx burners with two-stage combustion that could achieve a 50% NOx reduction, was calculated at $569/ton NOx removed from the flue gas, based on 1993 costs [27]. For a 25% reduction in NOx emissions, the use of low excess air levels could be implemented at a cost of $57/ton NOx removed. However, on tests performed on over 200 boilers [28], the cost of NOx abatement technology was found to decrease with increasing thermal capacity. Over a spectrum of boiler sizes ranging from 183 kW to 73 MW, the cost at 1993 levels to implement low NOx burners was found to decrease from $1500/ton to 700$/ton NOx removed, respectively. Similarly, the addition of both low NOx burners and flue gas recirculation cost between $5000/ton to $2000/ton of NOx removed, respectively.

2.3.2.5 **Reburning**

Reburning involves a three stage combustion process, resulting in the removal of NOx. The cost of natural gas reburn has been calculated for both 50% and 60% NOx removal [27]. It was calculated that a 50 % NOx decrease could be attained with a 10 % heat input by natural gas. In 1993 this resulted in a cost

of $1233/ton NOx removed. Similarly, for a 60 % NOx decrease, a natural gas heat input of 12.5% was required and cost $1656/ton NOx required. Reburning can also be performed through the recirculation of flue gas into the fuel rich combustion zone [21]. The process is initiated by a reaction, forming HCN, as given in equation (21). The hydrocyanide, HCN, produced further reacts to form nitrogen.

$$CH + NO = HCN + O \tag{21}$$

In the first stage, the primary fuel is fired under low excess air conditions. The reburn fuel is added in a second stage above the primary combustion zone, in an amount corresponding to approximately 18% of the primary fuel [29]. The reburn fuel produces a secondary fuel rich zone where a significant proportion of the NOx produced in the primary zone is converted to nitrogen. Natural gas is usually used as the reburn fuel as it is reactive, easily introduced to the combustion system and has good burnout properties. Over-fire air is then introduced in a third stage to complete the fuel burnout.

2.4 **POST COMBUSTION CONTROLS**

2.4.1 **Introduction**

Post combustion NOx reduction involves the removal of NOx from the flue gas after combustion is complete but before being released into the environment. The methods of NOx reduction are usually based on reactions with reducing agents, such as ammonia or urea, to form nitrogen. Catalytic reduction may also be used either with or without ammonia [5]. Details of these are given below.

2.4.2 **Selective non-catalytic reduction (SNCR)**

The SNCR process involves the injection of ammonia or urea into the furnace at relatively high temperatures to react with NO and oxygen forming nitrogen, water vapour and carbon dioxide. The temperatures at which the reaction is effective has been found to be between 871 °C and 1093 °C, leading to a NOx reduction of between 50 - 80% [28]. Optimum temperatures for the SNCR process, giving 70% NOx removal using ammonia and urea were found to be 950 °C and 1000 °C, respectively [30]. When injecting ammonia over a temperature range of 450 °C to 1000 °C, significant NOx reduction began at a temperature of 830 °C, and an optimum reaction temperature of 960 °C was found [31]. At temperatures above these a significant quantity of the ammonia was oxidised to form additional NOx. At temperatures below these, the reaction rate was too slow and resulted in high levels of ammonia and ammonia compounds being emitted into the environment. For a 60% NOx removal the SNCR processes was found to cost between $612/ton and $961/ton NOx removed, based on 1993 costs [32]. However, the cost of the SNCR process has been found to decrease with increasing thermal capacity [28]. For combustion facilities with a thermal rating of between 73 MW and 220 MW, the cost of SNCR was found to decrease from $3500 to $3000/ton NOx removed.

2.4.3 **Selective catalytic reduction (SCR)**

There are three classes of catalysts that have been used for the SCR process [33]. The classes were separated by the materials used and the temperature ranges at which they operated. Precious metal based catalysts operated at the lowest temperature range of 175 °C - 290 °C, base metal catalysts in the range of 260 °C - 450 °C and zeolites in a range of 454 °C - 593 °C.

The SCR reaction is similar to that of the SNCR process but has been found to give a normal NOx reduction of 80% [27]. However, the SCR process may

achieve a NOx reduction of up to 90% if the reagent injection nozzle location results in a good distribution [34]. It was also found that the cost of the SCR process was higher per ton of NOx removed than any other NOx reduction process, typically five times the cost of low NOx burners. To decrease the cost of total NOx reduction, flue gas recirculation and SCR has been used to achieve legislative emissions of 10 ppm NOx [35]. It was found that the use of flue gas recirculation decreased the number of SCR units by 26%.

2.5 **COMBUSTION SYSTEMS**

Low NOx combustion systems have been designed for use in utility combustion plants with great success [36], reducing NOx emissions from 973 ppm to 120 ppm. The underlying principles surrounding the reduction of NO are well established, and frequently occur either singularly or as a combined effort in order to reduce overall emissions. The legislation surrounding NOx emissions depends very much on the fuel being burnt, the age of the system and its size [5]. Small combustion systems at present need not have NOx emission controls as legislation is not currently in place to demand it.

To limit the quantity of material to be reviewed, only those burners working on similar principles shall be discussed. These primarily involve operation under fuel lean conditions, flue gas recirculation and staged combustion. Burners that are classed as industrial rather than those used in utility systems will also be included.

Wunning [23] designed a burner for flameless oxidation with low NO formation utilising natural gas. He found that through creating high levels of flue gas/air premixing, the flame temperature could be reduced so far as to largely suppress NO formation. By using several small jets of hot flue gas surrounding a central fuel jet, intense mixing and entrainment with the surrounding air resulted in complete combustion after only 6 mixing diameters. The total NO emissions were calculated as being 8.4 ppm when in flameless

oxidation mode, and 134 ppm in normal flame mode. This combustion system has been employed in the glass industry using very high air preheat temperatures, yet still producing low NOx emissions.

Meier et al [20] designed an integrated burner boiler system using cold flue gas recirculation to burn either gas or oil. They combined cold flue gas recirculation, high swirl, a pressurised combustion chamber and low excess air. Their findings led to the assumption that there was a critical level of excess air which led to high NOx formation. They also assumed that there must be an optimum oxygen concentration and temperature in the flame to produce low NOx. With only low levels of excess air, global soot free combustion was achieved once the recirculation rate was set above a critical limit. Further increases in recirculation led to blue flame combustion. Swirl was used to promote mixing through intense internal recirculation. This had the effect of compensating the stabilisation through a reduction in combustion intensity, due to the low temperature of the recycled gases. The flame colour regimes were compared to those of Cooper [15], and are displayed in figure (4). The transition from a soot free to blue flame was found to occur from 35% onwards, whereas Cooper found that at similar excess air levels, blue flame combustion would not occur until 55% recirculation. The NOx emission levels from the burner were given over a range of excess air levels between 1.0 and 1.4 and three recirculation rates. With no recirculation, the NOx emissions were typically 30 ppm. At recirculation rates of 30 and 60% (calculated based on equation (18)), the NOx emissions were typically 12 ppm and 10 ppm, respectively. The CO emissions under all cases were very low, and normally in the range of 5 to 10 ppm. The combustion system was designed principally for the use of domestic water heating.

Schefer [37], modelled and observed lean, premixed recirculating flows for the control of oxides of nitrogen. Using propane as a fuel, a two step reaction model was used. The first reaction with oxygen produced only CO and H_2O. The second reaction was between CO and O_2, completing the reaction to form

CO_2. The system was effectively composed of two opposing jets. The first was premixed propane and air at 300 - 600 K and travelling at 7 m/s. The second consisted of propane and air again but through a nozzle at a velocity of between 70 and 168 m/s. A stagnation region was created upstream of the narrower jet which created a recirculation zone capable of maintaining combustion. The combustion system was able to operate at an overall fuel lean stoichiometry of 0.45. Under these conditions, there was found to be generally good burnout of CO and unburnt hydrocarbons. The NOx emissions were measured as being between 12 and 15 ppm. Schefer [37] found that NOx increased with combustor residence time. Therefore, it was concluded that limiting the high temperature residence time would reduce the NOx emissions. However, the high temperature residence time must be matched with the burnout of CO if overall low emissions are required.

Syska [21] designed a low NOx burner using staged air and hot flue gas recirculation with the primary air preheated up to 1000°C. The burner was relatively large, having an output of 586 kW. NOx emissions were measured over a range of recirculation rates from 0% to 63%. The NOx emissions tended to vary from 200 ppm with no recirculation to below 10 ppm with 63% recirculation.

Cooper et al [15] designed a blue flame oil burner utilising attached jet entrainment, as shown in figure (5). The experimental data obtained over varying excess air levels of between 0 and 20% gives the description of the flames appearance and the CO emission levels. Recirculation rates are given in a percentage form but are based on volumetric recirculation rates to the air inflow rate and not the overall gas flow rate within the burner. The values of 58 to 75% recirculation represent the volumetric entrainment ratio of the air supply. They found that instability and blowoff occurred above excess air levels of 30%. However, CO emissions were measured as being up to 20 ppm with no excess air and at 0 ppm above 10% excess air. Unfortunately, no NOx measurements were taken.

Prior [38] designed a blue flame, low NOx Coanda ejector burner for kerosene combustion, as shown in figure (6). Operation at both fuel rich and fuel lean conditions were possible, leading to NOx emissions below 30 ppm. However, ignition of the burner proved to be difficult, and large quantities of CO were emitted, even under fuel lean conditions.

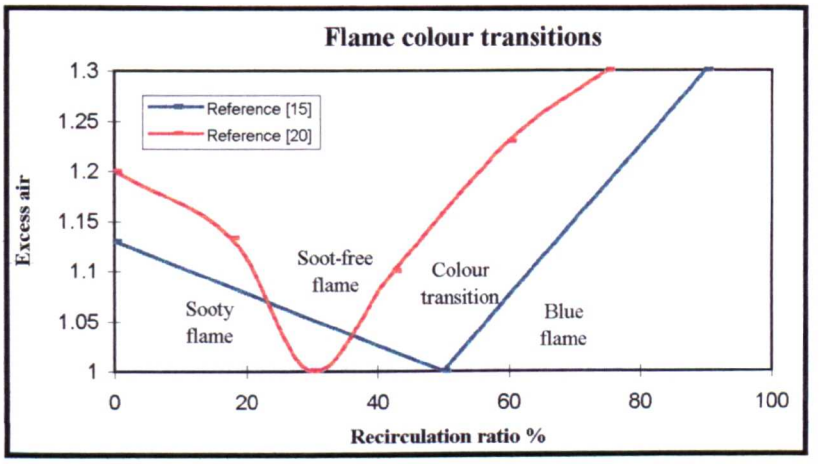

Figure 4. The effect of flue gas recirculation of flame colour and stability.

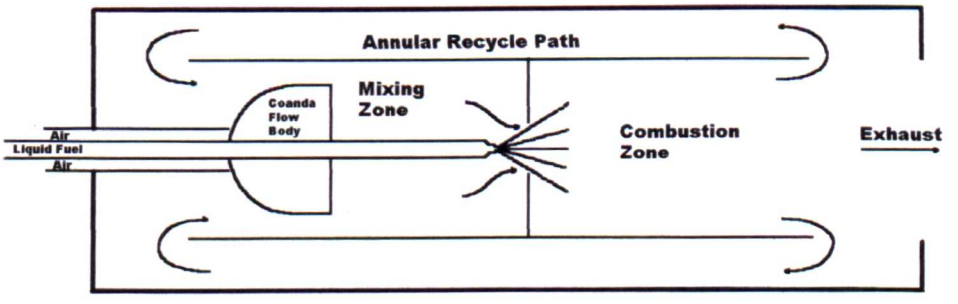

Figure 5. Attached jet blue flame burner designed by Cooper and Mareck [15]

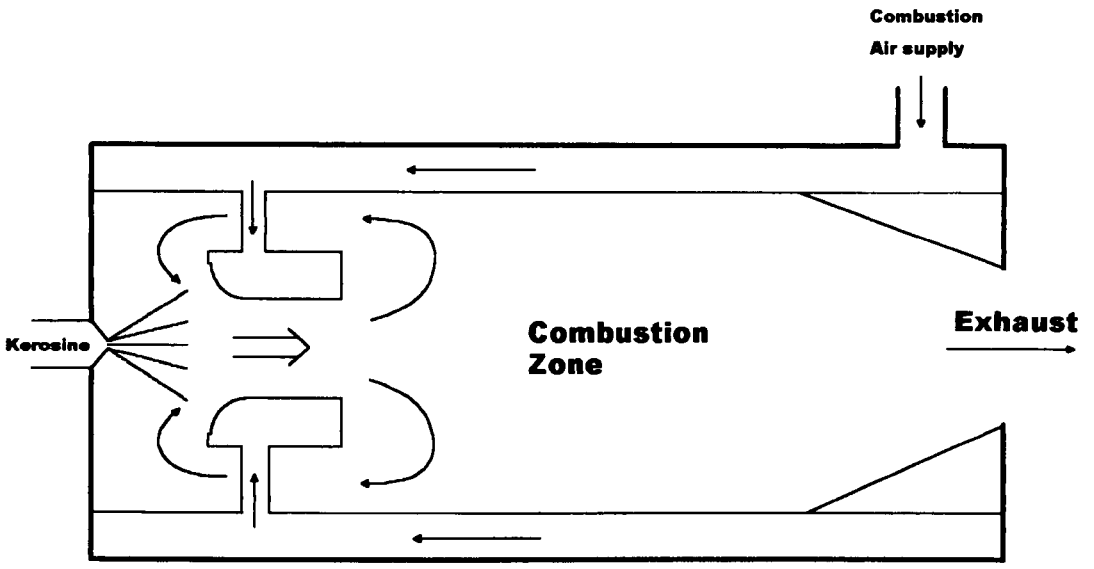

Figure 6. Blue flame Coanda burner designed by Prior [38].

2.6 COMBUSTION MECHANISMS OF HYDROCARBON FUELS

2.6.1 Introduction

The combustion of hydrocarbon fuels is highly complex, involving many reactions incorporating molecules, atoms and radicals. Propane combustion involves over 1000 reactions before combustion is complete [39].

2.6.2 Propane combustion

Degaut et al [39] studied the combustion of propane in detail, and revealed that propane initially reacts by thermal decomposition and with molecular oxygen, as given in equations (22) to (24).

$$C_3H_8 \rightarrow C_2H_5 + CH_3 \quad (22)$$

$$C_3H_8 + O_2 \rightarrow nC_3H_7 + HO_2 \quad (23)$$

$$C_3H_8 + O_2 \rightarrow iC_3H_7 + HO_2 \quad (24)$$

At high temperatures and under fuel rich conditions, equation (22) dominates. However, under fuel lean conditions and at high pressures, equations (23) and (24) dominate the start of the reaction process. After the initial reactions, propane consumption is dominated through reactions with atoms and radicals. The relative importance of the main reactive routes for propane is strongly dependent on stoichiometry. Under fuel lean conditions it was found that reaction with the OH radical dominated, and that under fuel rich conditions, reaction with the H atom dominated.

For modelling purposes, simplification of the reaction scheme is essential. A four step reaction mechanism for the combustion of lean propane flames was developed by Kennel et al [40] from an elementary 88 step reaction. The four step reaction derived is given in sequence through reactions (25) to (28).

$$C_3H_8 + O_2 + H_2O + 2H \leftrightarrow 3CO + 6H_2 \tag{25}$$

$$CO + H_2O \leftrightarrow CO_2 + H_2 \tag{26}$$

$$H + H + M \leftrightarrow H_2 + M \tag{27}$$

$$O_2 + 3H_2 \leftrightarrow 2H_2O + 2H \tag{28}$$

2.6.3 **Methane combustion**

The reaction sequence of methane-air flames were reduced through steady state and partial equilibrium assumptions to a 3 step reaction by Peters et al [41]. The three reactions involved are given in equations (29) to (31).

$$CH_4 + O_2 \rightarrow CO + H_2 + H_2O \tag{29}$$

$$CO + H_2O \leftrightarrow CO_2 + H_2 \tag{30}$$

$$O_2 + 2H_2 \rightarrow 2H_2O \quad (31)$$

A four step mechanism for methane combustion was evaluated by Chen et al [45], who found that flame temperatures were slightly over predicted.

2.6.4 **CO oxidation in flames**

The oxidation of CO to CO_2 in combustion systems is through reaction with the OH radical [43] [44], as given in equation (32).

$$CO + OH \rightarrow CO_2 + H \quad (32)$$

The reaction given in equation (32) has been found to give approximate agreement with experimental results [45], and that the rate of CO burnout is independent of fuel type provided the CO flames contained sufficient water vapour.

2.6.5 **Combustion reactions in numerical modelling**

Due to the limited number of species and reactions currently possible in commercial modelling packages, simplified combustion mechanisms need be used. Two step reactions are frequently used for methane combustion [12, 24, 43]. The reaction sequence follows that of equations (33) and (34).

$$CH_4 + 1.5O_2 \rightarrow CO + H_2O \quad (33)$$

$$CO + 0.5O_2 \rightarrow CO_2 \quad (34)$$

It has been found that the formation of the CO species leads to more accurate flame temperatures, and hence NO predictions. However, endothermic dissociation reactions were not taken into account which resulted in flame

temperatures being over predicted. Similar two step reaction mechanisms have been used for propane combustion [37] and the combustion of heavy fuel oil, where pentane was simulated as the gaseous components [46]. Coal combustion has also been modelled in a two step mechanism [36], where the first step involves the devolatilisation process of the coal, and the second step the reaction of CO with O_2.

2.7 **FLAME STABILIZATION**

2.7.1 **Introduction**

The stabilisation of flames is essential in the majority of practical combustion systems. Flame stabilisation is commonly achieved through forming a region in the burner that can support combustion and continually ignite the surrounding mixture. This stable region is normally formed through the use of bluff bodies and the aerodynamic properties of swirling flows.

2.7.2 **Bluff body flame stabilisers**

Williams et al [47] and Winterfield [48] studied the flame stabilisation characteristics behind various bluff body flame stabilisers for premixed gas air streams with very low inlet turbulent intensities. It was postulated that flame stabilisation was achieved through contact between the unburnt fuel air mixture with the eddy region of hot gases directly behind the bluff body. A rapid transfer of heat and chain reaction molecules from the eddy region to the colder unburnt stream caused the mixture to reach its ignition temperature and begin burning. During the remaining time that the recently ignited gas parcel was in contact with the eddy region, heat and chain reaction molecules flew back into the eddy region. The hot recirculating gases of the eddy region thus acted as a constant source of ignition for the unburned gases. Winterfield [48] found that the blow off velocity for a flame stabiliser was encountered when the flow velocity was increased such that the flame traversed the boundary of the

recirculation zone. When the blow off velocity was reached the flame was near the rear of the stagnation point. This resulted in the flame being unable to spread to the outer flow region. Williams et al [47] found that heating the bluff body stabiliser greatly increased the flame stability limits. The effect of the bluff body stabiliser shape on flame stability was found to be negligible, and increasing the inlet turbulence intensity of the fuel air mixture was found to decrease the stability limits. Wright et al [49] found that the wake after the bluff body expanded radially at an angle of 2^{o} as the flow travelled downstream. It was also found that the spreading rate of the wake was independent of initial bluff body diameter and of the laminar flame speed.

2.7.3 **Swirling flow**

Swirl can be used in the place of bluff body flame stabilisers. However, the recirculation zone is created through an aerodynamically formed blockage rather than a physical one [50]. The transport of heat and chemically reactive species from the recirculation eddy to the surrounding unburnt mixture is accomplished in a similar way to that when using a bluff body stabiliser. The angular momentum of the swirling fluid exerts a centrifugal force on the constraining boundary of the burner wall. This results in a radial pressure distribution within the burner, with the axis of the burner at a lower pressure. Once the swirling fluid exits the burner, the pressure along the axis of the burner is recovered further downstream. A balance exists between the low pressure at the axis of the burner exit and the momentum of the swirling fluid flowing in the axial direction. If the pressure differential at the burner exit can overcome the axial momentum of the fluid then a recirculation core is established. The occurrence of this recirculation can be determined through the swirl number, which is a function of the ratio between the angular and axial flux of the fluid. Wright et al [49] found that for turbulent burning free jets of propane - butane - air mixtures with swirl, the turbulent burning velocity was 80 times greater than the laminar flame speed.

2.8 **EJECTORS**

The principle upon which all types of ejectors work is that of conservation of momentum. Typically, a stream of fluid at high velocity is passed into a duct containing the fluid to be moved. Through viscous forces between the two fluids, the secondary fluid will increase in velocity. The increase in velocity in the duct creates a low pressure region which causes an inflow into the duct. The point at which the maximum amount of flow is attained is when the momentum between the two fluids is balanced. The term which defines the movement of the secondary fluid by the primary fluid is entrainment.

The most common ejector is a co-axial type, where the primary fluid is injected down the centreline of a circular duct [51]. Ejectors of this design have been commonly used as pressure boosters in gas distribution networks. Hoggarth [52] performed a theoretical evaluation and comparison with experimental results for co-axial ejectors in such applications [52]. The ejector was designed using a control volume approach, conserving mass and momentum throughout the ejector. The mathematical model used for the ejector design was simplified with the assumptions that a one dimensional model adequately represented the process, the injected gas was stationary and therefore did not contribute to momentum, no phase changes occurred, and that buoyancy was unimportant. It was found that at near design conditions, the theoretical results were in close approximation with the experimental results. However, discrepancies occurred when deviating from the design conditions. These discrepancies were attributed to recirculation of the injected fluid.

The Coanda effect was named after Henri Coanda, a Romanian engineer. In the year 1910 he discovered that if a fluid is passed at high velocity over a curved surface, that fluid would attach itself to the surface and may be turned through angles. In addition to this attachment effect, the high velocity stream of fluid has entrainment properties similar to those of a co-axial ejector.

The Coanda effect has been incorporated into the design of ejectors which have been used in a number of industrial situations such as gas extraction systems and jet pumps. Coanda surfaces are also found in the design of flaps on aircraft. Fricker [53] found that the Coanda has no effect other than to deflect the jet of the primary fluid. Coanda ejectors have been used in combustion systems, such as flarestacks burning waste or excess gas [54]. In the latter, the waste gas was passed through a Coanda ejector which was positioned in the flare stack. Entrainment of the combustion air by the gas produced a premixed combustible gas. This process not only decreased the atmospheric air pollution as compared to normal flare stacks, but was also found to produce low noise levels. The low noise levels resulted from modifications to the size of the turbulent eddies which shifted the combustion roar frequency from a low level to a higher frequency. The flare stack using the Coanda ejector was found to be 10 - 20 dB quieter than a conventional burner operating with the same mass throughput. Fricker et al [53] found that in a comparison of equally sized co-axial and Coanda ejectors, the sound power level decreased by 10 - 15 dB when the Coanda ejector was used in a combustion system. The Coanda effect has also been utilised by Reba [55] in creating a ground - effect machine. The machine used the Coanda effect to decrease the pressure over the upper surface of the machine, causing a pressure differential between the upper an lower surfaces, lifting the device off the ground.

The entrainment performance of a Coanda ejector has not been found to exceed that of a well designed co-axial ejector [53]. However, the Coanda ejector has the ability of giving good performance over a wider range of flow and area ratio conditions. It also has a mixing advantage due to having a far larger initial surface to volume contact than a normal ejector. This enables the Coanda ejector to achieve complete mixing after only 6 diameters. The increased rate of mixing is beneficial in combustion systems as the length of the burner is decreased.

There are three methods that can be used to predict the entrainment performance of a Coanda ejector [56]. The most common method, the control

volume approach, is similar to that of co-axial ejectors where the mass and momentum of the fluids are conserved. This method has also been used by other researchers [38, 53, 57]. It was found by Ameri et al [56] that the control volume approach predicted the experimental results to within 10% error. The second method used was the physical phenomena approach. This method solved the continuity and momentum equations using a marching finite difference method. The predicted results were found to closely approximate the experimental results. However, both the control volume and physical phenomena approach needed initial flow input conditions in order to predict the ejector flow properties. A third model was developed on the theory based on experimental results, predicting the entrainment ratio to within 5% error. This model was assumed to be capable of designing ejectors.

In common with co-axial ejectors, Coanda ejectors commonly have a diffuser section after the mixing section. Such diffusing sections increase the static pressure of the fluid and have been found to give an efficiency of 80 - 90% when using an included angle of 5 to 10° [52].

3. THE COANDA EJECTOR BURNER

3.1 THE COANDA EJECTOR

3.1.1 Introduction to ejectors

All types of ejectors work on the principle of conservation of momentum. Typically, a stream of fluid at high velocity is passed into a duct containing the fluid to be moved. Through viscous forces between the two fluids, the secondary fluid will increase in velocity. The increase in velocity in the duct creates a low pressure region which causes an inflow into the duct. The maximum amount of entrained flow is attained when the momentum between the two fluids is balanced.

A co-axial ejector, where the primary fluid is injected down the centreline of a circular duct, is the most common type. Optimum operation can only take place for a given design under specific flow conditions, otherwise losses will occur and the entrainment ratio will be reduced. Mixing between the streams of primary and secondary fluid is relatively poor, and on average ten mixing diameters are required before mixing is complete [53]. This type of ejector is incapable of working over a wide range of conditions due to the strict limitations in the optimum design.

3.1.2 The Coanda ejector

The Coanda effect was named after Henri Coanda, a Romanian engineer in the year 1910, who discovered that if a fluid is passed at high velocity over a curved surface, it will attach itself to that surface and may be turned through angles. This effect is illustrated in figure (7). The jet of high velocity fluid exiting the ejector becomes attached to the curved surface due to a pressure differential between the atmospheric pressure on one side of the jet and a low pressure region created at the Coanda surface wall. The jet of fluid that flows

over the Coanda surface has the ability to entrain the surrounding fluid through viscous forces. The amount of surrounding fluid that is entrained will depend upon the physical properties of the fluids used and the velocity of the ejected fluid. The entrainment capacity of the ejector is satisfied when a momentum balance is reached between the fluids. The Coanda ejector works on the same principle as a normal ejector, but allows the fluid to be injected radially.

It is interesting to note that the amount of entrainment that can be achieved by a Coanda ejector will not exceed that of a well designed 'normal' ejector, ejecting the fluid in the axial direction. However, the Coanda ejector has the ability to give a good performance over a wider range of flow conditions and area ratios. Its mixing potential is greater due to having a far larger initial surface to volume contact than a 'normal' ejector. This enables the Coanda ejector to achieve complete mixing after only six diameters [53]. The introduction of fluid over the Coanda surface can be achieved either radially inwards or outwards. Introducing the fluid radially inwards from a circular arrangement has the benefit of requiring lower fluid pressures and smaller Coanda gap widths, which lead to greater quantities of secondary fluid entrainment for an equivalent flow rate. The Coanda effect is used in many applications, such as flaps on aircraft, ventilation equipment and flare stacks for waste gases [54].

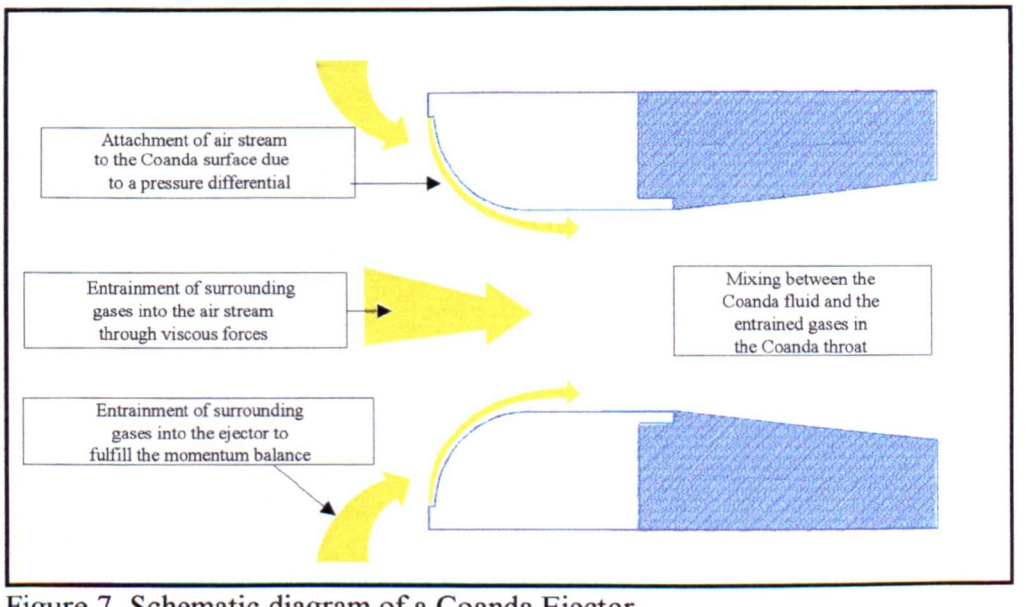

Figure 7. Schematic diagram of a Coanda Ejector.

3.2 DETERMINATION OF THE THEORETICAL ENTRAINMENT RATIO

3.2.1 Introduction

The entrainment performance of the Coanda ejector was determined mathematically through equations describing the conservation of mass, momentum and energy. The entrainment ratio calculated was then used to verify that the design dimensions of the Coanda unit, as calculated in sections 3.3.2 to 3.3.7, would satisfy the burner design characteristics, given in section 2.3.2.3.

The physical process taking place in the Coanda ejector were analysed mathematically through mass and momentum balances, along with energy conservation. The mathematical analysis of the Coanda ejector was performed for a variety of geometrical designs and fluid conditions. It was possible to calculate the resultant entrainment ratio of the Coanda ejector when operating at different air supply temperatures and pressures and flue gas temperatures and densities. These changes in supply conditions were coupled with variations in the ejector design which can be brought about by changing the Coanda gap area and the Coanda throat diameter. Analysing the ejector in this way led to an evaluation of its entrainment performance.

3.2.2 Mass and momentum balances

Using the nomenclature shown in figure (8), and assuming constant area mixing, the mass balance equation is given by:

$$\rho_i \int U_i dA_i + \rho_j U_j A_j - \rho_o \int U_o d(A_j + A_i) = 0 \qquad (35)$$

and the momentum balance is given by:

$$\rho_i \int U_i^2 dA_i + \rho_j U_j^2 A_j - \rho_o \int U_o^2 d(A_j + A_i) = \int (p_o - p_i) d(A_j + A_i) \quad (36)$$

Equations (35) and (36) assume that the velocity profiles of the external and exit streams may not be uniform and that the densities of the jet and external fluids may be different.

Applying the Bernoulli equation between points i and o, gives equation (37),

$$P_o - P_i = \frac{1}{2} \rho_i U_i^2 \quad (37)$$

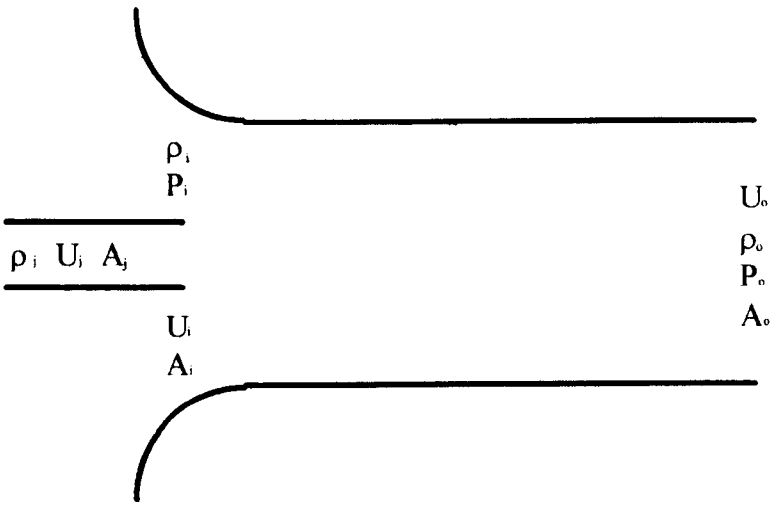

Figure 8. Nomenclature used in the control volume approach for an ejector.

3.2.3 **Determination of the entrainment ratio, φ.**

The theoretical entrainment ratio, φ, can be calculated through rearrangement and substitution of equations (35), (36) and (37). The introduction of λ, an experimentally determined value, was made to account for the non uniformity of the inlet and exit streams.

Substituting equation (37) into equation (36), and taking $A_i/a_j >> 1$, gives

$$\rho_i \int U_i^2 dA + \rho_j U_j^2 A_j - \rho_o \int U_o^2 dA = \frac{1}{2} \rho_i \int U_i^2 dA \tag{38}$$

where, $dA \approx dA_i \approx dA_o$

Rearranging equation (38) gives equation (39)

$$U_j = \left\{ \frac{1}{\rho_j A_j} \left(\rho_o \int U_o^2 dA - \frac{1}{2} \rho_i \int U_i^2 dA \right) \right\}^{\frac{1}{2}} \tag{39}$$

The non uniformity of the inlet and exit streams can be expressed as a parameter, λ [57].

$$\lambda = \frac{\frac{\rho^2}{A} \int U^2 dA}{\left(\frac{\rho}{A} \int U dA \right)^2} \tag{40}$$

It can be found from equation (40) that for a flat velocity profile λ tends to 1, and increases for a non uniform profile. Rearranging equation (40) yields equation (41).

$$\rho \int U^2 dA = \frac{\lambda \dot{m}^2}{\rho A} \tag{41}$$

Inserting equation (41) into equation (39) gives equation (42)

$$U_j = \left\{ \frac{1}{\rho_j A_j} \left(\frac{\lambda_o \dot{m}_o^2}{\rho_o A_o} - \frac{\lambda_i \dot{m}_i^2}{2 \rho_i A_i} \right) \right\}^{\frac{1}{2}} \tag{42}$$

The mass entrainment ratio is then given by equation (43), which can be rearranged to give equation (44).

$$\varphi = \frac{\dot{m}_o}{\dot{m}_j} = \frac{\dot{m}_o}{\rho_j A_j U_j} = \frac{\dot{m}_o}{\rho_j A_j}\left\{\frac{\rho_j A_j}{\frac{\lambda_o \dot{m}_o}{\rho_o A_o} - \frac{\lambda_i \dot{m}_i^{\bullet 2}}{2\rho_i A_i}}\right\}^{\frac{1}{2}} \tag{43}$$

$$= \left\{\rho_j A_j \left(\frac{\lambda_o}{\rho_o A_o} - \frac{\lambda_i \dot{m}_i^{\bullet 2}}{\rho_i A_i \dot{m}_o^{\bullet 2}}\right)\right\}^{-\frac{1}{2}} \tag{44}$$

But

$$\frac{\dot{m}_i^{\bullet 2}}{\dot{m}_o^{\bullet 2}} = \left(1 - \frac{1}{\varphi}\right)^2$$

The entrainment ratio, φ is now defined through equation (45),

$$\varphi = \frac{\dot{m}_o}{\dot{m}_j} = \frac{\dot{m}_o}{U_j A_j \rho_j} = \frac{\dot{m}_i + \dot{m}_j}{\dot{m}_j} \tag{45}$$

For perfect mixing, equation (46) can be deduced

$$\rho_o = \frac{\dot{m}_j}{\dot{m}_o}\rho_j + \frac{\dot{m}_i}{\dot{m}_o}\rho_i = \rho_i\left(1 + \frac{\frac{\rho_j}{\rho_i} - 1}{\varphi}\right) \tag{46}$$

Substituting equation (46) into equation (44) gives equation (47)

$$\varphi = \left\{ \frac{\left(2\frac{A_i\rho_1}{A_j\rho_j}\right)}{\left(\frac{2\lambda_o}{\left(1+\left(\frac{\rho_j}{\rho_i}-1\right)/\varphi\right)} - \lambda_i\left(1-\frac{1}{\varphi}\right)^2\right)} \right\}^{\frac{1}{2}} \qquad (47)$$

Equation (47) can be used through an iterative process to calculate the entrainment ratio for a Coanda ejector. The variables required to calculate the entrainment ratio are the Coanda gap area, Coanda throat area, the densities of the Coanda and entrained fluid, and the uniformity in velocity of the entering and exiting fluids. As this is an iterative process to determine φ, an initial guess of φ was needed to start the calculation. The iterative process was complete when the desired error value of 0.001 for φ was obtained. The results obtained for the theoretical entrainment ratio through increasing the air supply pressure and Coanda gap width are displayed in figure (9).

It can be seen that equation (47) may be reduced to the conventional ejector equation of (48) if it is assumed that $\lambda_i = \lambda_o = 1$, and the density is constant.

$$\varphi = \sqrt{2\frac{A_i}{A_j}} \qquad (48)$$

When φ is large but the gas densities are variable, equation (47) may be approximated to give equation (49)

$$\varphi = \left\{ \left(\frac{2\frac{A_i\rho_i}{A_j\rho_j}}{\left(2\lambda_o - \lambda_i\right)_1} \right) \right\}^{1/2} \qquad (49)$$

Swithenbank [57] found that λ_i =1.2 and λ_o = 1.02.

From equation (49), it can be noted that decreasing the density of the Coanda ejector supply fluid, ρ_j, and increasing the non uniformity of flow at the Coanda inlet, λ_i, will result in the greatest entrainment ratio for any geometrical design.

3.2.4 **Limitations of the mathematical analysis**

Equations (47), (48) and (49) allow the determination of the entrainment ratio achieved in an ideal situation. The value of φ was calculated in a way that assumed that there were no pressure or frictional losses between the entrance and exit of the ejector. It also assumed that there were no pressure or density variations within the system. Also, the experimentally derived values of λ were found for a Coanda ejector systems that did not include combustion.

The introduction of combustion causes pressure and density variations throughout the burner. Equation (47) will not give accurate entrainment predictions of the Coanda burner. The introduction of combustion, recirculation and flame stabilisers will cause pressure and density variations throughout the burner, resulting in a decreased value of φ. However, the computational fluid dynamics package, FLUENT, was used to predict the entrainment and mixing properties of the Coanda ejector when incorporated into the burner. The entrainment ratio of the Coanda burner predicted by the modelling package was significantly lower than that calculated through equation (14). Detailed use of the computational package and the entrainment ratios predicted are given in sections 3.4 and 5.1, respectively.

3. 3 BURNER DESIGN PARAMETERS

3.3.1 Introduction

In order to design the Coanda burner, parameters must be set for the operating conditions such that the designs of the subsequent individual components will meet the operating specifications. To limit the many possible design variations in the Coanda ejector and to provide initial guidelines for the Coanda ejector design, values were assumed concerning the following variables:

- Air mass flow rate required for combustion
- Air supply pressure
- Coanda gap area
- Coanda gap width

3.3.2 Determination of air mass flow rate

The air mass flow rate is governed by the thermal rating of the burner and the air to fuel ratio at which it operates. The burner was required to operate up to a maximum thermal rating of 30 kW, which is small for industrial burners but should provide an ideal rating for a prototype system. With a variable thermal rating of up to 30 kW, the Coanda burner could be used for domestic heating applications.

The calorific value of propane is 46.389 MJ/kg [68]. Therefore, the flow rate of propane required for a thermal rating of 30 kW was found to be $1.4697*10^{-5}$ mols/s.

Under lean conditions, to account for the burner operating at a stoichiometry of 0.7, the quantity of oxygen needed to be increased by a factor of 1.4286. Therefore, the molar rate of oxygen required was calculated to be $1.0498*10^{-5}$

mols/s. This is equivalent to $3.3595*10^{-3}$ kg/s of oxygen, and $1.4418*10^{-2}$ kg/s of combustion air.

3.3.3 **Air supply pressure**

The air supply pressure was kept to a maximum of 4 bar. This was chosen because it is a pressure that is attainable by most industrial compressors. Ideally, a lower pressure would be more advantageous as it would enable the system to be utilised over a wider range of industrial environments.

3.3.4 **Coanda gap area**

From section 3.2.3, it has been found that increasing the ratio between the Coanda throat area and the Coanda gap area increased the entrainment ratio of a Coanda ejector. In accordance with literature, [20, 21, 23], recirculation quantities of between 30% and 500% were successfully utilised in flue gas recirculation systems to reduce NOx emissions. Following the literature, the Coanda ejector was subsequently designed to obtain mass entrainment ratios of between 0.3 and 5.

The Coanda gap area was calculated using the assumption that the air supply pressure was at 4 bar, and the mass flow requirement was to suit a 30 kW burner operating at a fuel to air ratio of 0.7.

Using the variables given in sections 3.2.2 and 3.2.3, equation (50) was used to evaluate the Coanda gap area [58].

$$A_j = \sqrt{\frac{\left(\frac{\gamma-1}{2\gamma}\right)\frac{\dot{m}^2}{p_o\rho_o}}{\left(\frac{p}{p_o}\right)^{2/\gamma}-\left(\frac{p}{p_o}\right)^{\gamma+1/\gamma}}} \qquad (50)$$

Under these conditions, equation (50) yielded an area of $1.6359*10^{-5}$ m^2. Equation (50) assumes adiabatic, frictionless flow. However, for a small sharp edged orifice, the coefficient of discharge is in the range of 0.6 to 0.65 [58]. To correct the area from the ideal situation , a discharge coefficient of 0.63 was incorporated, which gave an equivalent area of $2.5966*10^{-5}$ m^2.

3.3.5 **Coanda gap width**

The Coanda gap width is a function of the Coanda gap area and the diameter of the ejector. The Coanda gap area was calculated in section 3.4 above. A number of Coanda gap widths could be used to give the required area. However, the implications of the Coanda gap width and the resultant ejector diameter on the mechanical design of the burner must be considered.

The following assumptions were made regarding the mechanical design of the Coanda ejector:

- The Coanda surface radius must be more than 25 times greater than the Coanda gap width, [57].
- For a given flow rate of fluid, a larger Coanda throat diameter results in a reduction in the flow velocity through it, but similarly increases the length of the burner to provide complete mixing.
- The Coanda gap width must be easily measured and reproducible, and of a width that will not be clogged by particulate matter.

A small Coanda gap width is preferable, as it results in a large Coanda throat diameter and a greater quantity of flue gas recirculation. Choosing a Coanda slit width of 0.1 mm, led to the ejector diameter through equation (51),

$$D = \frac{A}{\pi L} \tag{51}$$

giving a diameter of 0.08 m.

Figure (8) displays the air flow rate through the Coanda ejector in terms of stoichiometric thermal rating. The diameter of the Coanda gap was maintained at 0.08 m. It can be seen that it is unnecessary to dramatically increase the Coanda gap width in order to allow equivalent air mass flow rates at reduced air supply pressures.

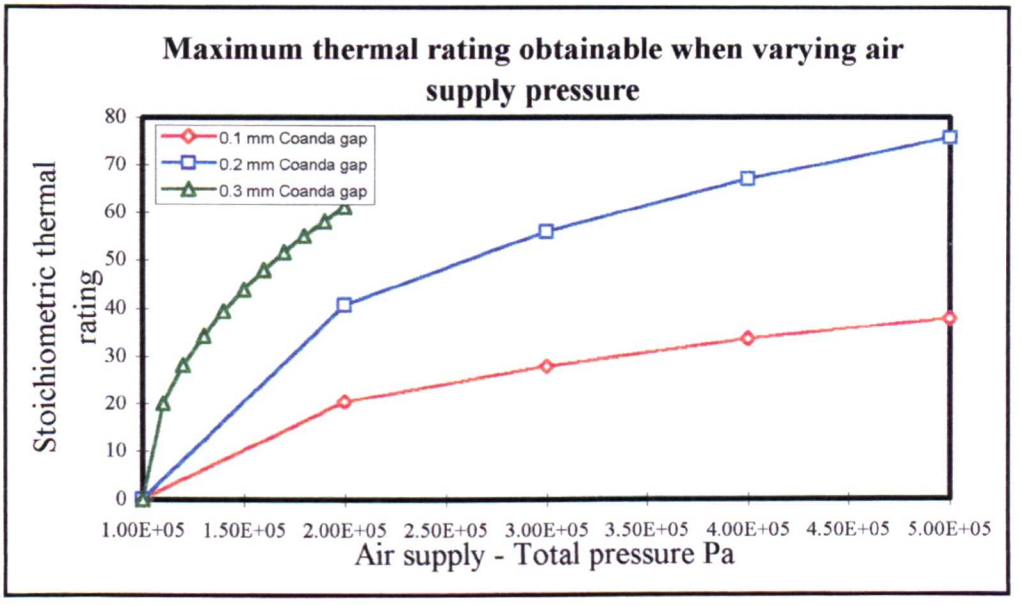

Figure 8a. The variation in air flow rate through the Coanda ejector with pressure.

3.3.6 **Internal burner diameter**

3.3.6.1 **Air flow to the Coanda gap**

An increase in the diameter of the Coanda ejector beyond that of the 80 mm Coanda gap diameter was needed to allow the combustion air to flow smoothly from the Coanda cavity, through the Coanda gap, and over the Coanda surface. This was accomplished by increasing the diameter of the Coanda to 90 mm.

3.3.6.2 **Flue gas recycle annulus**

From section 5.1 a mass entrainment ratio in the order of up to 1.5:1 was expected. At a thermal rating of 30 kW, a flow of $2.1627*10^{-2}$ kg/s of recirculating flue gas was obtained. The recirculating flue gas was at approximately 1300 K which gave a volumetric flow rate of $7.9822*10^{-2}$ m^3/s. If a nominal radius of 0.01 m beyond the radius of the air chamber was chosen, then the velocity in the annulus would have been in the order of 25 m/s. Using Bernoulli's equation, and taking the flue gas density at 1300 K as 0.27 kg/m^3 a pressure drop of 87 Pascals was achieved. Bernoulli's equation does not take into account the reduction in viscosity due to temperature or frictional losses. However, it does give the indication that the pressure drop is small. The addition of the recycle annulus caused the internal diameter of the burner to increase to 0.11 m.

3.3.7 **Coanda throat diameter and diffuser length**

To ensure that the construction of the burner was kept as simple as possible, the burner was cased in a cylindrical tube. This ensured that the maximum internal diameter of the burner was maintained along the whole length of the burner. To allow for materials of construction and flow, the Coanda radius was increased by 5 mm. Allowing for the recycle path, this implied that the exit of the burner could not exceed 90 mm (as the recycle path would reduce the maximum internal diameter by 20 mm).

Both the diffuser angle and mixing length are important parameters concerned in the design of the burner. Due to Coanda ejectors having an extremely good mixing capability over ordinary ejectors, the mixing length was reduced from 8 - 10 mixing diameters to 6 - 7 [53]. To decrease the pressure loss along the burner but prevent recirculation along the burner length, the angle of the diffuser was chosen to lie between 6 and 10 degrees, inclusive of both angles [58]. With the burner outlet diameter fixed at 90 mm, the diffuser lengths and

angles could be determined for a variety of Coanda throat diameters and mixing lengths.

For a mixing length of 7 diameters,

Throat diameter mm	diffuser length mm	included angle
30	210	16.26
40	280	10.2
50	350	6.4

Table 2. Diffuser lengths and angles when using a mixing length of 7 diameters.

For a mixing length of 8 diameters,

Throat diameter mm	diffuser length mm	included angle
30	240	14.24
40	320	8.93
50	400	5.72

Table 3. Diffuser lengths and angles when using a mixing length of 8 diameters.

From tables 2 and 3, it can be seen that a minimum throat diameter of about 40 mm and a maximum of about 50 mm will give acceptable diffuser dimensions. From the considerations given in section 3.5, a Coanda throat diameter of 50 mm was preferable. With a Coanda throat diameter of 50 mm, the maximum Coanda gap width was 0.6 mm.

Figure (9) displays the entrainment ratios calculated from equation (47). When using a 50 mm Coanda throat diameter and a variety of Coanda gap widths, the calculated entrainment ratios, through the use of equation (47), were between the required values of 0.33 and 5.

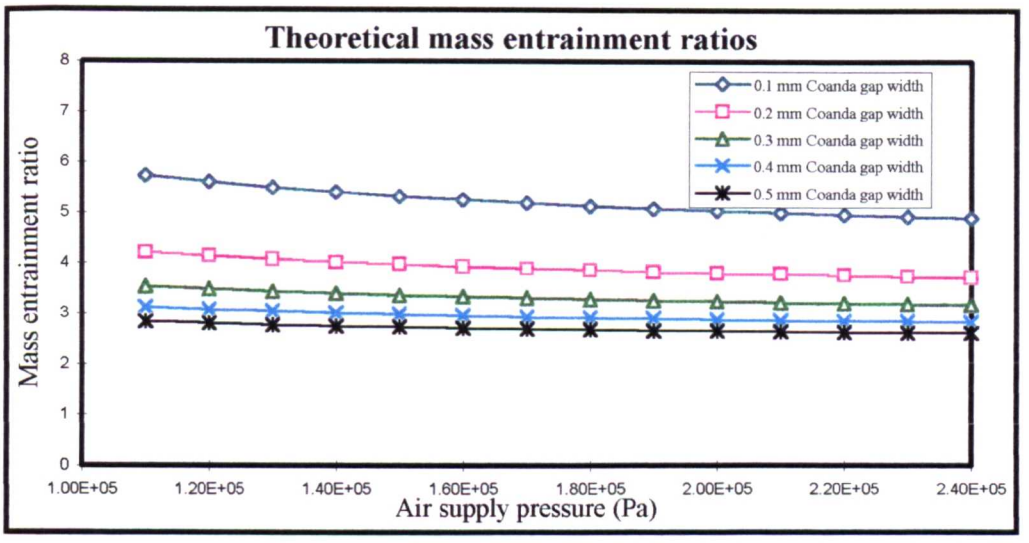

Figure 9. Theoretical mass entrainment for the Coanda ejector calculated from equation (47).

3.4 CFD THEORY

3.4.1 Introduction

The CFD package used, Fluent, relies on a control volume based technique to solve the conservation equations for mass, momentum, energy, species and turbulence. The technique involves converting the differential conservation equations to algebraic equations, which can be solved numerically. Fluent uses a non-staggered grid storage scheme, whereby all variables are stored at the centre of the control volume cell. The face fluxes are obtained such that the face velocities obey an averaged momentum balance, and the face pressures are obtained such that the velocities stored at the cell centres obey the mass balance. Interpolation of the stored cell centre values to the control volume faces can be performed through using a number of techniques, these being the power law differencing scheme, quick, simple and simplec schemes. The power law interpolation scheme interpolates the face value of a variable using the exact solution to a one dimensional convection-diffusion equation. This implies that when the flow is dominated by convection, interpolation can be accomplished by letting the face value of a variable be set equal to its upstream value. The QUICK and second order interpolation schemes compute the face value of an unknown, based on the values stored at the two adjacent cell centres and on a third cell centre at an additional upstream point. These higher order schemes provide greater accuracy, however, numerical instabilities can occur unless the interpolation is properly bounded. Fluent linearly combines the methods to provide a scheme that is both accurate and numerically stable.

3.4.2 The governing equations used by FLUENT

The conservation of mass, momentum, energy and species in a laminar flow can be expressed as differential equations as follows:

3.4.2.1 **Mass conservation equation**

$$\frac{\partial \rho}{\partial t} + \frac{\partial}{\partial x_i}(\rho u_i) = S_m \tag{53}$$

Equation (53) is valid for both compressible and incompressible flows, S_m is the mass added to the continuous phase from the dispersed phase.

3.4.2.2 **Momentum conservation equation**

Conservation of momentum in the i^{th} direction in a non accelerating reference frame is given by equation (54).

$$\frac{\partial}{\partial t}(\rho u_i) + \frac{\partial}{\partial x_i}(\rho u_{iu_j}) = -\frac{\partial p}{\partial x_i} + \frac{\partial \tau_{ij}}{\partial x_j} + \rho g_i + F_i \tag{54}$$

3.4.2.3 **Species conservation equation**

$$\frac{\partial}{\partial t}(\rho m_{i'}) + \frac{\partial}{\partial x_i}(\rho u_i m_{i'}) = \frac{\partial}{\partial x_i}(J_{i',i}) + S_{i'} \tag{55}$$

The conservation of species, equation (55), is linked to the conservation of mass equation, such that the summation of species and volumes changing with chemical reaction remains constant.

3.4.2.4 **Energy conservation equation**

Fluent solves the conservation of energy in terms of conservation of enthalpy, which is given by equation (56)

$$h = \sum_{i'} m_{i'} h_{i'} \tag{56}$$

3.4.3 **Fluid properties**

Fluent allows all fluid properties to be defined as constant or as temperature and/or composition dependent. Defining the characteristics of each species present as it varies with temperature will lead to a more accurate prediction, especially when temperatures vary greatly throughout the system. A linear piecewise or polynomial description of how the property varies with temperature can be used to calculate the values of each species. For multi-component mixtures, the mass fraction of each species can be used to predict the fluid properties.

3.4.3.1 **Density, ρ**

Density can be calculated by the ideal gas law. When compressibility effects are negligible, the gas can be calculated through equation (57)

$$\rho = \frac{p}{RT\sum_{i'} \frac{m_{i'}}{M_{i'}}} \tag{57}$$

The values for viscosity, thermal conductivity and specific heat capacity are variable with both species and temperature. Fluent calculated each property for each species through the use of a polynomial as given in tables 4, 5 and 6. The local value for each variable was then calculated in accordance to the species concentration.

Species	Specific heat capacity, Cp
Propane	$-1.71E^{1}+6.44T-3.25E^{-3}T^{2}+5.93E^{-7}T^{3}$
carbon monoxide	$9.83E^{2}+2.01E^{-1}T+6.37E^{-6}T^{2}-1.35E^{-8}T^{3}$
oxygen	$8.33E^{2}+3.58E^{-1}T-1.24E^{-4}T^{2}+1.63E^{-8}T^{3}$
nitrogen	$9.92E^{2}+1.5E^{-1}T+3.57E^{-5}T^{2}-1.75E^{-8}T^{3}$
CO_2	$9.83E^{2}+1.32T-7.27E^{-4}T^{2}+1.41E^{-7}T^{3}$
H_2O	$1.76E^{3}+2.93E^{-1}T+3.26E^{-4}T^{2}-9.84E^{-8}T^{3}$

Table 4. Polynomial used to calculate the specific heat capacity, Cp, of the combustion gases.

Species	Viscosity, μ
Propane	$-1.86E^{-6}+3.66T-1.49E^{-11}T^2+3.43E^{-15}T^3$
carbon monoxide	$2.47E^{-6}+5.87E^{-8}T-2.63E^{-11}T^2+6.83E^{-15}T^3$
oxygen	$3.385E^{-6}+6.488E^{-8}T-2.2407E^{-11}T^2+4.591E^{-8}T^3$
nitrogen	$3.387E^{-6}+5.325E^{-8}T-2.132E^{-}11T^2 4.849E^{-15}T^3$
CO_2	$2.433E^{-7}+5.467E^{-8}T-1.895E^{-11}T^2+4.849E^{-15}T^3$
H_2O	$-3.08E^{-6}+4.077E^{-8}T-2.132E^{-23}T^2-2.456E^{-26}T^3$

Table 5. Polynomial used to calculate the viscosity, μ, of the combustion gases.

Species	Thermal conductivity, k
Propane	$-3.05E^{-3}+3.09E^{-5}T+1.3E^{-7}T^2-6.94E^{-12}T^3$
carbon monoxide	$4.14E^{-3}+7.23E^{-5}T-6.73E^{-9}T^2$
oxygen	$-1.52E^{-3}+1.03E^{-4}T-3.62E^{-8}T^2+5.01E^{-12}T^3$
nitrogen	$-1.41E^{-3}+1.04E^{-4}T-5.6E^{-8}T^2+1.66E^{-11}T^3$
CO_2	$-1.58E^{-2}+1.16E^{-4}T-3.87E^{-8}T^2+6.08E^{-12}T^3$
H_2O	$-1.68E^{-2}+1.19E^{-4}T-2.61E^{-8}T^2+7.91E^{-12}T^3$

Table 6. Polynomial used to calculate the thermal conductivity, k, of the combustion gases.

3.4.3.2 **Viscosity, μ**

For a single component ideal gas, the viscosity is calculated through equation (58).

$$\mu = \mu(T) \tag{58}$$

For a multi component mixture, the viscosity is calculated through equation (59).

$$\mu = \sum \frac{X_{i'}\mu_{i'}}{\sum_{i'} X_{i'}\phi_{i'j'}} \tag{59}$$

3.4.3.3 **Thermal conductivity, k**

For a single component ideal gas, the thermal conductivity is calculated through equation (60).

$$k = k(T) \tag{60}$$

For a multi component mixture, the viscosity is calculated through equation (61).

$$k = \sum_{i'} \frac{X_{i'} k_{i'}}{\sum_{i'} X_{j'} \phi_{i'j'}} \tag{61}$$

3.4.3.4 **Specific heat capacity, Cp**

For a single component ideal gas, the specific heat capacity is calculated through equation (62).

$$c_p = c_p(T) \tag{62}$$

For a multi component mixture, the specific heat capacity is calculated through equation (63).

$$c_p = \sum m_{i'} c_{p,i'} \tag{63}$$

3.4.4 **Chemically reacting flow models**

The computational package is capable of modelling multiple reactions between chemical species. The chemical reactions create sources/sinks of chemical species and enthalpy, which are governed by the reaction rates.

From equation (55), the source term $S_{i'}$ includes the source due to reaction, $R_{i'}$. $R_{i'}$ is computed as the sum of the reaction sources over all reactions that the species may participate in. The rate of creation/destruction of species I is given in equation (64).

$$R_{i'} = \sum_{k} R_{i'k} \tag{64}$$

The term $R_{i'k}$ is the rate of creation/destruction of species i' in reaction k.

The enthalpy source due to reaction is given in equation (65)

$$S_{h,reaction} = \sum_{i'} h_{i'}^{o} R_{i'} \tag{65}$$

3.4.4.1 **Reaction rate**

A two step reaction model was employed for both propane and methane combustion. The first reaction involved oxidation of the fuel to form CO and H_2O, such as those given in equations (66) and (67), followed by the oxidation of CO to form CO_2, as given in equation (68). This has found to lead to more accurate flame temperatures [12].

$$C_3H_8 + 3.5O_2 \rightarrow 3CO + 4H_2O \tag{66}$$

$$CH_4 + 1.5O_2 \rightarrow CO + 2H_2O \tag{67}$$

$$CO + 0.5O_2 \rightarrow CO_2 \tag{68}$$

The Arrhenius reaction rate, $R_{i'k}$, is controlled by a kinetic rate expression (69). In laminar flows, only the Arrenhius reaction rate is calculated.

$$R_{i'k} = -\nu'_{i',k} M_{i'} T^{\beta_k} A_k \prod_{j' reactants} C_{j'}^{\nu j'k} e^{-E_k/\bar{R}T} \tag{69}$$

Modelling the source terms in the energy and species transport equations due to chemical reactions requires a description of turbulence chemistry interaction. Fluent employs the Magnussen and Hjertager model [59]. To calculate the rate of production/destruction, equation (70) is used.

$$R_{i',k} = -Cm\rho\frac{\varepsilon}{k}\sum_{i'}\frac{m_{i'}}{v_{i'k}} \qquad (70)$$

This model relates the reaction time scale to the eddy lifetime, k/ε, following the eddy break up model of Spalding [60]. It is assumed that coherent structures are formed within the flame, consisting of various non uniform mixtures of fuel and oxidant [61]. These coherent structures form the large eddies in combustion, travelling as 'parcels' through the flame until viscous forces have dissipated the large eddies into smaller eddies and so gradually release and mix the fuel and air. The reaction rate is governed by the rate at which the turbulent eddies release their reacting contents. In premixed and turbulent flows, both the Arrenhius reaction rate and the turbulent mixing rate are calculated, the slower of which is the rate determining step.

In the two step combustion model employed, the oxidation of fuel and carbon monoxide were expressed as Arrhenius rate constants. The fuel oxidation rate was set to be faster than the carbon monoxide burnout rate. The rate constants used are displayed in table 7.

	Arrhenius constant	Activation energy
Fuel	$1.3e^{14}$	4883 J/kgmol
Carbon monoxide	$5.6e^{11}$	4490 J/kgmol

Table 7. Reaction rates used for modelling fuel and CO oxidation.

An alternative combustion model has been developed, known as the equilibrium chemistry/Probability density function (PDF) model that calculates individual

species concentrations on a mixture equilibrium basis. The conservation of a singular scalar, the mixture fraction, allows the derivation of other scalars, such as temperature and density without the need for great computational effort. Individual species, including intermediate species are inserted into a pre-processor which calculates the equilibrium concentrations. A look up table is formed to which the model references during the iterative calculations. The interaction of turbulence on the mixture fraction is calculated through the use of the PDF.

The advantages of the equilibrium chemistry/PDF model over that of the Arrenhius reaction rate mixing model are that the species concentrations are predicted with greater accuracy, endothermic dissociation reactions are accounted for, and that turbulent interactions on combustion are calculated in a more rigorous manner. However, the equilibrium chemistry/PDF model has a disadvantage in that it cannot predict NOx formation.

3.4.5 **Discrete radiation heat transfer model (DTRM)**

The DTRM provided by Fluent predicts surface to surface radiation heat transfer. The simplified model assumes grey radiation, i.e. no wavelength dependence. The change in radiation intensity, dI, along a path, ds is described by equation (71). Fluent also allows for a variable absorption coefficient, based on local concentrations of CO_2 and H_2O, which are common gases present in combustion systems. To increase the accuracy of temperature prediction in the model, the CO_2 and H_2O species are specified.

$$\frac{dI}{ds} = -(\alpha_{abs} + \alpha_s)I + \frac{\alpha_{abs}\sigma T^4}{\pi} \qquad (71)$$

Equation (71) is integrated along a series of rays emanating from a single point in each discrete control volume on a surface. The enthalpy source in the fluid due to radiation is then computed by summing the change in intensity along the

path of each ray. Increasing the number of rays will increase the accuracy of the prediction but will require greater computational power.

3.4.6 **Boundary conditions**

Inlet flow quantities may be set through either velocity or pressure boundaries. When using velocity boundaries, the velocity may be either positive or negative so as to allow the boundary to be used as a fixed inlet or outlet condition. The velocity, composition, temperature and turbulence is set by the user.

When using pressure boundaries, the inlet velocity is calculated by solving the flow condition as a loss free momentum balance, through the Bernoulli equation. Again, temperature, composition and turbulence are set by the user.

Velocity boundaries were used at the air and fuel inlets. This gave accurate mass flow rates of air and fuel into the burner. Due to the high velocities obtained through the air inlet at large air mass flow rates, viscous dissipation was turned on. This addition represents the effect of the dissipation of turbulent eddies on the heating of the fluid. At the inlet boundaries, species mass fractions were used. The air inlet had an oxygen mass fraction of 0.233, a temperature of 300 K and a turbulence intensity of 40% [56]. The fuel inlet had a fuel mass fraction of 1.0, a temperature of 300 K and a turbulence intensity of 10%. The temperature at the outlet boundary was 300 K so that radiation loses could be accounted for.

As the burner was well insulated, no heat loses were accounted for through the burner walls. This was done through specifying the external walls as heat flux walls and setting the heat flux to 0. The walls of the fuel injector and the diffusing section were made of refractory material and conducted heat, especially the diffusing section. For this reason these walls were set as conducting walls with a thermal conductivity of 2 $W/m^{2o}C$ [62].

3.4.7 **Turbulence modelling**

There are a number of approaches that can be adopted to model turbulence. The fundamental approach uses direct numerical simulation, whereby the 3-dimentional Navier-Stokes equations are calculated. This approach requires powerful computers and is impractical in engineering applications. Similarly, the use of large eddy simulation solves the Navier-Stokes equations in the grid size of large eddies but still needs a model for the small scale turbulence and again requires great computational power.

The most practical way to model turbulence is through Reynolds time averaged equations and the transport equations [63]. The idea of turbulence modelling is to simulate the unknown higher order correlation terms by using lower order correlations to calculate the mean flow properties and hence close the time averaged equations. Even though the prediction will not accurately model the turbulent structure in great detail, it is acceptable for engineering purposes where only the time averaged velocity, temperature, turbulence, etc. are needed.

For any scalar quantity, such as velocity, the scalar is assumed to be comprised of a mean value and a fluctuating part, such as that given in equation (72):

$$\phi = \bar{\phi} + \phi' \tag{72}$$

where $\bar{\phi}$ is the time averaged value of ϕ. $\bar{\phi}$ is defined by equation (73).

$$\bar{\phi} = \frac{1}{\Delta t}\int_0^{\Delta t} \phi dt \tag{73}$$

where Δt is a time scalar much larger than the largest time scale for turbulent fluctuations.

Fluent is able to use three closure models for the turbulent correlations, these being

- k-ε model
- Differential Reynolds stress mode
- RNG k-ε model

For the modelling of the Coanda burner, the k-ε turbulence model was employed.

3.4.7.1 **k-ε Turbulence model**

The k-ε turbulence model is an eddy viscosity model in which the Reynolds stresses are assumed to be proportional to the mean velocity gradients. This assumption for the viscosity is known as the Boussinesq hypothesis and is given by equation (74). The two parameters, k and ε represent the turbulent kinetic energy and the dissipation rate of k, respectively.

$$\rho \overline{u_i' u_j'} = \rho \frac{2}{3} k \delta_{ij} - \mu_t \left(\frac{\partial u_i}{\partial xj} + \frac{\partial u_j}{\partial x_i} \right) + \frac{2}{3} \mu_t \frac{\partial u_l}{\partial x_l} \partial_{ij} \qquad (74)$$

Here, k is the turbulent kinetic energy and is represented by equation (75).

$$k = \frac{1}{2} \sum_i \overline{u_i'^2} \qquad (75)$$

The final term in equation (74) is ignored by Fluent under the assumption that the divergence of velocity has a negligible effect on the turbulent stress tensor.

3.4.7.2 **Reynolds stress model (RSM)**

The limitation of the k-ε model is that it is an isotropic model, this means that the length and velocity for the turbulent viscosity are equal in all three directions. In anisotropic flows, this simplification can lead to incorrect predictions in the flow field. The RSM computes the individual Reynolds stresses and thus provides a better alternative to the k-ε model in such situations.

3.4.7.3 **Renormalization group theory (RNG)**

This is a modified k-ε model that maybe used for highly swirling or separated flows to give improved prediction. In the standard k-ε model, the turbulent viscosity is obtained from semi-empirical data. The RNG method uses a fundamental approach to calculate the turbulent viscosity. The RNG method, as related to turbulence involves an iterative process whereby the small scale eddies are incorporated into the larger eddies, leading to modified Navier Stokes equations. The use of this model leads to improved prediction of swirling flows, flows with high streamline curvature and near - wall flows. For these reasons, the RNG k-ε turbulence model was used in the modelling of the Coanda burner.

3.4.8 **Techniques used in modelling the Coanda burner**

To decrease the computational requirements, the Coanda burner was modelled in two dimensions. Two dimensional modelling was sufficient as the vast majority of the burner could be considered in this way, except for the flame stabilisers which would require highly detailed, time consuming three dimensional grid structures. Also, the burner was axially symmetric. This implied that only half of the burner needed to be modelled.

The geometry of the burner, and especially the Coanda surface required accurate dimensions and smooth surfaces. This was accomplished through the use of body fitted co-ordinates, using the computer package PreBFC, which enabled the use of body fitted co-ordinates. The complete computational grid structure created for the Coanda burner is displayed in figure (10), which has been mirrored about its axis. Live cells to calculate temperature were required in both the fuel injector and diffuser sections and were modelled as conducting walls as specified in section 3.4.6. A uniform, highly detailed grid structure was required throughout the burner. The air and fuel inlets required multiple cells to achieve accurate results. However, the multiple cells and small dimensions of the inlets in comparison to the overall dimensions of the burner required careful manipulation of surrounding grid lines, as shown in figure (11). Grid structures were successfully created that provided stable, convergent modelling.

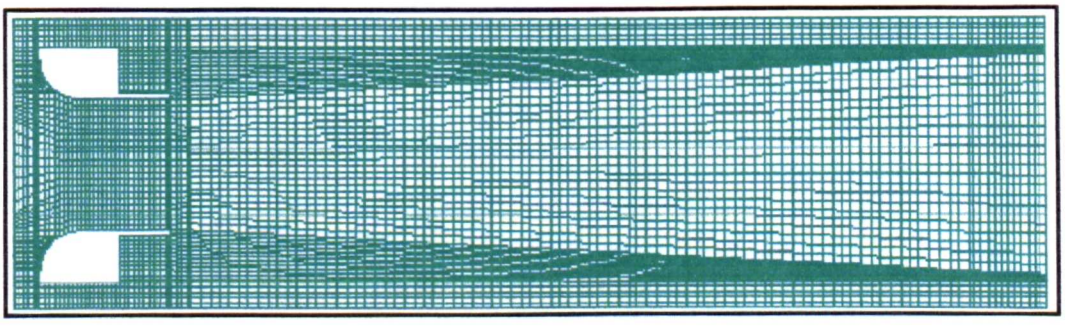

Figure 10. Computational grid structure used for the Coanda burner.

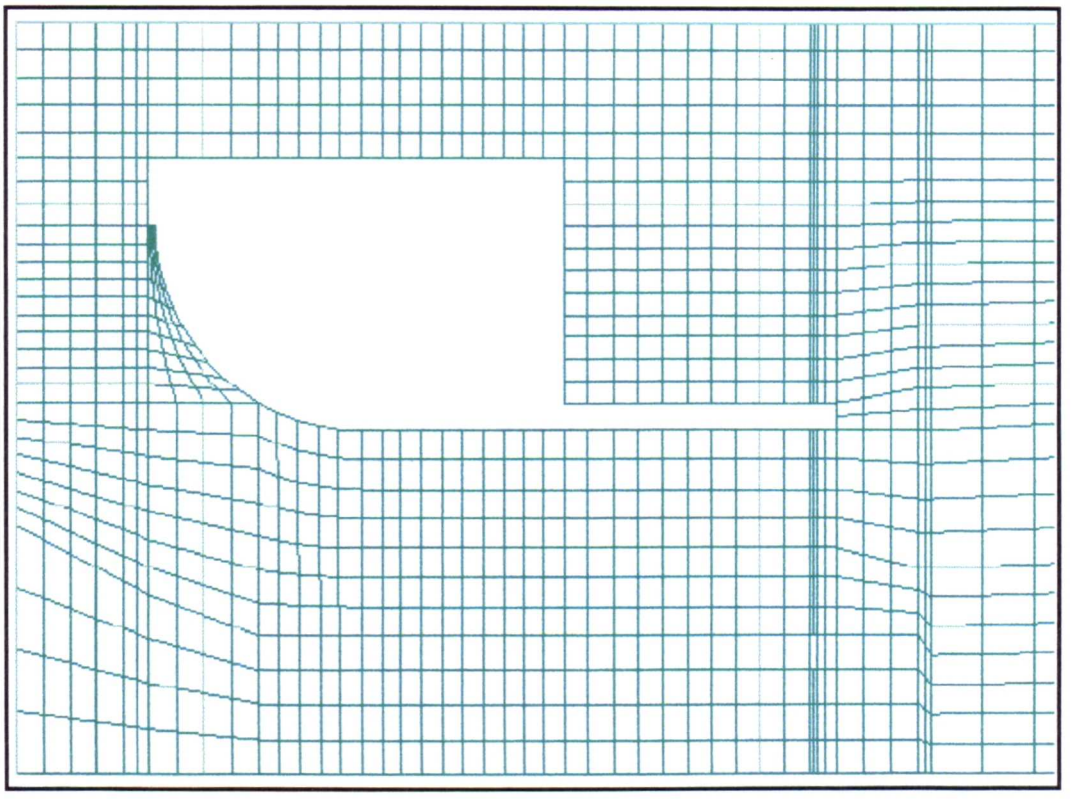

Figure 11. Detailed computational grid structure around the Coanda ejector.

3.4.9 **NOx post processing model**

The NOx post processor was capable of determining thermal, prompt and fuel NOx formation. However, as the gaseous fuels used contained negligible quantities of chemically bound nitrogen, only thermal and prompt NOx formation was calculated.

The kinetics of the thermal NOx formation rate are much slower than the main hydrocarbon oxidation rate, and so most of the thermal NOx is formed after completion of combustion. Thermal NOx formation is decoupled from the main combustion process through assuming equilibrium values of temperature, stable species, O atoms and OH radicals. However, at higher flame temperatures, radical overshoots of O atom concentration are accounted for through the use of supra-equilibrium O atom concentrations. Thermal NOx formation is then calculated through the mechanism given by Zeldovich [7].

The prompt NOx formation mechanism used by the model follows that given by Fenimore [9]. In order to calculate the NOx formation, the model requires inputs for the number of carbon atoms per fuel molecule and the overall fuel-air stoichiometry.

The effect of turbulent mixing results in temporal fluctuations in temperature and species concentrations in the flame. If these fluctuations are not included and time averaged composition and temperature are used, significant errors would result in the NOx formation rate. The post processor takes these fluctuations in composition and temperature into account by considering the probability density functions which describe the time variation.

The NOx post processor did not include NOx destruction mechanisms, such as in-flame NO removal through reduction from a hydrocarbon fragment. Due to the use of flue gas recirculation, this mechanism may be important in accurately predicting NOx in the Coanda burner.

4. EXPERIMENTAL RIG

4.1 CONSTRUCTION

4.1.1. Introduction

The Coanda burner was designed around the concept that it emitted low concentrations of NOx and CO, was manufacturable, and could be adjusted or modified with ease.

As this was an experimental burner, adjustability was extremely important for both minor and major changes in design to evaluate the performance of the burner. The burner was capable of being separated into five major parts, these being the Coanda ejector, the diffusing section, the fuel injection system, the outer casing and the ignition system. Each of these parts were easily accessible for alterations and modifications when combined together in the constructed burner. Figure (12) demonstrates how the Coanda burner was separated into components for inspection or adjustment. Figure (13) displays the complete diagram of the Coanda burner, incorporating all the internal components.

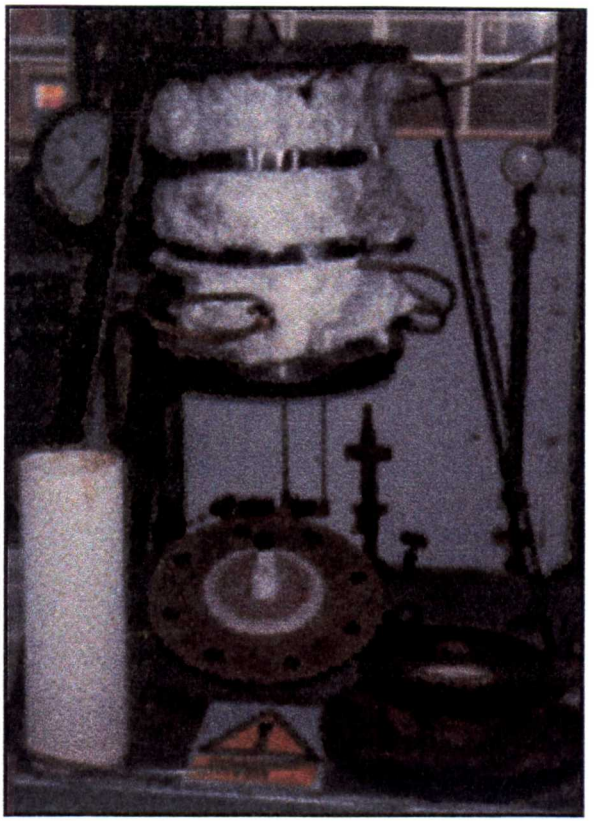

Figure 12. Components of the Coanda burner separated for inspection.

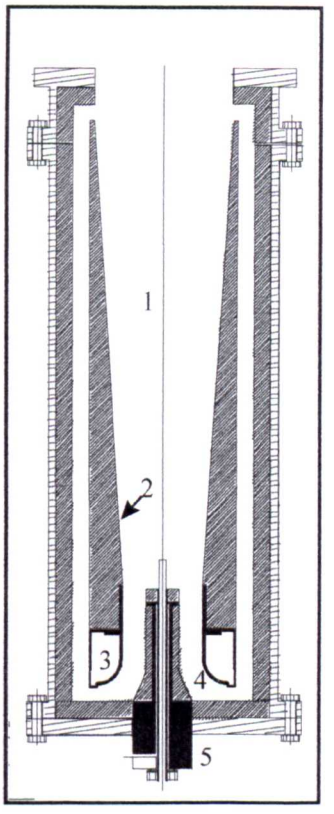

Figure 13. Diagram of the complete Coanda burner

1. Combustion chamber.
2. Diffusing section.
3. Coanda ejector cavity.
4. Coanda surface.
5. Fuel injector.

4.1.2. **Coanda burner components**

4.1.2.1. **Coanda unit**

The various sections of the Coanda ejector may be seen in figure (14). These include the gap width, Coanda surface and the Coanda's cavity.

The Coanda gap width is an important part of the burner as it controls both the primary air mass flow-rate, and affects the entrainment ratio. Altering of the gap width will enable the burner to operate at different pressures, and over a wider range of thermal ratings. It would therefore follow that the gap setting must be accurate, measurable, and easy to adjust, but be fixed in position when required.

The Coanda gap setting can be maintained in a number of ways. Firstly, it can be permanently fixed at one width, as they are in many industrial Coandas that can be purchased. These gaps are set to comply with the physical dimensions of the ejector and the fluids used, to give maximum entrainment performance. Clearly, in an experimental burner a set Coanda gap width is not acceptable as a number of Coanda units will then be needed to obtain a range of gap settings to asses the performance of the burner. An adjustable form of the set Coanda gap width was used by Prior [38]. This method utilised a set thickness shim which was used as a spacer ring around the circumference of the burner. The Coanda was manufactured in two parts, and then bolted together. The required gap width could then be formed through changing the spacer ring, as displayed in figure (15).

Another common method to adjust the gap setting is through using a screw thread. By twisting the thread, the gap setting can be altered. This allows easy adjustability and a wide range of settings. However, it is difficult to measure the gap width to a high degree of accuracy and even more so to obtain repeatability. In addition, the loss of air passing through the thread, rather than through the Coanda slit is difficult to eliminate when the thread is loosened. The margins of error are too great to rely on this technique. An alternative method is to combine both the screw thread and the spacer ring techniques. By doing this, the accuracy and repeatability of the gap settings can be guaranteed to be higher, whilst the ease of altering the gap is simple and does not affect the diffuser section. Tightening the thread ensures negligible passage of air through the screw thread. As long as the contacting surfaces of the Coanda are parallel to each other and smooth, the gap setting is completely controlled by the width of the spacer ring.

For manufacturing purposes, the Coanda ejector was split into three parts. A diagram of the construction of the Coanda ejector, incorporating its dimensions is shown in figure (16).

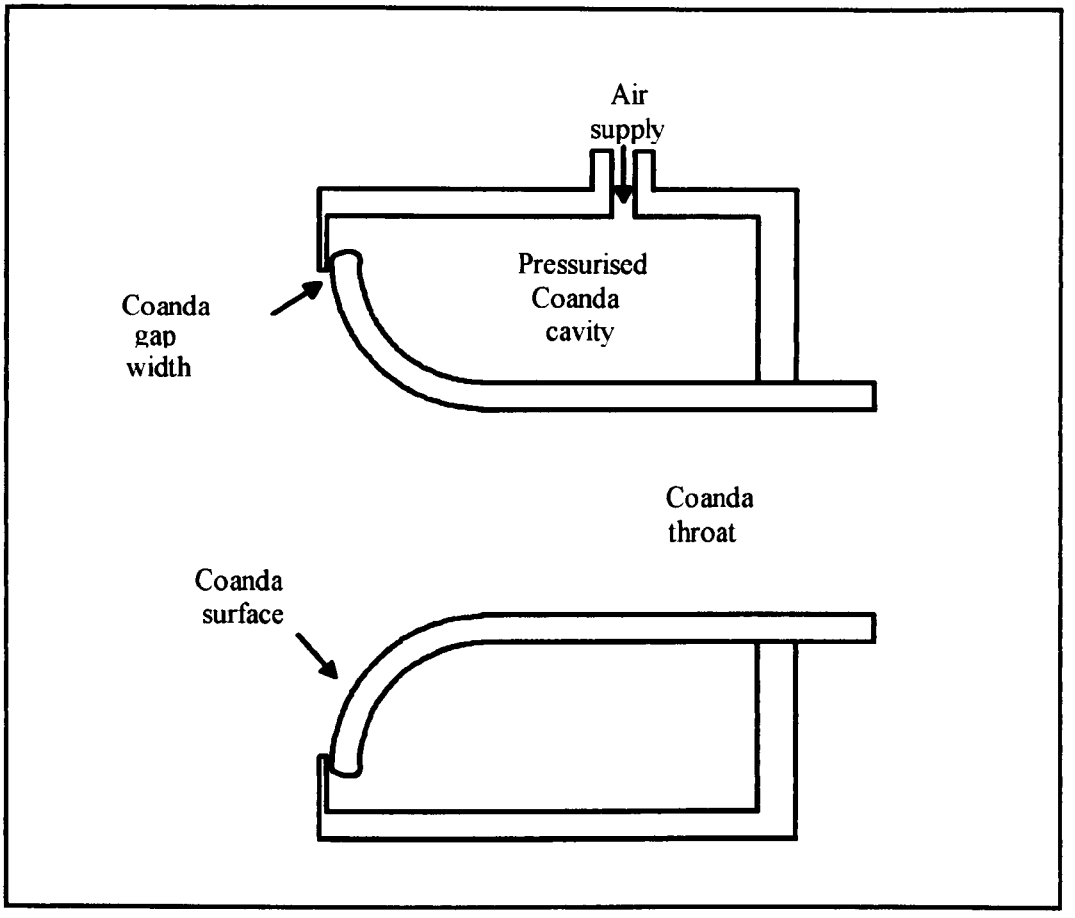

Figure 14. Parts of a Coanda ejector

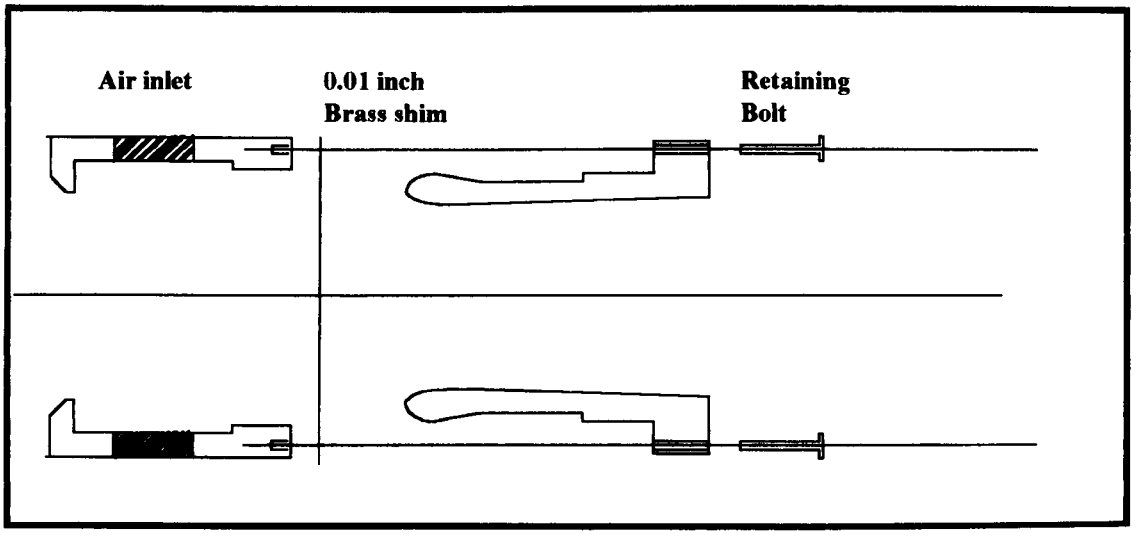

Figure 15. Setting the Coanda gap width through the use of a brass shim, as used by Prior [38].

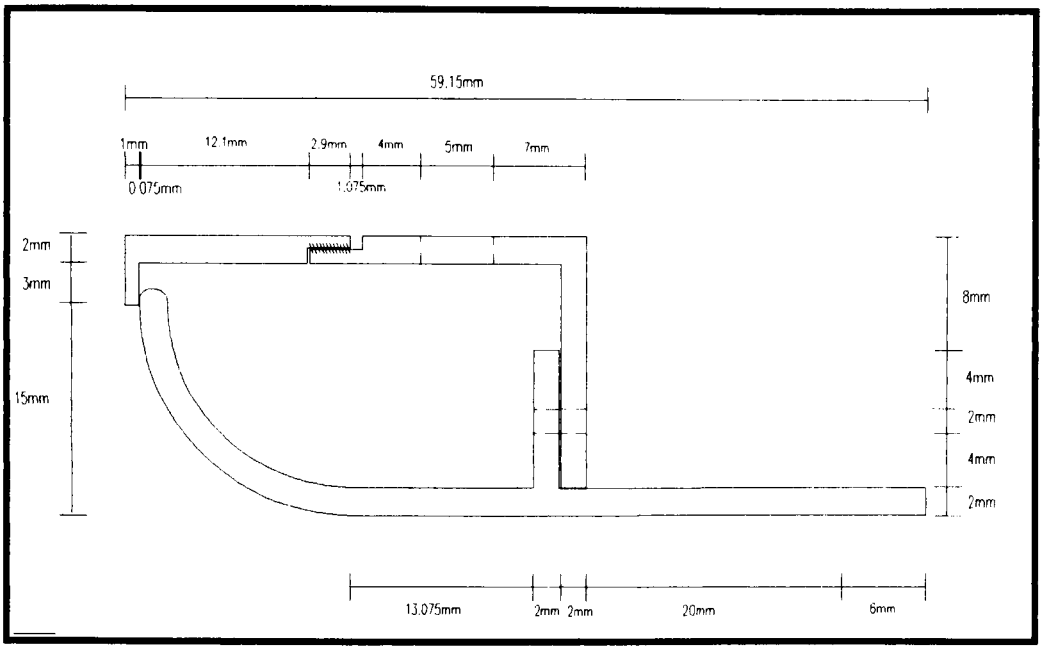

Figure 16. Detailed construction and dimensions of the Coanda unit

4.1.2.2. **Diffusing section**

The length and diffusing angle of the diffusing section were determined from the dimensions obtained through using the Coanda burner design equations, and the recommended lengths for complete mixing when using a Coanda ejector, as given in section 3.3.7. This led to a choice of design options. The first possibility was to manufacture the diffusing section from 1 mm high temperature metal plate, such as inconel. As displayed in figure (17), the use of a cylindrical casing with such a unit would not allow a good recirculating flow pattern.

The second choice was to construct a solid diffusing section, cast from refractory cement. This would allow a constant diameter recirculation path for the flue gases as displayed in figure (18). It also decreased pressure drops associated with bends and increased the entrainment ratio.

The final design selection was based on the modelling results and the manufacturing requirements. The diffusing angle of the solid diffuser was the same

as the metallic design but the thickness of the diffuser was substantially increased to give it mechanical strength. The diffuser was created by making a wooden mould, into which the refractory material was poured and allowed to set over a period of 24 hours. The diffuser was interchangeable, allowing longer diffusers and alternative diffusive angles to be used. It was connected to the Coanda ejector in the vertical position, supported centrally by interlocking connections between the Coanda unit and the diffuser, as displayed in figure (19), which also gives its dimensions.

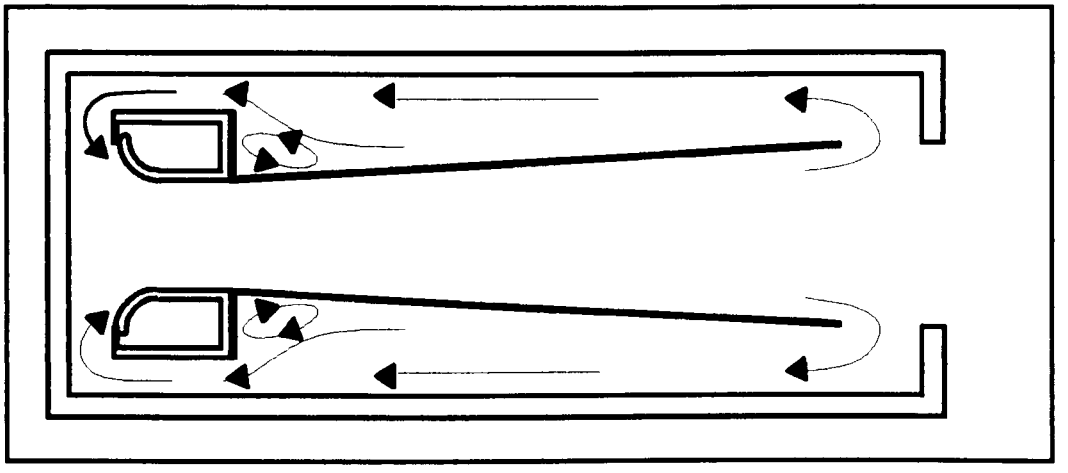

Figure 17. Recirculating flow pattern with metal plate

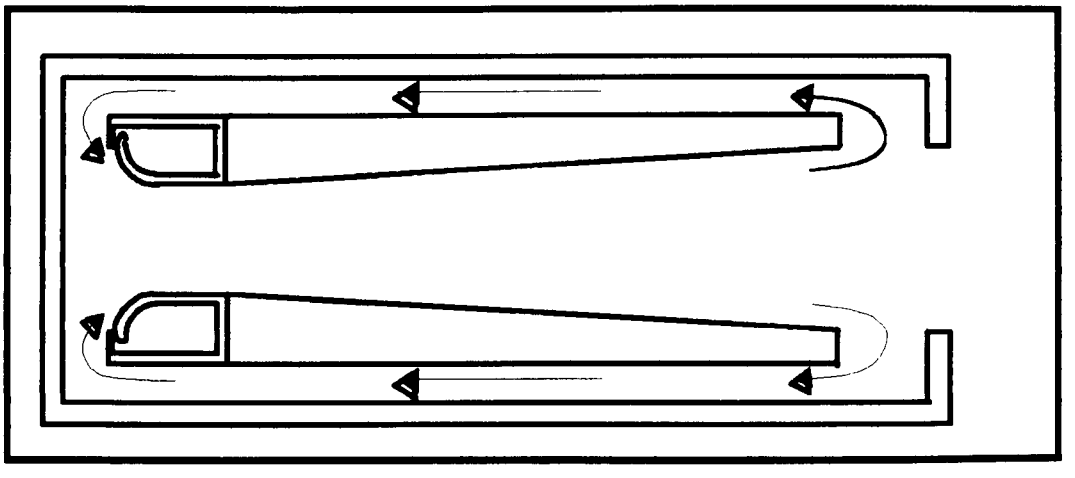

Figure 18. Recirculating flow pattern with solid diffuser

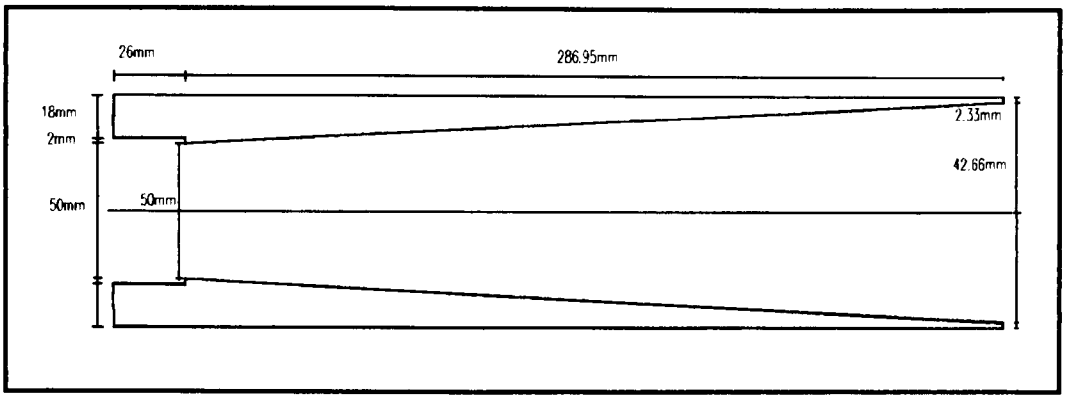

Figure 19. Dimensions of the solid diffuser section.

4.1.2.3. **Fuel injection system**

In the final model designed, the fuel was injected 10 cm inside the burner, allowing a fuel rich zone to be produced at the end of the fuel injector, which was also to act as a source of flame stabilisation.

To form the external surface of the injector, high temperature insulating string was wrapped around the metal surface and bonded using a high temperature mastic cement. The smooth external surface was formed by coating excess mastic cement over the string. Once hardened, the cement could easily be removed through using a file to produce the desired shape.

Modelling had shown that the temperatures in that region reached a maximum of 1000 K next to the surface of the injector, so stainless steel was used as the main construction material. The passage of gaseous fuel through the injector provided additional cooling of the metal surfaces.

The injector was constructed from two components as shown in figure (20). The fuel flowed in the annulus between the two components, separated by fixed diameter spacers along the interior component's axis. The fuel then travelled radially outwards through a 0.5 mm gap, which was maintained by spacer bars

between the two metal surfaces. The bore hole in the centre of the fuel injector was used for the ignition system, and was electrically insulated from the metal injector by a section of hollow, high temperature silica glass. A diagram of the fuel injector system and the front section is shown in figure (21).

To seal the two components, a rubber 'O' ring was used, compressed to form the seal by a washer and tightened by a nut. Although the temperature of the fuel injector outside the burner body did increase, it was not enough to damage the rubber seal. The temperature did have a detrimental effect at the interface between the burner body and the fuel injector. When continually heated and cooled, the screw thread connecting the components tightened. The use of high temperature, Teflon based anti-seize compound was needed to ensure that the threads were not damaged and the components could be easily separated.

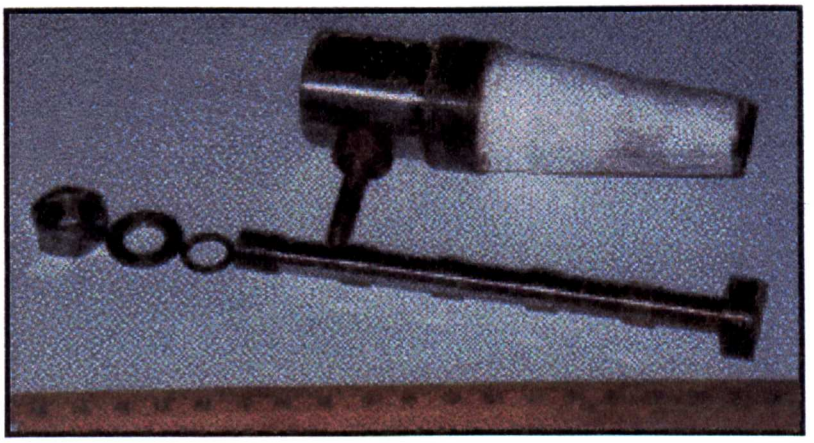

Figure 20. The components used in the construction of the fuel injector.

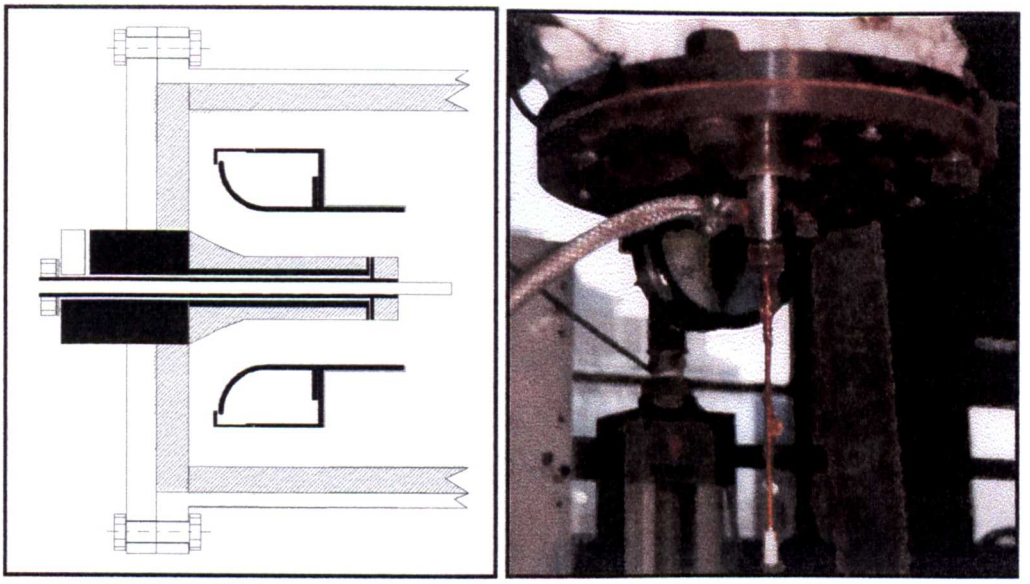

Figure 21. Construction and positioning of the fuel injection device and the burner front wall.

4.1.2.4. **Ignition and flame detector system**

The ignition system is an important and integral part of a burner. Most ignition systems utilise a high tension spark to ignite a gaseous mixture. The gaseous mixture may be either the primary fuel and air or it may be a pilot light. Pilot lights are common in domestic combustion appliances and most large industrial systems. The use of pilot lights are advantageous as they provide a constant source of ignition. Their disadvantage is that they use up a small amount of fuel over long periods, and tend to be highly polluting diffusion flames. Due to the compact, sophisticated design of the burner the use of a pilot flame was not needed. A high tension spark positioned directly in the flame stabilisation region was used to instantaneously light the burner.

There are generally two types of flame detectors, these being ultra violet detectors and flame ionisation detectors. Ultra violet flame detectors are more expensive but have the advantage of being placed away from the flame zone. Being faced directly towards the flame, the detection of ultra violet radiation is passed to a

control system which maintains the flow of the fuel and air. Flame ionisation detectors must be placed directly in the flame zone. Ionisation occurs within the flame which registers as a minute voltage at the control system. With the casing of the burner being reliably earthed, this minute voltage may be interpreted as a flame. The advantage of this system is that it is very compact and can be combined with the spark ignition through the use of a single metal rod.

In the system selected, a high tension spark was sent by the control system along a kanthal rod to provide a source of ignition at the flame stabilisation zone. A voltage was simultaneously sent to open a solenoid valve connected in the gas supply line. A spark was maintained for two seconds with the solenoid valve kept open for a further 3 seconds. If ionisation was not detected in this time, then the solenoid valve was closed. Similarly, if during combustion operation the flame were to extinguish, flame ionisation would cease and the control system would automatically close the solenoid valve, halting the flow of fuel into the combustion chamber.

4.1.3. **Material selection**

The material selected for use in the construction of the Coanda burner was a composite of metal and refractory material. The casing of the burner was protected by a refractory material lining the entire inner surface of the burner, which decreased the temperature at the metal wall. For this reason, and also cost effectiveness, mild steel was chosen. The Coanda unit within the burner was required to tolerate high temperatures, be relatively inexpensive and be easily machined. As hot, recycled combustion gases at a temperature of about 1800 K passed over the Coanda's surface, and cold primary air passed through the chamber, the actual temperature of the metal separating the two flows needed to be known. A simple heat transfer equation would not give accurate results, due to both the unknown flow pattern of the primary air and convection effects over the

surfaces. The Fluent package was employed to model this aspect of heat transfer, as given in section 3.4, using the thermal conductivity coefficients for different metals. Two models were investigated, one using mild steel and the other using brass. The thermal conductivities and melting points were taken as 41.9 W/m°C and 188 W/m°C and 1743 K and 1317 K, respectively [64].

To evaluate the suitability of various materials for the construction of the Coanda ejector, modelling of the flow through the Coanda cavity, and the entrained hot combustion products around the Coanda unit was necessary. The heat transfer model incorporated into the computational package was then used to determine the wall temperatures and hence the suitability of different materials. Figure (22) is for mild steel and displays a magnified section from the top surface of the metal, which was in contact with the recycled gases. This surface was expected to be the hottest region, as the stream of air passing through the Coanda gap would cool the external surface of the ejector, due to the Coanda effect. As can be seen from figure (22), the hottest temperature which the outside surface of the metal was expected to reach was approximately 900 K, with a sharp temperature gradient to the inner surface of the ejector, being at about 400 K. Figure (23) shows the flow pattern throughout the whole ejector. The external flow pattern around the ejector was similar to that found in the models describing the whole system, such as in figure (32), except for a recirculation region at the lower left corner which was due to the fuel injector not being included in the model. It was found to be impossible to use the complete geometry when creating the grid, so the angled section was therefore omitted. The fuel injector had very little effect over the region of interest, as it was the gases flowing directly over the Coanda surface that contributed to the temperature gradients. The recirculation region existed after the point of jet attachment where the cooling properties of the entering air were present in greatest quantities, creating a relatively cool region. The flow through the pressurised Coanda chamber was seen to take a backwards U effect. Dead regions occurred towards the back end of the ejector and the centre of the top

centre of the top surface. The dead region at the rear of the ejector was not expected to create any cooling problems due to the rear surface being covered by refractory material, and the underside being cooled by the mixing gases. Using brass as a material, no alterations in flow pattern were encountered. The temperature gradient across the inner and outer surfaces were very similar to those of the mild steel construction, having only a slightly lower peak temperature.

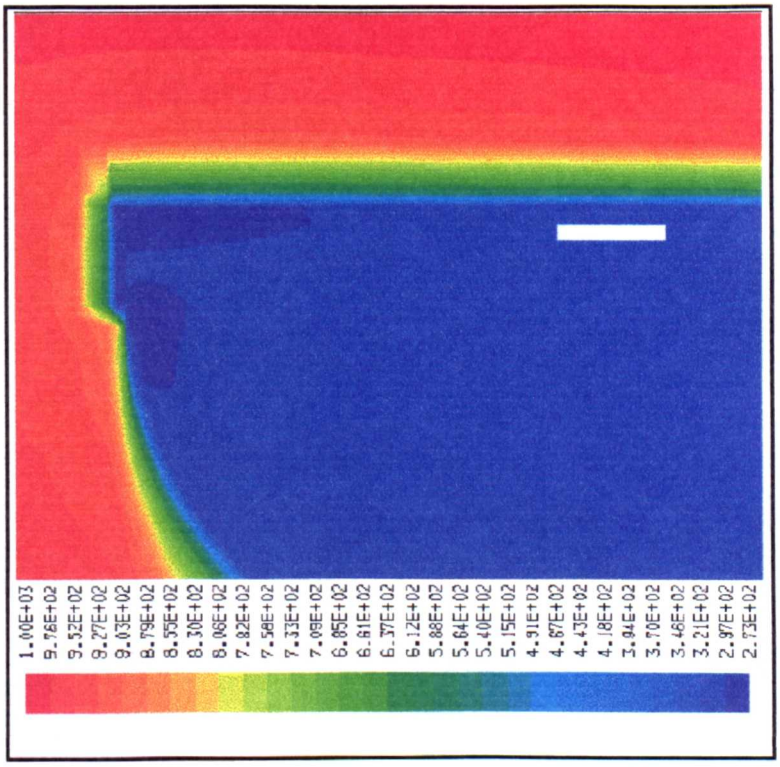

Figure 22. Modelled temperature predictions on the outer surface of the Coanda ejector.

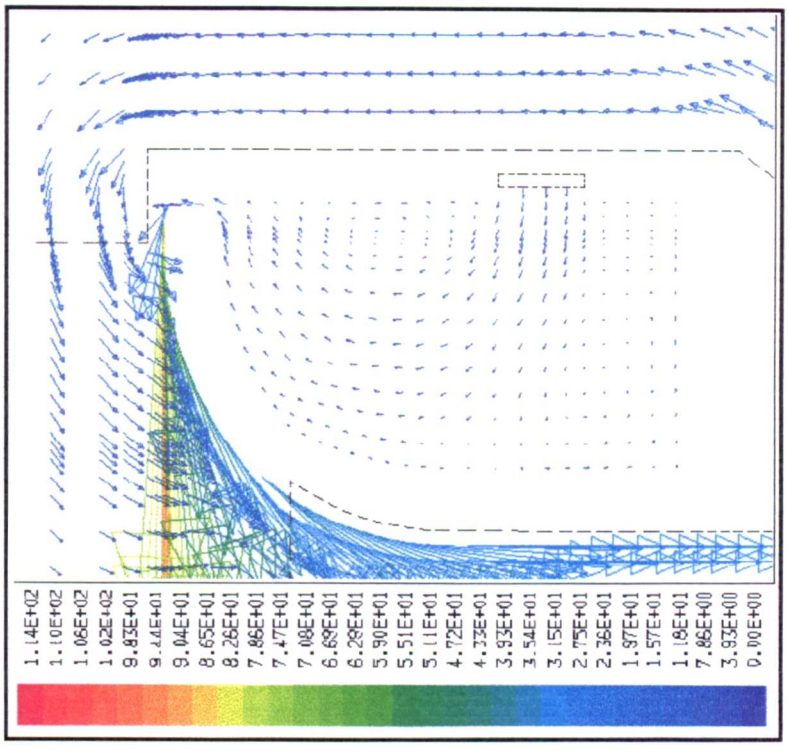

Figure 23. Modelled flow pattern through the Coanda ejector.

Due to the small differences in temperature changes, and the fact that the brass would be approaching its melting point at the predicted temperatures, manufacture from mild steel was considered to be appropriate. However, if mild steel was used it would be expected that the Coanda ejector would oxidise rapidly at the predicted temperatures and oxygen concentrations. This would lead to blockages of the Coanda gap and a decrease in the smoothness of the spacer ring. As the accuracy of the Coanda gap width was essential, the possibility of reproducing identical conditions would be decreased. It was possible to construct the Coanda unit from stainless steel which has a thermal conductivity and melting point of 50.2 W/m°C and 1743 K, respectively. These values are very close to those of mild steel mentioned above. Therefore, similar flow and temperature patterns as found in figures (22) and (23) would be expected to occur.

4.1.3.1. **Refractory material selection**

The choice of refractory material was based upon its upper temperature limit, the thermal conductivity of the cast material and the average stone size contained within the casting cement. After discussion with manufacturers [65], the refractory cement Durax 1550C was suggested as being the best available.

4.2 BURNER OPERATION

4.2.1. Introduction

The burner was designed so that it could be taken apart, adjusted or modified with ease. This allowed the burner to be run and tested over a wide range of conditions, in order to investigate specific design features. The variations made to the burner configuration and operating conditions are listed below.

4.2.2. Variations in configuration included the following:

- The Coanda gap width was varied between 0.2 mm and 0.5 mm.
- Addition or removal of external insulation.
- Different flame stabilisers of various shape.

Variations in operating conditions and fuel type included the following:

- The air to fuel ratio was varied over a range from stoichiometric conditions up to a ratio of 2 to 1.
- Two gaseous fuel types were used, namely propane and methane.
- Combustion air inlet temperatures of either 20°C or 150°C were used.
- The thermal rating was varied over a range from 3 to 20 kW.

Each of the above variables are discussed below.

Coanda gap width

The width of the gap used in the Coanda ejector will have a dramatic effect on the overall operation of the burner. A narrow gap width, such as 0.2 mm, will cause an increase in the recirculation ratio, but will also require a high air supply pressure

for a given mass throughput of air. Through having a high entrainment ratio, the velocity of gases passing through the centre of the burner will also increase.

Increasing the gap width to 0.5 mm will reduce the entrainment ratio of flue gas, but will also require a lower air supply pressure for a given mass flow rate of air. The reduction in recirculation will also cause a decrease in the velocity of gases passing through the centre of the burner.

Air to fuel ratio

Alteration in the air to fuel ratio is important as it will allow the burner to operate under a variety of conditions, depending on its application. Increasing the quantity of air above the stoichiometric requirement will lead to a reduction in the outlet temperature, and an increase in the mass flow rate of gases. Operation under fuel lean conditions will also reduce carbon monoxide emissions up to a point where the kinetics involved in CO burnout are slowed.

Increasing the air to fuel ratio decreases the outlet temperature of the burner and hence thermal NOx production, but the peak temperature will depend on how well the fuel and air are mixed prior to combustion. The increase in the availability of oxygen throughout the burner will enhance the rate of formation of NOx produced. The mixing process between the air and fuel is dependent upon the flame stabiliser used. The way in which NOx emissions varied with excess air and stabiliser design were determined experimentally.

Fuel types

The design of the fuel injector used in the Coanda burner allowed only gaseous fuels to be used. As the fuel and air were supplied separately, different gaseous fuels could be burnt. Two gaseous fuels were used, the first fuel was propane as it

lights easily, and its chemistry of combustion is well understood. The second fuel used was methane, which is a more commercially attractive fuel, being readily available in the form of natural gas.

When methane was used, minor modifications to the burner were needed to attain the best overall performance in terms of stability and pollutant emissions. These modifications are detailed in section 6.2.4.

Air preheat

Air preheat can be used to increase the overall efficiency of a combustion system, increase the temperature of the flue gases within the furnace or to provide hot gases to increase flame stability.

To provide the burner with air preheat, the thin copper tubing which supplied air to the ejector was wrapped around the outside of the burner and lagged with 30 mm thick insulating material. Using this system, air preheat temperatures of 150°C were obtained after operating for a period of approximately 20 minutes.

The air preheat arrangement was designed so as to increase the temperature of the incoming air and therefore ensure lower CO emissions.

Thermal rating

A commercial burner must be able to operate with a variety of fuel mass flow rates, be stable and have low emissions. The thermal rating could be adjusted by varying the gas flow into the burner. This was controlled by adjusting a valve in the gas line, and recording the flow on a calibrated rotameter. The air supply was similarly controlled in accordance with the gas flow in order to ensure stability and complete burnout of the fuel.

Lagging

Insulation is an important way of increasing the efficiency of the system. Both high temperature insulating refractory cement, and low temperature external fibre glass insulation were used. The internal refractory cement was cast on to the internal wall surface of the burner casing. Being 10 mm thick, it provided protection for the metal casing and insulation from the hot recycled gases. The external fibre glass insulation was 30 mm thick, covering the lower two thirds of the burner. This provided enough insulation so that it could be assumed there were negligible heat losses through the walls of the burner.

Flame stabilisers

The use of flame stabilisers was implemented in the Coanda throat, prior to combustion, through using a variety of metal shapes, as shown in figure (24). The flame stabilisers had a hole drilled through their middle so that they would fit over the flame detector. A second, 3 mm diameter hole was drilled at a slightly larger radius so that it was in line with the 3 mm tapped hole in the end of the fuel injector. When the stabiliser was positioned centrally over the injector, a 3 mm diameter screw was used to hold the two together and prevent movement. The screw also held the ignition contact so that the point of ignition could be varied along the axis of the burner. The screw was sufficiently long to hold the ignition contact and two stabilisers firmly in place. This allowed a greater number of stabilisers to be tested, a typical configuration is shown in figure (25) which displays how the ignition contact and flame stabiliser are attached to the fuel injector.

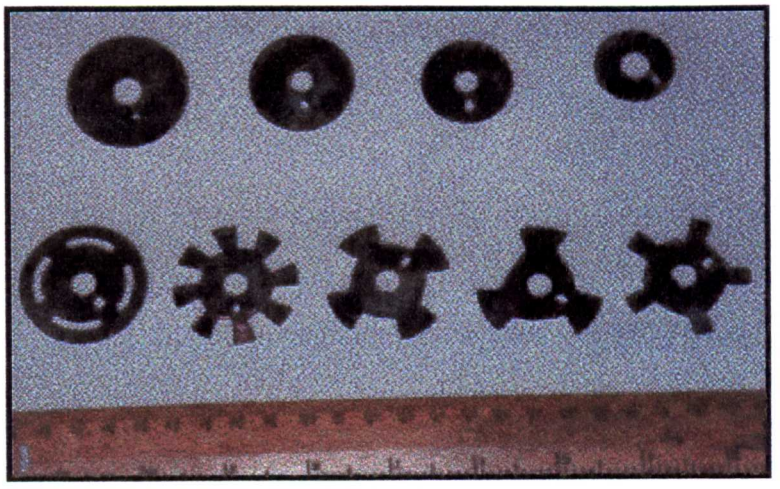

Figure 24. Various flame stabilisers used in the development of the Coanda burner.

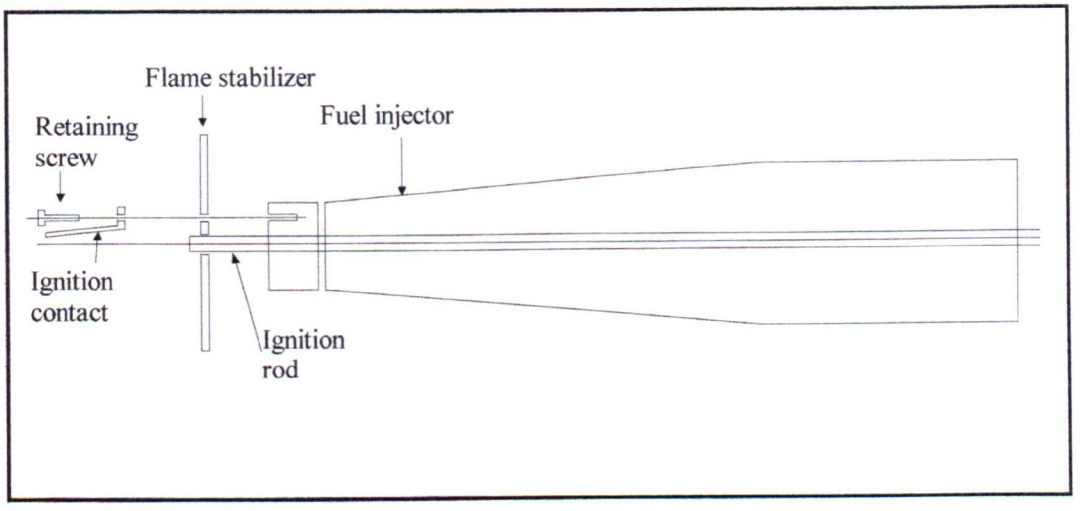

Figure 25. Fuel injector, flame stabiliser and ignition contact attachment.

4.2.3. **Flame stabilisation in the Coanda burner**

Flame stabilisers are used to provide a stable combustion region in a stream of high velocity that exceeds the rate of flame propagation. From this stable combustion region, there exists a source of constant ignition for the rest of the reactants. Aerodynamic flame stabilisers usually rely on a recirculation region behind a bluff body to maintain a flame.

The use of flame stabilisers was found to be essential to the low emission operation of the burner. The end of the fuel injector was found to be inadequate at mixing sufficient portions of fuel and air to allow operation near to stoichiometric conditions. At the point where the fuel was injected radially outwards from the injector, there existed a high velocity, tangential flow of air and recycled combustion gases. The fuel, being injected very near to the initial stabiliser formed a fuel rich zone, limiting the amount of oxygen in the recirculation zone. This limitation of oxygen in the stabilisation region would cause the flame to extinguish. The only method of increasing the amount of oxygen in this region was to increase the air inlet flow rate. Operating under very lean conditions has the detrimental effect of lowering the combustor temperature. This low temperature ultimately leads to very low NOx emissions but very high emissions of CO and possibly UHC's. This was clearly unacceptable and development work was needed to remedy this problem. The development work is detailed in section 5.2.2.

4.2.4. **Experimental method and data collection**

Experimental results were taken at two conditions. Firstly, results were taken with a constant gas flow. This enabled the burner to be evaluated at thermal ratings of between 3 and 15 kW, over a range of air to fuel ratios. Secondly, a more detailed analysis at one particular level of excess air was studied over a variety of similar thermal ratings. This involved manipulating the air and gas valves to the exact requirements.

4.2.4. **Overview of experimental procedure**

The lighting, running and extinguishing of the burner followed a series of steps to ensure that all the necessary safety precautions were taken. The sequence of lighting could begin once the experimental configuration of the burner had been

established, and the components of the burner were securely connected in their correct position.

4.2.4.1. **Lighting the burner**

The lighting of the burner followed the simple sequence given below:

- The laboratory and overhead extraction fans were switched on and checked.
- The air flow regulator was set to a low flow rate.
- The gas rotameter valve was securely closed.
- The power was switched on to the ignition system and tested to ensure a satisfactory spark was produced.
- The outside gas bottle was opened and set to a pressure of 0.1 bar.
- The internal gas line valve was opened.
- The gas rotameter valve was opened to allow a low flow rate of fuel.
- The ignition system was activated, which opened the solenoid valve in the gas line and formed a spark in the burner.
- The air flow rate was manually controlled to sustain combustion.
- If the burner switched off automatically or the flame extinguished, then the burner was purged with combustion air before re-ignition was attempted.

4.2.4.1. **Running the burner**

When operating the burner, the following precautions and procedures were followed:

Precautions:

- Lab coat and safety glasses were worn at all times.
- Ear protection was used when operating under noisy conditions.

- Tests were carried out by standing to the windward side of the burner.
- The burner was never left unattended whilst in operation.

4.2.4.3. **Operating procedure:**

- Gas analysers were calibrated.
- Air and gas flow rates were set manually to provide the desired experimental conditions.
- Experimental results were taken.

4.2.4.4. **Extinguishing the burner**

The following procedure was used to safely extinguish the burner:

- The air and gas flow rates were manually reduced to a low level.
- The gas rotameter valve was firmly closed, but the air flow was maintained at a low flow rate to cool the air preheat tubes.
- The flame detector was allowed enough time to deactivate the solenoid valve.
- The power to the ignition system was switched off.
- The internal gas line valve was closed.
- The gas cylinder valves were closed.
- The fume extraction units were switched off.
- The gas analysers were purged with atmospheric air before switching off.
- The gas analysers were switched off.

4.3 GAS ANALYSERS AND TEMPERATURE MEASUREMENT

4.3.1. Nitric oxide and nitrogen dioxide gas analysers

There are a number of methods available for measuring NOx. The most common are infra red absorption and chemiluminescence. These methods are commonly used in industrial and research sampling applications. The methods used vary in cost and accuracy, and are hence suitable for different applications.

4.3.1.1. Infra red gas analysers

Solid state infra - red gas analysers are commonly used to determine the concentration of a multitude of gases, working on the principle of infra - red absorbance of various gases at certain distinct wavelengths. These include O_2, CO, CO_2, NO, SO_2, CH_4 and many other chemical species. Being solid state, the analysers are not sensitive to vibration unlike the Luft type analysers.

Infra red radiation is emitted from a heated element and directed to pass through a reference gas cell and an inert gas cell. These cells rotate, causing bursts of radiation to pass through the cells at regular intervals. The radiation is then collimated by a lens and passed through an interference filter to select the spectral region of interest. The radiation then passes through the sample gas cell, another lens and is then directed onto a solid state detector. A series of pulses in time with the speed of cell rotation is then detected. Comparison between the various amplitudes created can be used to determine the sample gas concentration.

4.3.1.2. chemiluminescence

This is perhaps the most sensitive and accurate method for measuring NOx and is used in the majority of research applications. To measure the total NOx in the gas

sample, conversion from NO_2 to NO is accomplished through the use of a high temperature carbon converter. When NO is reacted with ozone to form NO_2, approximately 10% of the NO_2 produced is in an electronically excited state. Transition from the excited state to normal means that the molecule loses energy, and this results in a light emission. The overall reaction is given by equation (76). The photons are detected in a photo multiplier tube, and are directly proportional to the concentration of nitric oxide entering the analyser.

$$NO + O_3 \Rightarrow NO_2 + O_2 + light \qquad (76)$$

To determine the ratio of NO to NO_2 in the sample gas, the sample may be diverted from the carbon converter hence reacting only the NO present in the sample with ozone via reaction (76). Together with the total NOx measurement of the sample the ratio can be calculated.

This type of analyser can operate using unconditioned flue gas. This implies that the water does not need to be condensed out of the gas sample. Using a heated sampling line, the combustion gas sample can pass to, and through the analyser without condensing. Condensation of water in the flue gas will impair the results because NO_2 is soluble in water.

Some chemiluminescent analysers operate under vacuum conditions. It is believed that this gives greater sensitivity in the photomultiplier tube due to the diffraction that may occur from air molecules.

The accuracy of measurement associated with chemiluminescent NOx analysers is generally good, typically within 1% of the full scale deflection. Other errors which are important in the overall degree of accuracy are noise, linearity and other gaseous components such as CO_2 and H_2O. A 1% reduction is associated with either 10% CO_2 or 3% H_2O in the sample, which would be common concentrations for hydrocarbon combustion.

From the degree of accuracy required and the ability to measure low concentrations of NOx, the chemiluminescent NOx analyser was chosen over alternative techniques.

4.3.2. **Oxygen analysis**

The most common and accurate technique for measuring the concentration of oxygen in a gas sample is through paramagnetic analysis. Electrochemical cells may also be used but have the disadvantage of being accurate to only 0.1%, which is generally accurate enough for most combustion system analyses. They also have a short lifetime of only 2 years before the electrochemical cell needs to be replaced.

4.3.2.1. **Paramagnetic analysers**

Oxygen is one of the few gases which are attracted to a magnetic field. This effect is called paramagnetism.

The sample gas is passed into a dumbbell arrangement within a magnetic field. The quantity of oxygen contained in the sample gas creates an angled deflection. A light source is shone at the dumbbell arrangement, which is reflected to photocells. Depending on the degree of deflection caused by the oxygen concentration, the amount of light received by the photocells will vary. The amount of light received by the photocells may then be interpreted as a concentration for display purposes.

To prevent any damage to the analyser, the gas sample must be free of condensable water vapour and not be from a pressurised source.

On the basis of cost, maintenance and accuracy, the paramagnetic oxygen analyser was chosen over the cheaper electrochemical cell option.

4.3.3. **Carbon monoxide**

Infra red absorption is the most common type of analysis technique used. The luft type analyser uses two gas cells. One gas cell contains a reference gas and the other the sample gas. The two cells are separated by a thin sheet of metal, sensitive to distortion by pressures from the two gases. Pulses of infra red light in a frequency susceptible to heating carbon monoxide are given to each cell by means of a rotary chopping disc. The relative expansion of the carbon monoxide within both cells is measured as a distortion on the thin metal sheet.

In many large industrial applications, the concentration of CO in the flue gas may be determined without extracting a sample from the system. An infra - red absorption technique may be employed using a transmitter and receiver spanning across the gas flow. A beam of chopped radiation is directed from the transmitter unit through internal reference cells, across the flue gases to an infra - red filter and detector in the receiver unit. The level of radiation received and the corresponding processed output from the transmitter are a measure of the CO present in the gas. There is not a high degree of accuracy involved with this method, typically with an error of 5%. This error and the arrangement of transmitter and receiver units make it unsuitable for scientific evaluation of emission performance.

On the basis of the above descriptions and the accurate sample concentrations required, a choice was made between the solid state infra - red and the luft - type analysers. Either analyser would be suitable, but the luft type analyser was chosen due to financial advantages.

4.3.4. **Calibration gases**

To ensure that the analysers displayed the correct emission concentrations, calibration gases were used. Nitric oxide and carbon monoxide are accurately mixed together in a nitrogen balance in concentrations of 98 ppm and 498 ppm, respectively. These gases were used to calibrate the NOx and CO analysers, using bottled nitrogen as a zero point. For the oxygen analyser, nitrogen was again used as the zero gas with air being used as the span gas, and calibrated to 21% oxygen. Calibration of the analysers was carried out frequently, and normally before any readings were taken.

4.3.5. **Temperature measurement**

The measurement of temperature in combustion systems can be accomplished in a number of ways, some of these being through the use of thermocouples, radiative pyrometry and acoustic pyrometry. Thermocouples are the simplest and cheapest measurement technique, utilising a difference in EMF from the junction of two metals to determine the temperature.

4.3.5.1. **Thermocouples**

A variety of thermocouples exist and are standardised by letters, corresponding to the metals used. These thermocouple metal combinations have properties that enable them to operate at different temperatures. K - type thermocouples are the most commonly used, and being made from chromel alumel they are relatively cheap but have a maximum measurable temperature of 1000 K. This limitation makes them unsuitable for the majority of temperature measurements in combustion systems. For high temperature measurements, R - type platinum - platinum (13%) rhodium are usually used. These thermocouples are far more expensive due to the precious metals being used but have a maximum measurable

temperature of 2000 K. For this reason, R-type thermocouples were used to measure the combustion gas temperature from the Coanda burner.

The construction of thermocouples can be varied and will depend upon their use. For long term temperature measurement, it is preferred to encase the delicate wires in a ceramic casing. This provides a relatively slow response to changes in temperature but gives better mechanical strength. Ceramic casings are also used where the wires may come into contact with corrosive gases. For research purposes, a bare thermocouple bead in which the connecting wires pass through a ceramic sheath are generally used.

The voltage created at the thermocouple bead can be registered as a temperature, but this is usually inaccurate due to radiation loses from the thermocouple to the surroundings. A balance exists between heat transfer to the thermocouple through convective heat transfer from the combustion gases and the radiation loses [66].

Calculations to correct the error are based on an iterative procedure to balance the convective and radiative heat transfers through equation (77).

$$h_c\left(T_{gas} - T_{TC}\right) = \delta\sigma\left(T_{TC}^4 - T_{amb}^4\right) \qquad (77)$$

To reduce the error between the measured and actual temperatures, a number of steps can be taken. Firstly, increasing the temperature of the surroundings to nearer the gas temperature can be achieved through shielding the thermocouple with a ceramic casing, decreasing the heat lost through radiation from the thermocouple.

Secondly, decreasing the diameter of the thermocouple will drastically reduce the radiation loses. This, however, is limited by the thickness of the wires available

and the ability to manufacture the thermocouple with reasonable mechanical strength.

Finally, increasing the convective heat transfer to the thermocouple will also decrease the temperature error involved. This technique is used in a suction pyrometer, where the gases are drawn over the thermocouple bead at a higher temperature, due to the suction from a pump.

4.3.5.2. **Alternative temperature measurement methods**

Acoustic pyrometry utilises time measurement of a sound pulse between two points in order to calculate the gas temperature. The speed of sound can be calculated from equation (78). The value of γ can be calculated from the gas composition. Through rearranging equation (78), the temperature can be calculated relatively simply. This method would be most useful in large combustion systems.

$$C = \sqrt{\frac{\gamma RT}{M}} \tag{78}$$

4.3.6 **Sampling Probes**

The sampling of gases from a combustion system can be accomplished in a number of ways. For continuous sampling, double skinned water cooled probes are commonly used. These are of a solid construction and need a pressurised water supply. They have the disadvantage of being relatively large and would be obstructive to the flow pattern in the Coanda burner. They also have the disadvantage of condensing the water from the sample gases thereby reducing the total NOx measured due to NO_2 being soluble in water. Hot water cooled stainless steel probes can be used to negate this effect. However, Horio [67] found that

discrepancies exist between NOx concentrations when using different probes on the same combustion system. The reason for this was not fully understood but was believed to be due to wall reactions inside the probe between the NOx in the sample gas and the wall lining material.

With a typical diameter of 3 mm, quartz microprobes are relatively unobtrusive, inexpensive, and require no cooling. The quenching effect in the probe relies on a downstream low pressure being present to draw the sample gas through a divergent nozzle. The rapid expansion of the gas cools the sample, quenching the reaction. The short time period within the high temperature region of the probe has little effect on reheating the gases. The quartz material is not known to have any side reactions with the NOx. The disadvantage of the microprobe is that it is very fragile and has a limited temperature. The temperature at which quartz softens is 1250 °C. However, the actual temperature that the quartz will reach will be somewhat below this due to radiation effects to the surroundings. Problems may occur when sampling within the flame, where the highest temperatures are expected, velocities are highest and the nearby surroundings are at high temperatures. Figure (26) shows how the probes were positioned to sample the combustion gases.

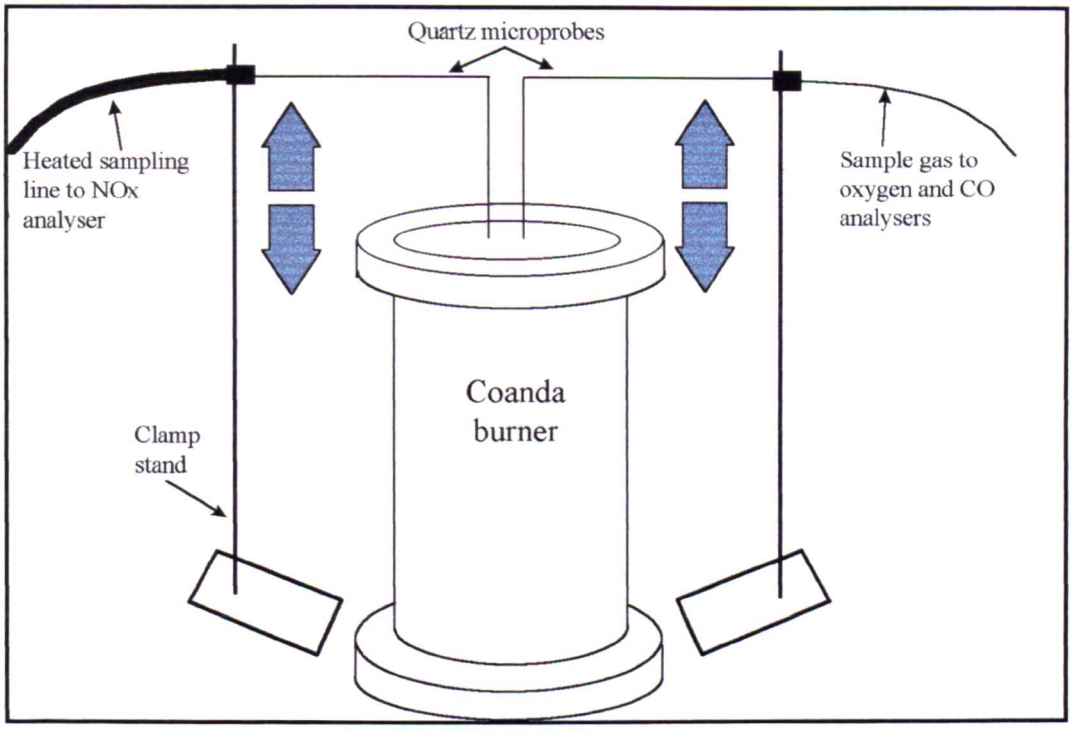

Figure 26. Positioning of the probes to sample the combustion gases.

The probes were manufactured from 3 mm diameter quartz tubing with a 1 mm diameter bore. The end which drew the gas was created by axially rotating the glass in a lathe. An oxy-fuel flame was then used to heat a small section of the glass which was manually stretched along its axis. Once the glass had been stretched by about 8 mm, the centre of the stretched section was separated to form two parts. As the probe was to sample along the axis of the burner, a 90° bend was created so that the sampling lines could be connected horizontally. The tapered end was closed with glass and needed to be ground back to give the desired entrance diameter of about 100 μm, expanding to 1 mm. To determine the orifice diameter accurately, a travelling microscope and fine emery paper were used. A diagram of a typical probe is displayed in figure (27).

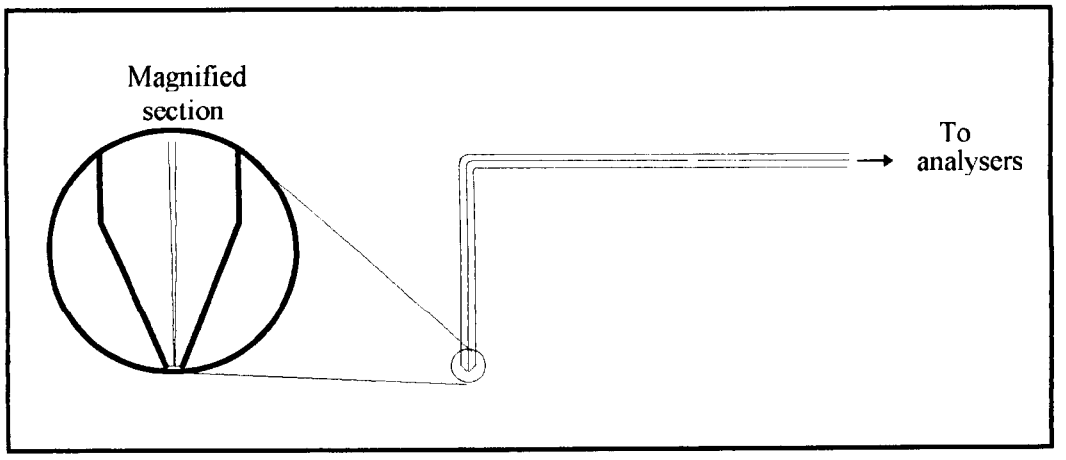

Figure 27. Diagram of a quartz probe used for sampling combustion gases.

5. RESULTS

5.1 MODELLING RESULTS

5.1.1 Initial model of the Coanda burner

The preliminary design of the Coanda burner led to a configuration that utilised the end of the fuel injector to act as a flame stabiliser. The model predicted high quantities of flue gas recirculation, typically three times the air mass flow rate. The resultant NOx emissions for such a design, and its formation region is shown in figure (146). When corrected to 0% oxygen and dry conditions, the predicted outlet NO emissions were 4.8 ppm.

5.1.2 Modelling of the experimentally modified design

The graphical outputs obtained from the computational modelling were analysed by considering the two main sections of the burner. The first section was concerned with the region which included the Coanda ejector, the Coanda mixing throat and the flame stabiliser. The second section included the main combustion region, the flue gas recycle point and the burner exit.

5.1.3 Gas compositions in the Coanda throat 10 mm behind the stabiliser

5.1.3.1 Introduction

This section analyses the modelling results taken directly from the Coanda throat, behind the fuel injection point. In order to obtain modelling results that could be easily compared, the gas compositions and temperatures in the Coanda mixing throat were averaged over the radius of the Coanda mixing throat. The NOx emissions at the exit of the burner are also shown. However, further detail concerning the distribution and mixing of the gases in the combustion chamber are given in sections 5.1.5.1 and 5.1.5.2. Detail has been

focused on the Coanda throat region to diagnose the effects of changing the Coanda gap width, flame stabiliser diameter, fuel type and air to fuel ratio on the processes occurring within the burner, and upon the emissions from the burner.

5.1.3.2 **Effect of Coanda gap width on gas composition**

Table 8 below displays modelling results which were taken from a cross section of the Coanda mixing throat, behind the fuel injection point. In order to allow a comparison between the modelling predictions and typical experimental results, the fuel used in both models was propane. A 30 mm disc was used to simulate the flame stabiliser, and the air to fuel ratio was approximately 1.3.

Coanda gap width mm	Air to fuel ratio	φ %	O_2 %	CO_2 %	H_2O %	Temp K	U velocity m/s	Final NOx ppm, DAF
0.2	1.26	101.2	13.7	4.8	6.46	1040	9	76.65
0.5	1.3	50.2	16.6	2.4	3.25	856	8.72	194

Table 8. Composition, temperature and velocity of the gaseous mixture, in the Coanda mixing throat when using 0.2 and 0.5 mm Coanda gap widths.

The air to fuel ratios in both cases were very similar, but the entrainment ratio of the 0.2 mm Coanda gap was more than double that of the 0.5 mm Coanda gap. The higher entrainment obtained by using the 0.2 mm Coanda gap width resulted in a greater quantity of flue gas, which had a low oxygen concentration, to be recycled. When the recycle stream was mixed with the combustion air supplied through the Coanda ejector, the average oxygen concentration in the Coanda mixing throat, behind the fuel injection point, was 13.7%. The increased entrainment also increased the concentrations of CO_2 and H_2O in the Coanda mixing throat. Similarly, the temperature in this region increased to 1040 K, 740 K above the air inlet temperature.

When using a 0.5 mm Coanda gap width, an entrainment ratio of 50.2% was achieved. This resulted in an oxygen concentration of 16.2% in the Coanda throat and an increase in the temperature to 856 K. A comparison between using the 0.2 and 0.5 mm Coanda gap widths showed that the smaller Coanda gap widths resulted in an increase in entrainment, local temperatures and non combustible gases such as CO_2 and H_2O in the Coanda mixing throat, with a subsequent decrease in oxygen concentration. The NOx emissions given in table 8 show that these differences in oxygen and non reactive gases in the Coanda mixing throat resulted in a large decrease in overall NOx emissions. The effect of the Coanda gap width upon the burner is further discussed in section 5.1.4.1.

5.1.3.3 **Change in fuel type**

Table 9 displays the effect of fuel type on the composition of the gaseous mixture at the Coanda mixing throat. The model used simulated a 0.5 mm Coanda gap width with a 40 mm flame stabilising disc. The composition of the gases in the Coanda mixing throat were very similar for the two fuels. The only exception was the difference in concentrations of CO_2 and H_2O which was due to the difference in the ratio of carbon to hydrogen in the fuels used. From the modelling results, there was a 38% reduction in NOx emissions when changing fuels from propane to methane.

Fuel used	Air to fuel ratio	φ %	O_2 %	CO_2 %	H_2O %	Temp K	U velocity m/s	Final NOx ppm, D.A.F.
Propane	1.33	25.8	17.9	1.68	2.25	687	5.74	86
Methane	1.28	23.7	18	1.36	2.72	668	5.2	53

Table 9. Modelling results at the Coanda mixing throat when burning propane and methane.

5.1.3.4 **Change in flame stabiliser diameter**

Table 10 below details the differences in entrainment and composition encountered when changing the size of the flame stabilisation disc. The modelling results were obtained using a 0.5 mm Coanda gap width and propane as the fuel.

Diameter of flame stabiliser mm	Air to fuel ratio	φ %	O_2 %	CO_2 %	H_2O %	Temp K	U velocity m/s	Final NOx ppm, DAF
40	1.33	25.8	17.9	1.68	2.25	687	5.74	86
30	1.3	50.2	16.6	2.4	3.25	856	8.72	194

Table 10. Modelling results at the Coanda mixing throat when using 30 mm and 40 mm flame stabilisers.

From table 10, it can be seen that the entrainment obtained using a 0.5 mm Coanda gap width with 30 mm and 40 mm flame stabiliser discs were 50.2% and 25.8%, respectively. The decrease in entrainment when using a 40 mm disc was due to a reduction in the ratio of the Coanda throat area to Coanda gap area, and pressure losses through the larger recirculation region after the stabiliser.

The reduction in entrainment resulted in less flue gas being recycled, causing the local oxygen concentration to increase, whilst the local concentrations of CO_2, H_2O and temperature decreased. Due to the decrease in entrainment, the average velocity of gases passing through the Coanda throat decreased. The higher NOx emissions when using the 30 mm disc were due to the mixing process between the fuel and oxygen, as explained in section 6.1.2.

5.1.3.5 **Changes in air to fuel ratio**

Tables 11 and 12 display the modelling results taken from the Coanda mixing throat over a range of air to fuel ratios. In each case, a 0.5 mm Coanda gap width was modelled and propane was used as the fuel.

Diameter of flame stabiliser mm	Air to fuel ratio	φ %	O_2 %	CO_2 %	H_2O %	Temp K	U velocity m/s	Final NOx ppm, D.A.F.
40	1.18	21.9	18	1.62	2.16	680	4.86	223
40	1.29	25.8	17.9	1.69	2.25	687	5.74	118
40	1.44	28	17.9	1.71	2.28	693	6.33	86.2
40	1.66	33.3	17.8	1.77	2.37	695	7.77	33.8
40	2.26	39.6	17.8	1.77	2.37	694	9.8	12.5

Table 11. Modelling results at the Coanda mixing throat over a series of air to fuel ratios using a 40 mm stabilising disc and a 0.5 mm Coanda gap width.

Diameter of flame stabiliser mm	Air to fuel ratio	φ %	O_2 %	CO_2 %	H_2O %	Temp K	U velocity m/s	Final NOx ppm, D.A.F.
30	1.2	45.4	16.6	2.43	3.24	842	7.35	150.2
30	1.27	50.2	16.6	2.44	3.25	856	8.72	194.1
30	1.42	53.1	16.6	2.44	3.26	862	9.62	83.1
30	1.64	61	16.5	2.49	3.31	859	11.7	94.8
30	2.24	70.7	16.5	2.46	3.29	843	14.7	46.5

Table 12. Modelling results at the Coanda mixing throat over a series of air to fuel ratios using a 30 mm stabilising disc and a 0.5 mm Coanda gap width.

From tables 11 and 12, it can be noted that the proportions of each component in the Coanda mixing region did not change as the air to fuel ratio was increased. This phenomenon was caused by an increase in the entrainment ratio and oxygen concentration in the recycled flue gases as the air to fuel ratio increased. The mixed gas temperature also remained almost constant over the range considered but the axial velocity increased by a factor of 2, from 7.35

m/s to 14.7 m/s. The reduction in NOx emitted from the burner as the air to fuel ratio was increased was caused by the fuel being dissipated and allowed to react into a larger volumetric flow. This dilution effect resulted in lower average temperatures throughout the burner. However, as displayed in table 13, due to the increased volume of combustion gases entrained, the temperatures and oxygen concentration prior to fuel and air mixing were at over 1000 K and at approximately 14 %, respectively.

Diameter of flame stabiliser mm	Air to fuel ratio	φ %	O_2 %	CO_2 %	H_2O %	Temp K	U velocity m/s	Final NOx ppm, D.A.F
30	1.09	92.2	13.48	5.03	6.7	1026	7.6	58.3
30	1.26	101.2	13.7	4.8	6.46	1040	9	76.7
30	1.42	111.2	14.26	4.74	6.33	1051	10.75	80.5
30	1.65	120	14.6	4.5	6.0	1043	12.37	65.1
30	2.18	135.3	15.36	4.09	5.46	1017	15.48	36

Table 13. Modelling results at the Coanda mixing throat when using a 0.2 mm Coanda gap width.

When comparing the 0.5 mm and 0.2 mm Coanda gap widths, greater entrainment was obtained by the latter, and the rate of recirculation increased with increasing the air to fuel ratio. Tables 12 and 13 display the modelling results at the Coanda throat for Coanda gap widths of 0.5 mm and 0.2 mm, respectively. When using the 0.2 mm Coanda gap width and operating near stoichiometric conditions, the oxygen concentration in the Coanda mixing throat was approximately 3% lower than when using a 0.5 mm Coanda gap width.

When comparing the results for the 0.5 mm and the 0.2 mm Coanda gap widths given in tables 12 and 13, the greater entrainment obtained when using the latter gap width resulted in an increase in the rate of recirculation when increasing the air to fuel ratio. The concentrations of CO_2 and H_2O increased by a factor of up to two when the air to fuel ratio was increased from 1.1 to

1.2. Through the combination of both lower oxygen concentrations and higher CO_2 and H_2O concentrations, the overall NOx emissions were significantly reduced, especially when operating with an air to fuel ratio of between 1.1 to 1.4, where approximately only a third of the NOx was produced.

5.1.4 **Modelling comparisons**

The following section considers further the distribution and mixing of the gases in the Coanda mixing throat. Comparison of results in this region were based on changing the Coanda gap width, stabiliser diameter, fuel type and air to fuel ratio. In sections 5.1.5.1 to 5.1.5.2, further comparisons are made of the gas compositions and temperatures in the diffusing section, where combustion occurred.

5.1.4.1 **Changing the Coanda gap width from 0.2 mm to 0.5 mm**

Figures (28) to (31) and figures (32) to (35) both simulated a 30mm stabilising disc with Coanda gap widths of 0.2 and 0.5 mm, respectively. Propane was used as the fuel in each case, with an air to fuel ratio of 1.28. When using the 0.5 mm Coanda gap width, it can be seen from figures (32) to (35) that the oxygen concentration in the Coanda throat increased slightly with radial distance. The average oxygen concentration was approximately 16%, and the temperature was 800 K. The 0.2 mm Coanda gap width resulted in a uniform oxygen concentration of 13% in the Coanda throat behind the fuel injection point, and with a temperature of 1000 K. The composition of the recycled gases was different in each case. When using a 0.5 mm Coanda gap width, the recycled gases had an oxygen concentration of 8.5% but when using a 0.2 mm Coanda gap width the recycled oxygen concentration was 5.5%. However, the temperature of the recycled flue gases was 1600 K in both cases.

The use of the 0.5 mm Coanda gap width resulted in a slightly higher peak CO concentration after the flame stabiliser as compared to when using the 0.2 mm

Coanda gap width. The higher concentration of CO also stretched over a longer axial distance and maintained a higher concentration when using a 0.5 mm Coanda gap width.

5.1.4.2 **Changing the stabiliser diameter from 30 mm to 40 mm**

Figures (32) to (35) and figures (36) to (39) were used to contrast the differences between the stabilisers, both of which used a 0.5 mm Coanda gap width and propane as the fuel.

To satisfy the entrainment requirement of the ejector, a recirculation region was formed whereby the ejector entrained gases from a point downstream of the ejector. This recirculation region can be seen in both figures (32) and (36) as a flow of gas travelling radially outwards along the burner's inner wall. The recirculation region was larger when using the 40 mm diameter stabiliser. This was due to the reduction in the flow area caused by the larger diameter disc. As shown in figures (33), (34), (37) and (39), the recirculating gases had a temperature and an oxygen concentration similar to that at the Coanda throat, indicating that the recirculating gases originated from that region.

The use of a 40 mm disc as compared to a 30 mm disc resulted in a reduction in flue gas entrainment. Figures (33), (34), (37) and (39) show that the reduction in flue gas entrainment caused both a reduction in temperature and an increase in oxygen concentration at the Coanda throat. The recycled gas oxygen concentration for the 40 mm and 30 mm discs were 6% and 9%, respectively, with similar temperatures in each case.

Through comparing figures (32) and (36), it can be seen that the recirculation zone directly after the flame stabiliser was larger in both diameter and length when using the 40 mm disc as compared to the 30 mm disc. The flow around the flame stabiliser resulted in greater mixing between the air and fuel with the 40 mm disc. This increase in mixing was illustrated through comparing figures

(34) and (39) which show the oxygen concentrations near the walls of the diffuser, where the 30 mm disc exhibited a greater oxygen concentration than the 40 mm disc. A similar observation was made for CO concentrations from figures (35) and (38). The peak concentration of CO when using the 40 mm disc extended over a greater volume but similar axial length. The concentration of CO next to the wall of the diffuser was also of a far higher concentration. The 40 mm disc displayed a greater rate of decrease in CO concentration with axial distance than the 30 mm disc. This reduction of CO for the 40 mm disc resulted in a higher temperature in the region directly after the flame stabiliser.

5.1.4.3 **Changing the fuel type from propane to methane**

Figures (36) to (39) and figures (40) to (43) display modelling results simulating a 0.5 mm Coanda gap width with a 40 mm disc as the flame stabiliser, burning propane and methane, respectively. The velocity vectors for both fuels were almost identical, the only difference being that methane was injected at a far higher velocity, due to its lower density. Figures (39) and (42) show that the oxygen concentrations are virtually identical for both fuel types, indicating that there was little difference in mixing. However, the peak temperature obtained when using methane was slightly lower than that for propane. This could be due to the simplified reaction sequence used in the model, producing greater quantities of water vapour which had a high specific heat capacity and radiation absorption capabilities. Due to the difference in the ratio of carbon to hydrogen between methane and propane, the concentrations of CO in the burner varied significantly. Methane had a peak CO concentration of 1.97% and propane a concentration of 2.58%. When using propane, the higher concentration of CO existed over a larger volume than for methane. The concentration of CO when using methane was also far lower behind the stabiliser. The reduction in concentration of CO along the axis of the burner for both methane and propane followed a similar trend in relative concentrations, indicating that the mixing mechanisms were similar.

5.1.4.4 **Increasing the air to fuel ratio**

Figures (44) to (55) display simulations of propane combustion using a 0.5 mm Coanda gap width, and a 40 mm flame stabiliser disc. The air to fuel ratio in figures (44) to (47), (48) to (51) and (52) to (55) were 1.18, 1.44 and 2.26, respectively.

A comparison between these figures shows that the re-entrainment of gases decreased with increasing air to fuel ratio. The flow of gas travelling radially outwards along the front wall decreased with distance, indicating that the entrainment achieved was closer to that required by the ejector. When operating at an air to fuel ratio of 1.18, figure (45) shows that the recycled gas temperature was at approximately 1500 K, but when operating at an air to fuel ratio of 2.26 the recycle temperature was at approximately 1300 K, as shown in figure (53). This difference in temperature resulted in a difference in recycle gas density and hence the amount of entrainment. The ejector entrained more gas at the lower temperature, resulting in a smaller recirculation region near the Coanda ejector.

The recirculation region behind the flame stabiliser increased in axial length with increasing air to fuel ratio, due to an increase in velocity over the stabiliser. When increasing the air to fuel ratio from 1.18 to 2.24, the concentration of CO directly in front of the stabiliser decreased from 1.35% to 0.65%. The relative concentration of CO decreased with axial distance and it also decreased radially inwards with increasing axial length. The temperature in the recirculation zone after the flame stabiliser increased slightly with increasing air to fuel ratio, due to a larger proportion of the fuel being burned in this region.

Figures (56) to (59), (60) to (63), and (64) to (67) represent models using propane as fuel, a 30 mm disc stabiliser and a 0.5 mm Coanda gap width, operating at air to fuel ratios of 1.2, 1.42 and 2.24, respectively. The flow

pattern near the Coanda ejector was similar to that of the 40 mm stabiliser cases, in that the re-entrainment of primary air decreased with increasing excess air. This is similarly explained through a reduction in temperature of the recycled gases, from 1600 K to 1400 K when increasing the air to fuel ratio from 1.2 to 2.24.

The oxygen concentration in the Coanda throat behind the fuel injection point was almost constant at 16% for all the air to fuel ratios modelled. For all air to fuel ratios, the concentration of oxygen increased with radial distance in the Coanda throat, the largest concentration difference being 2% oxygen at an air to fuel ratio of 2.24. In the combustion region after the stabiliser, the oxygen concentration profiles for air to fuel ratios of 1.2 and 1.42 were very similar, with no oxygen present along the axis of the burner over the region considered. Figure (66) shows that there was a high concentration of oxygen along the wall of the diffuser, and that the concentration of oxygen slowly increased radially inwards with axial distance.

Concentrations of CO reached similar peak values for each air to fuel ratio. However, when operating at an air to fuel ratio of 1.2, peak concentrations existed over a greater volume. Directly after the flame stabiliser, CO concentrations of 1%, 0.9% and 0.75% were found for air to fuel ratios of 1.2, 1.42 and 2.24, respectively. These decreases in CO concentration directly after the stabiliser were thought to be due to an increase in the reaction rate in this region, which caused the temperature to rise from 1900 to 2050 K when the air to fuel ratio was increased from 1.2 to 2.24, respectively.

5.1.5 **The effects of air to fuel ratio on the temperature and gas compositions in the combustion chamber**

5.1.5.1 **Effects using a 30 mm flame stabiliser**

Figures (68) to (70), (71) to (73) and (74) to (76) display models of the burner using a 30 mm flame stabilising disc, a 0.5 mm Coanda gap width and air to fuel ratios of 1.2, 1.42, and 2.24, respectively. A comparison of figures (70), (73) and (76) showed that the CO emissions at the burner exit decreased with increasing air to fuel ratio. The axial distance through the burner at which the CO was un-reacted, decreased with increasing air to fuel ratio. The inverse effect was displayed with the concentrations of oxygen over the same air to fuel ratios, as shown in figures (69), (72) and (75). No oxygen was present along any part of the burner axis when operating at an air to fuel ratio of 1.2, but a high concentration of oxygen was present along the diffuser wall, which was then entrained into the recycle annulus by the Coanda ejector. The difference in oxygen concentrations between the average outlet gas composition and the recycle gas was significantly large. As shown in figure (75), when operating at an air to fuel ratio of 2.24, a high oxygen concentration existed along the axis of the burner shortly after the flame stabiliser. At the exit of the burner, the oxygen concentration profile between the axis and the outer diameter of the exhaust duct showed that the oxygen concentration was almost uniform, and that the oxygen concentration of the outlet gases and the recycled gases were similar.

Similarly, the regions of peak temperature were changed by the air to fuel ratio. At an air to fuel ratio of 1.2, figure (68) shows that the peak temperature extended over a larger volume that started roughly half way along the axis of the burner and continued until the exit. At an air to fuel ratio of 1.4, figure (71) shows that the peak temperature region occupied a smaller volume in the middle of the burner, along the axis. At an air to fuel ratio of 2.24, figure (74) shows that the peak temperature region occupied the smallest volume and was

located a short distance behind the flame stabiliser. The temperatures of the recycled gases were different to those of the exit gas when operating at air to fuel ratios of both 1.2 and 1.4. The decrease in temperature was caused by heat transfer from the gases in the recycle annulus to the cooler, oxygen rich gases, flowing in the opposite direction along the inside surface of the diffuser wall.

5.1.5.2 **Effects using a 40 mm flame stabiliser**

Figures (77) to (79), (80) to (82) and (83) to (85) display model simulations using a 40 mm flame stabilising disc with a 0.5 mm Coanda gap width. The effect of air to fuel ratio on the temperature and concentrations of CO within the combustion chamber were similar to those for the 30 mm disc, described in section 5.1.5.1. A direct comparison between the results obtained from the model incorporating the 40 mm stabiliser and that of the 30 mm stabiliser can aid to highlight the changes encountered within the combustion chamber.

Comparison of the effect of the use of the 40 mm and 30 mm stabilising discs in a burner operating at an air to fuel ratio of 1.2, is shown in figures (68) to (70) and (77) to (79), respectively. The 40 mm stabilising disc caused a reduction in the oxygen concentration along the diffuser wall, but did not result in a significant change in the concentration of CO within the burner. The volume over which the peak temperature existed was larger when using a 40 mm stabilising disc, starting from a point slightly closer to the stabiliser but similarly continuing to the burner exit.

Figures (71) to (73) and (80) to (82), which are for operation at an air to fuel ratio of 1.42, show that with a 40 mm stabilising disc the axial distance along the burner for CO burnout was shorter than for the 30 mm stabilising disc. Similarly, the point at which oxygen was present along the burner axis began at a shorter axial distance, after the depletion of CO. When using the 40 mm stabilising disc, the radial oxygen concentration at the burner outlet was more

uniform than when using the 30 mm stabilising disc. However, the overall oxygen concentration of the recycled gases and the outlet gases were not quite the same. The peak temperature region occupied when using the 40 mm stabilising disc was slightly smaller and was located closer to the stabiliser than when using the 30 mm stabilising disc.

Figures (74) to (76) and (83) to (85), which are at an air to fuel ratio of 2.24, show that when using a 40 mm flame stabiliser, the CO occupied a smaller volume than when using a 30 mm flame stabiliser and that it existed over a shorter axial distance. When using a 40 mm stabilising disc, the radial oxygen concentration at the exit of the burner was uniform, having the same concentration as the recycled gases. The peak temperature region was of a similar volume when using both the 40 mm and 30 mm discs. However, when using the 40 mm disc, the peak temperature region was close to the stabiliser. The radial outlet temperature profile was constant when using the 40 mm stabilising disc, having the same temperature as the recycled flue gases.

5.1.5.6 **NOx formation in the combustion chamber**

The region of NOx formation and the quantities produced in the combustion chamber changed with fuel type, air to fuel ratio and diameter of the flame stabiliser. Figures (86) and (87) show the positions of thermal NO formation when burning methane at air to fuel ratios of 1.64 and 2.57, respectively. Under these air to fuel ratios, and when corrected to dry 0% oxygen conditions, 21 and 1.8 ppm of NO was emitted, respectively. As the air to fuel ratio was increased, the NOx formation region moved in the direction of the flame stabiliser. Figure (88) shows the position of thermal NO formation when burning propane with a 30 mm disc and an air to fuel ratio of 1.36. The majority of the NO was formed near the exit of the burner, when the combustion of the fuel was complete.

Figures (89) and (90) show the prompt NO formation in the combustion zone when using a 40 mm flame stabilising disc for methane and propane operating at air to fuel ratios of 1.64 and 1.39, respectively. Under these air to fuel ratios and when corrected to dry 0% oxygen conditions, 0.65 and 2.5 ppm NO was emitted for methane and propane, respectively. The quantity of NO formed was found to be negligible for both fuels, as compared to thermal NO formation. Prompt NO formation was located near the flame stabilisation region, where there was a high concentration of unburnt fuel.

5.2 EXPERIMENTAL RESULTS

5.2.1 Introduction

This chapter contains an account of the experimental results obtained for operation of the Coanda burner. During the development of the burner, extensive modifications were made to the design of the flame stabiliser. For each design of flame stabiliser, the effect of variations in air and gas flow rates and Coanda gap widths on pollutant emissions and burner stability have been summarised. Where experimental results were taken incorporating swirl, the swirl was induced through the use of swirl vanes at an angle of 80° to the horizontal.

5.2.2 Developments in the stabiliser design

The Coanda burner was designed and manufactured according to the configuration and dimensions of the modelled burner, which predicted very low NO emissions, as discussed in section 5.1.1. The original burner utilised the end of the fuel injector, which was 20 mm in diameter, to act as the flame stabilisation region. In conjunction with the end of the fuel injector, the hot recirculated combustion gases were utilised to increase the flame stability. In practice, as predicted by the model, operation at lean conditions led to very low NOx emissions, typically 5 ppm. However, operating the burner with a high air to fuel ratio led to emissions of CO that were unacceptably high. This was due to incomplete combustion of the fuel through low combustion gas temperatures. The burner was unable to operate near stoichiometric conditions as flame stabilisation was not achieved. The reason for the limited range of operation was due to the fuel-air mixing in the stabilisation region which is described in section 6.1.2. Consequently, the development of the burner required the use of a flame stabiliser which was attached to the end of the fuel injector.

The experimental results obtained when using a 30 mm stabilising disc alone proved unable to support combustion under any air to fuel ratios or fuel mass flow rates. Modifications in the design of the flame stabiliser provided methods of increased stability and reduced NOx emissions. The flame stabiliser consisted of stainless steel discs of 30 and 40 mm diameters, as shown in figure (24), and described in section 4.2.2.1. Discs with three, four, five and eight fingers were used, occupying up to 50% of the difference in area between the 30 and 40 mm discs. These fingers provided small mixing regions in which the fuel and oxygen mixed to form flammable mixtures and stabilised the flame. A reduction in the number and thickness of the fingers resulted in a decrease in the overall area of the stabiliser. As the stabiliser area approached that of the 30 mm disc, through a decrease in the number and thickness of the fingers, the emission of NOx decreased. The stabilisers, which were of similar area but with a differing number of extensions gave similar emissions of NOx. However, the three finger flame stabiliser resulted in the highest quantity of NOx being emitted when compared to the other stabiliser designs. This was because each extension was broader than the other designs, resulting in greater mixing between the fuel and air, leading to higher NOx formation.

Experimental NOx emissions were highest when using the 40 mm stabilising disc alone, and decreased with decreasing stabiliser area. It is possible that the increase in entrainment ratio and resultant lower mixed oxygen concentration caused the reduction in NOx emission. In comparison to other stabilisers considered, a 40 mm disc proved to have the greatest gradient of NOx decrease with increasing air to fuel ratio. The NOx emission results taken from the eight finger stabiliser were almost uniform over a large range of air to fuel ratios. This adds to the theory from the modelling assumption that the 40 mm disc produced a larger amount of premixing between the fuel and oxygen prior to combustion, leading to high NOx emissions at low air to fuel ratios and low NOx emissions at high air to fuel ratios.

5.2.3 **Experimental results for different burner configurations**

5.2.3.1 **Burner configuration utilising the five finger flame stabiliser**

Figures (91) to (99) display NOx and CO emissions obtained experimentally for the burner configurations utilising the five finger flame stabiliser. Figures (91), (92) and (93) display the emissions obtained when burning propane with a 0.2 mm Coanda gap width, and operating at 5, 10 and 15 kW, respectively. NOx emissions less than 30 ppm were obtained for all the air to fuel ratios used, which ranged from approximately 1.25 to 1.65 in all cases. The burner was unable to operate below an air to fuel ratio of 1.25.

Figures (94) to (99) show the NOx and CO emissions for the burner utilising the five finger flame stabiliser with a 0.5 mm Coanda gap width. This resulted in flame stability for a range of air to fuel ratios from 1 up to a maximum of 2.4.

Figures (94) to (96), and (97) to (99), display the NOx and CO emissions with and without swirl, respectively. At 5 and 10 kW, lower NOx emissions were obtained when swirl was employed. Differences in NOx concentrations of up to 5ppm and 10 ppm were obtained for 5 and 10 kW, respectively.

Figures (96) and (99) show the results for the operation of the burner at 15 kW, with and without swirl, respectively. The NOx emissions for these configurations were almost identical. CO emissions were similar with and without swirl at all fuel mass flow rates.

5.2.3.2 **Burner configurations utilising the 40 mm disc flame stabiliser**

Figures (100) to (102) show NOx and CO emissions when burning propane with a 40 mm flame stabilising disc, a 0.5 mm Coanda gap width and swirl at 5, 10 and 15

kW, respectively. Using the 0.5 mm Coanda gap width resulted in flame stability near stoichiometric fuel to air ratios. Figure (103) and (104) show the NOx and CO emissions obtained with the Coanda gap width set at 0.2 mm. For this configuration, the flame stability of the burner decreased, and operation was only possible from an air to fuel ratio of approximately 1.15 and 1.2 at thermal ratings of 10 and 15 kW, respectively.

From figures (100) to (102), it can be seen that when using the 0.5 mm Coanda gap width, NOx emissions decreased significantly with increasing air to fuel ratio, typically by 20 ppm over the experimentally measured range, which was approximately 1.0 to 1.6. CO emissions were high near stoichiometric conditions, up to 1600 ppm, decreasing to between 20 to 50 ppm at an air to fuel ratio of 1.2, and increasing again with increasing excess air from an air to fuel ratio of about 1.45.

When using either the 0.2 or 0.5 mm Coanda gap widths, increasing the mass flow rate of fuel through the burner had the effect of increasing the NOx emissions. However, figure (100) shows that at the lowest fuel mass flow rate, corresponding to a thermal rating of 5 kW, the NOx emissions nearest stoichiometric conditions were the highest, decreasing rapidly with increasing excess air. The 0.2 mm Coanda gap width resulted in NOx emissions which were approximately 15 ppm lower than those obtained when using the 0.5 mm Coanda gap width, but CO emissions were comparable.

Figure (105) shows that increasing the length of the diffuser had little effect on CO emissions but increased NOx emissions by approximately 5 to 10 ppm.

5.2.3.3 **Burner configurations utilising the three finger flame stabiliser**

Figures (106) to (108) and, (109) to (111) show the NOx and CO emissions obtained when burning propane with 0.5 mm and 0.2 mm Coanda gap widths at 5, 10 and 15 kW, respectively. The flame stabiliser used consisted of both the three finger stabiliser and the 30 mm disc, which were placed on top of each other, which resulted in greater flame stability.

Figures (106) to (108) show that when using a 0.5 mm Coanda gap width, the flame was stable near stoichiometric conditions. However, figures (109) to (111) show that the burner became less stable when using a 0.2 mm Coanda gap width. Stable operation when using a 0.2 mm Coanda gap width was only possible from an air to fuel ratio of about 1.1 to 1.25, with the burner least stable when operating at 15 kW.

NOx emissions were highest when using a 0.5 mm Coanda gap width, and increased with increased fuel mass flow rate, ranging from approximately 35 ppm to 45 ppm when increasing the equivalent fuel flow from 5 kW to 15 kW. A similar increase in NOx emissions occurred when using a 0.2 mm Coanda gap width with identical fuel mass flow rates, increasing from approximately 16 ppm to 40 ppm.

It can be seen from figures (106) to (109) that CO emissions decreased rapidly with increasing air to fuel ratio up to 1.4, after which the emissions increased.

5.2.3.4 **Burner configurations utilising a four finger flame stabiliser**

Figures (112) to (114) display the NOx and CO emissions obtained when burning propane with a four finger flame stabiliser, a 0.5 mm Coanda gap width and swirl at 5, 10 and 15 kW, respectively. The flame was stable from near stoichiometric

conditions, with NOx emissions measured at approximately 35 ppm. NOx emissions peaked at an air to fuel ratio of 1.1 and 1.2 for fuel mass flow rates of 15 and 10 kW, respectively but had an overall downward trend when increasing the air to fuel ratio. However, when operating at 5 kW, NOx emissions increased slightly with increasing air to fuel ratio.

CO emissions were generally low for all thermal ratings, typically at 20 - 30 ppm at an air to fuel ratio of 1.3. Increasing the air to fuel ratio above 1.4 resulted in an increase in CO emissions.

5.2.3.5 **Burner configurations utilising the 40 mm sectioned flame stabiliser**

Figures (115) and (116) show the NOx and CO emissions obtained when burning propane with a 40 mm sectioned stabiliser, a 0.2 mm Coanda gap width and swirl at 10 and 15 kW, respectively. The flame was stable from an air to fuel ratio of 1.15, up to a maximum of 1.38. The NOx emissions at both 10 and 15 kW decreased slightly with increasing air to fuel ratio, and were approximately 35 and 50 ppm, respectively. At an air to fuel ratio of 1.35, CO emissions at 10 and 15 kW were 50 ppm and 100 ppm, respectively. The CO emissions decreased with increasing air to fuel ratio.

Figures (117) to (119) display the NOx and CO emissions obtained when burning methane with a 40 mm sectioned stabiliser and a 0.5 mm Coanda gap width at 7.5, 15 and 22 kW, respectively. The flame was stable at air to fuel ratios in excess of 1.1, up to a maximum air to fuel ratio of 1.5. The NOx emissions were approximately 37 ppm and 45 ppm for fuel mass flow rates equivalent to 15 and 22 kW, respectively. The NOx emissions decreased by only about 5 ppm when the air to fuel ratio was increased from 1.1 to 1.4. From figure (117), it can be observed that when using a fuel mass flow rate equivalent to 7.5 kW, 50 ppm of NOx was measured at an air to fuel ratio of 1.15 which steadily decreased to 30 ppm at an

air to fuel ratio of 1.5. CO emissions of up to approximately 50 ppm were measured for all fuel mass flow rates.

5.2.3.6 **Burner configurations utilising the eight finger flame stabiliser**

Figures (120) to (123) show the NOx and CO emissions obtained when burning methane with a 0.5 mm Coanda gap width. The flame stabiliser used consisted of a 30 mm disc and an eight finger stabiliser positioned on top of each other. Figures (120) and (121), and figures (122) and (123) show the emissions when operating at 8 and 12 kW both with and without swirl, respectively. The flame was stable over a short range of air to fuel ratios, which were between approximately 1.1 and 1.4.

In all cases, NOx emissions increased with increasing air to fuel ratio and fuel mass flow rate, from a minimum of 18 ppm to a maximum of 25 ppm. A NOx reduction of 2 ppm was obtained when not using swirl. CO emissions decreased rapidly with increasing air to fuel ratio. CO emissions of approximately 20 ppm and 50 ppm were measured with and without swirl, respectively.

Figures (124) and (125) show the NOx and CO emissions for propane combustion when using a 0.5 mm Coanda gap width at 8 and 12 kW, respectively. The flame stabiliser used consisted of a 30 mm disc and an eight finger stabiliser placed on top of each other. The flame was stable between an air to fuel ratio range of 1.1 to a maximum of 1.7. The NOx emissions over this range of air to fuel ratios were almost constant at both thermal ratings. Over the air to fuel ratio range considered, figure (124) shows that there was a decrease in NOx emissions from 40 ppm to 35 ppm. However, figure (125) shows that there was an increase in NOx emissions from 45 ppm to 50 ppm.

5.2.3.7 In flame measurements utilising the eight finger flame stabiliser and the 30 mm disc

Figures (126) to (129) show NOx and CO emissions along the axis of the burner when burning methane with a 0.5 mm Coanda gap width. The flame stabiliser consisted of a 30 mm disc and an eight finger stabiliser placed on top of each other. Figures (126) and (127), and figures (128) and (129) show the results obtained when operating with outlet oxygen concentrations of 3.0% and 4.8%, with and without swirl, respectively. It was found that with an outlet oxygen concentration of 3.0%, approximately 30 ppm and 32 ppm of NOx were measured with and without swirl, respectively. Along the axis of the burner, the concentration of NOx increased only slightly, whereas the concentration of CO increased dramatically. There was little difference in the concentration of CO measured when swirl was introduced.

Figures (126) and (127) show that the NOx concentration increased slightly at 12 to 15 cm inside the burner, whereas figures (128) and (129) show that the NOx concentration decreased by up to 5 ppm over the distance measured. At both oxygen outlet concentrations, CO emissions were not significantly affected by swirl. CO emissions were below 100 ppm up to 12 cm inside the burner but increased rapidly with distance as samples were taken nearer the flame stabiliser.

5.2.4 Quantities of NO and NO_2 in the measured NOx

Figure (130) shows that the proportion of NO_2 in the NOx emissions for propane combustion using an eight finger stabiliser was approximately 10% over all of the air to fuel ratios measured. When burning methane with an eight finger stabiliser, figure (131) shows that the NO_2 contributed to between 0 and 5% of the total NOx measured. The low level of NO_2 within the flue gas was due to both the high

flue gas temperatures, and the re-burning of the recycled flue gas that contained NO_2, reducing it to NO through thermal decomposition.

6. DISCUSSION OF THE RESULTS

6.1 DISCUSSION OF MODELLING RESULTS

6.1.1 Introduction

This section discusses the NO and CO emissions obtained from the modelling results. Possible reasons as to how the burner operates to achieve low pollutant emissions are identified and evaluated. The significance of the findings are highlighted to aid the understanding of the burner operation, with a view to reducing pollutant emissions.

6.1.2 The effect of flame stabiliser diameter, air to fuel ratio and thermal rating on NO and CO emissions

Figures (132) and (133) display the NOx and CO emissions obtained for 30 mm and 40 mm flame stabilising discs at outlet oxygen concentrations of 3% and 5%, respectively. The fuel used in both cases was methane. The emissions of NO associated with the use of the various stabilisers were found to vary, depending upon the flue gas oxygen concentration and fuel mass flow rate. Figure (132) shows that when operating the burner with an outlet oxygen concentration of 3%, NO emissions for the 40 mm disc were higher over the majority of the range considered. However, figure (133) shows that when operating the burner with an outlet oxygen concentration of 5%, NO emissions were significantly higher when the 30 mm disc was used.

Figures (132), (133) and (134) show that NO emissions increased and CO emissions decreased as the fuel mass flow rate was increased. From figure (132), it can be seen that under all conditions, the 40 mm disc was found to result in the emission of lower concentrations of CO, and that increasing the amount of oxygen in the outlet flue gas reduced CO emissions.

From the results given in table 8, increased flow rates of flue gas recirculation decreased the formation of NOx. Table 10 showed that the quantity of recirculated gases was greater when using the 30 mm flame stabiliser as compared to the 40 mm stabiliser. However, the NOx emissions for the 30 mm flame stabiliser were significantly higher than when using a 40 mm flame stabiliser. Therefore, the reason for the difference in NOx and CO emissions is unlikely to be attributed to the quantity of flue gas recirculation.

From figures (132) and (133), the emissions of CO decreased as the thermal rating of the burner was increased. Due to radiation heat loses through the burner exit, lower gas temperatures were expected at low thermal ratings, leading to a decrease in the reaction rate and increased CO emissions. However, due to high gas temperatures and the fast reaction chemistry used in the model, this reason was unlikely. Also, the decrease in CO emissions could not have been attributed to the quantity of flue gas recirculation, as at low thermal ratings the entrainment ratio was low. This gave high concentrations of oxygen in the Coanda mixing throat which should have lowered the CO emissions.

However, the decrease in CO emissions as the thermal rating was increased can be explained through the increased velocity through the burner as the thermal rating was increased. The increased velocity led to an increase in the turbulent mixing energy and hence an increase in the reaction rate. Similarly, from figures (132) and (133), the increase in NOx emissions with increasing thermal ratings can be explained through the same reasons.

An alternative reason for the difference in NOx emissions can be explained through the mixing intensity obtained through the use of the 30 mm and 40 mm stabilising discs. Figures (132), (133) and (134) show that when using the 40 mm flame stabilising disc, the emissions of CO were less than when using 30 mm disc, except at very high air to fuel ratios, where the concentration of oxygen was such that the CO emissions were 0 ppm. As the combustion

reaction model used was mixing rate controlled, it can be assumed that the 40 mm disc was superior in mixing the fuel and oxygen.

Considering that the 40 mm stabilising disc provided a mechanism for increased mixing of fuel and oxygen over that of the 30 mm disc, an explanation can be made for the NOx results given in figures (132), (133) and (134). It was possible that the fuel and oxygen mixing differences led to the formation of near premixed mixtures after the flame stabiliser when using the 40 mm disc, whereas the use of the 30 mm disc resulted in a relatively fuel rich region.

Figures (132) and (133) show that the modelled NO emissions when using the 40 mm disc with oxygen outlet concentrations of 5% and 3% over the range of thermal ratings considered averaged between approximately 40 ppm and 80 ppm, respectively. Assuming that the 40 mm disc produced a near premixed mixture of air and fuel as it entered the combustion zone, this would imply that there was an increase in flame temperature when the air to fuel ratio was decreased. The increase in gas temperature led to increased production of thermal NO when using an outlet oxygen concentration of 3% as compared to 5%.

The theory that the use of the 40 mm disc produced a premixed mixture of air and fuel is also supported by figure (134). Figure (134) displays modelled NO and CO emissions for both 30 mm and 40 mm flame stabilising discs burning propane over a range of air to fuel ratios. When using the 40 mm disc, the gradual decrease in NO emissions as the air to fuel ratio was increased is typical of premixed combustion. Similarly, the NOx emissions from models using the 30 mm disc followed the staged combustion theory for NO formation. At an air to fuel ratio of 1.25, NOx emissions were at their highest. However, NO emissions decreased at air to fuel ratios both above and below 1.25. At air to fuel ratios greater than 1.4, the NOx emissions remained at a level significantly higher than when using a 40 mm disc. Figure (132) shows that when using the 30 mm disc under low air to fuel ratios, such as 3% oxygen at the burner outlet, lower concentrations of NO were emitted at most fuel mass

flow rates as compared to operating with an outlet oxygen concentration of 5%. This was because the fuel and oxygen mixture concentrations in the flame zone led to high NOx formation rates.

The significance of these results regarding air to fuel ratio and flame stabiliser diameter is important for the burner operating conditions. Under fuel lean conditions, where low temperature exit gases are required, good mixing of the air and fuel can be achieved through the use of a 40 mm flame stabilising disc. This diluted the combustion zone with inert gases, such as nitrogen which led to a decrease in peak temperatures and NOx emissions. However, good mixing was not desirable near to stoichiometric conditions, where high gas temperatures resulted in high NOx emissions.

When high temperature exit gases are required, the air to fuel ratio must be decreased to near stoichiometric conditions. To decrease NOx formation at these high temperatures, the formation of a fuel rich region after the flame stabiliser proved successful. The use of the 30 mm flame stabilising disc resulted in slower mixing of the fuel and oxidant, decreasing the peak flame temperature and NOx emissions.

6.1.3 **The effect of Coanda gap width**

When using a 30 mm flame stabilising disc, it was found in section 5.1.3.2, from table 8 that the entrainment ratios for a 0.2 and 0.5 mm Coanda gap width were 101.2% and 50.2%, respectively. It was also found that the oxygen concentration in the Coanda mixing throat for the 0.2 mm and 0.5 mm Coanda gap widths were 13.7% and 16.6%, respectively. Similarly, the concentrations of CO_2 and H_2O in the Coanda mixing throat were greater for the 0.2 mm Coanda gap width.

Figure (135) displays the NOx and CO emissions for 0.2 mm and 0.5 mm Coanda gap widths, using a 30 mm disc over a range of air to fuel ratios. The

low emissions of NO when using a 0.2 mm Coanda gap width close to stoichiometric conditions was caused by a decrease in the oxygen concentration and an increase in CO_2 and H_2O concentration prior to combustion.

Figure (136) displays the modelled NO emissions when using Coanda gap widths of 0.2 mm and 0.5 mm, with an outlet oxygen concentration of 6.5%. At up to 7 kW, the NO emissions increased with increasing fuel mass flow rate. When using the 0.2 mm Coanda gap width beyond 7 kW, the NO emissions decreased with increasing fuel mass flow rate.

At less than 7 kW, the initial increase in NO emissions when using the 0.2 mm Coanda gap width was attributed to an increase in the mixing turbulence brought about by the higher flow velocity over the flame stabiliser. The increase in turbulent mixing through the use of the 0.2 mm Coanda gap width was confirmed by figure (135), which showed that lower CO emissions were obtained at lower air to fuel ratios. As the thermal rating was increased beyond 7 kW, the subsequent decrease in NO emissions was due to the increased entrainment, reducing the oxygen concentration and increasing the concentrations of CO_2 and H_2O prior to combustion.

If the flue gas entrainment is sufficiently high, the decrease in O_2 concentration prior to combustion will be dominant over turbulent mixing in the formation of NOx as the thermal rating is increased. Also, the greater turbulent mixing created through the use of the smaller Coanda gap width leads to low emissions of CO.

6.1.4 **The effect of changing the fuel**

Figure (137) displays NOx emissions when burning propane and methane over a range of thermal ratings form 3 to 15 kW. NOx emissions when burning propane were found to be higher than those for methane. The slight difference in outlet oxygen concentration between the fuels used was not expected to be

the cause for this difference, as a correction for this would increase the difference in NOx emissions.

The calorific value of propane and methane are very similar, but there is a difference in their molecular weight. For a given mass of fuel, on a volumetric basis, approximately 2.75 times as much methane must be injected as propane. The difference in volume may account for a difference in the mixing between the fuel and air, although no difference was observed from the modelling pictures. The molecular compositions of methane and propane are also different, propane having a higher carbon to hydrogen ratio than methane. As a two step reaction mechanism was used, this may have had a significant effect on the positions of heat release within the burner, and hence NOx emissions. Also, propane would be expected to produce more prompt NOx than methane due to its higher carbon content. However, prompt NOx was not the reason for the difference in NOx emissions as only thermal NOx was calculated.

Endothermic dissociation reactions are present for the combustion of both methane and propane. However, the two step combustion model provided only a very limited ability to cope with this effect. The difference in modelled NOx emissions between the combustion of propane and methane was not likely to be accounted for through dissociation reactions.

These results showed that NOx reduction can be achieved through a change in fuel type from propane to methane. Although methane and natural gas are common industrial fuels, alternative fuels may be used which could result in low NOx combustion.

6.2 DISCUSSION OF EXPERIMENTAL RESULTS

6.2.1 Introduction

In this chapter, comparisons are made between experimental results obtained from the Coanda burner. These results are used to identify how the emissions and stability of the burner were affected by the Coanda gap width, stabiliser type, air to fuel ratio and fuel type.

6.2.2 Effect of the Coanda gap width on burner stability and emissions

The Coanda gap width used in the Coanda ejector influenced the entrainment of flue gases within the burner, the smaller gap width giving the greatest entrainment. Two Coanda gap widths of 0.2 mm and 0.5 mm were used with a variety of flame stabiliser discs to determine the effect that this had on the stability and emissions from the burner.

Experimental results and observations led to the tables given below, representing the NOx emission for both Coanda gap widths over a range of air to fuel ratios from 1.2 to 1.5.

The results given in table 14 display NOx emissions at 10 and 15 kW using propane as fuel. The data was obtained from figures (101) and (103), and figures (102) and (104), respectively.

Thermal rating kW	10	15
Lowest air to fuel ratio at which the burner became unstable when using 0.2 mm gap	1.14	1.2
Lowest air to fuel ratio at which the burner became unstable when using 0.5 mm gap	1.03	1.05
NOx emissions over an air to fuel ratio range of 1.2 to 1.5 for a 0.2 mm Coanda gap	30 to 25 ppm	33 to 23 ppm
NOx emissions over an air to fuel ratio range of 1.2 to 1.5 for a 0.5 mm Coanda gap	42 to 31 ppm	45 to 38 ppm
Overall NOx reduction in changing the Coanda gap width from 0.5 mm to 0.2 mm.	9 ppm (24.6%)	13.5 ppm (32.5%)

Table 14. NOx reductions obtained for a 40 mm disc stabiliser burning propane.

The results displayed in table 15 for a three finger flame stabiliser using 0.5 and 0.2 mm Coanda gap widths were obtained from figures (106) to (108) and figures (109) to (111), respectively.

Thermal rating kW	5	10	15
Lowest air to fuel ratio at which the burner became unstable when using 0.2 mm gap	1.23	1.13	1.26
Lowest air to fuel ratio at which the burner became unstable when using 0.5 mm gap	1.01	1.03	1.04
NOx emissions over an air to fuel ratio range of 1.2 to 1.5 for a 0.2 mm Coanda gap	16 ppm	30 to 20 ppm	42 to 27 ppm
NOx emissions over an air to fuel ratio range of 1.2 to 1.5 for a 0.5 mm Coanda gap	37 to 30 ppm	37 to 28 ppm	42 to 30 ppm
Overall NOx reduction in changing the Coanda gap width from 0.5 mm to 0.2 mm.	17.5 ppm (52%)	7.5 ppm (23%)	1.5 ppm (4.2%)

Table 15. NOx reduction obtained for a three finger stabiliser burning propane.

The results displayed in table 16 for the five finger flame stabiliser using 0.2 and 0.5 mm Coanda gap widths were obtained from figures (91) to (93) and figures (94) to (96), respectively.

Thermal rating kW	5	10	15
Lowest air to fuel ratio at which the burner became unstable when using 0.2 mm gap	1.32	1.25	1.25
Lowest air to fuel ratio at which the burner became unstable when using 0.5 mm gap	1.03	1.05	1.05
NOx emissions over an air to fuel ratio range of 1.2 to 1.5 for a 0.2 mm Coanda gap	16 to 17 ppm	27 to 20 ppm	30 to 22 ppm
NOx emissions over an air to fuel ratio range of 1.2 to 1.5 for a 0.5 mm Coanda gap	23 to 24 ppm	24 to 19 ppm	31 to 27 ppm
Overall NOx reduction in changing the Coanda gap width from 0.5 mm to 0.2 mm.	7 ppm (24.6%)	-2 ppm (-9.3%)	3 ppm (10.3%)

Table 16. NOx reduction obtained for a five finger stabiliser burning propane.

From tables 14 to 16, it is clear that the NOx emissions can be expected to decrease by approximately 20% when using a 0.2 mm Coanda gap width as compared to a 0.5 mm Coanda gap width. The decrease in NOx emissions was due to increased entrainment through the use of the 0.2 mm Coanda gap width. The reason for this was due to an increase in the concentration of CO_2 and H_2O, and a decrease in the concentration of oxygen prior to combustion. This resulted in a decrease in the formation of NOx. Also, the increased recirculation of NOx containing flue gases provided a mechanism for NOx reduction through reburning, converting NO into N_2. This NOx reduction mechanism is displayed in section 2.3.2.5.

Tables 14 to 16 showed that when using a 0.2 mm Coanda gap width, a reduction in flame stability was encountered when operating at low air to fuel ratios. For both the 40 mm disc and the three finger stabiliser, stable operation was achieved from an air to fuel ratio of 1.2 and above. However, the five

finger stabiliser was found to be stable with air to fuel ratios above 1.25 for most thermal ratings.

The reduction in flame stability through changing the stabiliser type could have been due to the reduction in the diameter and surface area of the stabiliser. A decrease in surface area increased the amount of flue gas being entrained and hence increased the flow velocity over the stabiliser. This could cause the flame to become detached from the flame stabiliser and 'blow off'. This reason for flame instability was unlikely as the flame was least stable near stoichiometric conditions, where the flow velocities were at their minimum. Under fuel lean conditions there were higher flow velocities over the flame stabiliser, but under these conditions the flame was found to be stable.

Assuming that there was no difference in flow pattern for the individual flame stabilisers as the Coanda gap width was changed from 0.2 mm to 0.5 mm, the remaining variable was the concentration of oxygen prior to combustion. From section 5.1.3.2, it was found that the higher entrainment properties of the 0.2 mm Coanda gap width resulted in a lower oxygen concentration in the Coanda throat prior to combustion. It is possible that the fuel - air mixture formed after flowing over the stabiliser was deficient in oxygen and could not sustain combustion. From section 5.1.3.5, it was found that increasing the air to fuel ratio did not necessarily increase the concentration of oxygen prior to combustion. However, the quantity of oxygen available for mixing with the fuel did increase. For this reason, the increased quantity of oxygen enabled stable combustion in the recirculation zone behind the flame stabiliser.

6.2.3 **The effect of flame stabiliser geometry**

Flame stability and NOx emissions over a range of air to fuel ratios were experimentally measured to provide information concerning the effect of the flame stabiliser geometry. It was generally found that the 40 mm disc resulted in the highest NOx emissions near stoichiometric combustion and that the 30

mm disc could not support combustion at any air to fuel ratios. The introduction of 'fingers' provided stable combustion and low NOx emissions near stoichiometric conditions. It was found that thick fingers resulted in high NOx emissions, and that thin fingers resulted in low NOx combustion. This signified that mixing small quantities of fuel and air to initiate combustion was preferable to larger scale mixing in the reduction of NOx formation.

The significance of these findings indicates that for low NOx burner operation near stoichiometric conditions, a small cross sectional area flame stabiliser is required. This gives a fuel rich region, providing a method for slow mixing between the fuel and oxygen, resulting in low NOx emissions. However, for this to succeed in low NOx formation, a method of flame stabilisation must be used that does not vigorously mix large quantities of the fuel and air.

6.2.4 **Effects of changing the fuel from propane to methane**

Due to the different physical properties of propane and methane, the operation of the burner, and the emissions varied when changing from one fuel to the other. To aid in the identification of how and the extent to which the NOx emissions were affected through changing the fuel type, selected experimental results have been tabulated.

The results displayed in table 17 are for the burner configurations utilising the eight finger flame stabiliser when burning propane and methane, using a 0.5 mm Coanda gap width. The results were obtained from figures (122) and (124) and figures (123) and (125), respectively.

Thermal rating kW	8	12
Lowest air to fuel ratio at which the burner became unstable when using propane	1.1	1.1
Lowest air to fuel ratio at which the burner became unstable when using methane	1.1	1.125
NOx emissions over an air to fuel ratio range of 1.1 to 1.5 when burning propane	39 to 36 ppm	46 to 49 ppm
NOx emissions over an air to fuel ratio range of 1.1 to 1.5 when burning methane	18 to 16 ppm	20 to 23 ppm
Overall NOx reduction in changing the fuel from propane to methane	20.5 ppm (54.7%)	26 ppm (54.7%)

Table 17. NOx reductions obtained when using an eight finger stabiliser.

The results displayed in table 18 are for burner configuration incorporating the 40 mm sectioned flame stabiliser when burning propane and methane, using a 0.5 mm Coanda gap width. The results were obtained from figures (115) and (116) and figures (117) and (118), respectively.

Thermal rating kW	10	15
Lowest air to fuel ratio at which the burner became unstable when using propane	1.17	1.15
Lowest air to fuel ratio at which the burner became unstable when using methane	1.17	1.1
NOx emissions over an air to fuel ratio range of 1.15 to 1.4 when burning propane	36 to 27 ppm	50 to 58 ppm
NOx emissions over an air to fuel ratio range of 1.1 to 1.4 when burning methane	53 to 32 ppm	36 to 33 ppm
Overall NOx reduction in changing the fuel from propane to methane	-11 ppm (-35%)	19.5 ppm (36%)

Table 18. NOx reductions obtained when using a 40 mm sectioned stabiliser.

It can be seen from table 17 that when using the eight finger stabiliser, NOx emissions were reduced by over 50% when changing the fuel from propane to methane. Table 18 shows that when using a 40 mm sectioned stabiliser, there was a 36% reduction in NOx emissions when operating at 15 kW, but an increase of 35% when operating at 10 kW.

From tables 17 and 18, it was generally found that significantly lower emissions of NOx were measured when burning methane rather than propane. There are five possible reasons that could account for the large differences in NOx emissions, these being the stoichiometric air requirement for methane and propane, dissociation reactions, fuel air mixing differences brought about by a difference in the molecular weights of methane and propane, products of combustion and prompt NO formation.

6.2.4.1 **Stoichiometric air requirements**

The stoichiometric air requirements for methane and propane are 17.167 kg and 15.605 kg air per kg of fuel, respectively. However, the ratios of stoichiometric air requirement and calorific values for each fuel are such that methane is equivalent to 99.8% of that of propane. It was unlikely that this small difference had any significant effect on thermal NOx formation.

6.2.4.2 **Dissociation reactions**

Endothermic dissociation reactions during the combustion of fuels leads to decreased peak temperatures. The intermediate species formed and the sequence of chemical reactions are different for the combustion of methane and propane. The dissociation reactions could be a significant reason why less NOx was formed with methane combustion. The importance of dissociation reactions and their effects on flame temperatures is given in section 3.4.4.1.

6.2.4.3 **Volumetric flow rates of propane and methane**

The difference in molecular weights of methane and propane provide a significant difference in volumetric fuel requirement. For each kilogram of fuel, 2.75 times the quantity of methane was injected as propane. The quantities of fuel injected into the burner were small in comparison to the volumetric flow rate and were unlikely to have a significant effect on NOx emissions. However, it was found experimentally that when using the five finger flame stabiliser combustion could be achieved for propane but not for methane. The compatibility of one gaseous fuel with another is expressed through the use of the Wobbe number, and is defined by equation (79).

$$\text{Wobbe number} = \frac{\text{Gross calorific value (MJ / m}^3\text{)}}{\{\text{Relative air density (air = 1)}\}^{0.5}} \qquad (79)$$

The Wobbe numbers for methane and propane are 55 and 78 MJ/m^3, respectively. This large difference in volumetric heat release was likely to be the cause for a significant proportion of the difference in NOx emissions when comparing the performance of identical burner configurations. It also explains why certain burner configurations could be run with one fuel but not the other.

6.2.4.4 **Products of combustion**

The products of methane and propane combustion vary in concentration. Methane combustion produces a significantly higher ratio of water vapour to CO_2 than propane combustion. The concentrations of CO_2 and H_2O could have altered the specific heat capacity of the recycled flue gas, decreasing the flue gas temperature and hence thermal NOx formation.

6.2.4.5 **Prompt NOx contribution**

With a higher ratio of carbon to hydrogen atoms, prompt NOx formation was expected to be higher when burning propane rather than methane. However, it is difficult to quantify whether prompt NOx formation could have contributed fully or in part to the differences in NOx emissions.

From table 16, it can be seen that the NOx emissions for propane, operating at 10 kW were between 24 and 19 ppm over an air to fuel ratio of 1.2 to 1.5. The experiments with methane were conducted at 8 kW and 12 kW, the results from these ratings are displayed in table 17. It can be seen that the average NOx concentration in the exit gases was approximately 20 ppm across the range of air to fuel ratios of 1.1 to 1.5. The difference in NOx emissions shows that there was a 13% reduction over the range considered when comparing methane to propane. However, these figures were taken from the best results obtained for a specific combination between fuel type and stabiliser.

6.2.5 **The effect of using swirl**

Swirl was incorporated into the burner through the use of removable, angled vanes which were located at the end of the Coanda throat. The vanes were bent to an angle of 80° from the horizontal. This provided a maximum swirl number of 0.121. The aim of introducing swirl was to provide increased mixing of the post flame gases to decrease CO emissions. A swirl number of less than 0.6 was chosen so that aerodynamic recirculation would not modify the fuel-air mixing behind the flame stabiliser.

From studying figures (91) to (96), it can be seen that swirl had very little effect on the emissions of CO, and had no effect on burner stability. However, NOx emissions decreased by 2 to 5 ppm over most air to fuel ratios for all the fuel flow rates considered. Figures (120) to (123) showed that when burning methane with an eight finger stabiliser, there was little difference in CO emissions and flame stability when approaching stoichiometric conditions. However, there was a slight increase of approximately 2 ppm in NOx emissions when using swirl.

The small differences in NO and CO emissions suggest that the swirl vanes had a minimal effect on increasing the mixing process of the post flame gases. This was because the swirl number used was small and did not provide sufficient radial momentum of the flue gases to create an aerodynamic recirculation region. Also, the swirl vanes were positioned at a radial location in the Coanda throat that consisted of high concentrations of oxygen but low concentrations of fuel. If a greater swirling angle had been used then lower CO emissions but higher NOx emissions would have been expected.

6.2.6 **In flame measurements**

Figures (126) to (129) display NOx and CO measurements along the axis of the burner when burning methane with oxygen outlet concentrations of 3.0% and

4.8%, respectively. When operating with an oxygen outlet of 4.8%, the NOx concentration was found to decrease slightly as the exit of the burner was approached. The decrease in concentration was due to dilution of the NOx produced into the surrounding gases as they travelled along the axis of the burner. However, when operating the burner with an oxygen outlet concentration of 3.0%, the NOx concentration was found to increase slightly towards the burner exit. This indicated that NOx was formed after the flame zone where oxygen rich gases mixed with the high temperature combustion products.

The measured concentrations of CO along the axis of the burner indicated that combustion was almost complete at approximately 12 cm from the burner exit. As samples were taken nearer the flame stabiliser, the concentration of CO increased sharply. In figures (126) and (128), the concentration of CO appeared to remain constant at 1800 ppm. In reality, the concentration of CO increased beyond this value but the CO analyser had reached its maximum measurable limit.

These results signify that under fuel lean conditions, a large proportion of NOx was formed in the flame stabilisation region. However, as the air to fuel ratio was decreased, NOx was formed along the length of the burner. As NOx formation is a post combustion process, these results suggest that the fuel - air mixing process given in section 6.1.2 is confirmed.

6.3 COMPARISON OF THE MODELLING AND EXPERIMENTAL RESULTS

6.3.1 Introduction

In this section, the modelling results are compared to the experimental results. The trends in the flow patterns and emissions have been used to explain the low emissions obtained experimentally.

6.3.2 Comparison of emissions for identical experimental and modelled burner configurations

6.3.2.1 Propane combustion using a 0.2 mm Coanda gap width and a 30 mm flame stabilising disc.

From figure (138), it can be observed that the experimental results indicated that the burner was stable between an air to fuel ratio of 1.27 to 1.65. The NOx emissions from the experimental results ranged from 28 ppm to 16 ppm, over the range considered and with CO emissions between 15 ppm to 35 ppm. However, the modelling results predicted that 35 ppm to 47 ppm of NO were emitted over the same air to fuel ratio range with no CO being emitted.

6.3.2.2 Propane combustion using a 0.5 mm Coanda gap width and a 30 mm flame stabilising disc.

When using a 0.5 mm Coanda gap width and a 30 mm disc, figure (139) was used to compare the experimental and modelling emissions over a range of air to fuel ratios from 1.0 to 1.82. Over this range, the experimental NOx emissions remained almost constant at approximately 30 ppm and the CO emissions varied from 430 ppm to 60 ppm. The modelled NO and CO emissions over the same air to fuel ratio range were between 150 ppm and 70

ppm and 1700 ppm to 0 ppm, respectively, with the emission of NO peaking at 200 ppm at an air to fuel ratio of 1.25.

6.3.2.3 **Propane combustion using a 0.5 mm Coanda gap with and a 40 mm flame stabilising disc.**

When burning propane with a 0.5 mm Coanda gap width and a 40 mm disc, figure (140) was used for comparing the results. The experimental results indicated that the burner was stable over an air to fuel ratio range of 1.05 to 1.55, with NOx and CO emissions of between 47 ppm to 27 ppm and 430 ppm to 50 ppm, respectively. The modelled NO and CO emissions over this range predicted emissions of 230 ppm to 50 ppm and 700 ppm to 0 ppm, respectively.

6.3.3 **Accuracy of the predicted NOx and CO emissions**

From figures (139) and (140), it can be seen that there were significant differences in concentrations of NOx and CO between the modelling and experimental results when approaching stoichiometric conditions when using the 0.5 mm Coanda gap width. However, there was close approximation to the experimental NOx and CO emissions at an air to fuel ratio greater than 1.4. As shown in figure (138), modelled NOx and CO predictions when using a 0.2 mm Coanda gap width resulted in concentrations that were significantly closer to the experimental results near stoichiometric conditions than when using a 0.5 mm Coanda gap width.

The differences in NOx and CO emissions were due to simplifications made in the modelling procedure. The most significant of these simplifications was the two step combustion model. The reaction rates involved for each reaction were governed by the fuel-air mixing rate, which caused the oxygen concentration in the reaction zone to decrease to 0%, and only after the reaction was complete was oxygen present. From experimental results, a

constant oxygen concentration was measured along the axis of the burner. This signifies that the reaction rate used in the model between the fuel and oxygen was too fast, over predicting peak temperatures and under predicting oxygen concentrations. The numerical solution obtained for the combustion model was then used by the NOx post processor to calculate the formation of NOx. As NOx formation was dependent on temperature and species concentrations, the inaccurate temperature and gas concentrations in the burner led to inaccurate NOx predictions. Rapid mixing of hot combustion products with cooler surrounding gases decreased the formation rate of thermal NOx. This resulted in closer NOx predictions by the model under fuel lean conditions.

A possible cause for the over prediction of NOx near stoichiometric conditions could have been due to several factors. Firstly, the model did not take into account the NOx reduction method of reburning. The reburning NOx reduction process would be most significant near stoichiometric conditions, where high concentrations of NOx in the flue gas were recirculated into a fuel rich environment. Secondly, the quantity of entrained flue gas in the Coanda burner could have been under predicted. This would have led to an over prediction in the NOx emissions by the model. Unfortunately, no experimental results were taken for the entrainment ratio of the Coanda burner. However, this theory was supported by the decrease in predicted NOx emissions near stoichiometric conditions when using a 0.2 mm Coanda gap width, indicating that NOx emissions decreased when the entrainment ratio increased. Other reasons that could account for the over prediction in modelled NOx include the assumption that there were no heat losses through the walls of the burner and that the flame stabiliser shape was slightly different to those modelled. The assumption not to include heat loses led to a slight increase in gas temperature but was not expected to greatly effect the results as the burner was lagged with insulation. The shape of the flame stabiliser chosen to model that of the five finger flame stabiliser was the 30 mm disc. This simplified the modelling procedure and was not expected to significantly alter the general flow pattern or resultant emissions.

A possible method of obtaining more accurate combustion temperatures and oxygen concentrations could be obtained through the use of an alternative combustion mechanism, such as the equilibrium chemistry, pdf scheme or a mechanism that involves a greater number of reactions and intermediate species. The introduction of intermediate reactions and endothermic dissociation reactions would lead to decreased peak temperatures and lower thermal NOx formation. Unfortunately, at the time of modelling the burner, the equilibrium chemistry model was unavailable. When available, it was not used because it was incapable of calculating NOx formation.

6.3.4 **Temperatures**

Temperature measurements were taken at the burner outlet using two platinum - rhodium thermocouples. The diameters of the thermocouples used were 0.65 mm and 0.1 mm. For the thermocouple to accurately measure the temperature of the combustion gases, correction calculations were performed on the experimental data collected. The thermocouple bead diameter was an important consideration in the calculation procedure, a smaller bead diameter led to a decrease in the correction required and therefore gave a more accurate measurement. The correction calculations used an iterative process to equate the convective heat transfer to, and the radiation heat losses from the thermocouple. The equations used to correct the experimental temperatures and sample calculations using the two thermocouples used are given in section 8.1.

Figure (141) shows that when burning propane using a five finger flame stabiliser, the burner outlet temperatures were similar for operation at 5, 10 and 15 kW. The thermocouple used consisted of a 0.65 mm R-type thermocouple. There was a slight increase in temperature as the mass flow rate of fuel was increased, which was one reason why NOx emissions increased with increasing the fuel mass flow rate. Figure (141) also displays the temperature predictions from the model when operating at 10 kW with a 30 mm stabilising disc. The

modelled outlet temperature was approximately 200 K higher than the experimentally corrected temperatures over most of the range considered. The difference in modelled and experimental outlet temperatures could have been due to two reasons. Firstly, the model incorporated no heat loses other than those of radiation to the outside, through the burner exit. In practice, although the burner was insulated, heat losses through the burner walls did exist. Secondly, the temperature correction error calculation for the 0.65 mm diameter thermocouple was shown to be large, typically up to 450 K. The correction error was calculated using assumptions concerned with the surrounding conditions, such as average background temperature. The use of these assumptions resulted in errors in the correction calculation.

Figure (142) displays the corrected experimental temperatures when utilising a 0.1 mm diameter thermocouple, which had a typical correction error of 250 K. As shown in figure (143), the smaller difference between the modelled temperatures and the corrected temperatures through the use of the 0.1 mm diameter thermocouple confirmed that the corrected temperatures for the 0.65 mm diameter thermocouple were inaccurate. The more accurate temperature measurements also confirmed that the assumption not to include heat loses through the burner walls was correct.

Figure (144) displays experimental temperature measurements for methane and propane combustion when using an eight finger flame stabiliser. Temperature measurements for methane and propane were taken through the use of 0.65 mm and 0.1 mm diameter thermocouples, respectively. There was a temperature difference of approximately 250 K over the entire range considered. This was due to the different thermocouples used for the temperature measurement. Figure (145) displays experimental temperature measurements for burning both methane and propane, using a 0.65 mm diameter thermocouple. For each fuel, stabiliser configurations which led to the least concentration of NOx being emitted were used. At an air to fuel ratio of 1.15, the outlet temperature was measured at approximately 1900 K for both fuels. Similar outlet temperatures for both methane and propane combustion

were obtained over a range of air to fuel ratios, decreasing in temperature as the ratio was increased. It can therefore be assumed that the temperatures measured were lower than the actual temperatures due to the large correction errors incurred with the 0.65 mm diameter thermocouple.

6.3.5 **Comparing the similarities between the model and experimental results**

The trends found from the modelling results were used to explain why the experimental emissions and burner performance were affected by changing the burner configuration. The variation in flame stability between the different stabilisers used can be explained through the help of the modelling results. Initial modelling results, which used the end of the fuel injector as the flame stabiliser showed that there was a high concentration of fuel in the flame stabilisation zone. Similarly, the model predicted that there was a higher concentration of fuel in the flame stabilisation region when using a 30 mm flame stabiliser as opposed to a 40 mm stabiliser. It was found through experimental work that when using the end of the fuel injector as a flame stabiliser, the onset of flame stability occurred only at very high air to fuel ratios. Flame stability nearer stoichiometric conditions was increased when a flame stabiliser to represent a 30 mm disc was attached to the end of the fuel injector. This trend of increased fuel concentration after the stabiliser as the diameter of the stabiliser decreased was used to explain why the burner became unstable near stoichiometric conditions when a flame stabiliser diameter of less than 40 mm was used.

Similarities regarding NOx emissions existed between the modelling and experimental results when the width of the Coanda gap was changed from 0.5 mm to 0.2 mm. The model predicted that there would be a reduction in NOx and CO emissions when the 0.2 mm Coanda gap width was used. The experimental results confirmed this trend in NOx emissions. Also, there was agreement that near stoichiometric conditions, NOx emissions would decrease as the flame stabiliser diameter decreased.

7. CONCLUSIONS

1. The current trend of lowering NOx emissions from combustion systems of all sizes has led to the development of low NOx combustion technology. Stoichiometric combustion conditions are favoured by industrial processes for the high temperatures obtained but produce the greatest quantity of NOx. A review of NOx reduction options showed that combustor redesign was the most cost effective method for NOx reduction, modifying the combustion process in a way that inhibited NOx formation. A Coanda burner was selected as a possible design to achieve low NOx emissions over a broad range of operating conditions.

2. To achieve the Coanda effect, a smooth curved surface was required. The use of body fitted co-ordinates provided an accurate burner geometry, enabling the model to simulate the Coanda effect. The use of 2-D axi-symmetric modelling enabled the evaluation of many flow conditions and configurations. The 2-D model did not accurately represent the flame stabilisers used in experimentation. However, the use of the 2-D model to provide trends was assumed to be of greater importance than fewer, complex 3-D models.

3. NOx emissions from the Coanda burner were found to be lowest when using a 0.2 mm Coanda gap width, resulting in 16 ppm NOx being emitted at an air to fuel ratio of 1.5. However, the use of a 0.2 mm Coanda gap width required an air supply pressure of up to 4 bar. Low NOx emissions could be obtained with lower air supply pressures through increasing the Coanda gap width.

4. The ratio of NO_2 to total NOx was found to be between 0 to 10 % under all air to fuel ratios.

5. The optimum burner configuration with respect to both NOx emissions and burner stability near stoichiometric conditions was found when using a 0.5

mm Coanda gap width. When burning propane, a five finger flame stabiliser resulted in NOx emissions as low as 19 ppm and a corrected gas outlet temperature of 2200 K at an air to fuel ratio of 1.1. However, when burning methane, a combination of a 30 mm disc and an eight finger flame stabiliser resulted in NOx emissions as low as 16 ppm.

6. It was found that the lowest NOx emissions near stoichiometric conditions were obtained through a decrease in the surface area of the flame stabiliser and the use of thin 'fingers'.

7. The CFD model accurately predicted the exit gas temperatures at all air to fuel ratios. The two step combustion mechanism enabled the prediction of CO, but the fast chemistry reaction used did not accurately predict the in-flame gas species concentrations and temperatures. However, the model did predict the trends and exit gas CO concentration with reasonable accuracy.

8. The NOx post-processor used to predict NOx from the converged flow solution was inaccurate near stoichiometric conditions. It was thought that these inaccuracies were caused by simplifications in the combustion model and the exclusion of the NOx destruction process, known as reburn, in the large quantities of recycled flue gases.

9. The quantity of flue gas recirculation was predicted to increase as the Coanda gap width decreased for a given Coanda throat area. The mass of recirculated gas as a percentage of the air mass flow rate when using 0.2 mm and 0.5 mm Coanda gap widths were predicted by the model as 101.2 % and 50.2 %, respectively.

10. Flue gas recirculation quantity, flame stability, flame stabiliser shape and operational limits proved to be interlinked in the reduction of NOx emissions. It was found that fuel-air mixing was controlled by the entrainment properties of the Coanda ejector. The average oxygen

concentration entering the combustion chamber when using 0.2 mm and 0.5 mm Coanda gap widths were 13.7 % and 16.6 %, respectively. Due to the position of the fuel injector, a fuel rich region formed behind the flame stabiliser. With a suitable flame stabiliser geometry and the use of 'fingers', low NOx combustion and flame stability was achieved near stoichiometric conditions. This characteristic of high temperature flue gas with low NOx emissions makes the Coanda burner attractive for many commercial applications.

7.1 **FURTHER WORK**

Further work would include the following:

1. The scale of the burner could be increased to evaluate its NOx reducing potential when incorporated into a furnace.

2. The mechanisms of blue flame combustion could be investigated.

3. The use of this type of burner could be extended to include liquid fuels, such as kerosene or alcohols.

4. Following the success of low NOx emissions near stoichiometric conditions, the use of substantial air preheat could be evaluated with respect to NOx emissions. This would enable the investigation of the suitability of the burner for very high temperature processes, such as glass furnaces.

5. Detailed 3-D modelling of the flame stabilisers would be done to study the mixing processes obtained. This would lead to improved flame stabiliser designs for stable, low NOx combustion.

6. Gas sampling and flow measurements of the recycled gas would be obtained to experimentally verify the modelling predictions and be used to determine the effect this has on flame stability and colour.

8. APPENDIX

8.1 THERMOCOUPLE CORRECTION CALCULATIONS

A heat balance at the thermocouple bead is resolved in the following way:

convection to the bead = radiation from the bead

$$h_c\left(T_{gas} - T_{TC}\right) = \delta\sigma\left(T_{TC}^4 - T_{amb}^4\right) \qquad (77)$$

Where h_c is the convective heat transfer coefficient, δ is the thermocouple emmisivity and σ is the Stefan Boltzman constant ($5.6697E^{-8}$).

The convective heat transfer coefficient, h_c, is dependent on the local flow conditions and is expressed in terms of Nusselt number correlations, as given in equation (80)

$$Nu = a\,\mathrm{Re}^b\,\mathrm{Pr}^c \qquad (80)$$

For a thermocouple placed perpendicular to the flow of gas, the Nusselt number is calculated from:

$$Nu = (0.38 \rightarrow 0.5)\,\mathrm{Re}^{0.5}$$

Typical values used in the thermocouple correction calculations are given in table 19.

Bead diameter m	6.50E-04	Ambient temperature K	500
Outlet velocity m/s	5	Thermocouple temp K	1273
Density kg/m^3	0.235		
Viscosity	5.40E-05	Corrected gas temp K	1603.817
Reynolds number	14.14352	Error	330.8173
Nusselt number	1.617138		
Epsilon	0.5		
Stefan Boltzman constant σ	5.67E-08		
Heat transfer coefficient	219.682		

Table 19. Typical values used in a thermocouple correction calculation.

Figure (143) displays the deviation between the thermocouple and actual temperatures when using a 0.1 mm and 0.65 mm diameter thermocouple. The results are based on the assumption that the burner is operating at 10 kW. To allow for the differences in temperature that the thermocouple radiated heat to, the ambient temperature was estimated at 500 K.

8.2 **ROTAMETER CALIBRATION**

The two gas rotameters used to measure the flow rate of air and fuel were calibrated through the use of correlations for standard metric rotameter sizes using duralumin floats. The air supply pressure to the Coanda ejector was variable with flow rate. Pressure readings were taken between the rotameter outlet and the Coanda inlet at 1 cm intervals on the rotameter scale and the air flow rate was calculated at each of these points. This procedure was not required for the fuel rotameter as the pressure variation with flow rate was insignificant. Figure (147) displays the variation of air flow rate with rotameter scale. It also displays the air flow rate required over a range of air to fuel ratios as the fuel rotameter scale is increased.

8.3 CALCULATION OF SWIRL NUMBER

The angular momentum, G_φ, can be calculated from equation (81).

$$G_\varphi = 2\pi\rho U_0^{\,2} \tan\alpha \frac{r^3 - r_h^{\,3}}{3} \tag{81}$$

and the axial momentum, G_x can be calculated from equation (82).

$$G_x = \pi\rho U_0^{\,2}\left(r^2 - r_h^{\,2}\right) \tag{82}$$

Equations (81) and (82) can be combined and used to calculate the swirl number as given by equation (83).

$$Sw = \frac{G_\varphi}{G_x r} = \frac{2}{3}\left[\frac{1-\left(r_h/r\right)^3}{1-\left(r_h/r\right)^2}\right]\tan\alpha \tag{83}$$

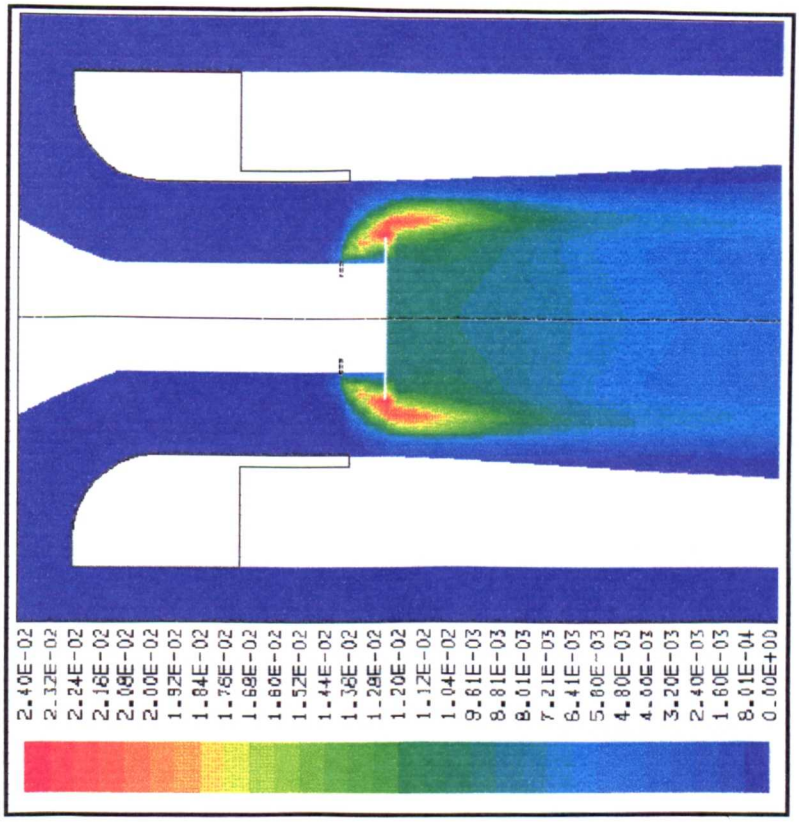

Figure 28. Mol fraction of CO when using a 0.2 mm Coanda gap width and burning propane

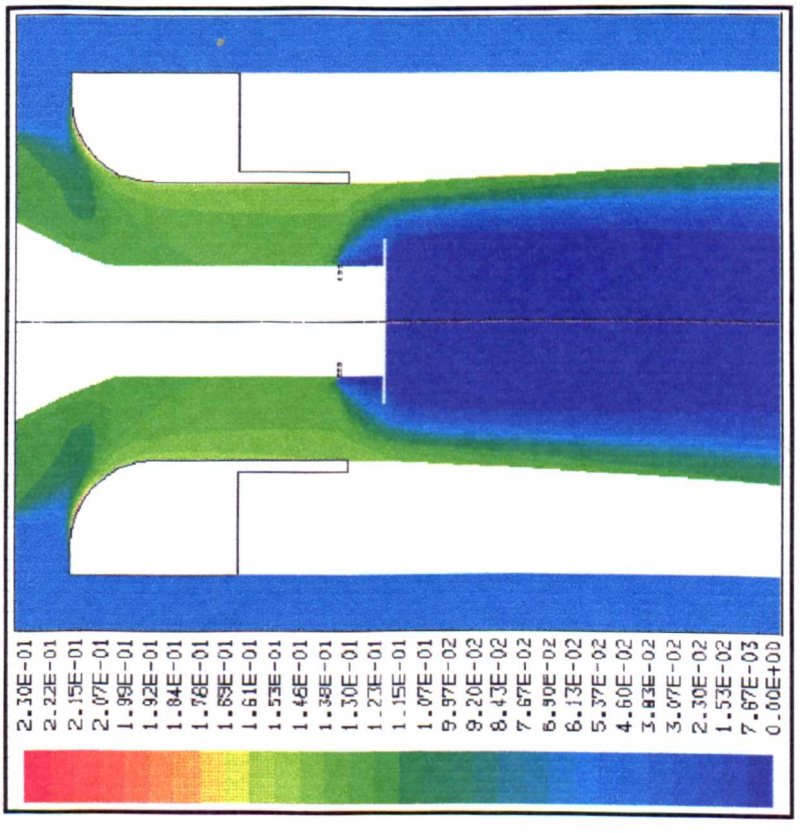

Figure 29. Oxygen mol fraction when using a 0.2 mm Coanda gap width and burning propane

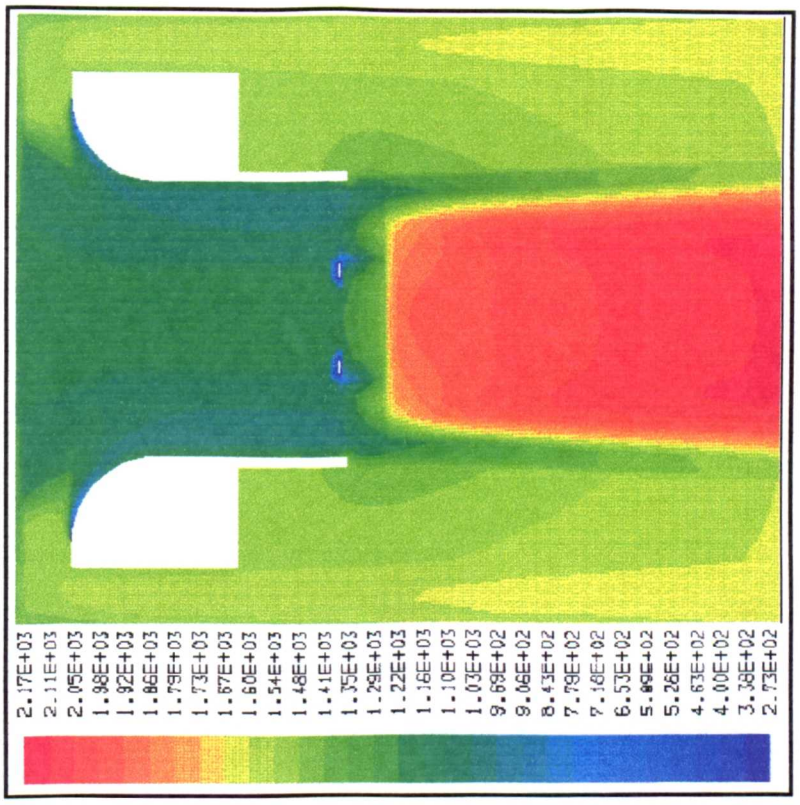

Figure 30. Temperature, Kelvin, when using a 0.2 mm Coanda gap width and burning propane

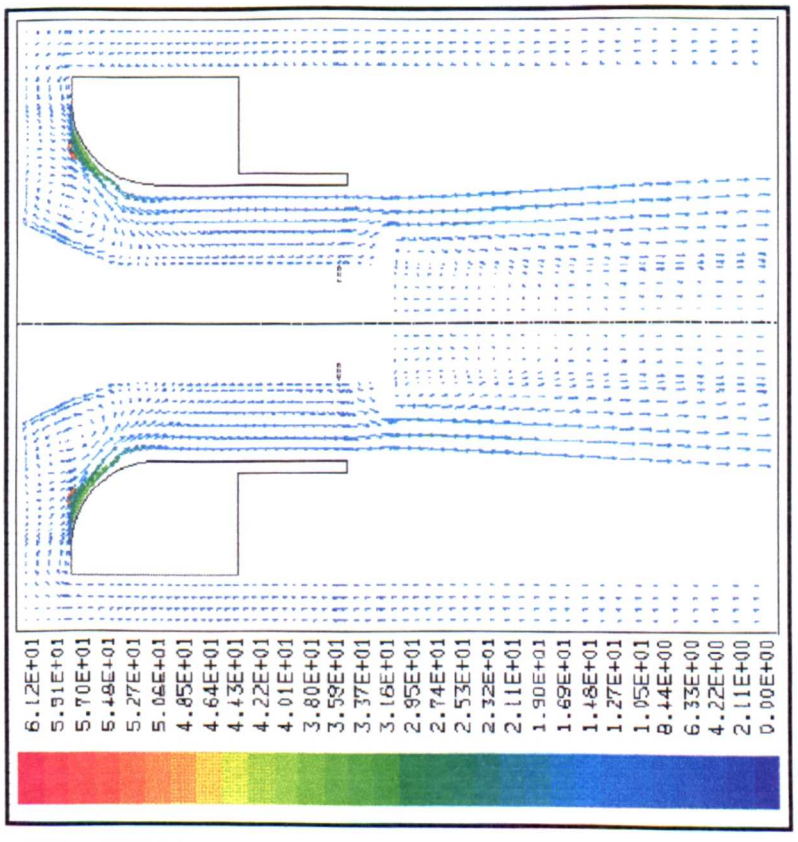

Figure 31. Velocity vectors when using a 0.2 mm Coanda gap width and burning propane

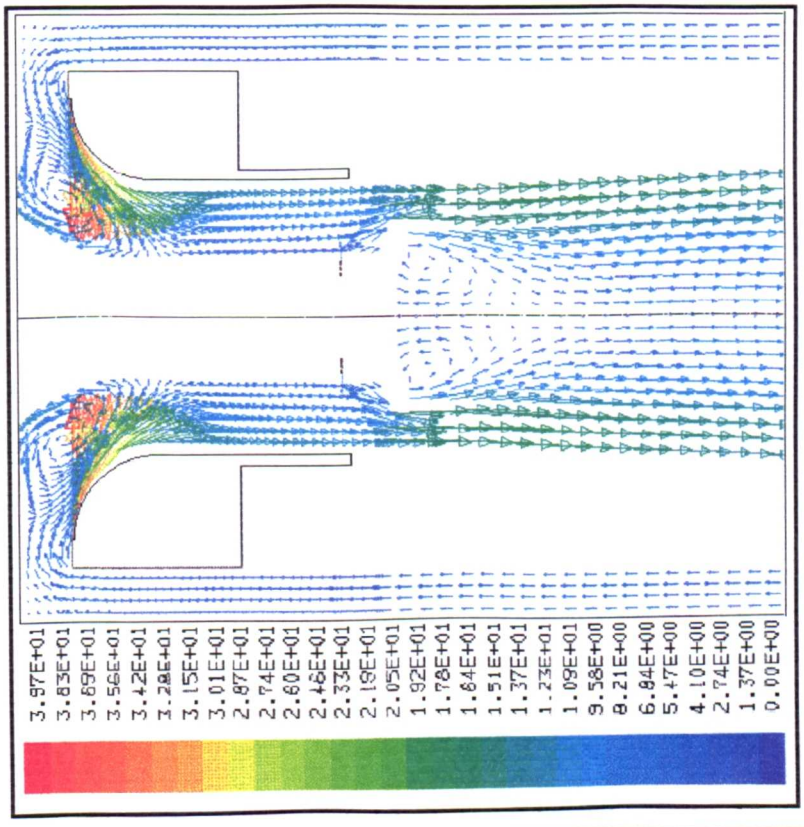

Figure 32. Velocity vectors, m/s, when using a 0.5 mm Coanda gap width and burning propane

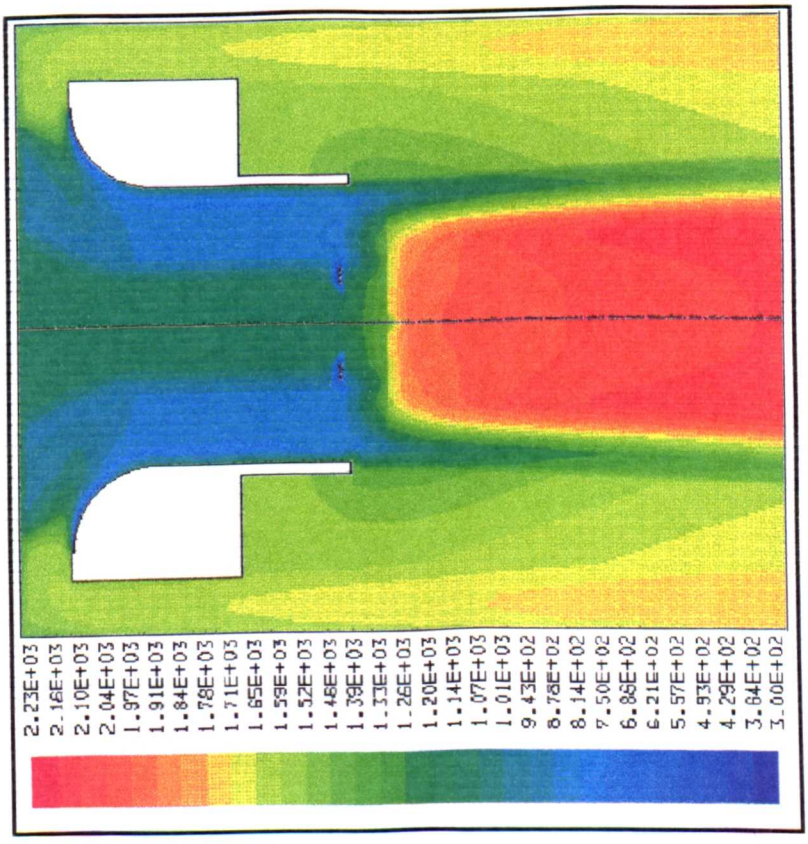

Figure 33. Temperature, Kelvin, when using a 0.5 mm Coanda gap width and burning propane

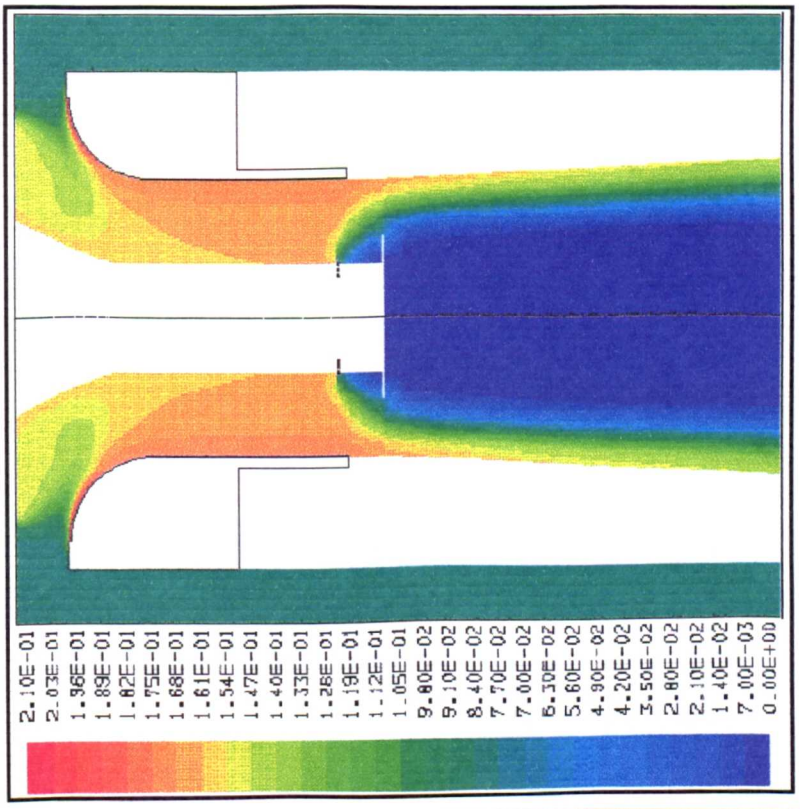

Figure 34. Oxygen mol fraction when using a 0.5 mm Coanda gap width and burning propane

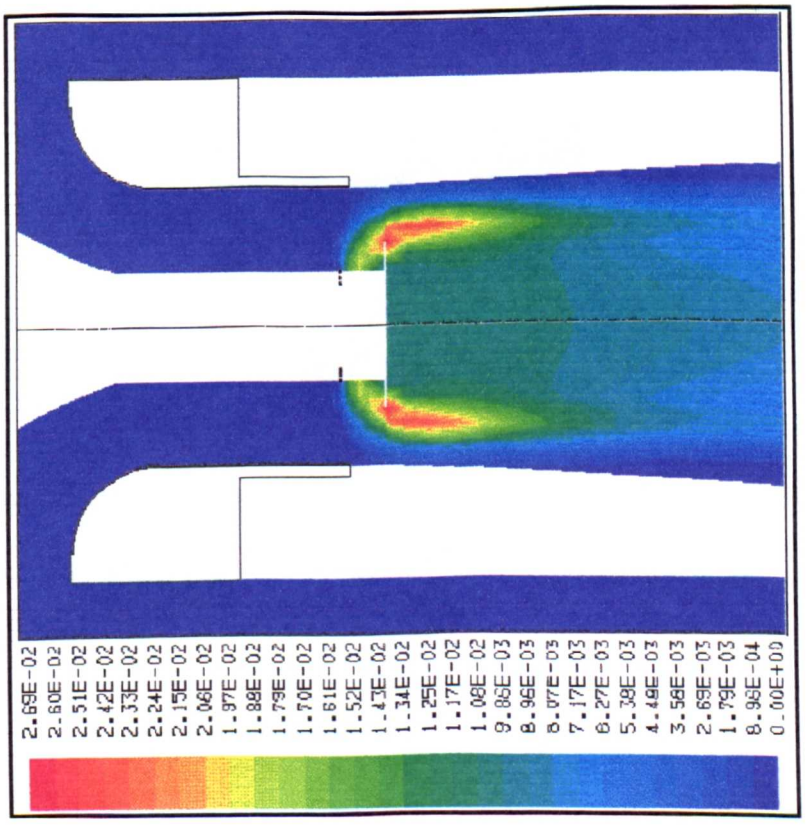

Figure 35. CO mol fraction when using a 0.5 mm Coanda gap width and burning propane

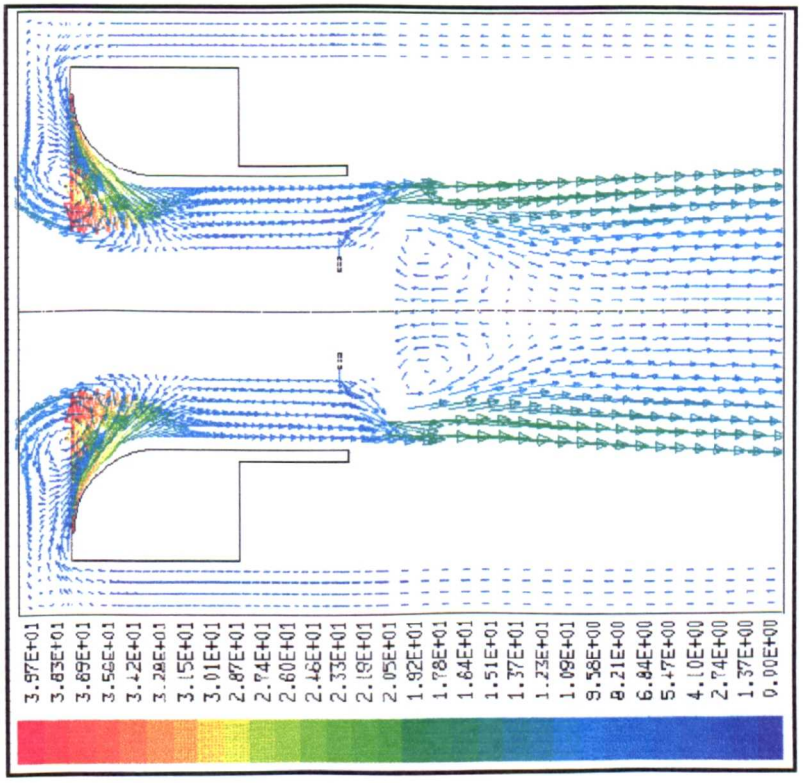

Figure 36. Velocity vectors, m/s, when using a 40 mm flame stabilization disc burning propane.

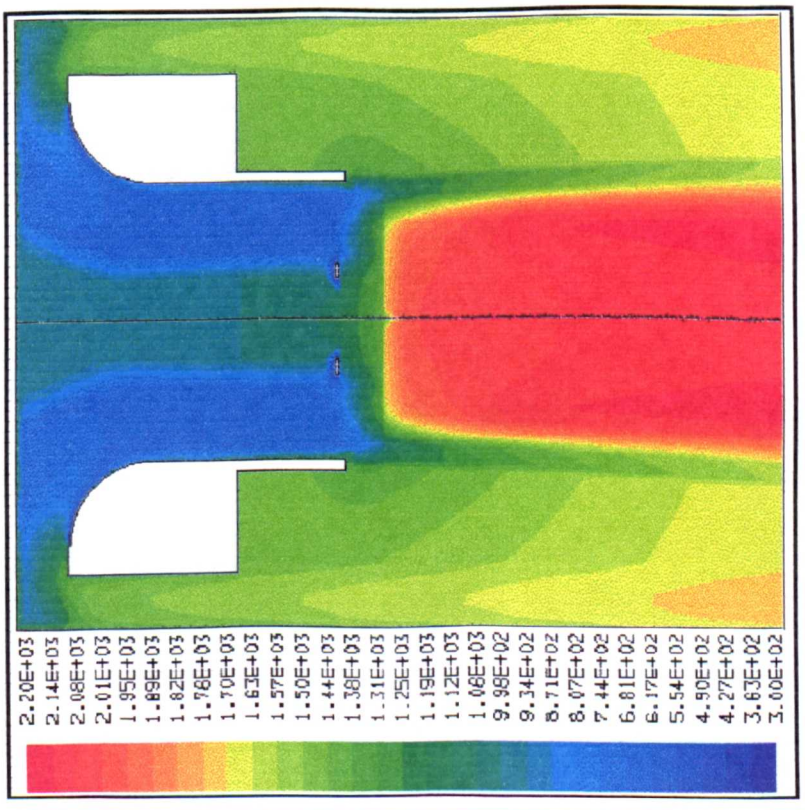

Figure 37. Temperature, Kelvin, when using a 40 mm flame stabilization disc burning propane.

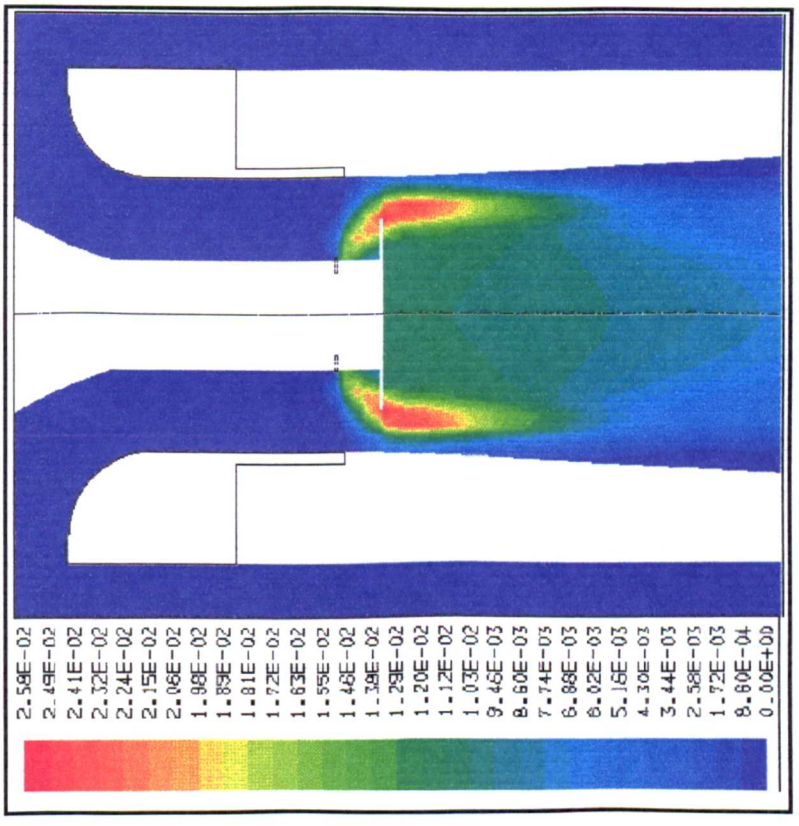

Figure 38. CO mol fraction when using a 40 mm flame stabilization disc burning propane.

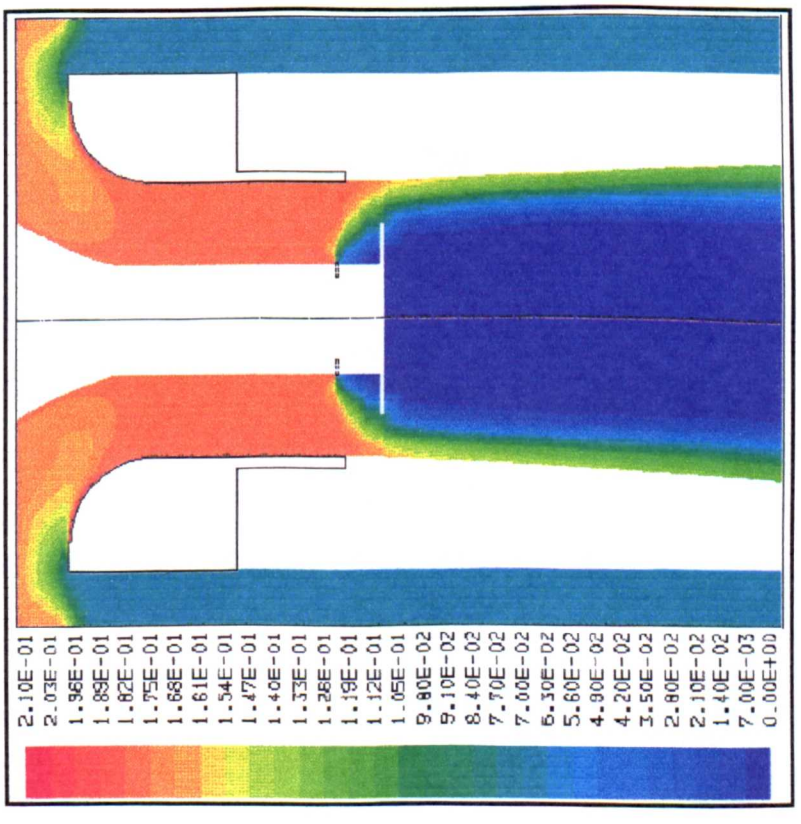

Figure 39. Oxygen mol fraction when using a 40 mm flame stabilization disc burning propane.

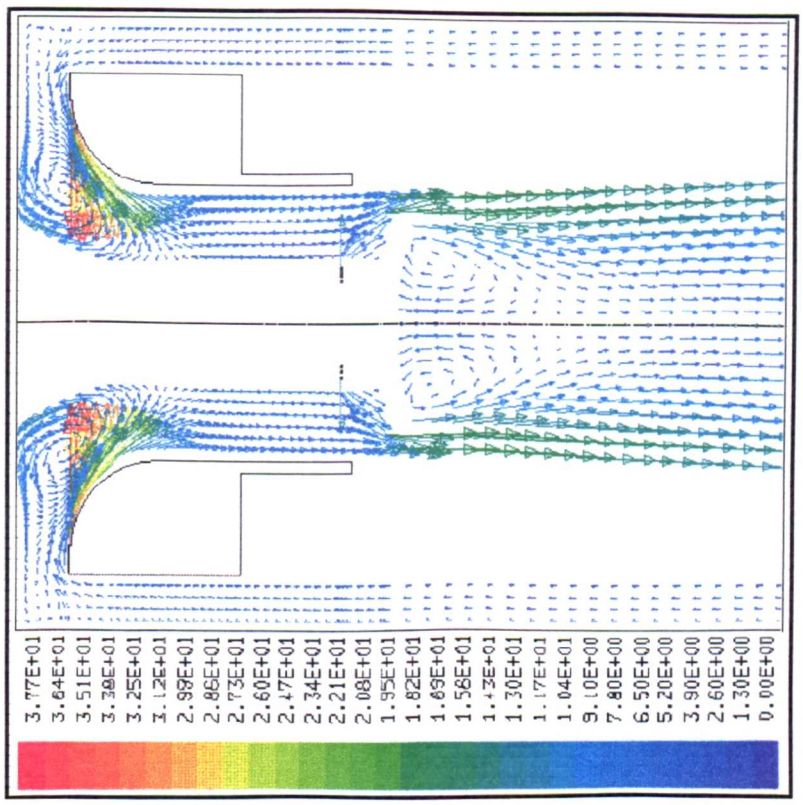

Figure 40. Velocity vectors, m/s, when using a 40 mm flame stabilization disc and burning methane.

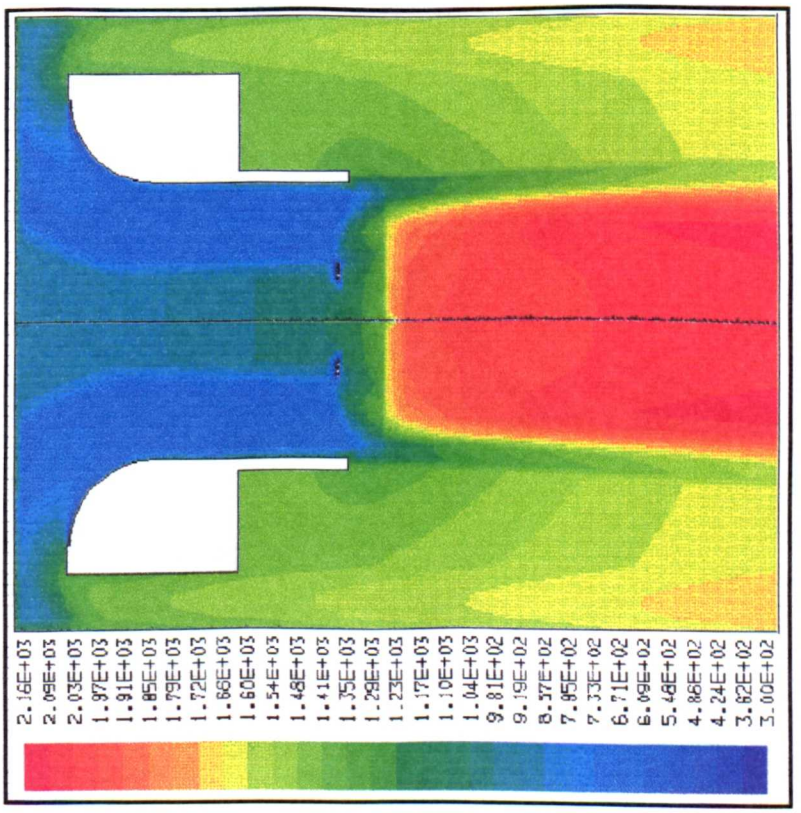

Figure 41. Temperature, Kelvin, when using a 40 mm flame stabilization disc and burning methane.

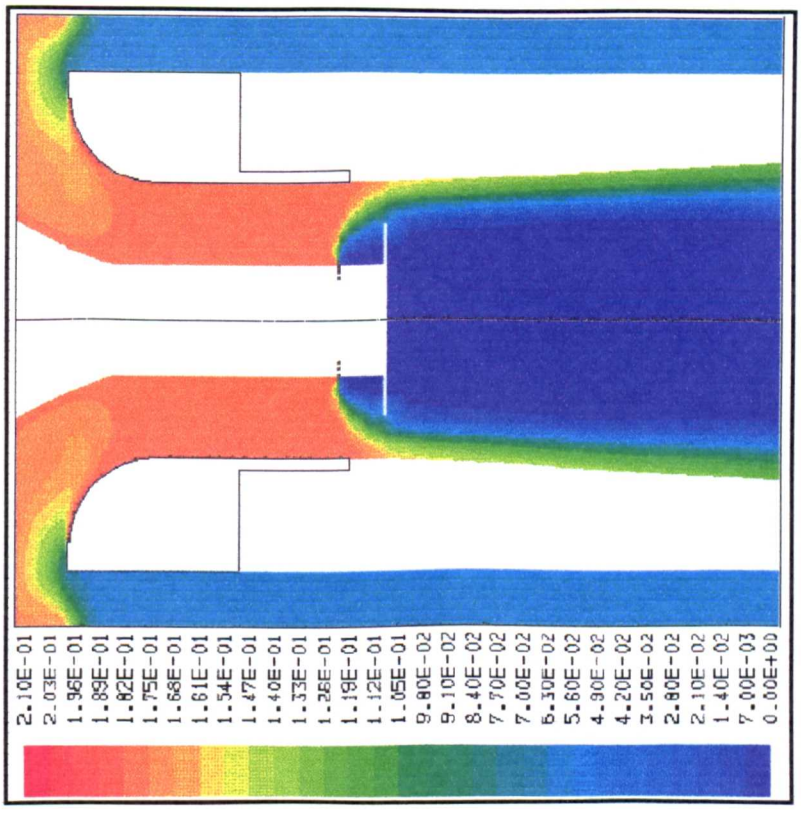

Figure 42. Oxygen mol fraction when using a 40 mm flame stabilization disc and burning methane.

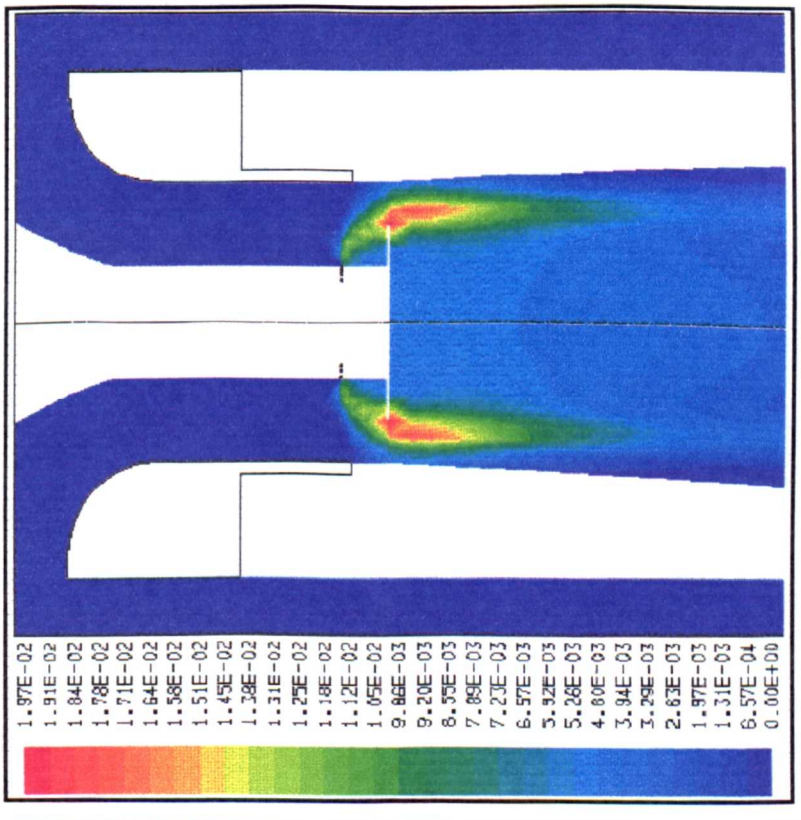

Figure 43. CO mol fraction when using a 40 mm flame stabilization disc and burning methane.

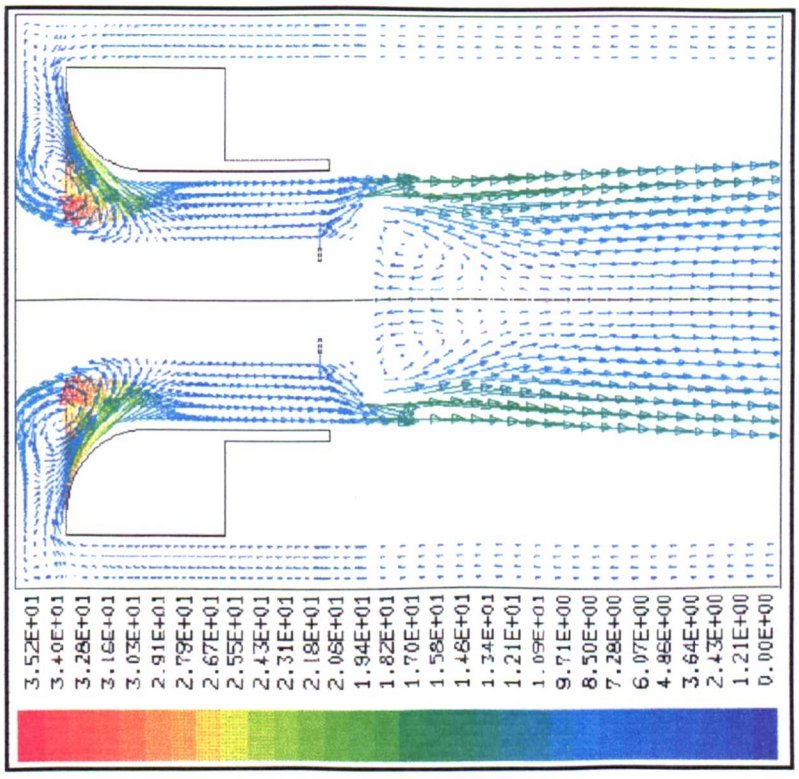

Figure 44. Velocity vectors, m/s, when burning propane using a 40 mm disc and an outlet oxygen concentration of 2.5%.

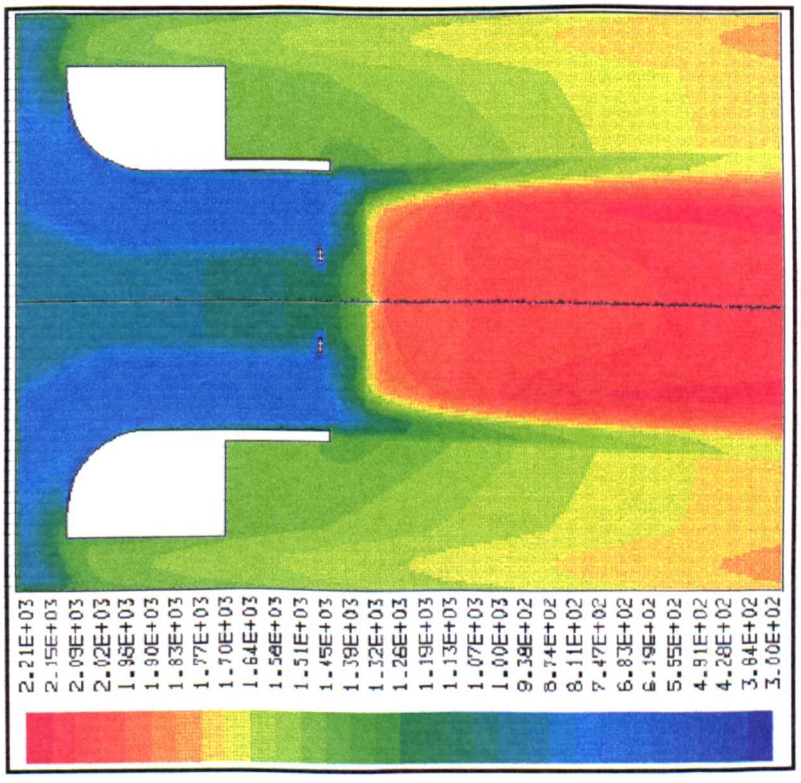

Figure 45. Temperature, Kelvin, when burning propane using a 40 mm disc and an outlet oxygen concentration of 2.5%.

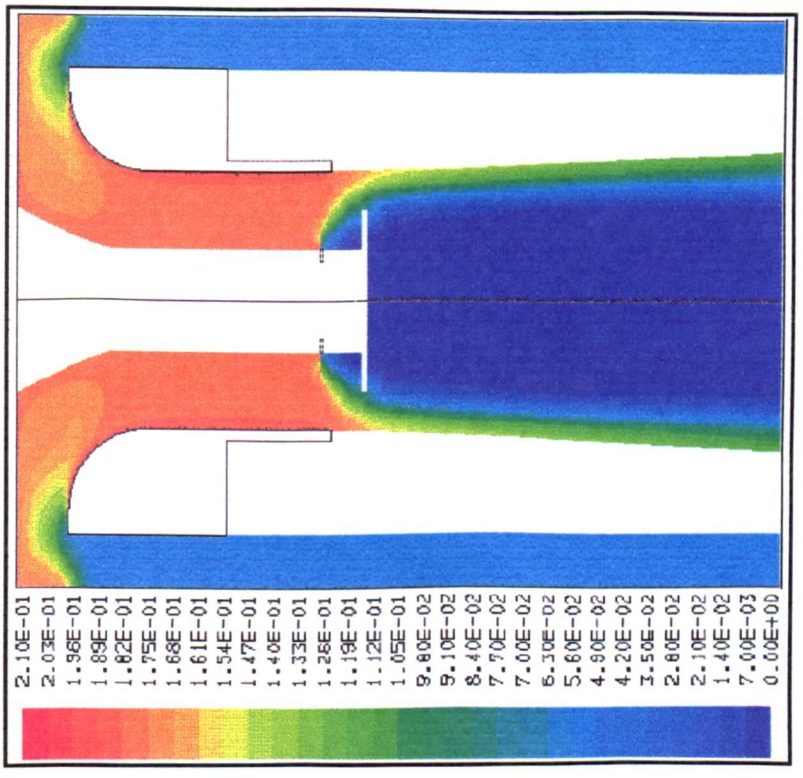

Figure 46. Oxygen mol fraction when burning propane using a 40 mm disc and an outlet oxygen concentration of 2.5%.

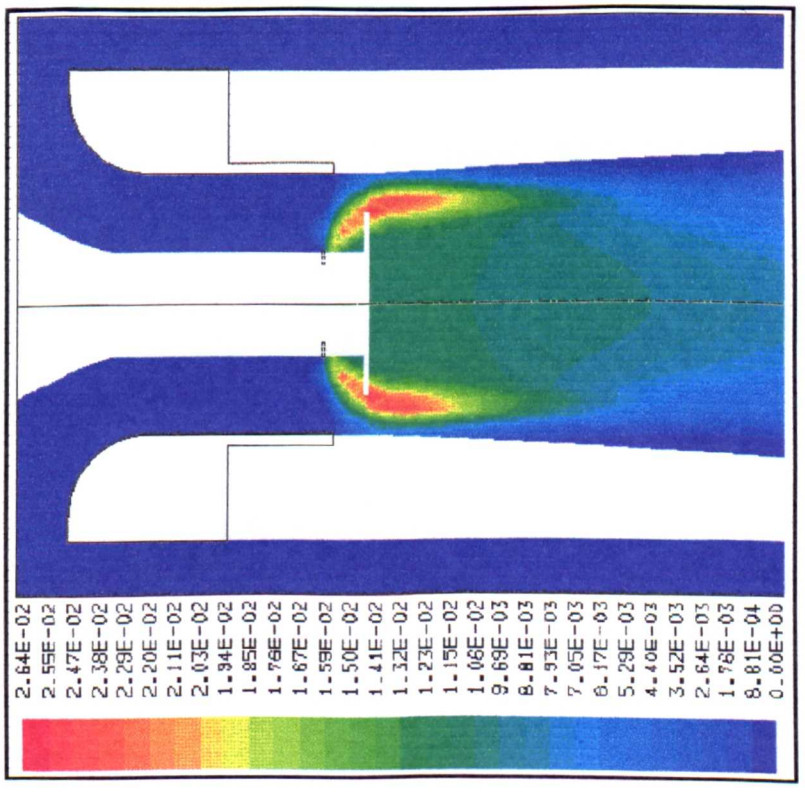

Figure 47. CO mol fraction when burning propane using a 40 mm disc and an outlet oxygen concentration of 2.5%.

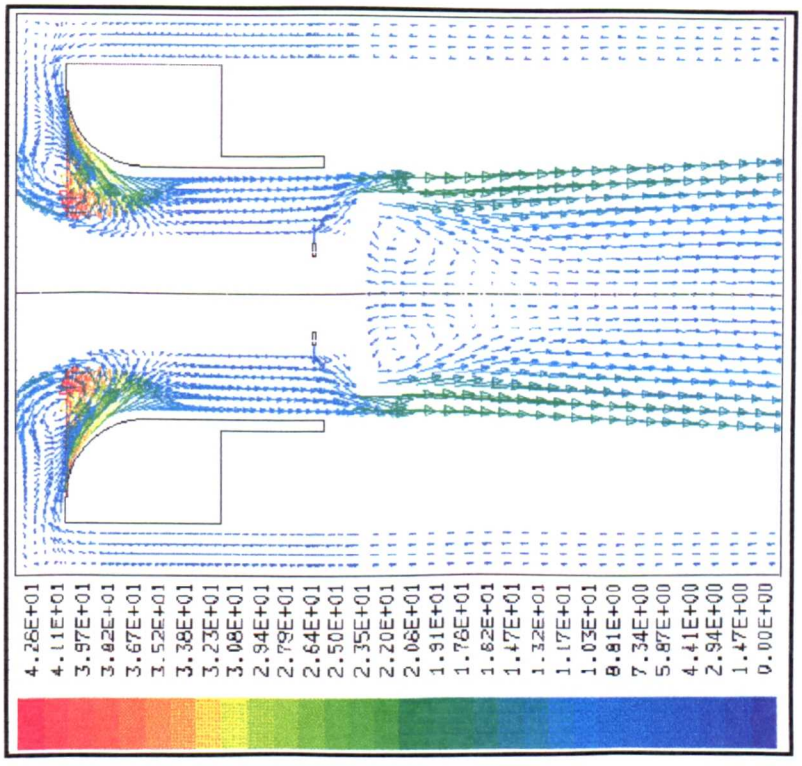

Figure 48. Velocity vectors, m/s, when burning propane with an outlet oxygen concentration of 5.1% and using a 40 mm flame stabilizing disc.

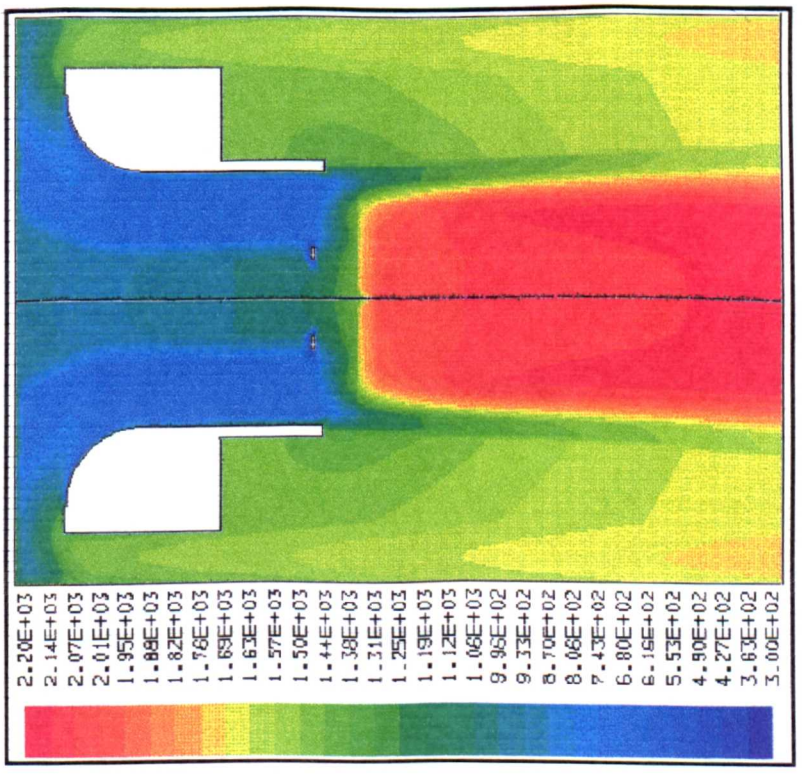

Figure 49. Temperature, Kelvin, when burning propane with an outlet oxygen concentration of 5.1% and using a 40 mm flame stabilizing disc.

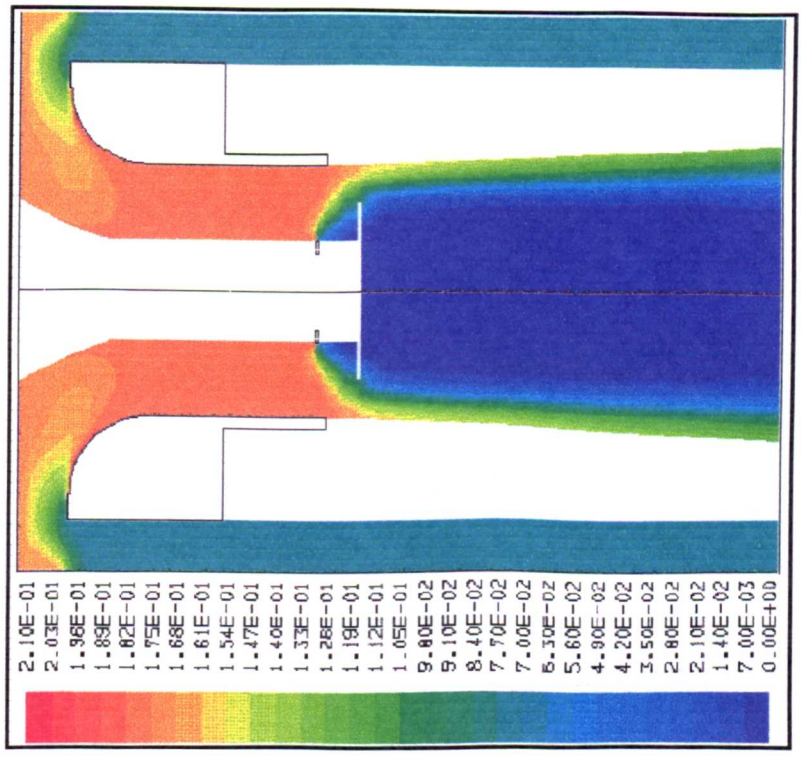

Figure 50. Oxygen mol fraction when burning propane with an outlet oxygen concentration of 5.1% and using a 40 mm flame stabilizing disc.

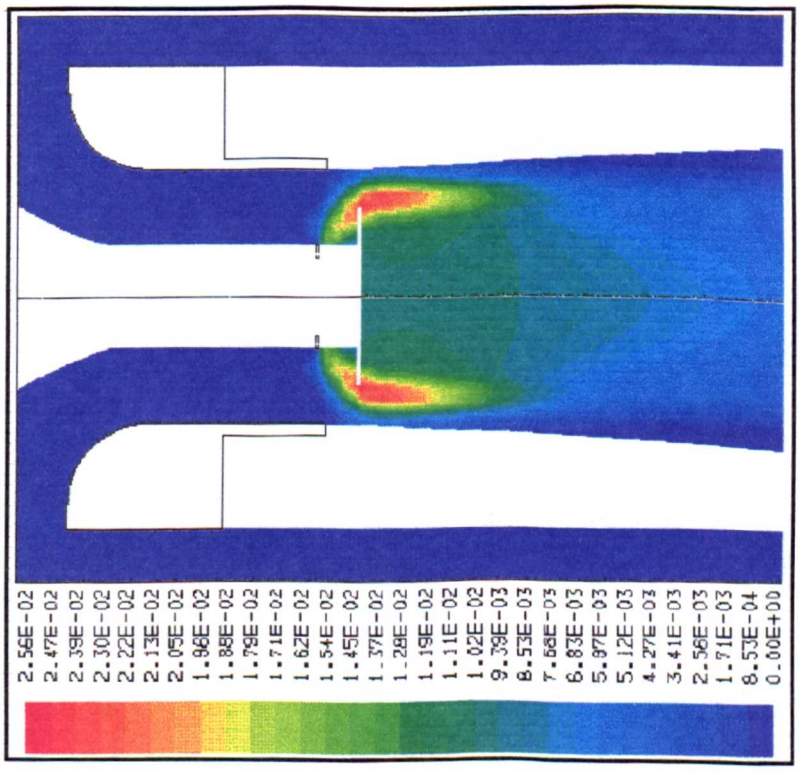

Figure 51. CO mol fraction when burning propane with an outlet oxygen concentration of 5.1% and using a 40 mm flame stabilizing disc.

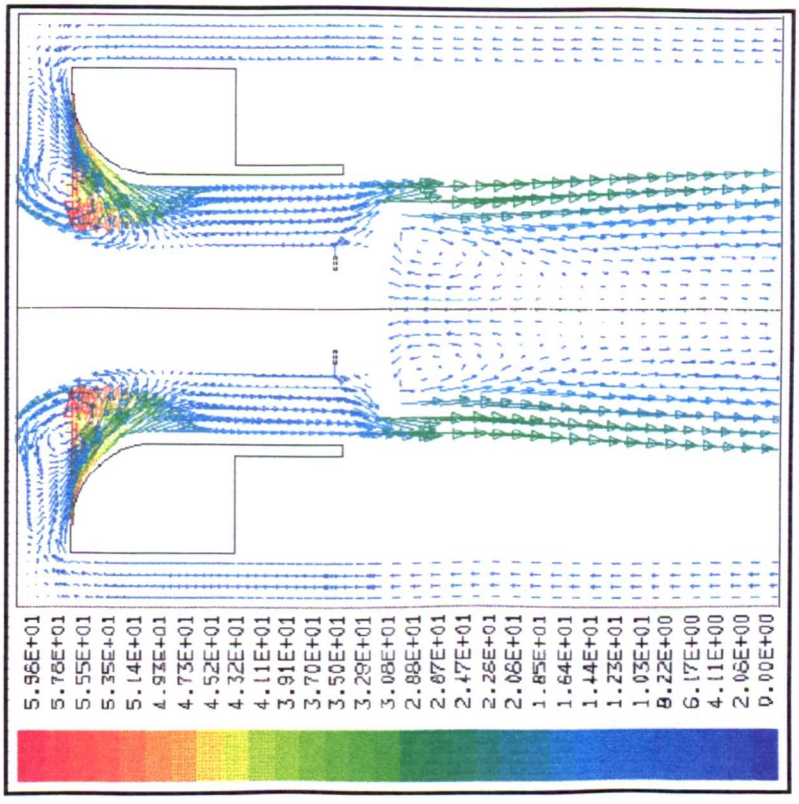

Figure 52. Velocity vectors, m/s, when burning propane with an oxygen outlet concentration of 9.4% and a 40 mm flame stabilizing disc.

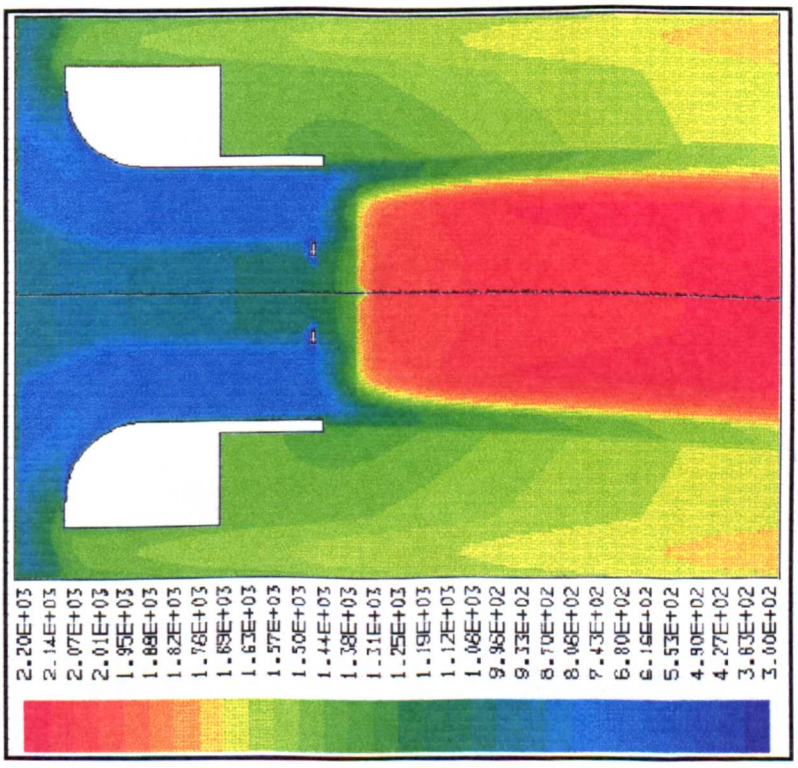

Figure 53. Temperature, Kelvin, when burning propane with an oxygen outlet concentration of 9.4% and a 40 mm flame stabilizing disc.

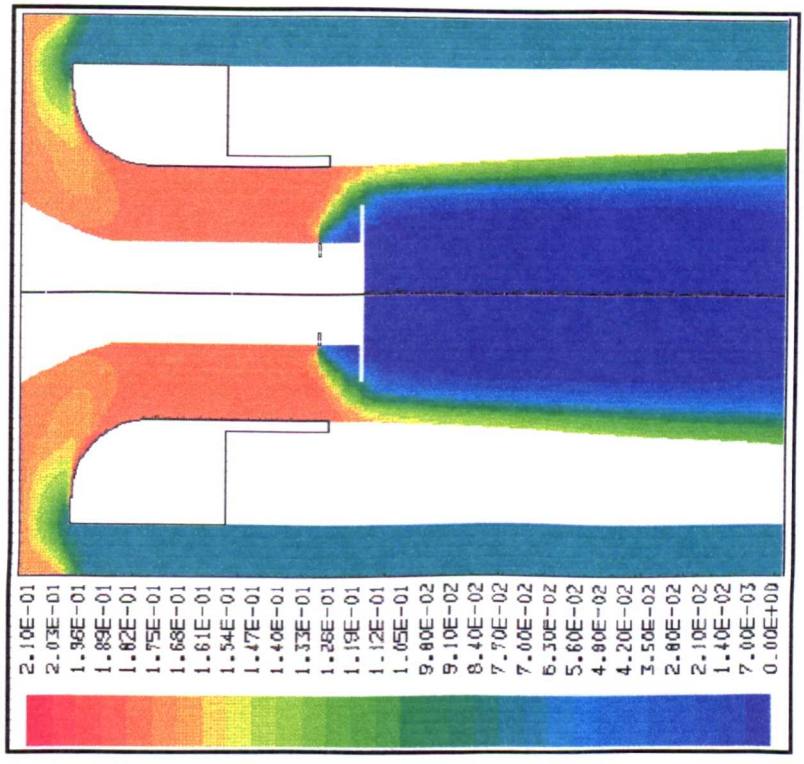

Figure 54. Oxygen mol fraction when burning propane with an oxygen outlet concentration of 9.4% and a 40 mm flame stabilizing disc.

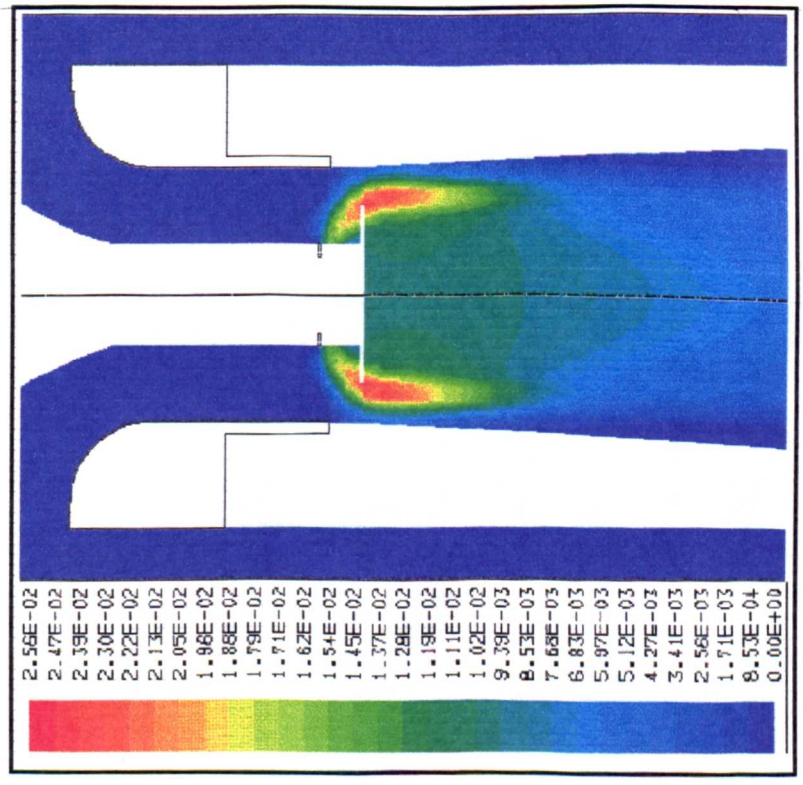

Figure 55.CO mol fraction when burning propane with an oxygen outlet concentration of 9.4% and a 40 mm flame stabilizing disc.

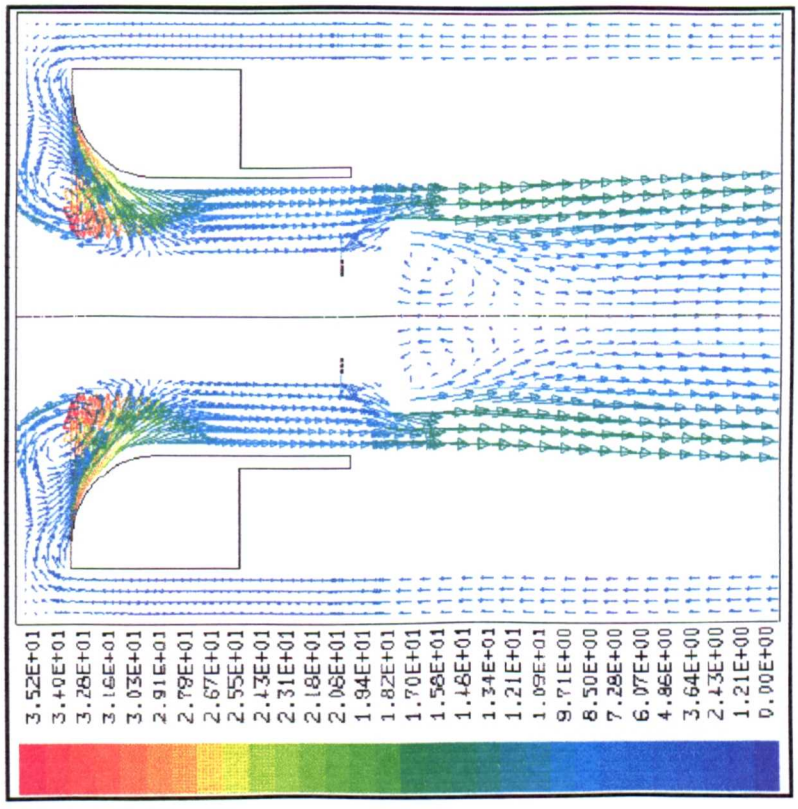

Figure 56. Velocity vectors, m/s, when burning propane with an outlet oxygen concentration of 2.7% and a 30 mm flame stabilizing disc.

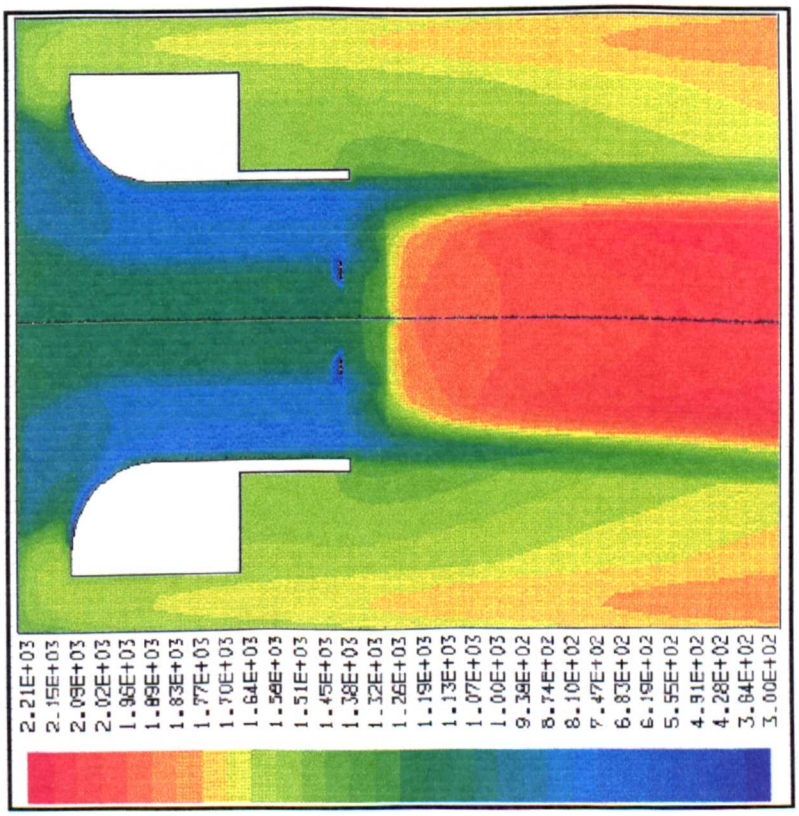

Figure 57. Temperature, Kelvin, when burning propane with an outlet oxygen concentration of 2.7% and a 30 mm flame stabilizing disc.

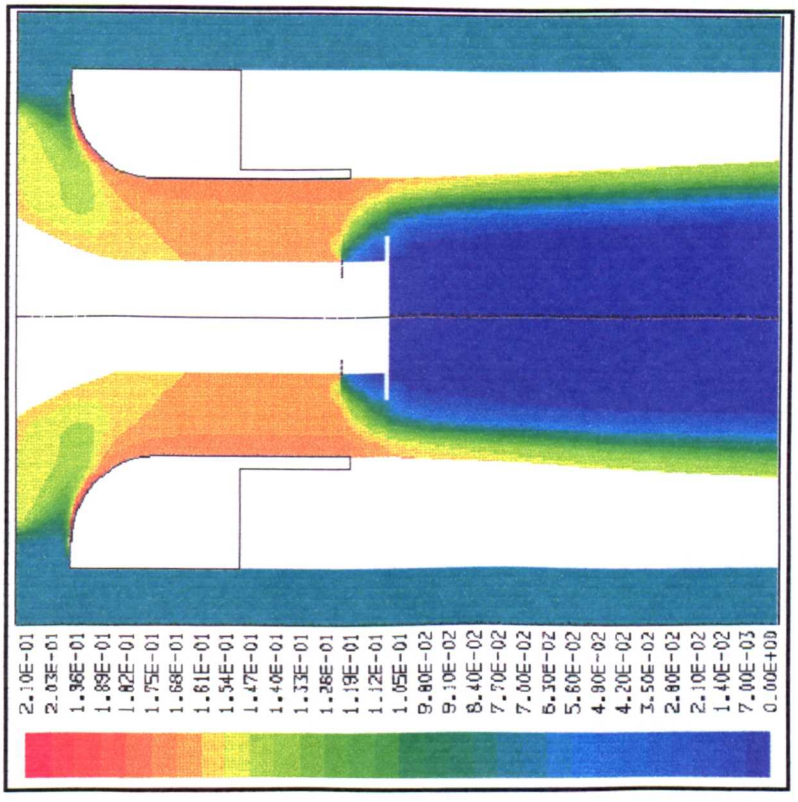

Figure 58. Oxygen mol fraction when burning propane with an outlet oxygen concentration of 2.7% and a 30 mm flame stabilizing disc.

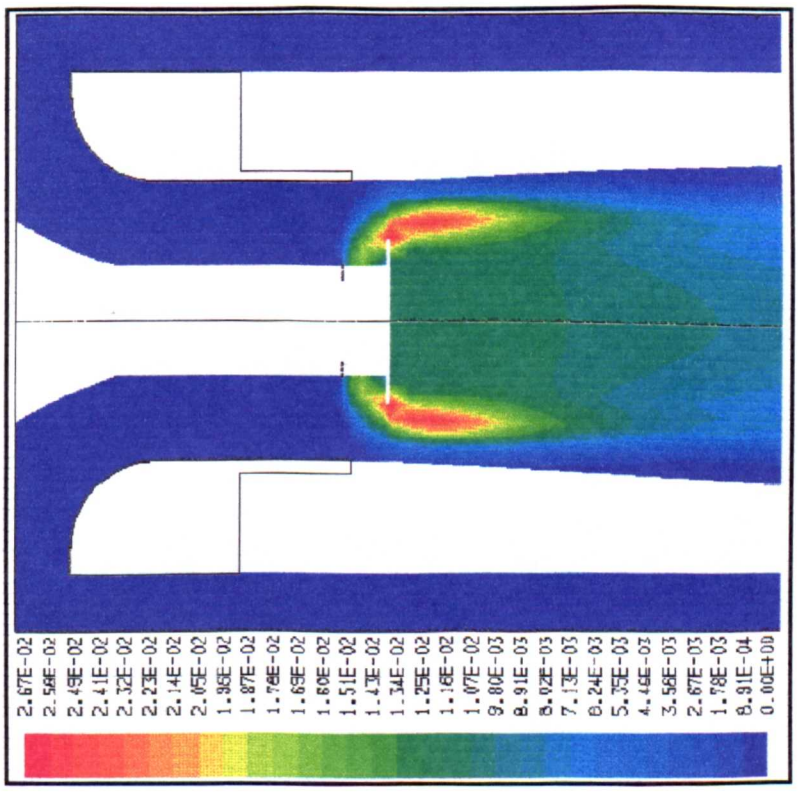

Figure 59. CO mol fraction when burning propane with an outlet oxygen concentration of 2.7% and a 30 mm flame stabilizing disc.

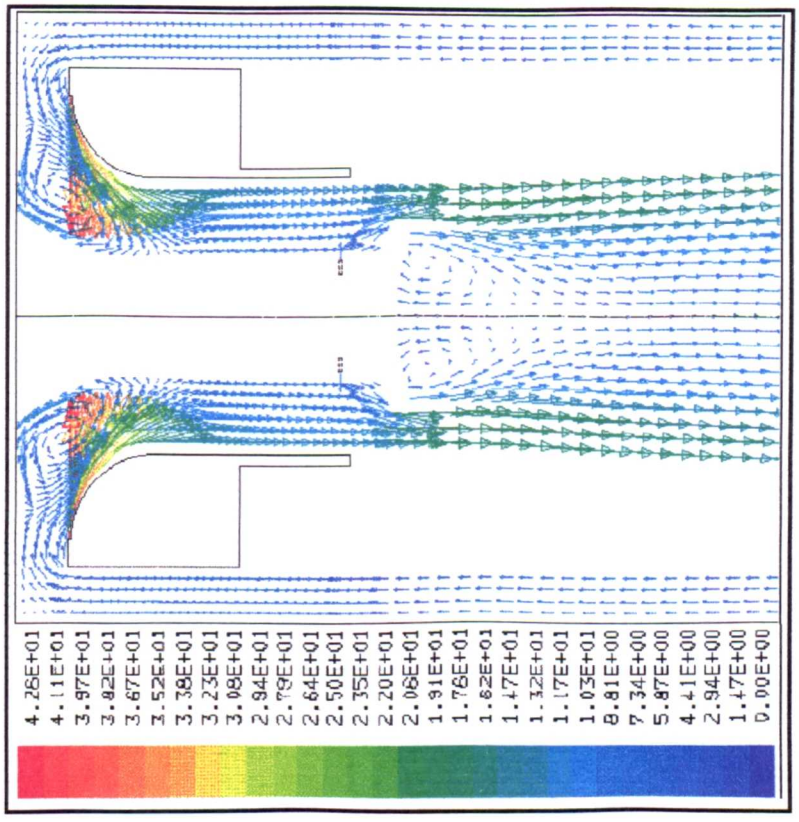

Figure 60. Velocity vectors, m/s, when burning propane with an oxygen outlet concentration of 4.9% and a 30 mm flame stabilizing disc.

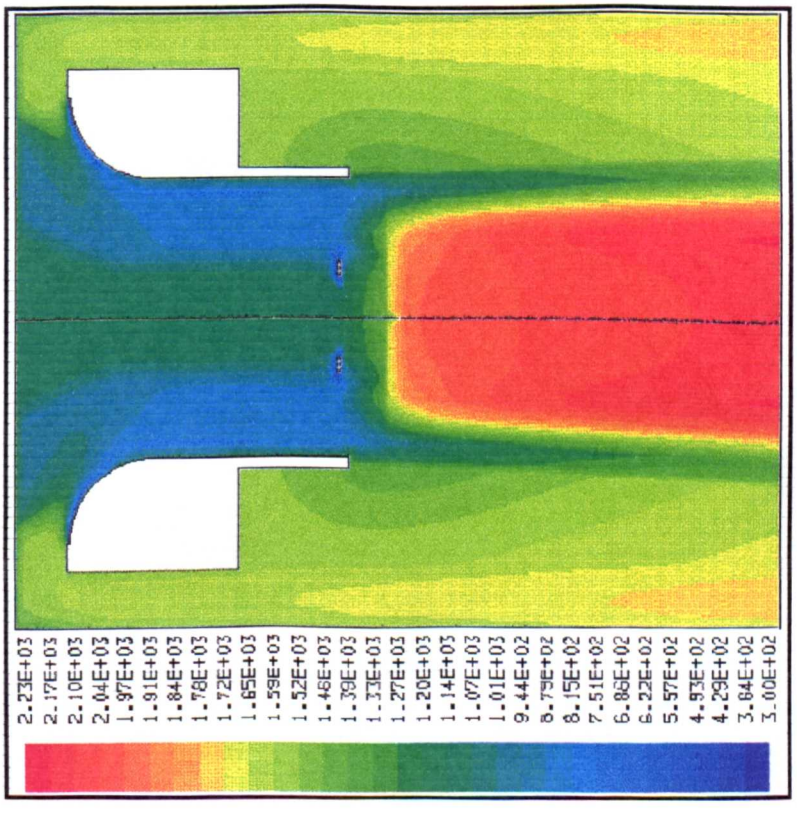

Figure 61.Temperature, Kelvin, when burning propane with an oxygen outlet concentration of 4.9% and a 30 mm flame stabilizing disc.

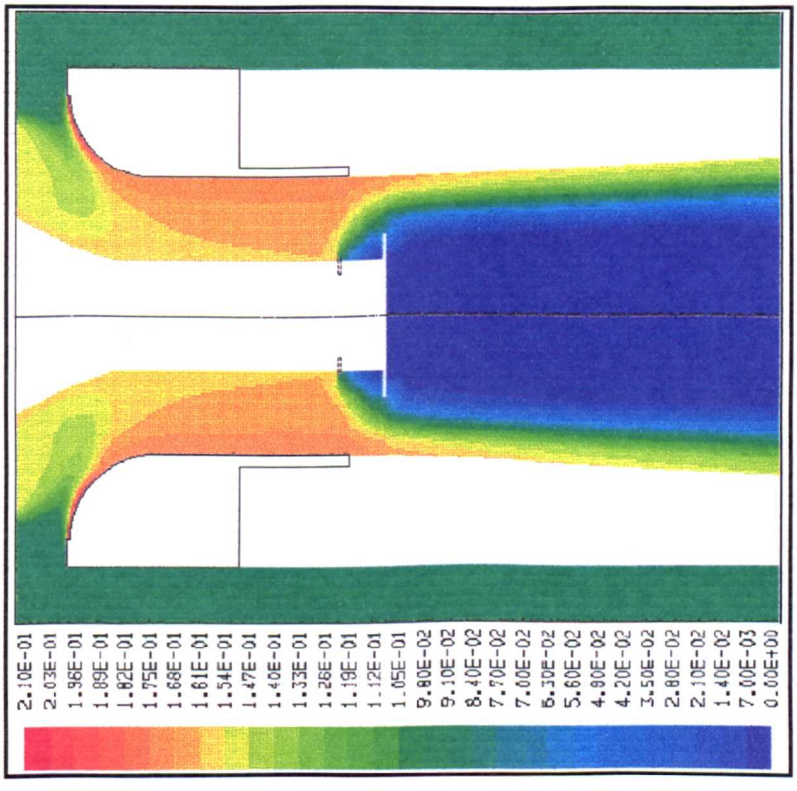

Figure 62. Oxygen mol fraction when burning propane with an oxygen outlet concentration of 4.9% and a 30 mm flame stabilizing disc.

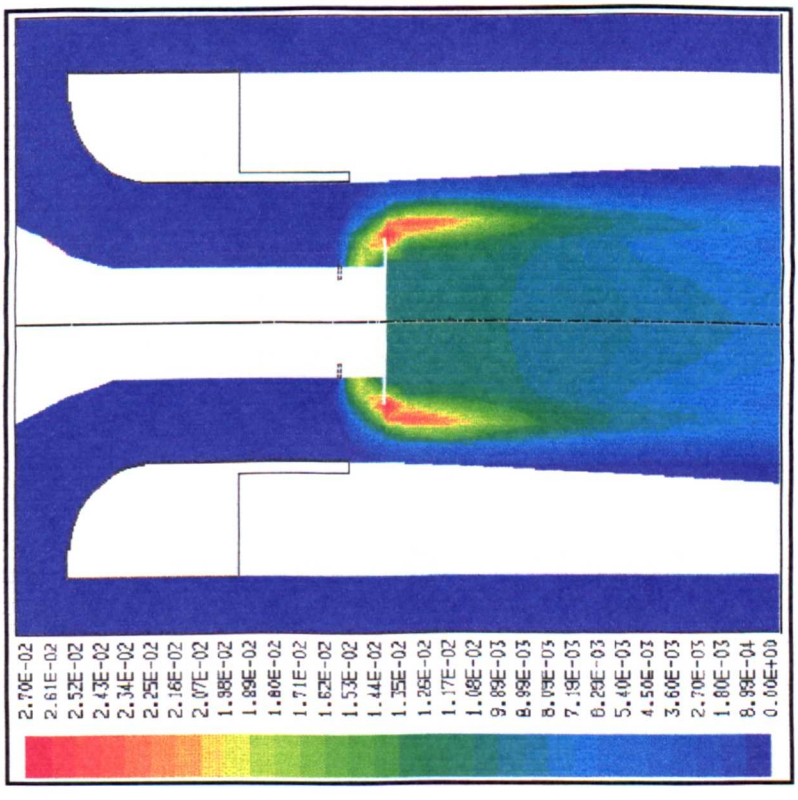

Figure 63. CO mol fraction when burning propane with an oxygen outlet concentration of 4.9% and a 30 mm flame stabilizing disc.

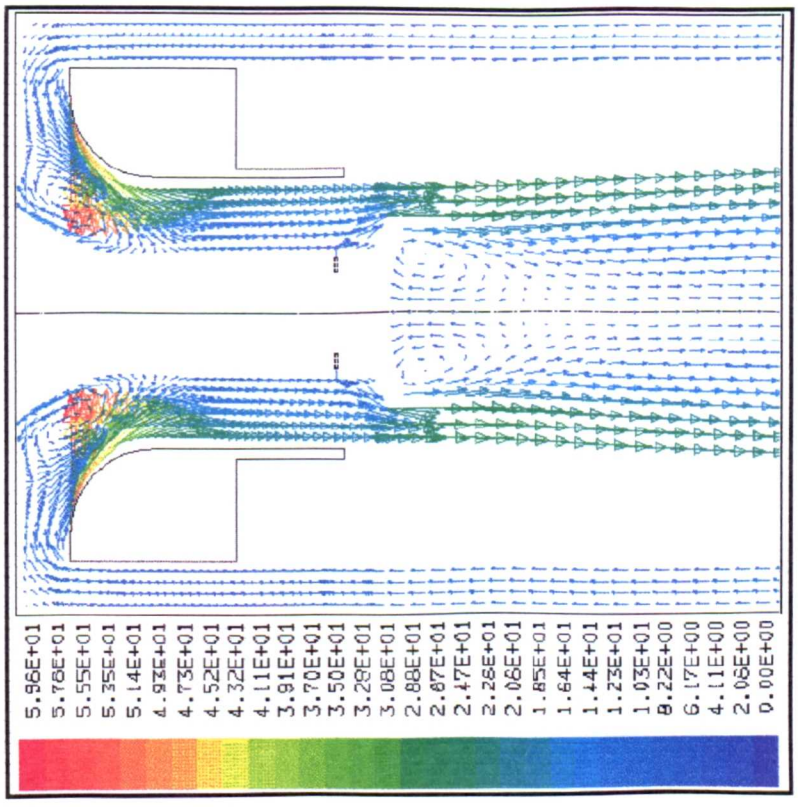

Figure 64. Velocity vectors, m/s, when burning propane with an oxygen outlet concentration of 9.3% and a 30 mm flame stabilizing disc.

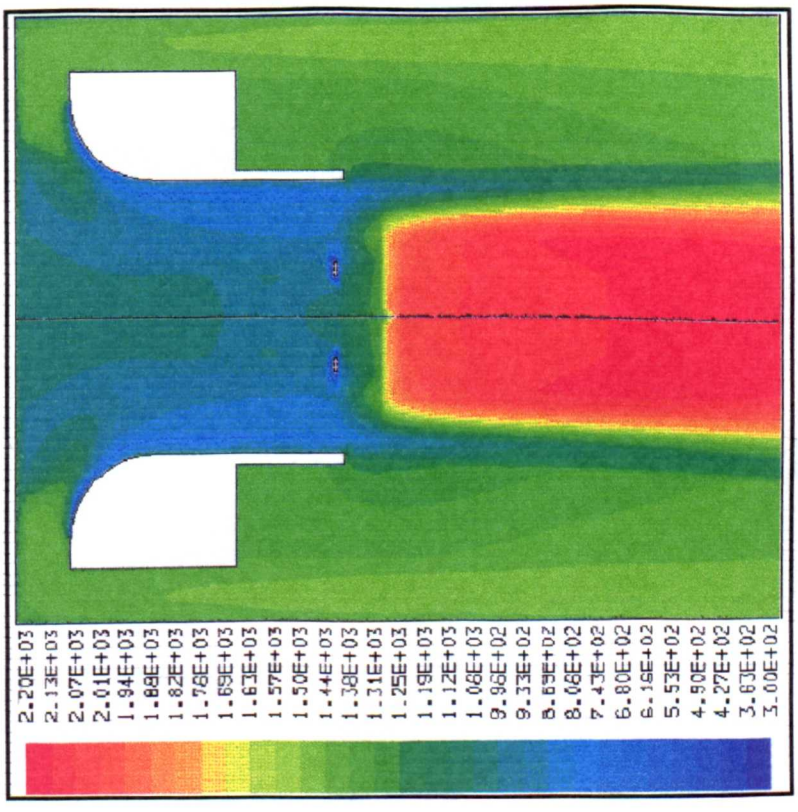

Figure 65. Temperature, Kelvin, when burning propane with an oxygen outlet concentration of 9.3% and a 30 mm flame stabilizing disc.

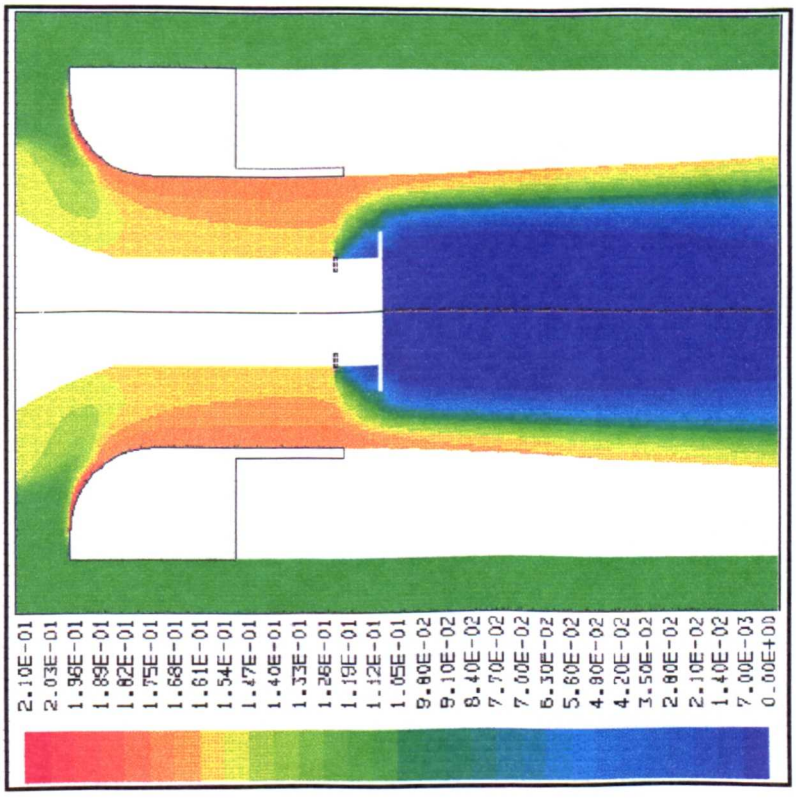

Figure 66. Oxygen mol fraction when burning propane with an oxygen outlet concentration of 9.3% and a 30 mm flame stabilizing disc.

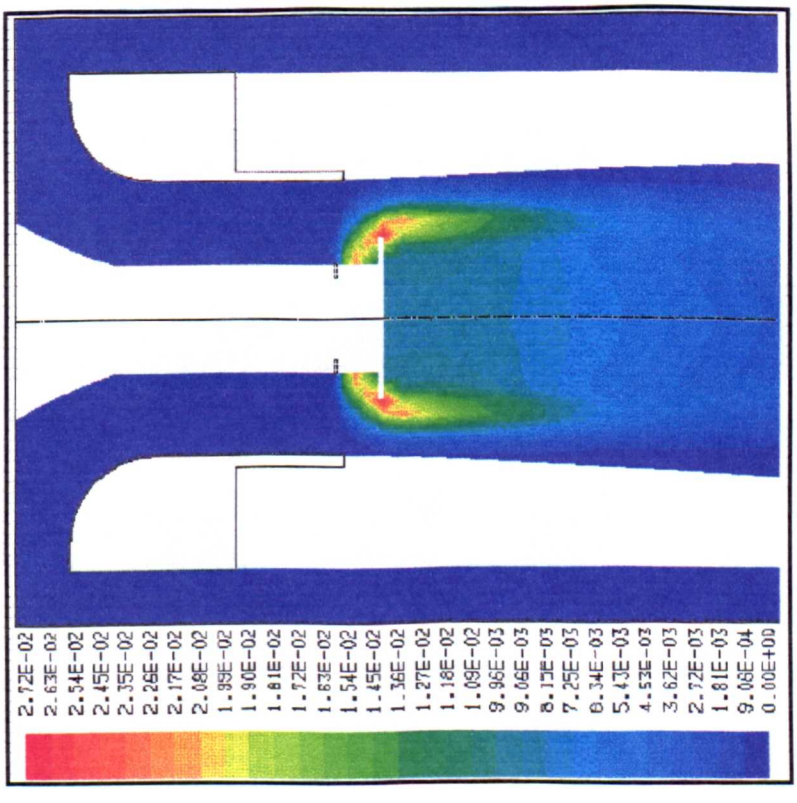

Figure 67. CO mol fraction when burning propane with an oxygen outlet concentration of 9.3% and a 30 mm flame stabilizing disc.

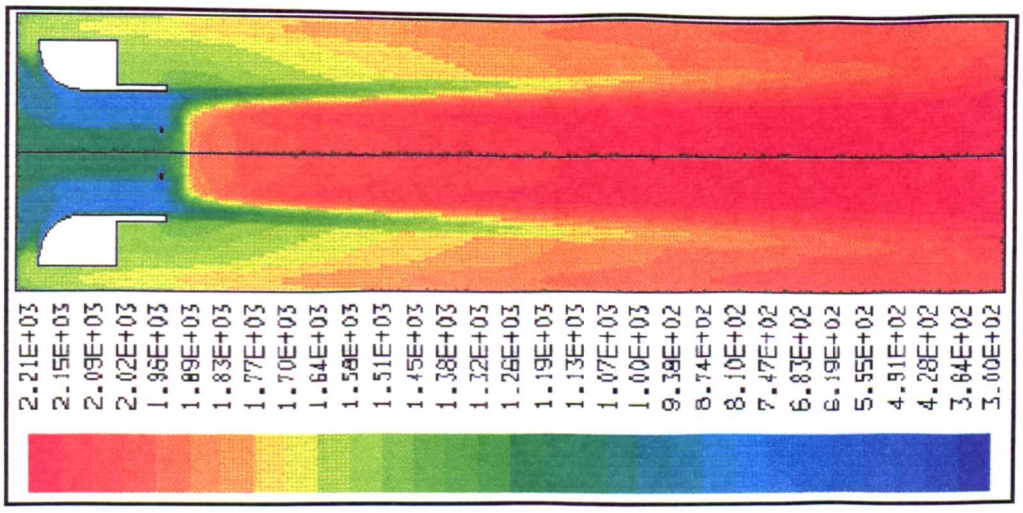

Figure 68. Temperature, Kelvin, when burning propane with an outlet oxygen concentration of 2.5% and a 30 mm flame stabilization disc.

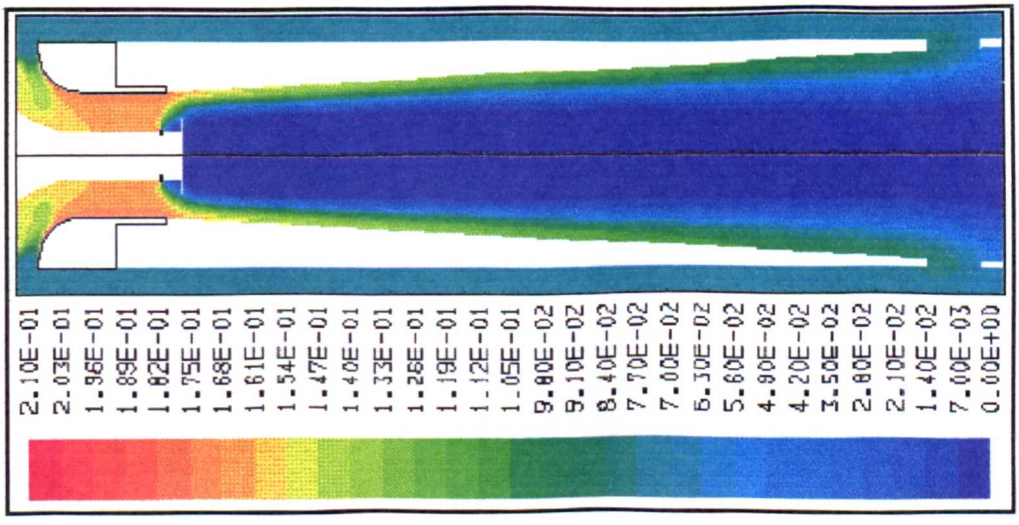

Figure 69. Oxygen mol fraction when burning propane with an outlet oxygen concentration of 2.5% and a 30 mm flame stabilization disc.

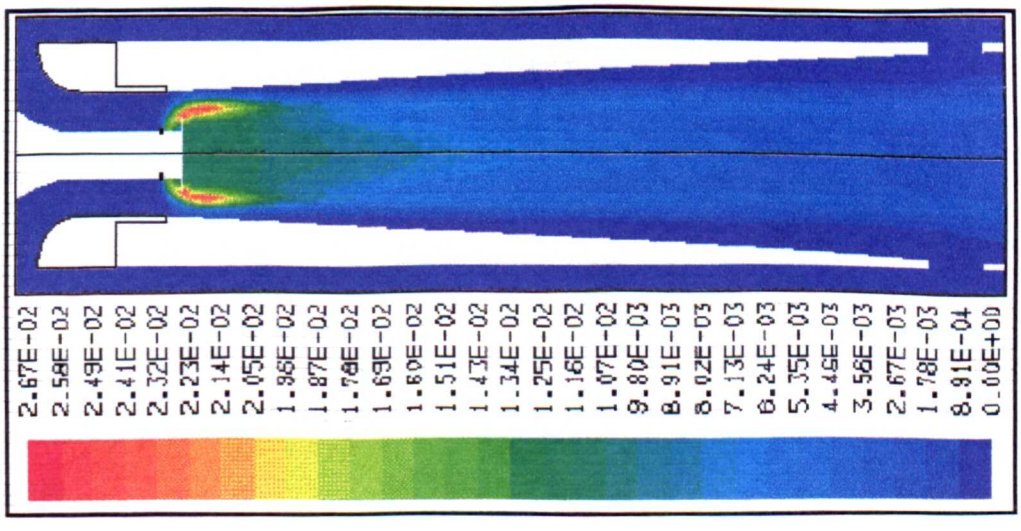

Figure 70. CO mol fraction when burning propane with an outlet oxygen concentration of 2.5% and a 30 mm flame stabilization disc.

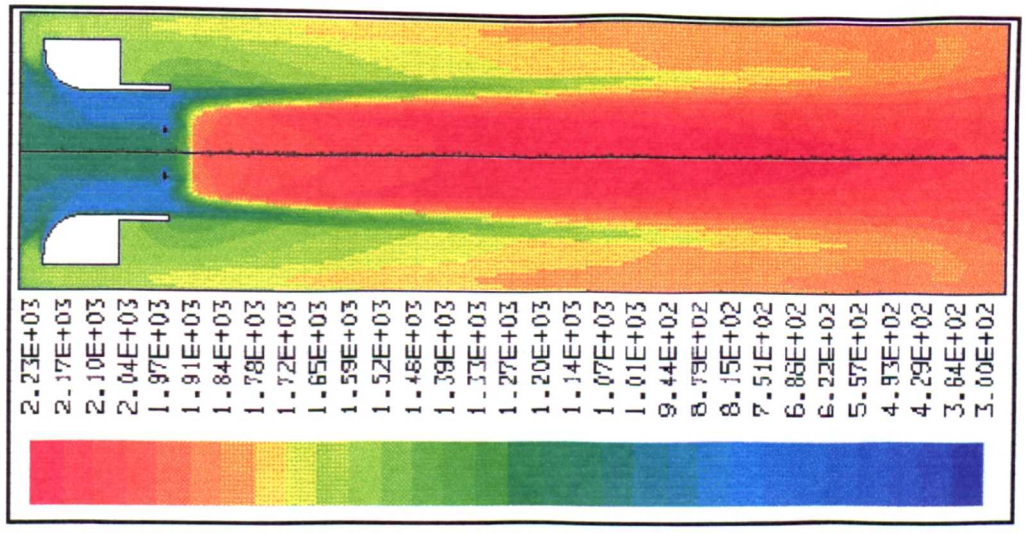

Figure 71. Temperature, Kelvin, when burning propane with an outlet oxygen concentration of 5.1% and a 30 mm flame stabilization disc.

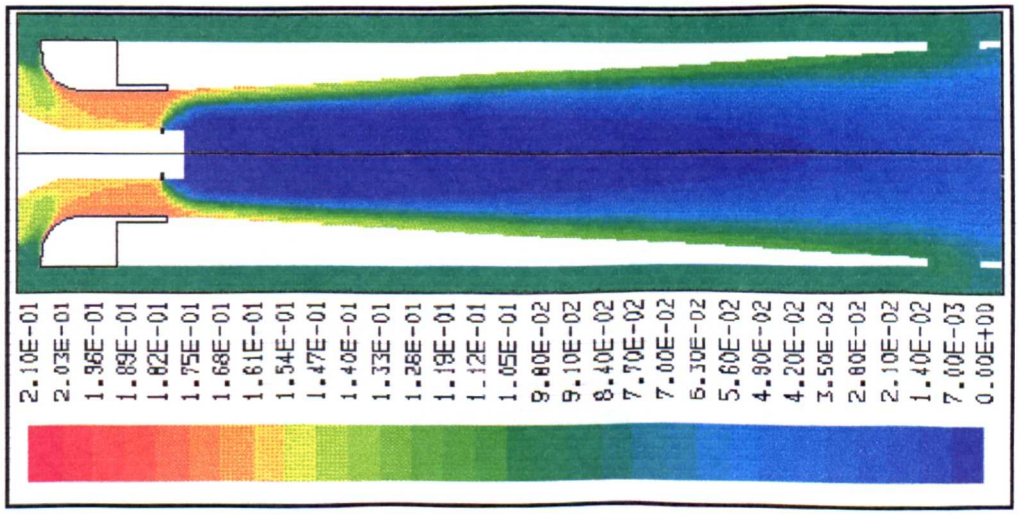

Figure 72. Oxygen mol fraction when burning propane with an outlet oxygen concentration of 5.1% and a 30 mm flame stabilization disc.

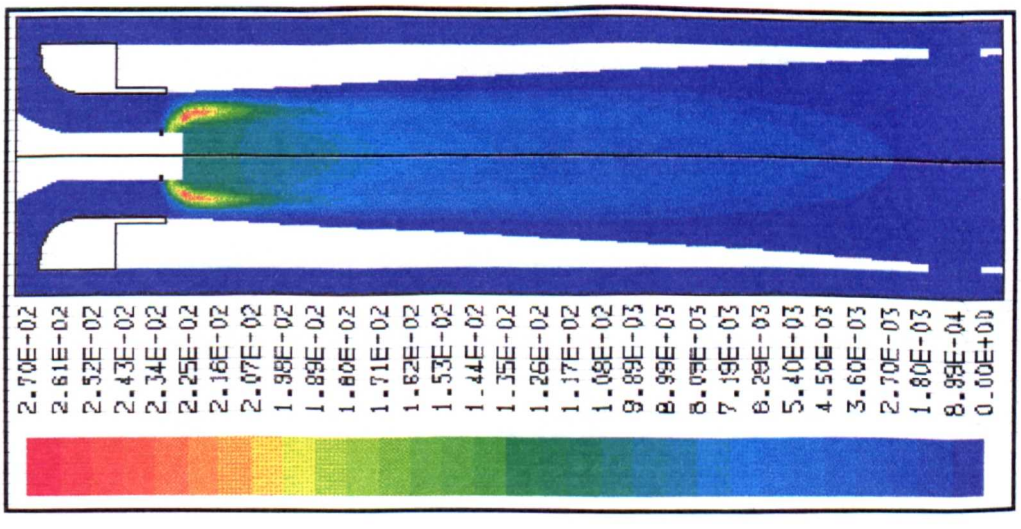

Figure 73. CO mol fraction when burning propane with an outlet oxygen concentration of 5.1% and a 30 mm flame stabilization disc.

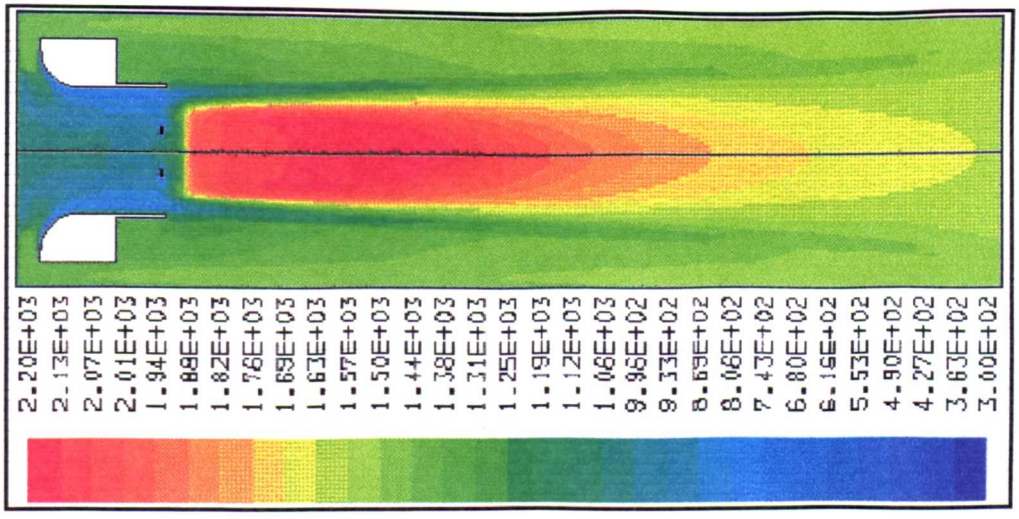

Figure 74. Temperature, Kelvin, when burning propane with an outlet oxygen concentration of 9.4% and a 30 mm flame stabilization disc.

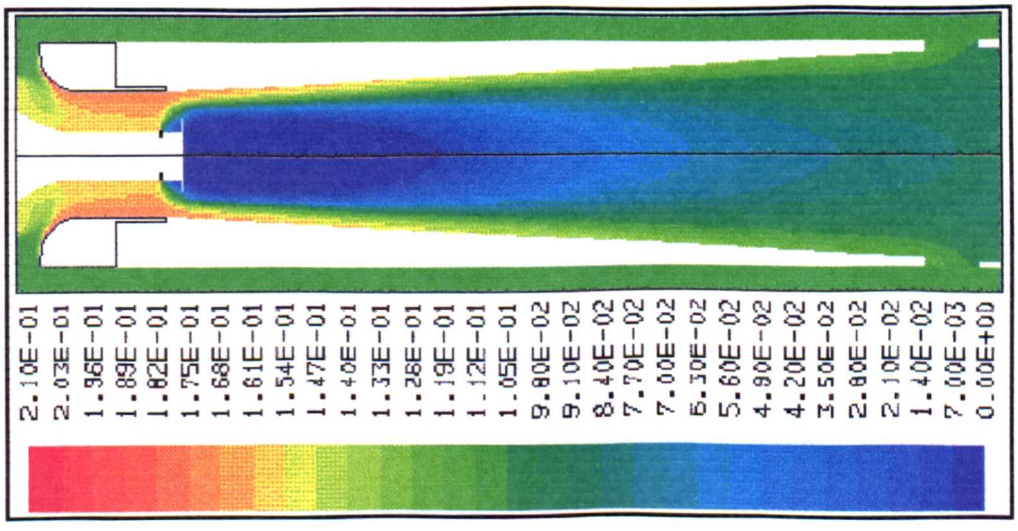

Figure 75. Oxygen mol fraction when burning propane with an outlet oxygen concentration of 9.4% and a 30 mm flame stabilization disc.

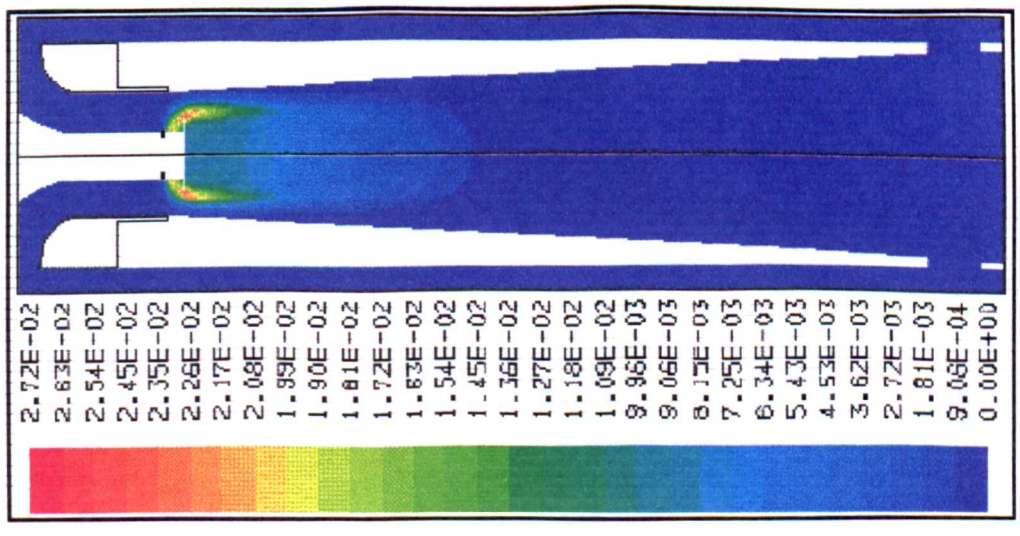

Figure 76. CO mol fraction when burning propane with an outlet oxygen concentration of 9.4% and a 30 mm flame stabilization disc.

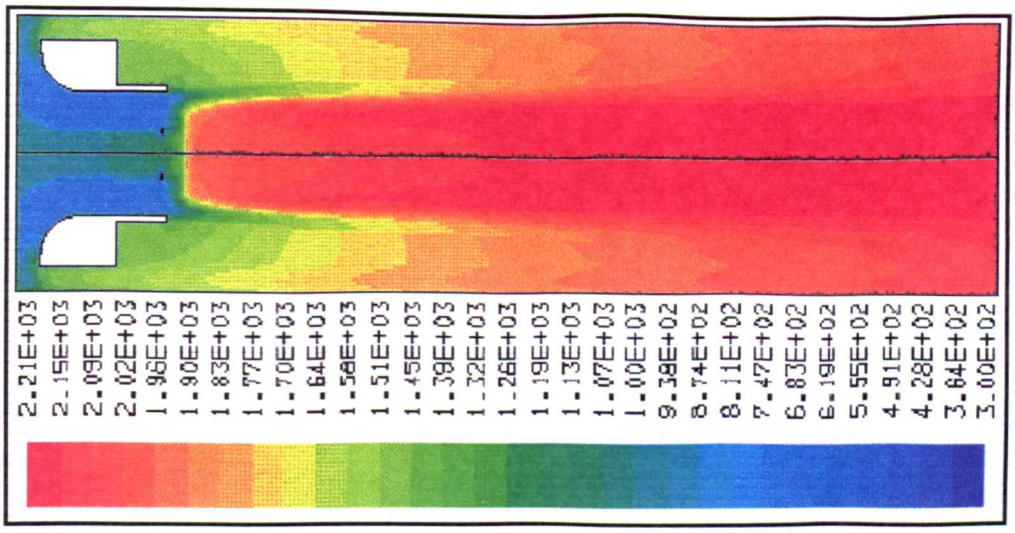

Figure 77. Temperature, Kelvin, when burning propane with an oxygen outlet concentration of 2.7% with a 40 mm flame stabilizing disc.

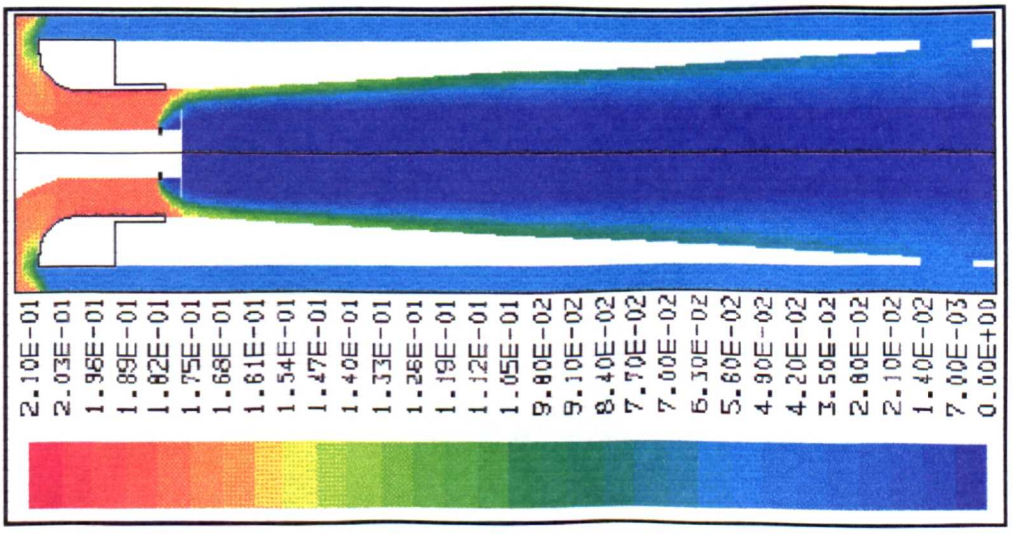

Figure 78. Oxygen mol fraction when burning propane with an oxygen outlet concentration of 2.7% with a 40 mm flame stabilizing disc.

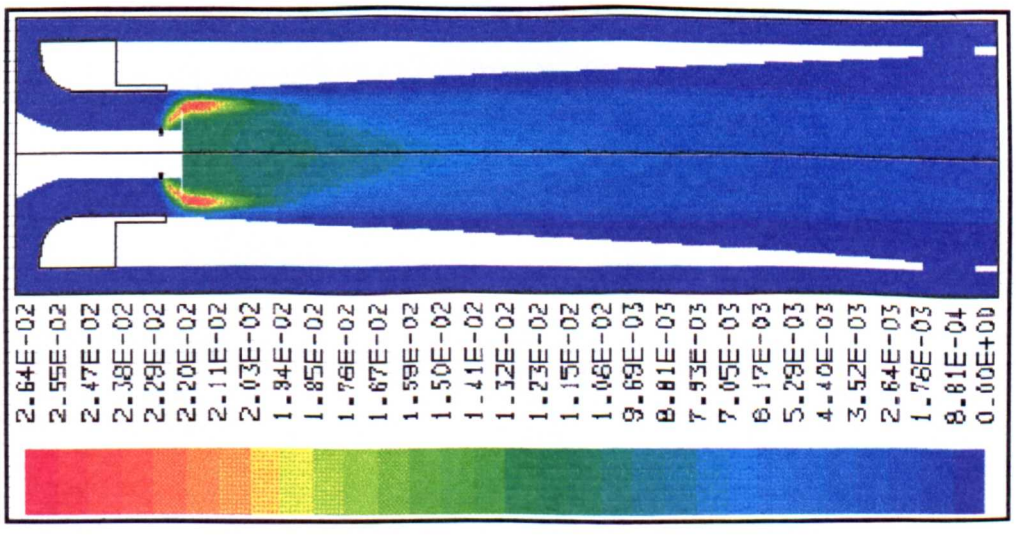

Figure 79. CO mol fraction when burning propane with an oxygen outlet concentration of 2.7% with a 40 mm flame stabilizing disc.

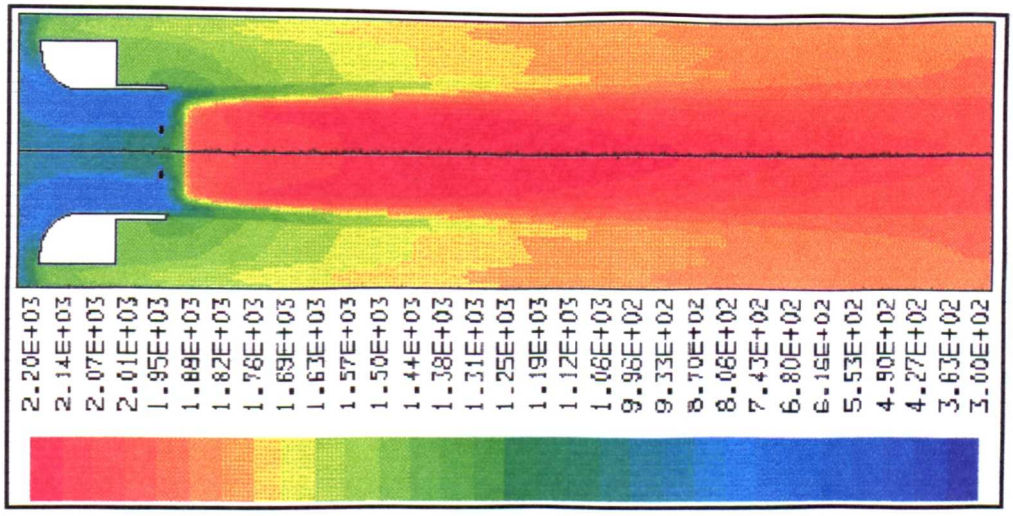

Figure 80. Temperature, Kelvin, when burning propane with an outlet oxygen concentration of 4.9% and a 40 mm flame stabilization disc.

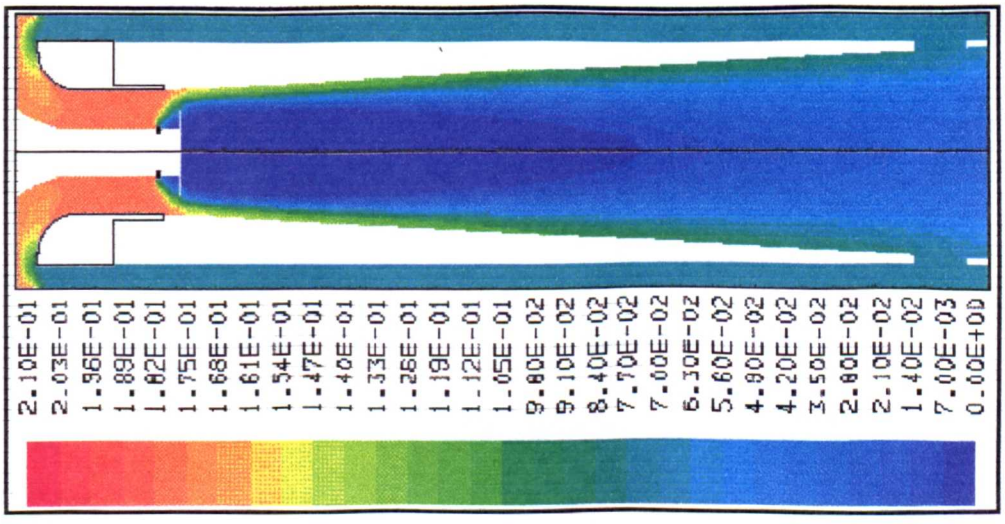

Figure 81. Oxygen mol fraction when burning propane with an outlet oxygen concentration of 4.9% and a 40 mm flame stabilization disc.

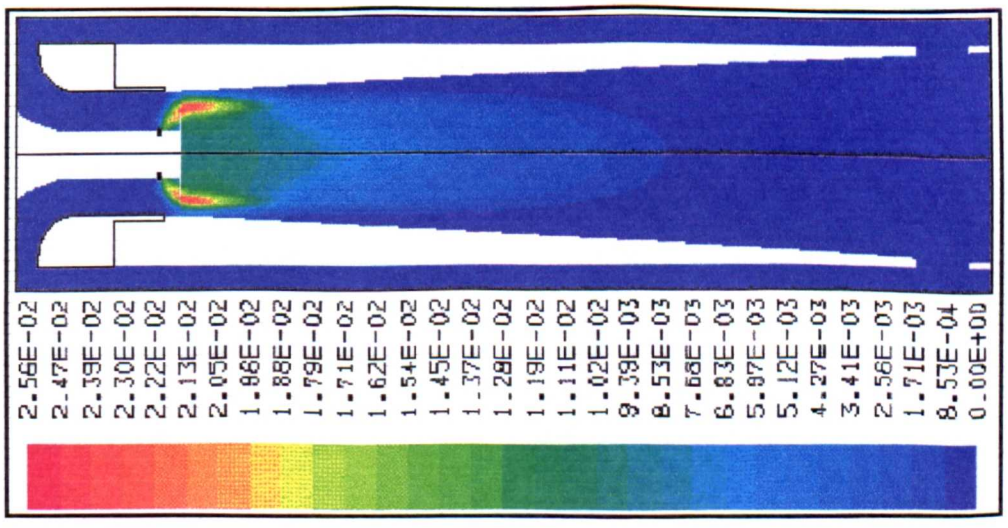

Figure 82. CO mol fraction when burning propane with an outlet oxygen concentration of 4.9% and a 40 mm flame stabilization disc.

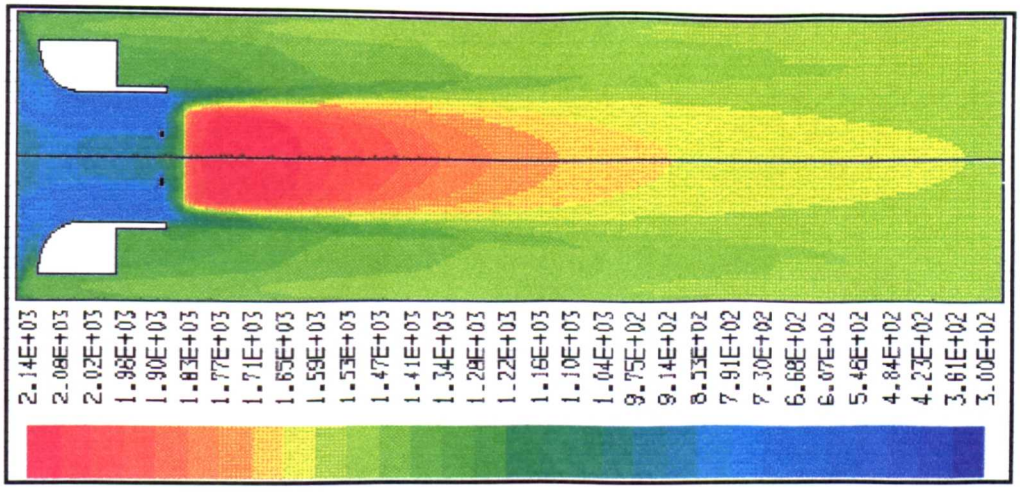

Figure 83. Temperature, Kelvin, when burning propane with an outlet oxygen concentration of 9.4% and a 40 mm flame stabilizing disc.

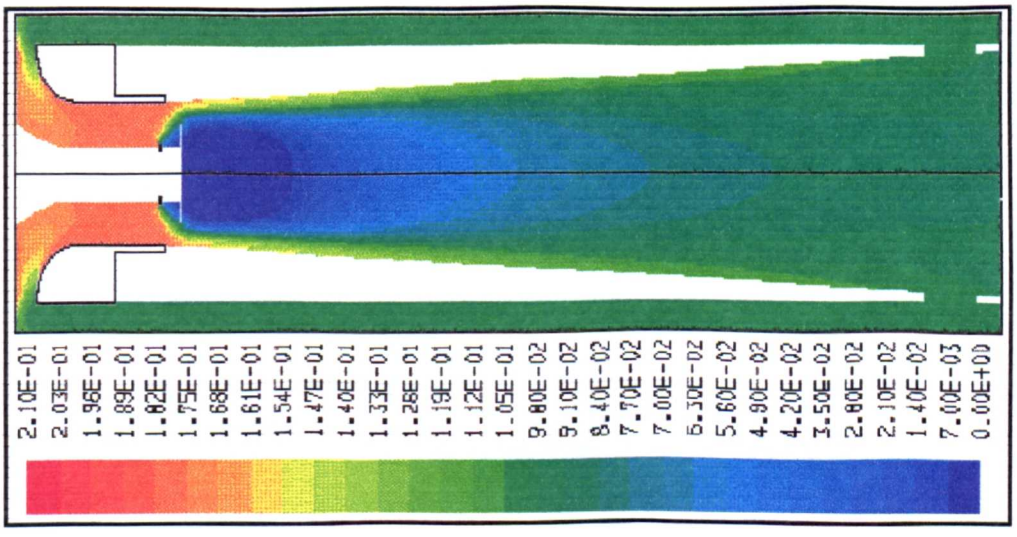

Figure 84. Oxygen mol fraction when burning propane with an outlet oxygen concentration of 9.4% and a 40 mm flame stabilizing disc.

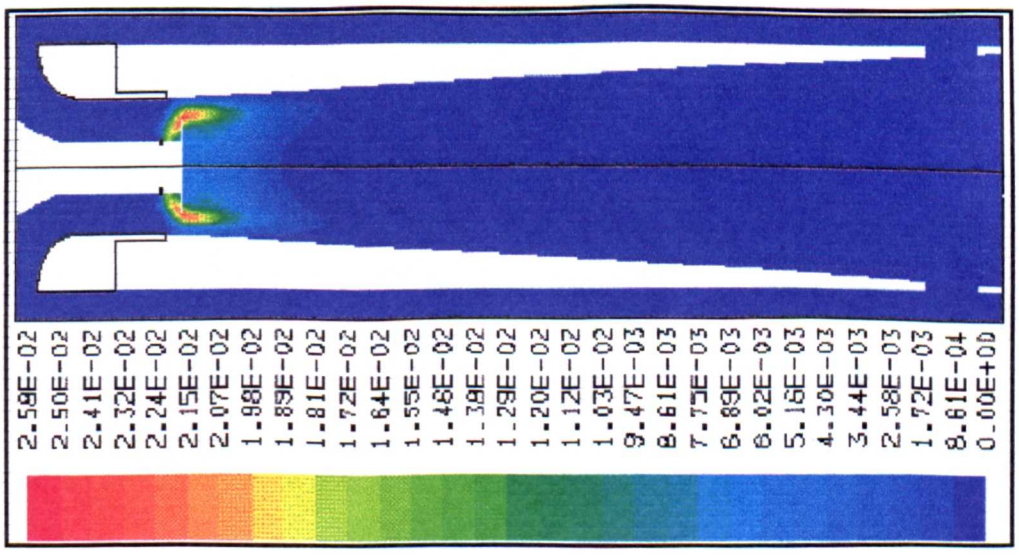

Figure 85. CO mol fraction when burning propane with an outlet oxygen concentration of 9.4% and a 40 mm flame stabilizing disc.

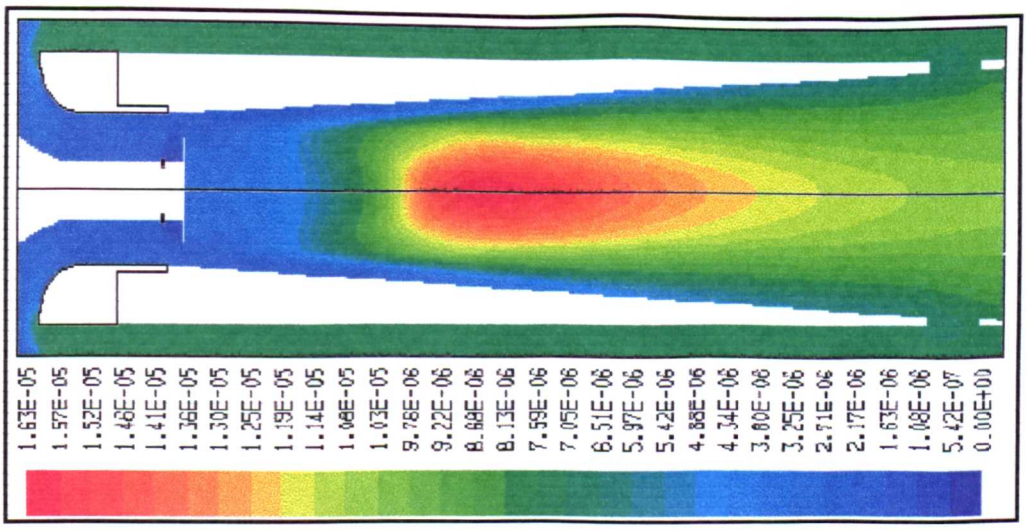

Figure 86. Thermal NOx formation when burning methane at an air to fuel ratio of 1.64.

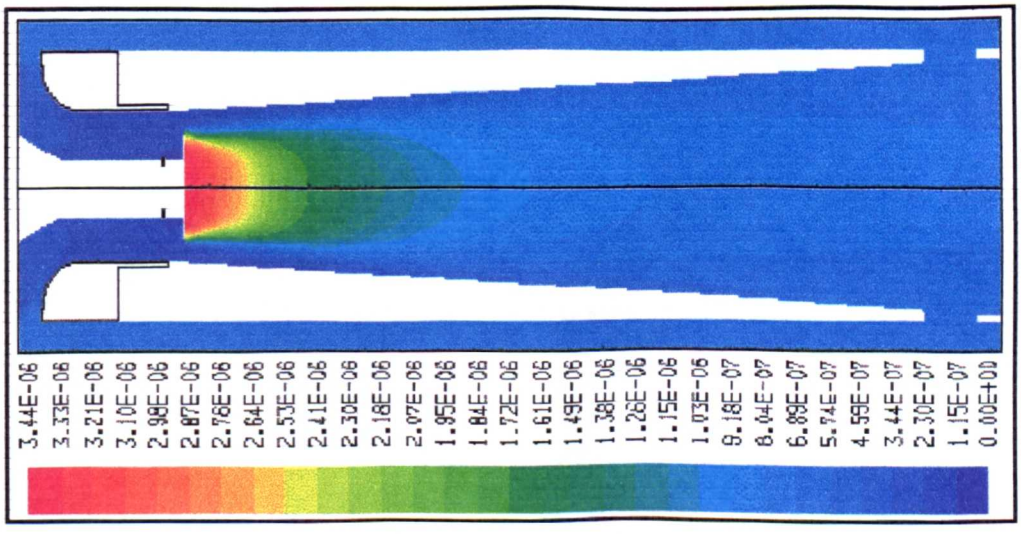

Figure 87. Thermal NOx formation when burning methane at an air to fuel ratio of 2.57.

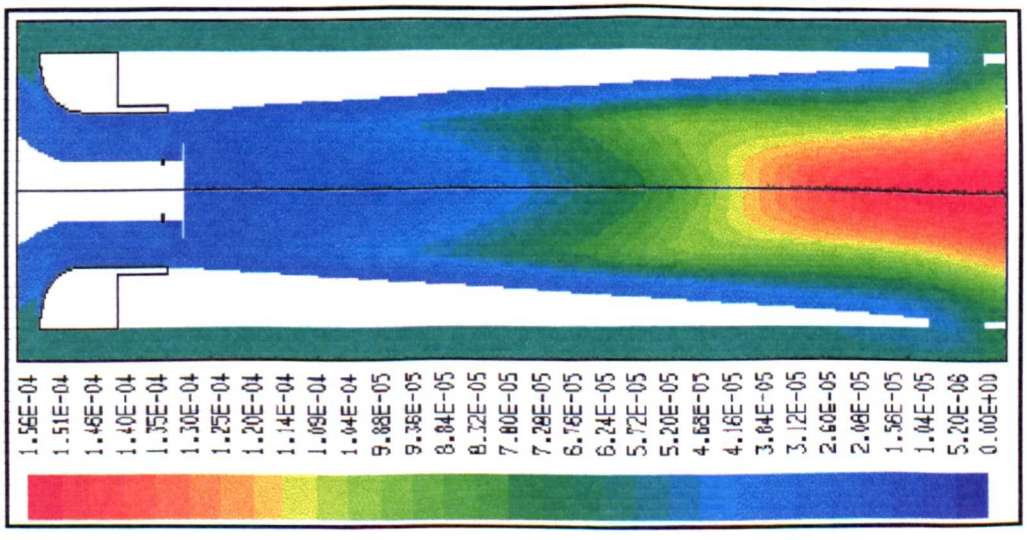

Figure 88. Thermal NOx formation when burning propane at an air to fuel ratio of 1.36.

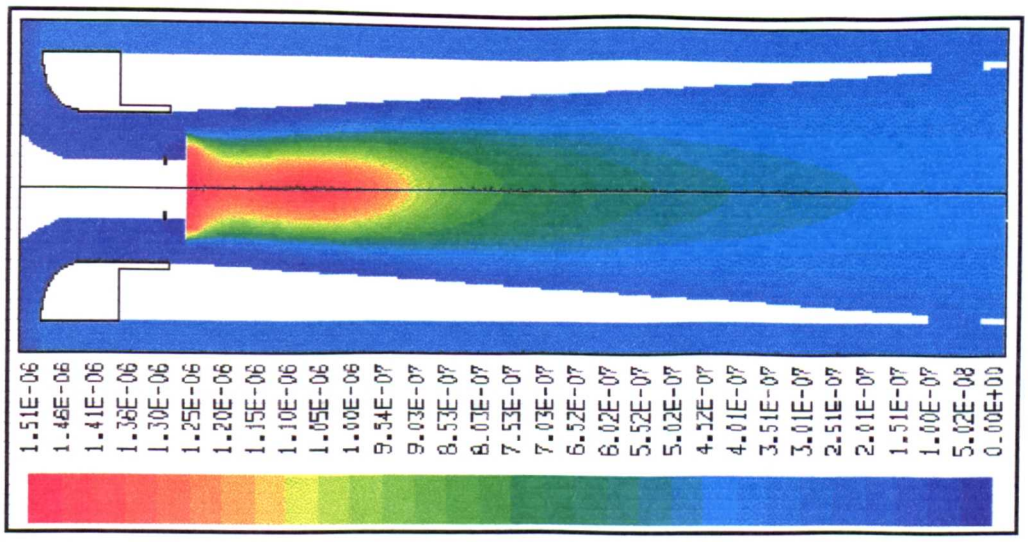

Figure 89. Prompt NOx formation when burning methane at an air to fuel ratio of 1.64.

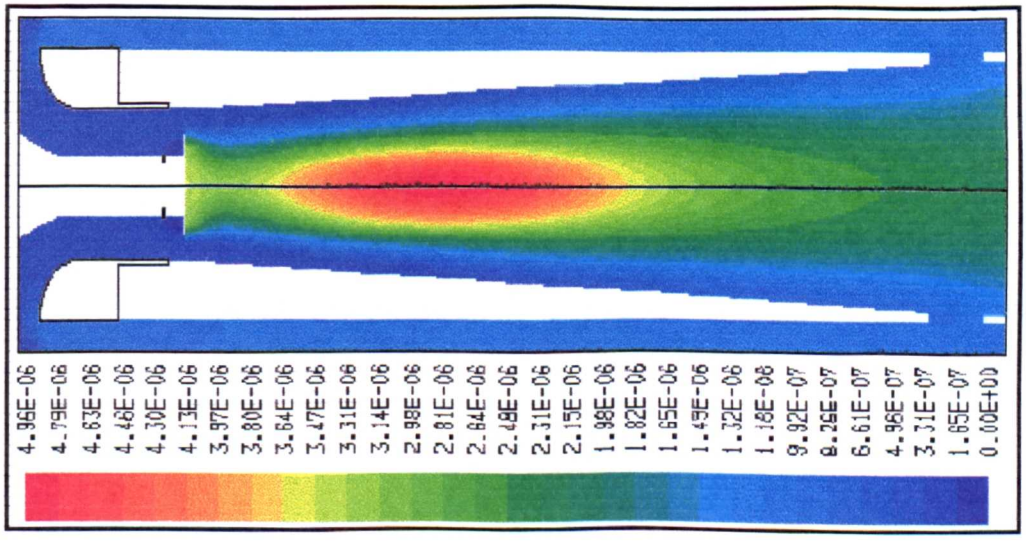

Figure 90. Prompt NOx formation when burning propane at an air to fuel ratio of 1.39.

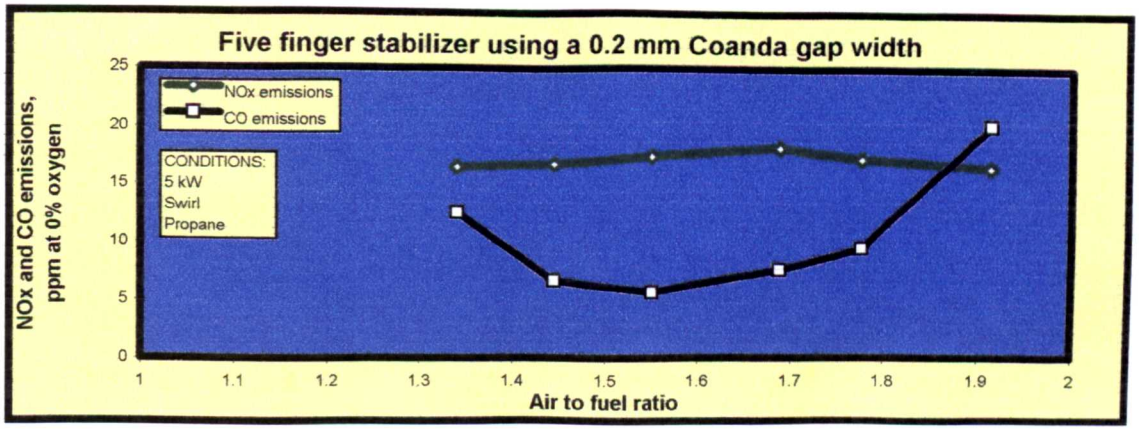

Figure 91. Experimental NOx and CO emissions when operating at 5 kW with a 0.2 mm Coanda gap width and swirl.

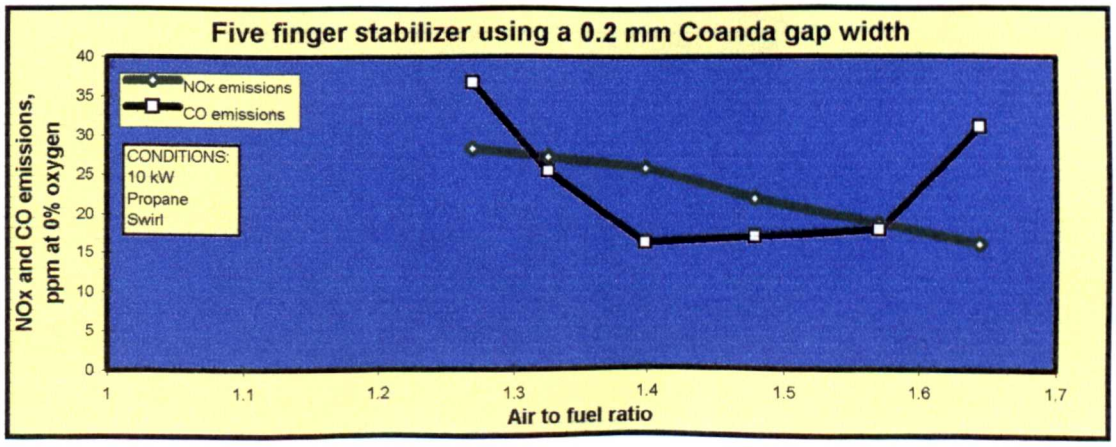

Figure 92. Experimental NOx and CO emissions when operating at 10 kW with a 0.2 mm Coanda gap width and swirl.

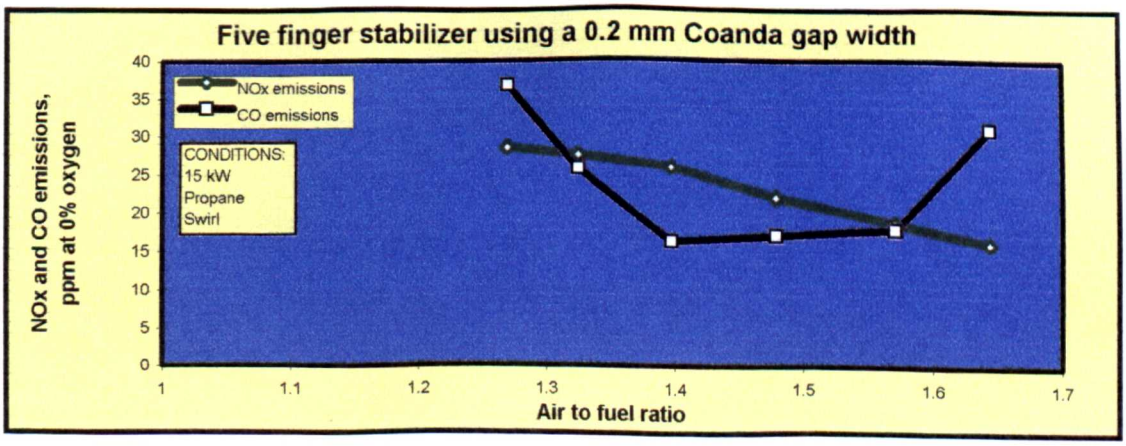

Figure 93. Experimental NOx and CO emissions when operating at 15 kW with a 0.2 mm Coanda gap width and swirl.

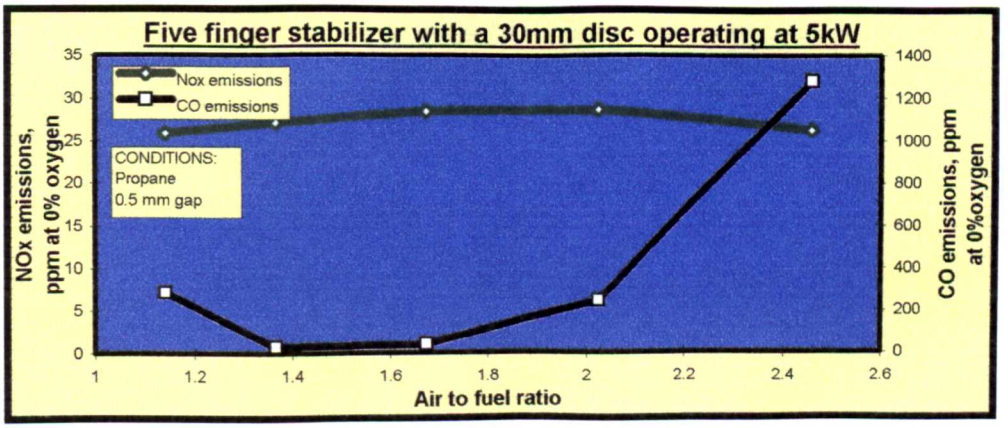

Figure 94. Experimental NOx and CO emissions when operating at 5 kW with a 0.5 mm Coanda gap width.

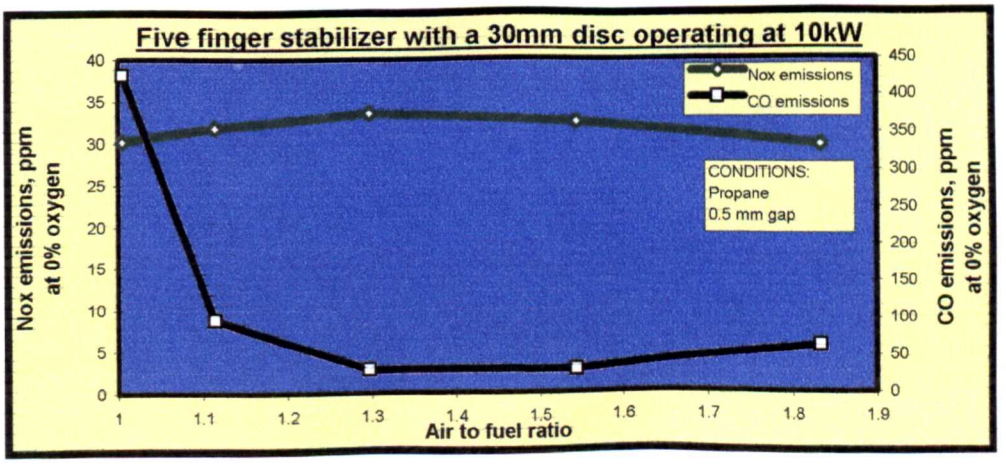

Figure 95. Experimental NOx and CO emissions when operating at 10 kW with a 0.5 mm Coanda gap width.

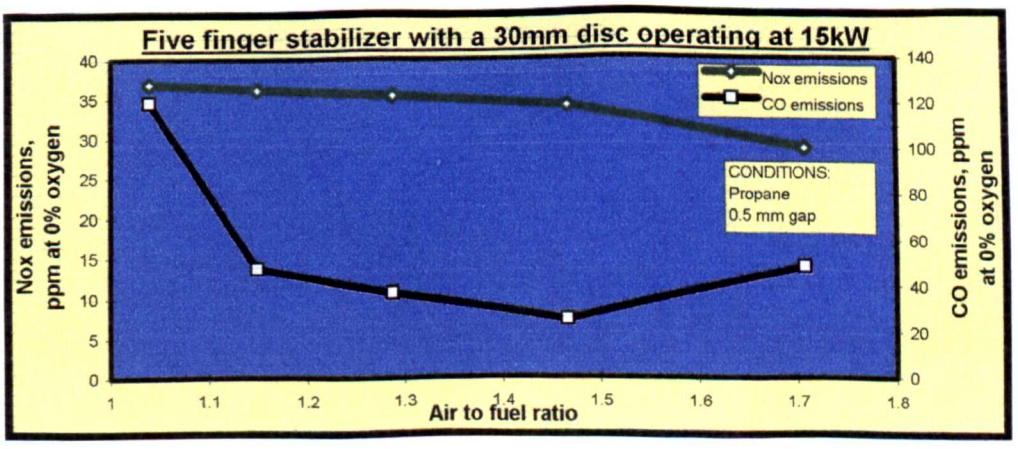

Figure 96. Experimental NOx and CO emissions when operating at 15 kW with a 0.5 mm Coanda gap width.

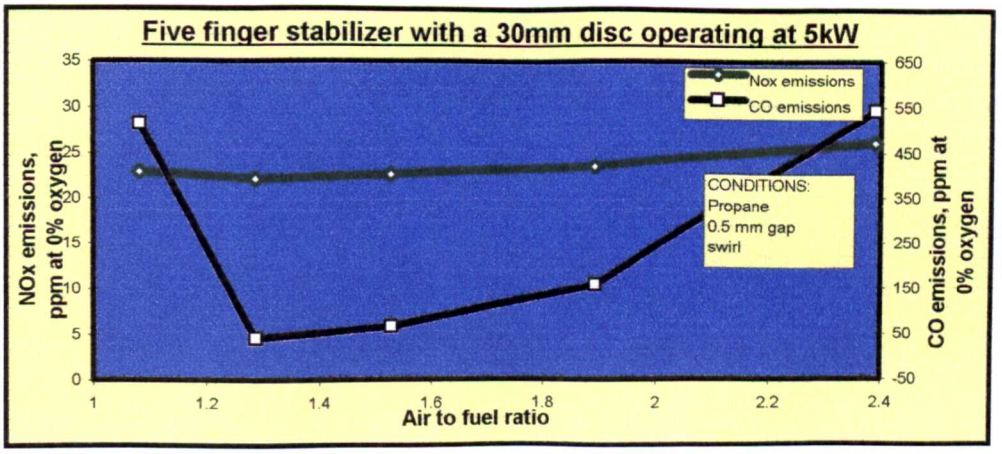

Figure 97. Experimental NOx and CO emissions when operating at 5 kW with a 0.5 mm Coanda gap width and swirl.

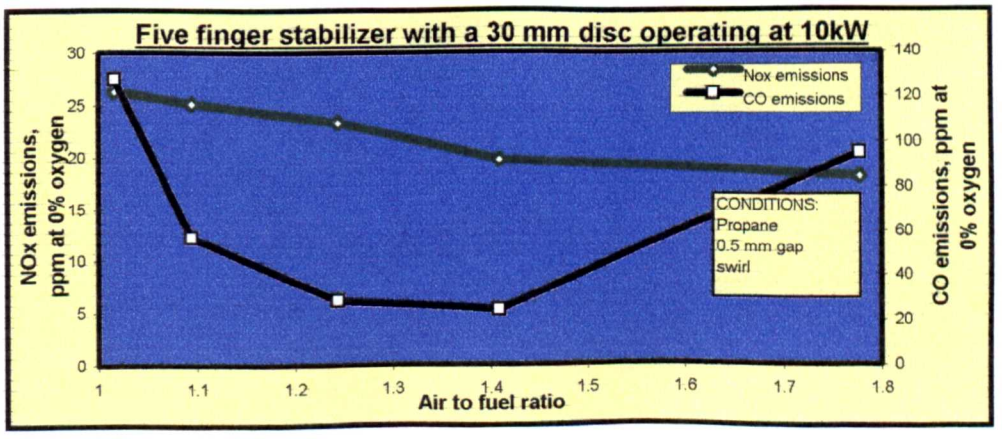

Figure 98. Experimental NOx and CO emissions when operating at 10 kW with a 0.5 mm Coanda gap width and swirl.

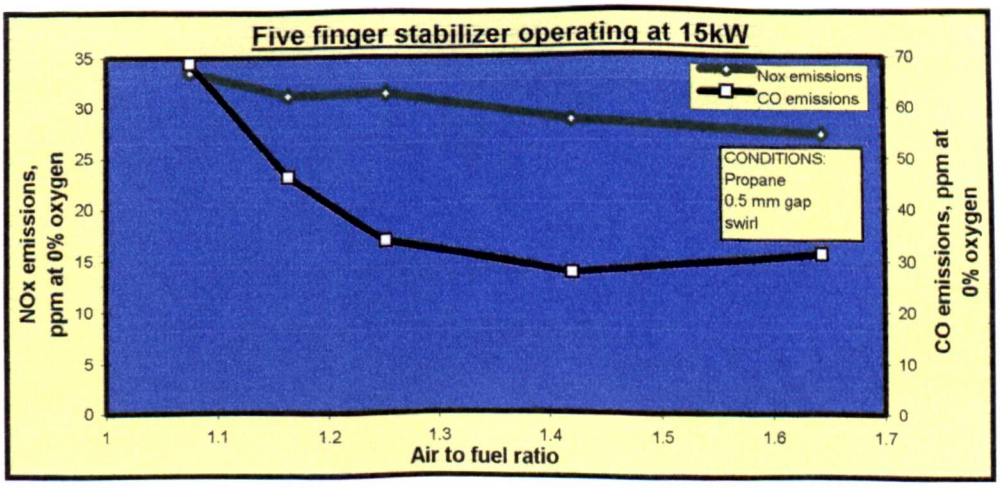

Figure 99. Experimental NOx and CO emissions when operating at 15 kW with a 0.5 mm Coanda gap width and swirl.

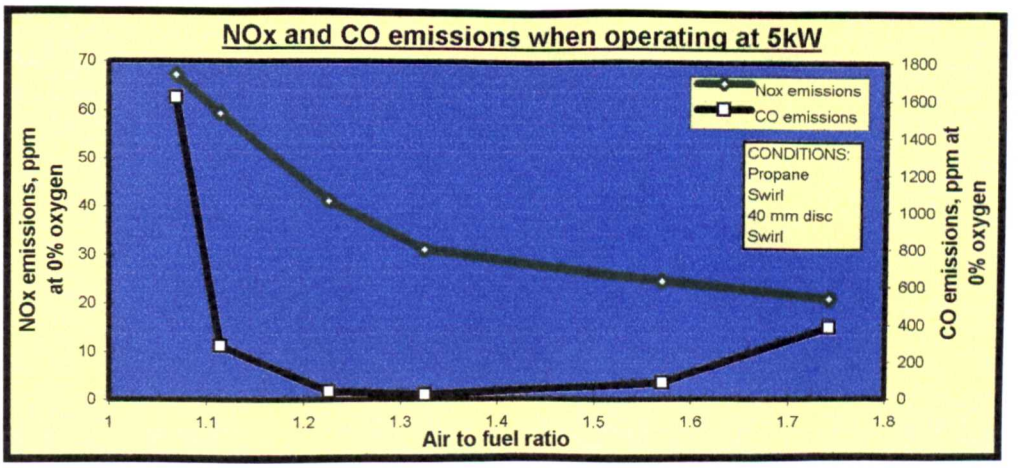

Figure 100. Experimental NOx and CO emissions when operating at 5 kW and a 0.5 mm Coanda gap width and swirl.

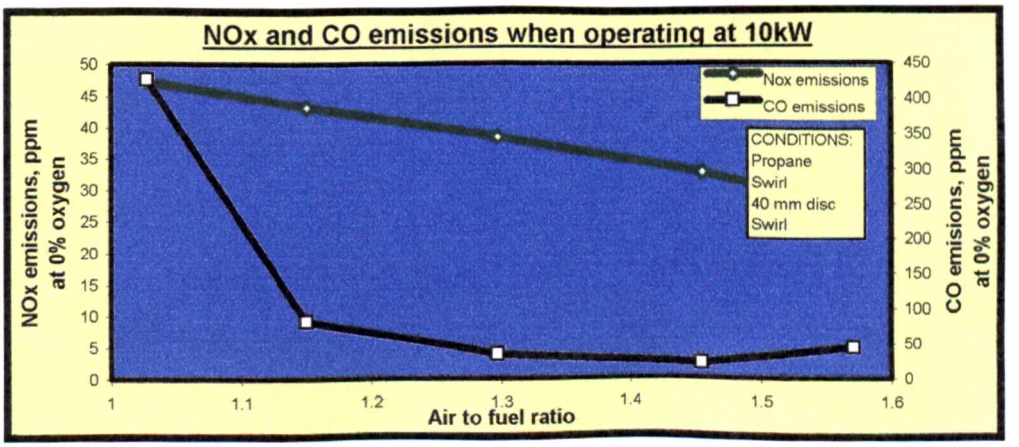

Figure 101. Experimental NOx and CO emissions when operating at 10 kW and a 0.5 mm Coanda gap width and swirl.

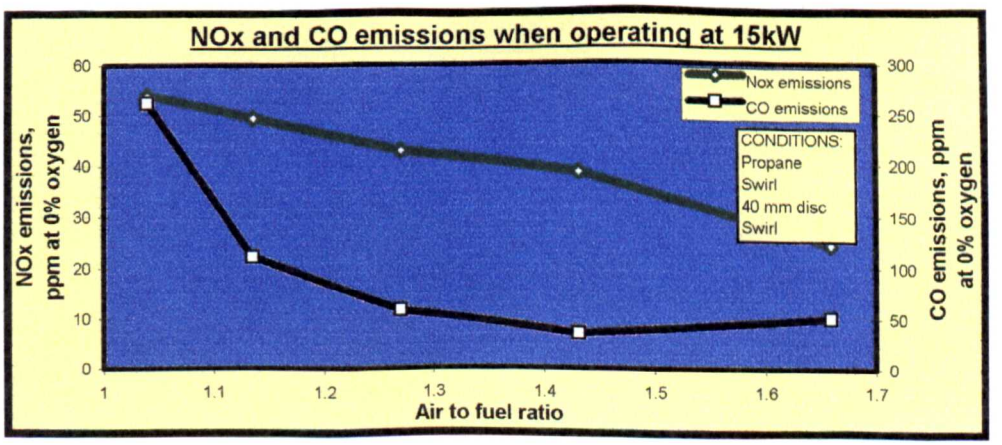

Figure 102. Experimental NOx and CO emissions when operating at 15 kW and a 0.5 mm Coanda gap width and swirl.

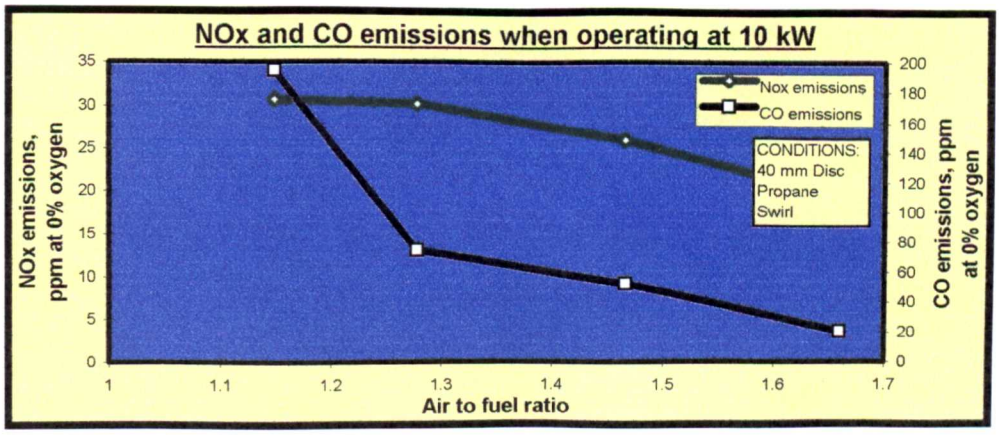

Figure 103. Experimental NOx and CO emissions when operating at 10 kW and a 0.2 mm Coanda gap width and swirl.

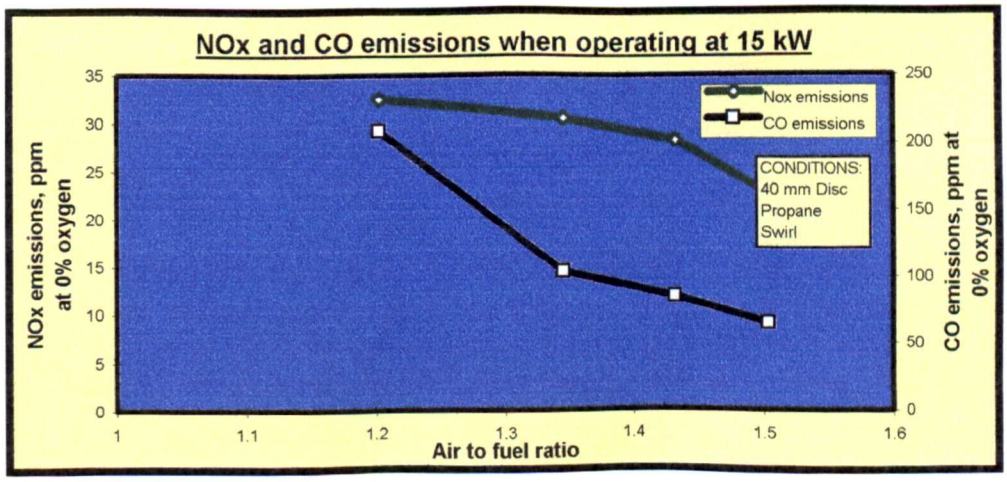

Figure 104. Experimental NOx and CO emissions when operating at 15 kW and a 0.2 mm Coanda gap width and swirl.

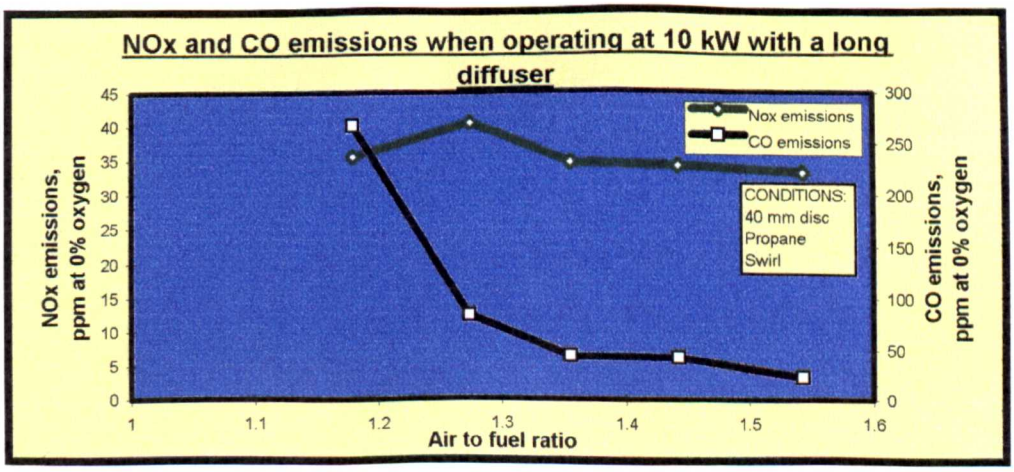

Figure 105. Experimental NOx and CO emissions when operating at 10 kW, a 0.2 mm Coanda gap width and a long diffusing section with swirl.

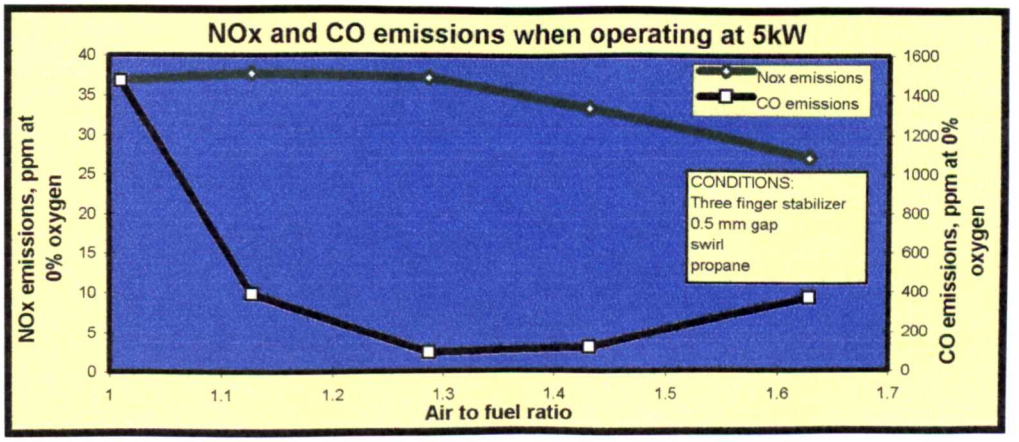

Figure 106. Experimental NOx and CO emissions when operating at 5 kW, a 0.5 mm Coanda gap width and a three finger flame stabiliser with swirl.

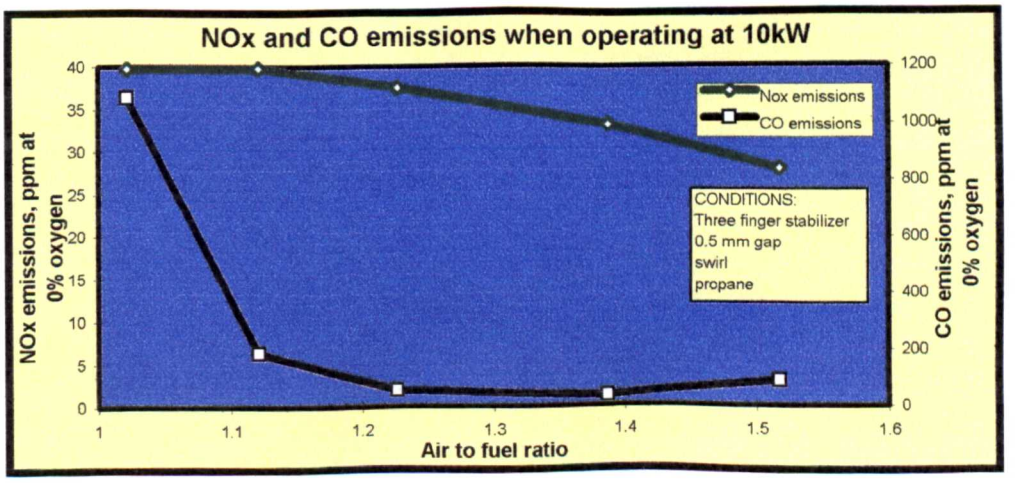

Figure 107. Experimental NOx and CO emissions when operating at 10 kW, a 0.5 mm Coanda gap width and a three finger flame stabiliser with swirl.

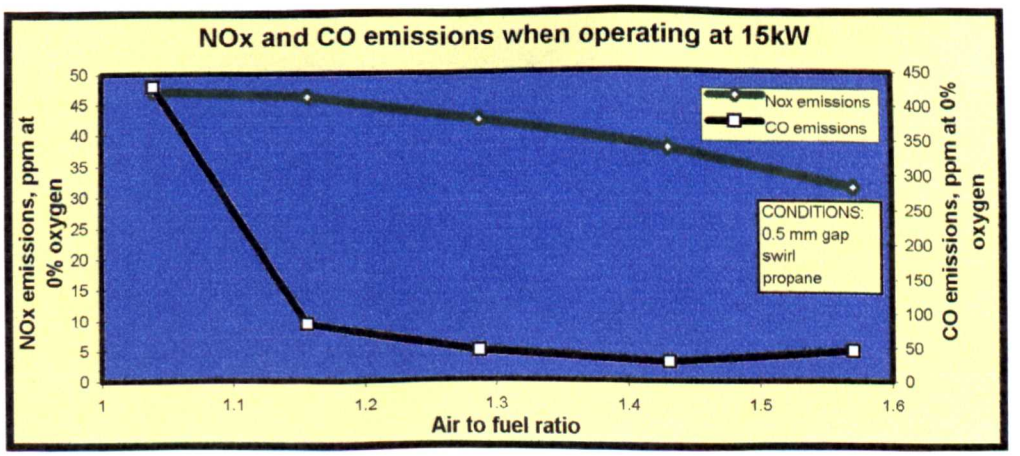

Figure 108. Experimental NOx and CO emissions when operating at 15 kW, a 0.5 mm Coanda gap width and a three finger flame stabiliser with swirl.

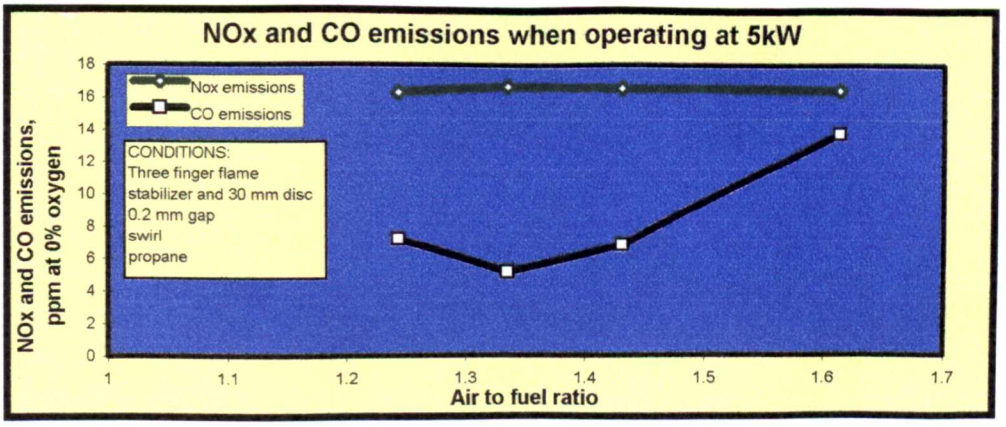

Figure 109. Experimental NOx and CO emissions when operating at 5 kW, a 0.2 mm Coanda gap width and a three finger, 30 mm disc flame stabiliser combination with swirl.

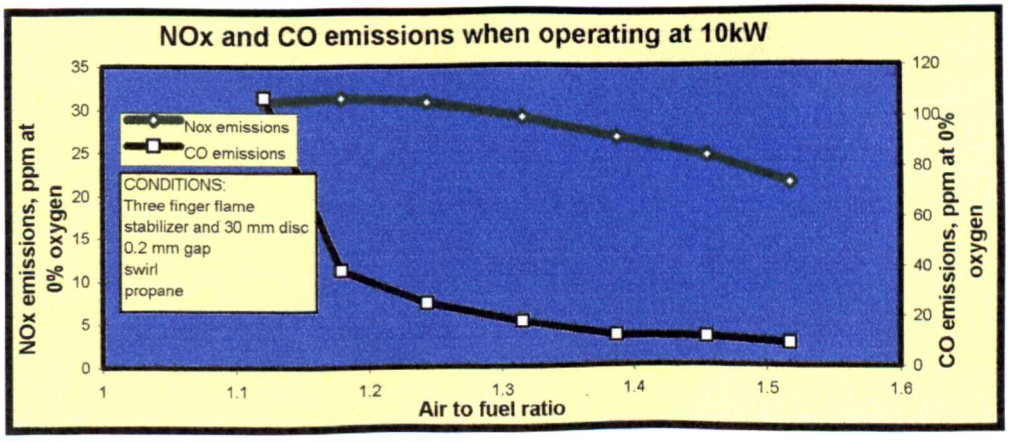

Figure 110. Experimental NOx and CO emissions when operating at 10 kW, a 0.2 mm Coanda gap width and a three finger, 30 mm disc flame stabiliser combination with swirl.

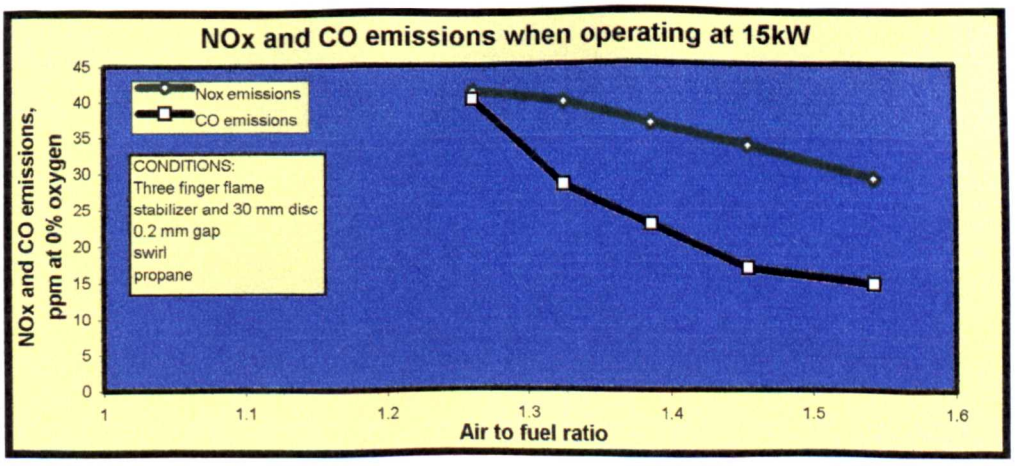

Figure 111. Experimental NOx and CO emissions when operating at 15 kW, a 0.2 mm Coanda gap width and a three finger, 30 mm disc flame stabiliser combination with swirl.

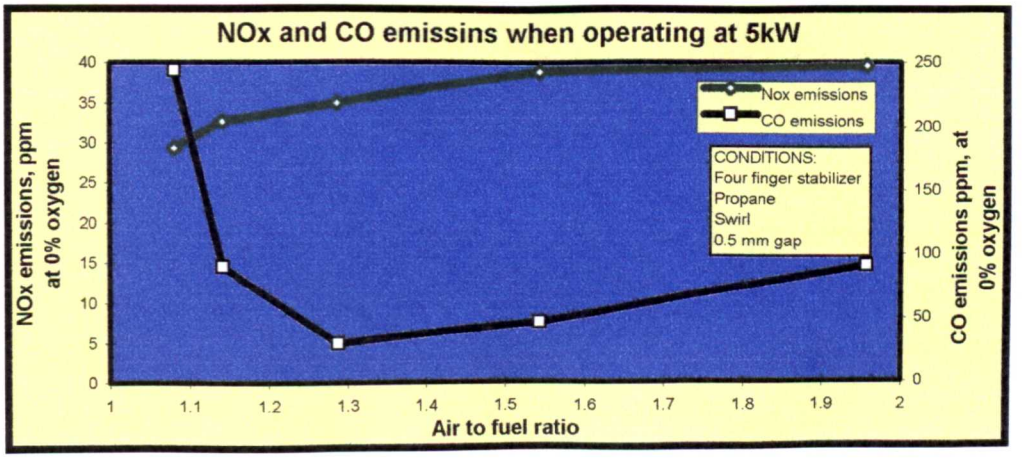

Figure 112. Experimental NOx and CO emissions when operating at 5 kW, a 0.5 mm Coanda gap width and a four finger flame stabiliser with swirl.

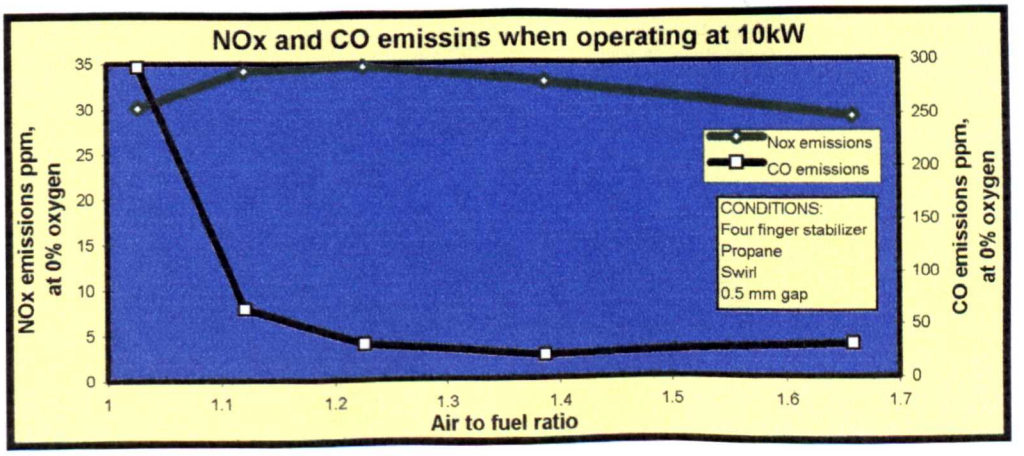

Figure 113. Experimental NOx and CO emissions when operating at 10 kW, a 0.5 mm Coanda gap width and a four finger flame stabiliser with swirl.

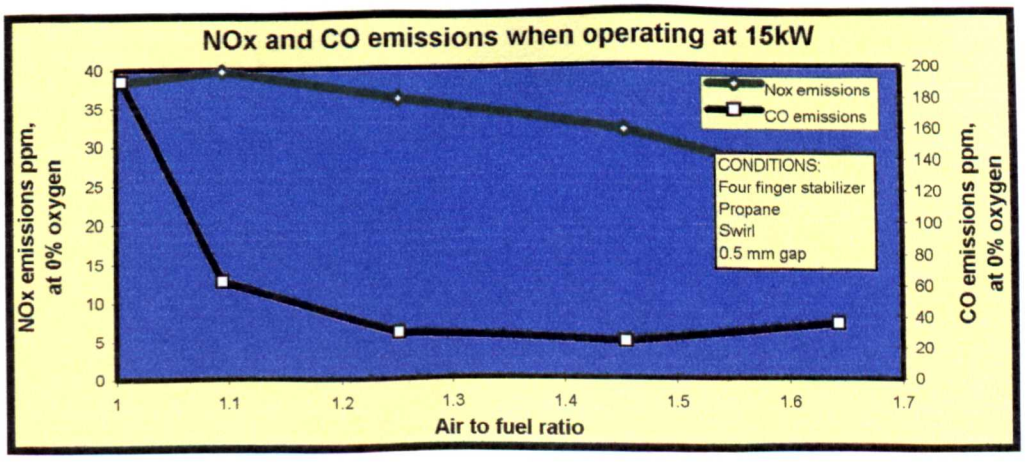

Figure 114. Experimental NOx and CO emissions when operating at 15 kW, a 0.5 mm Coanda gap width and a four finger flame stabiliser with swirl.

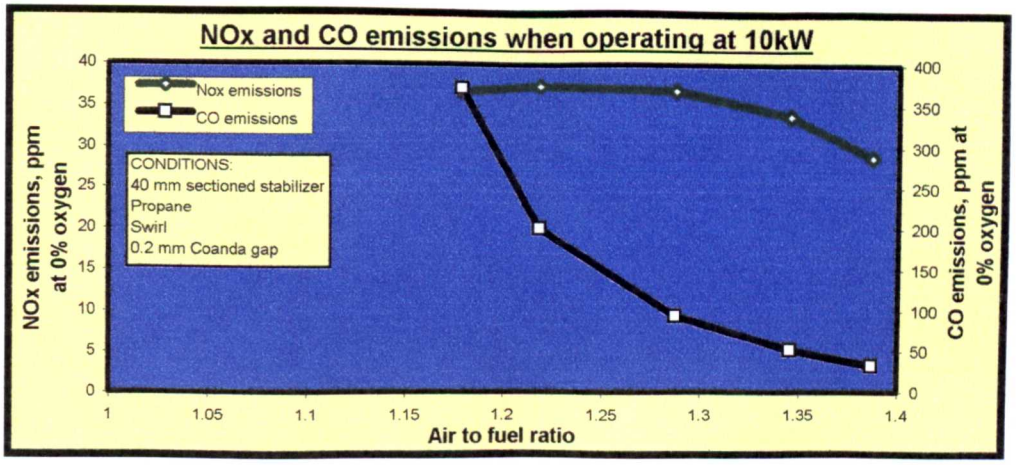

Figure 115. Experimental NOx and CO emissions when operating at 10 kW, with a 0.2 mm Coanda gap width and a 40 mm sectioned stabiliser with swirl.

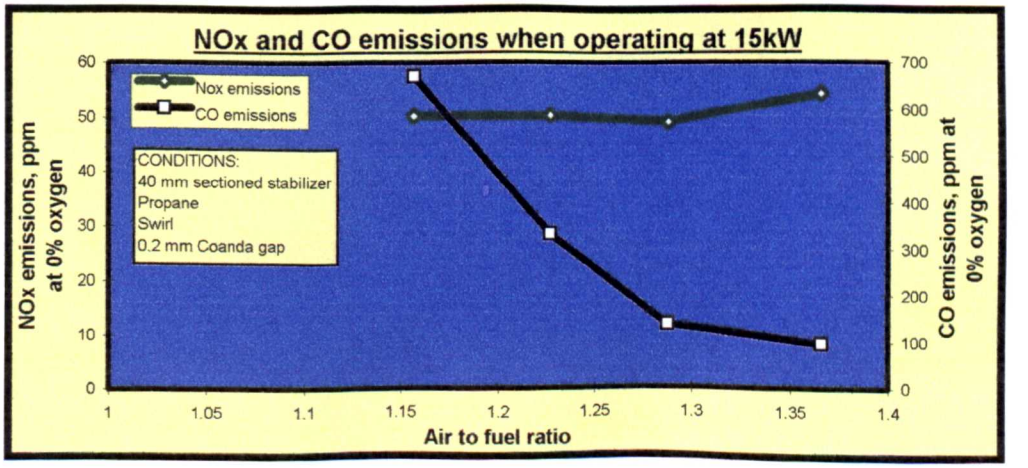

Figure 116. Experimental NOx and CO emissions when operating at 15 kW, with a 0.2 mm Coanda gap width and a 40 mm sectioned stabiliser with swirl.

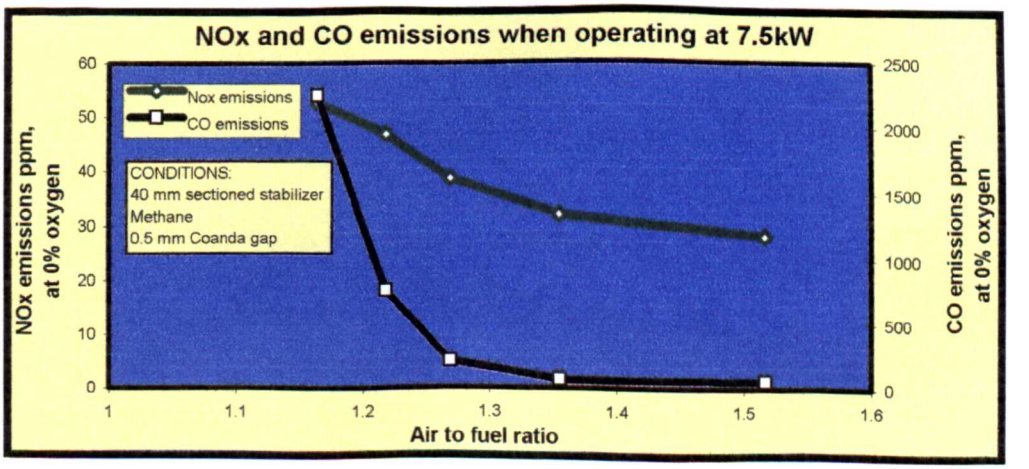

Figure 117. Experimental NOx and CO emissions when operating at 7.5 kW, with a 0.5 mm Coanda gap width and a 40 mm sectioned stabiliser.

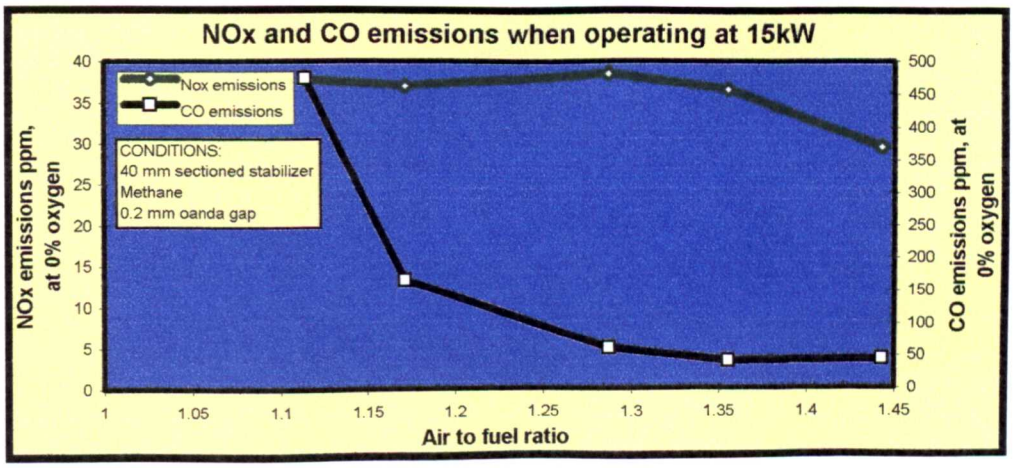

Figure 118. Experimental NOx and CO emissions when operating at 15 kW, with a 0.2 mm Coanda gap width and a 40 mm sectioned flame stabiliser.

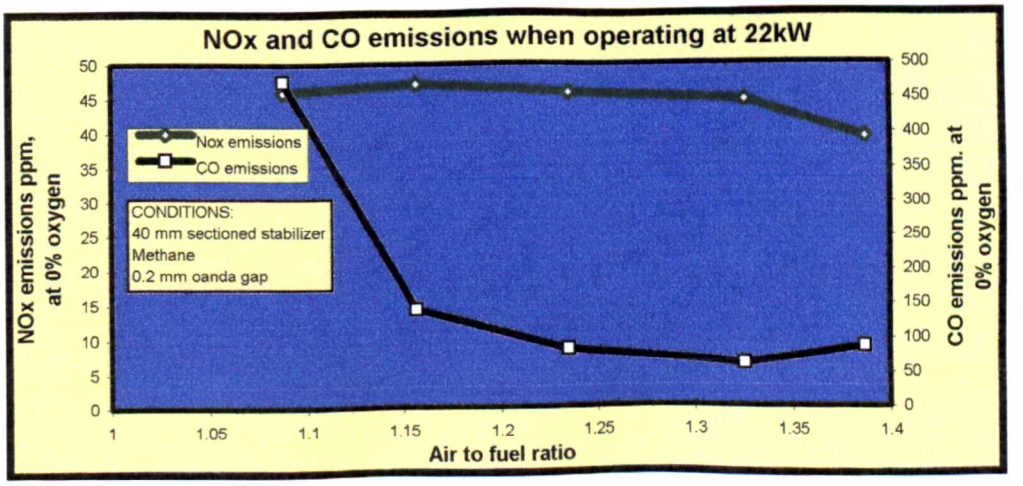

Figure 119. Experimental NOx and CO emissions when operating at 22 kW, with a 0.2 mm Coanda gap width and a 40 mm sectioned flame stabiliser.

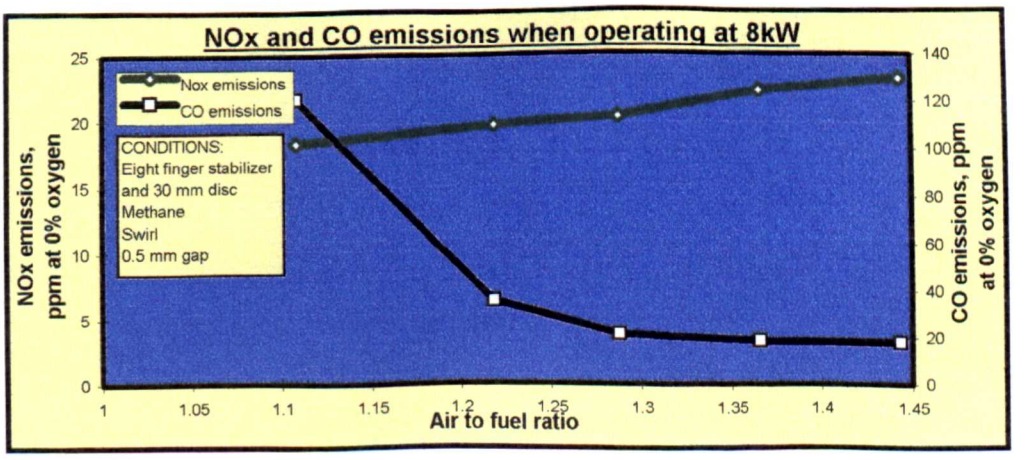

Figure 120. Experimental NOx and CO emissions when operating at 8 kW, with a 0.5 mm Coanda gap width and an eight finger flame stabiliser with swirl.

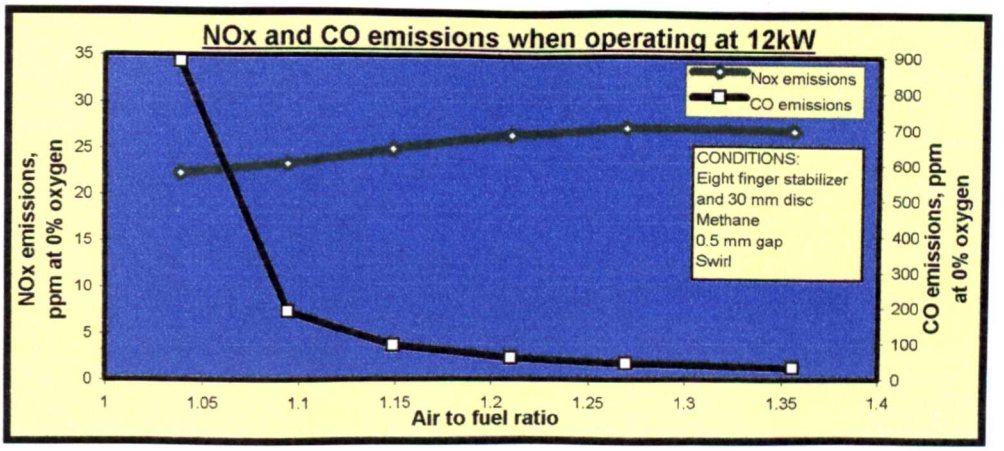

Figure 121. Experimental NOx and CO emissions when operating at 12 kW, with a 0.5 mm Coanda gap width and an eight finger flame stabiliser with swirl.

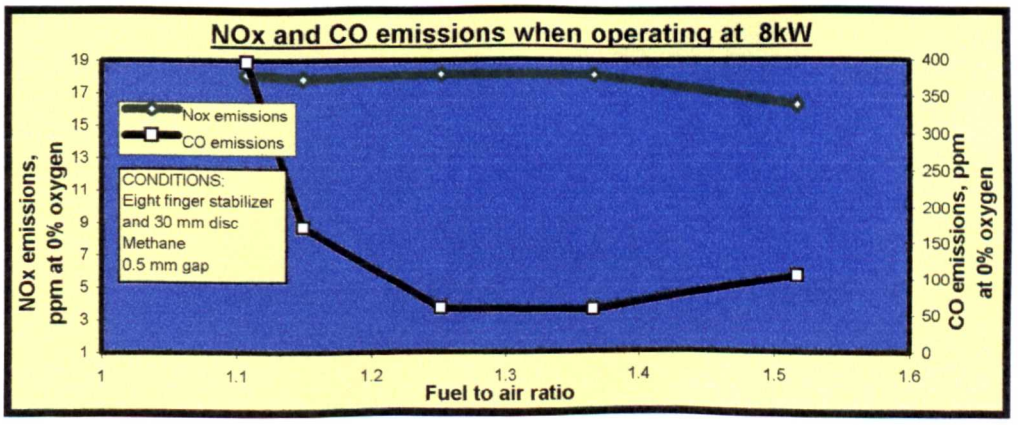

Figure 122. Experimental NOx and CO emissions when operating at 8 kW, with a 0.5 mm Coanda gap width and an eight finger flame stabiliser.

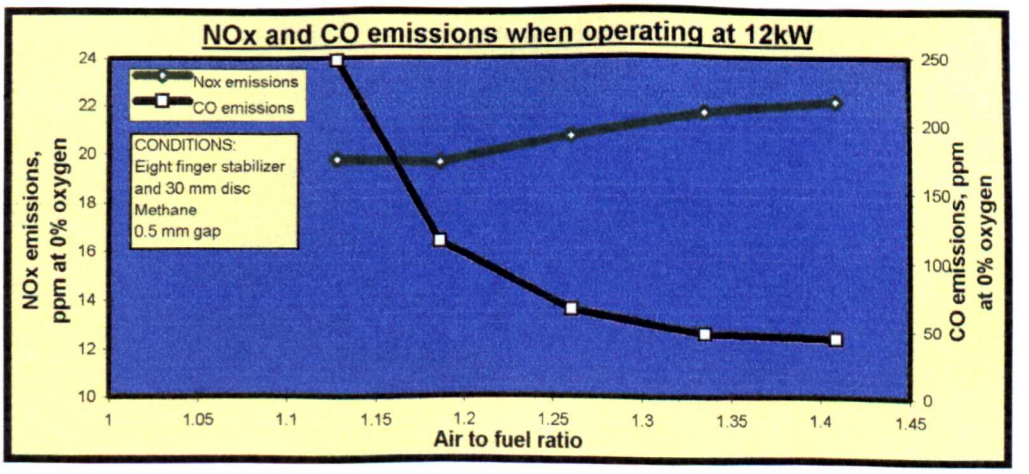

Figure 123. Experimental NOx and CO emissions when operating at 12 kW, with a 0.5 mm Coanda gap width and an eight finger flame stabiliser.

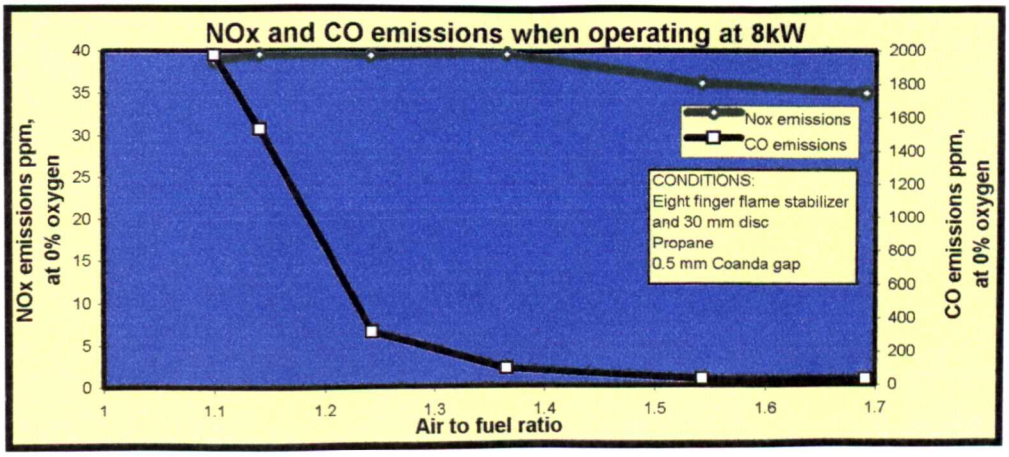

Figure 124. Experimental NOx and CO emissions when operating at 8 kW, a 0.5 mm Coanda gap width and an eight finger - 30 mm disc flame stabiliser combination.

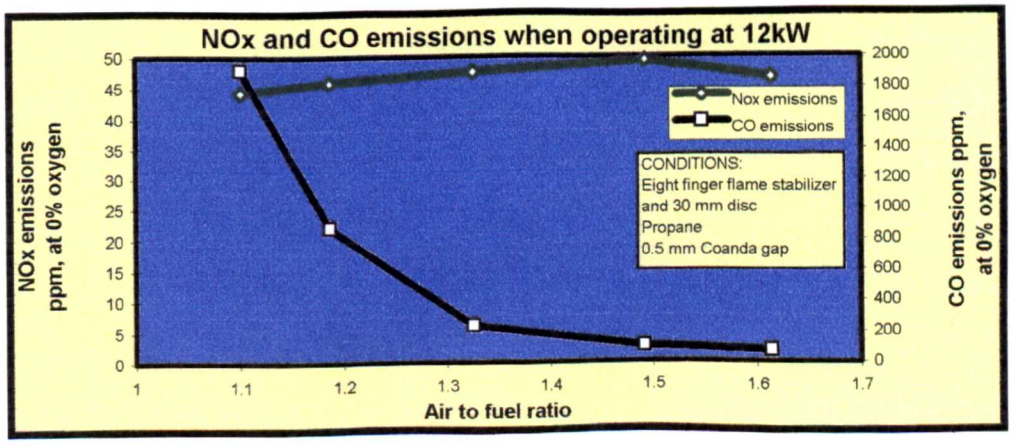

Figure 125. Experimental NOx and CO emissions when operating at 12 kW, a 0.5 mm Coanda gap width and a combined eight finger - 30 mm disc stabiliser.

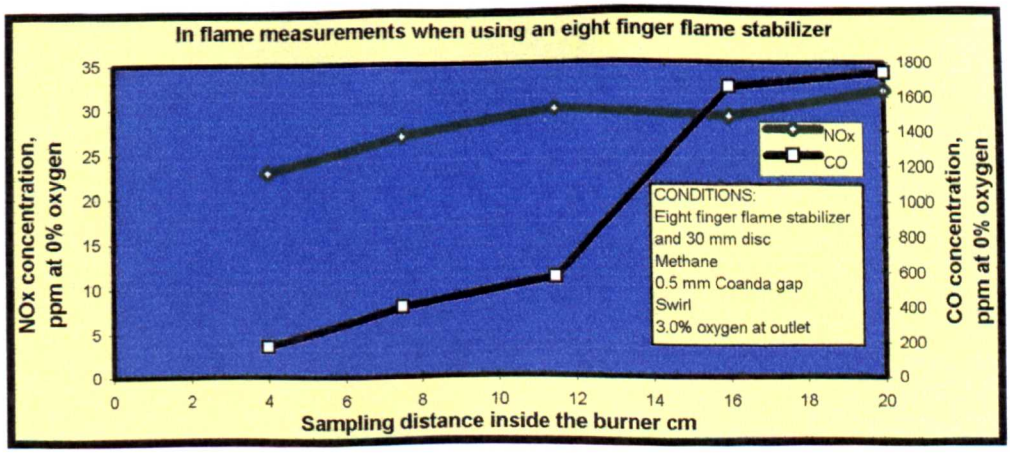

Figure 126. Experimental NOx and CO concentrations when sampling axially along the inside of the burner when using an eight finger flame stabiliser and 30 mm disc combination with swirl.

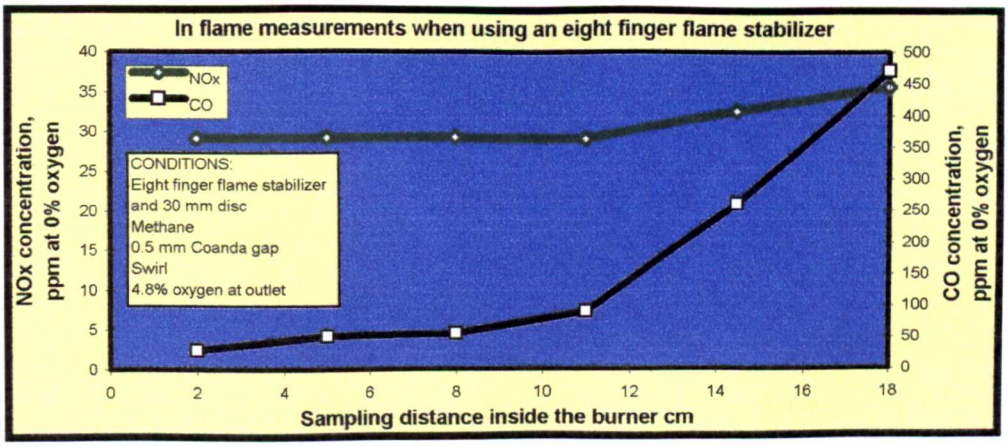

Figure 127. Experimental NOx and CO concentrations when sampling axially along the inside of the burner when using an eight finger flame stabiliser and 30 mm disc combination with swirl.

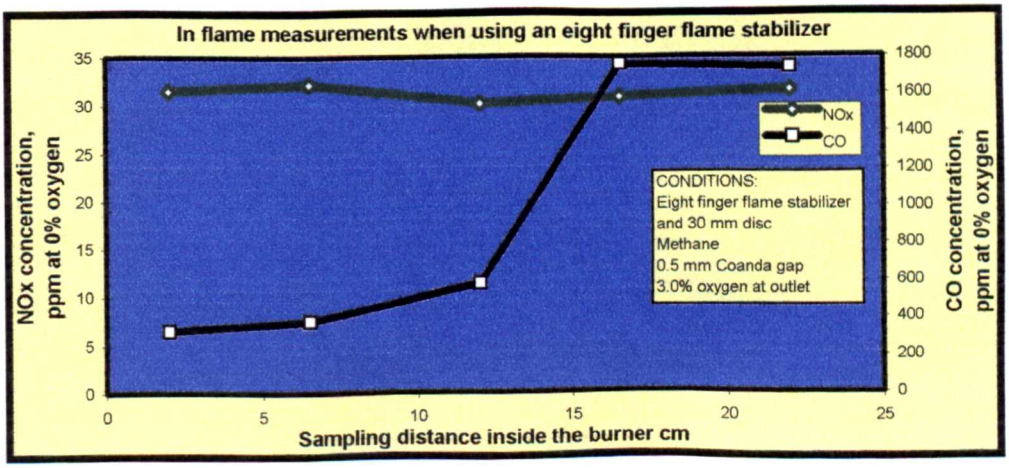

Figure 128. Experimental NOx and CO concentrations when sampling axially along the inside of the burner when using an eight finger flame stabiliser and 30 mm disc combination.

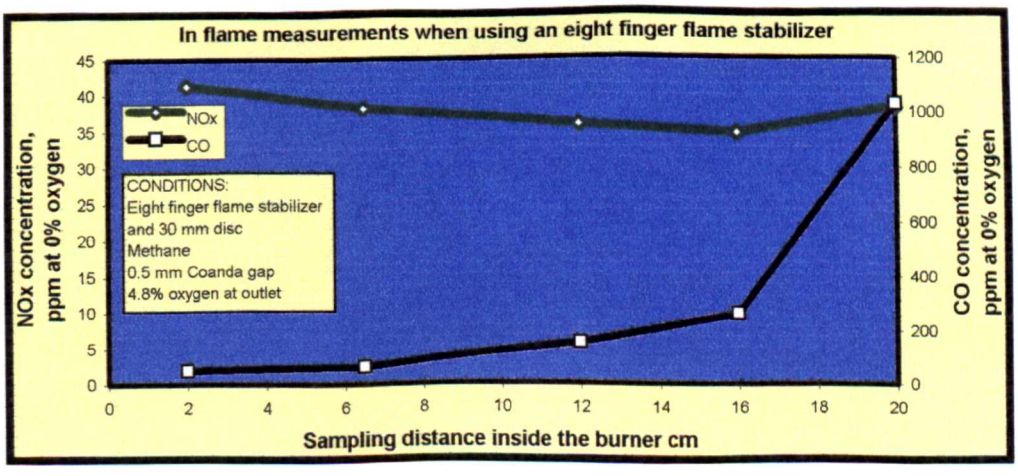

Figure 129. Experimental NOx and CO concentrations when sampling axially along the inside of the burner when using an eight finger flame stabiliser and 30 mm disc combination.

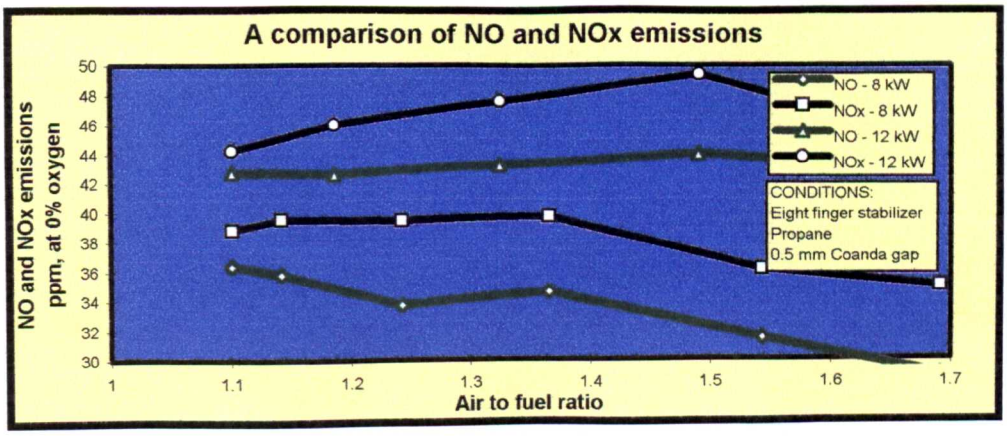

Figure 130. Experimental results comparing of NO and NO_2 emissions when burning propane with an eight finger flame stabiliser.

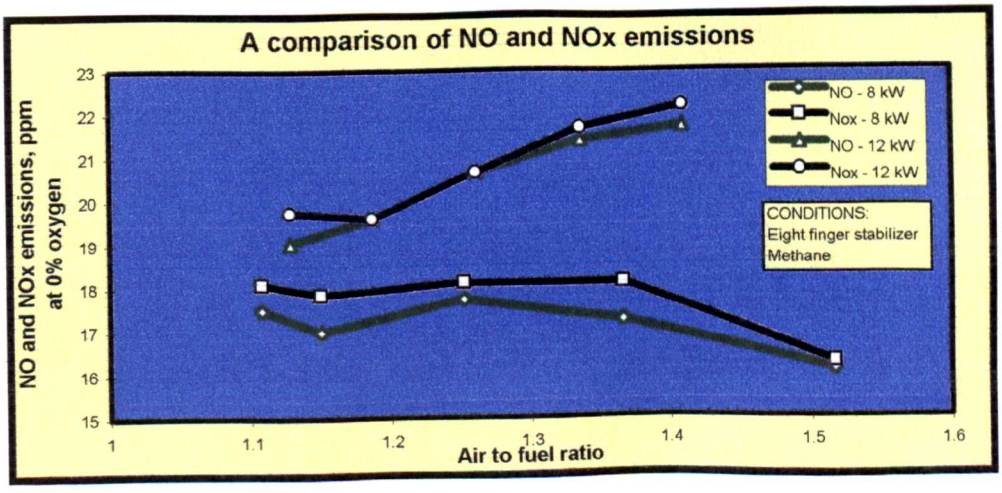

Figure 131. Experimental results comparing of NO and NOx emissions when burning methane with an eight finger flame stabiliser.

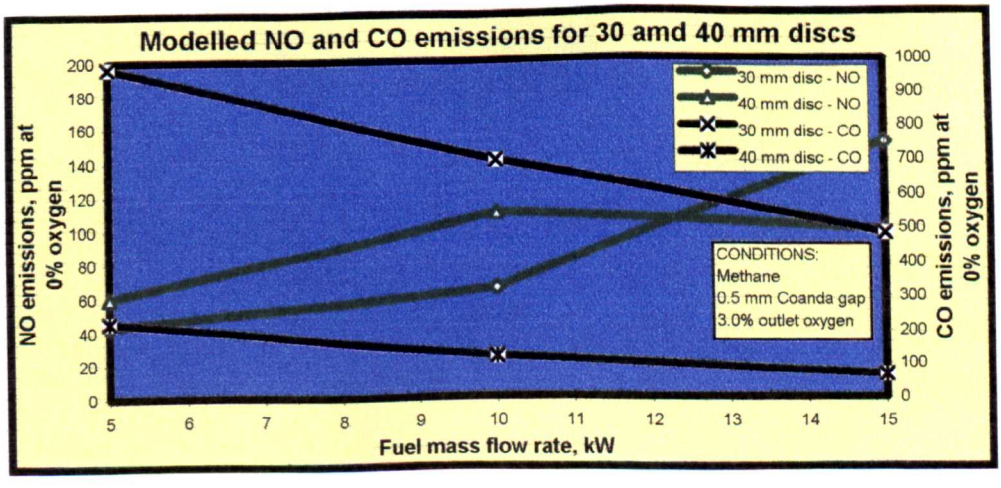

Figure 132. Modelling NOx and CO emissions when using an oxygen outlet concentration of 3.0%.

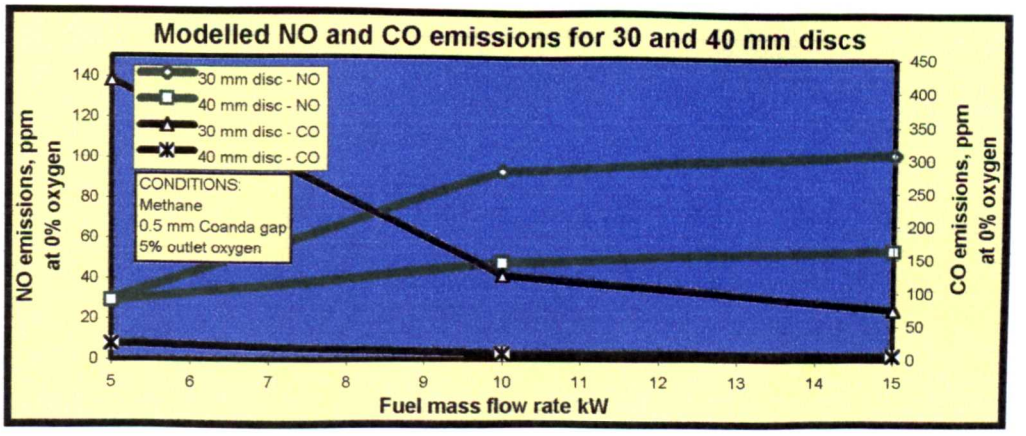

Figure 133. Modelled NOx and CO emissions when using an oxygen outlet concentration of 5.0%.

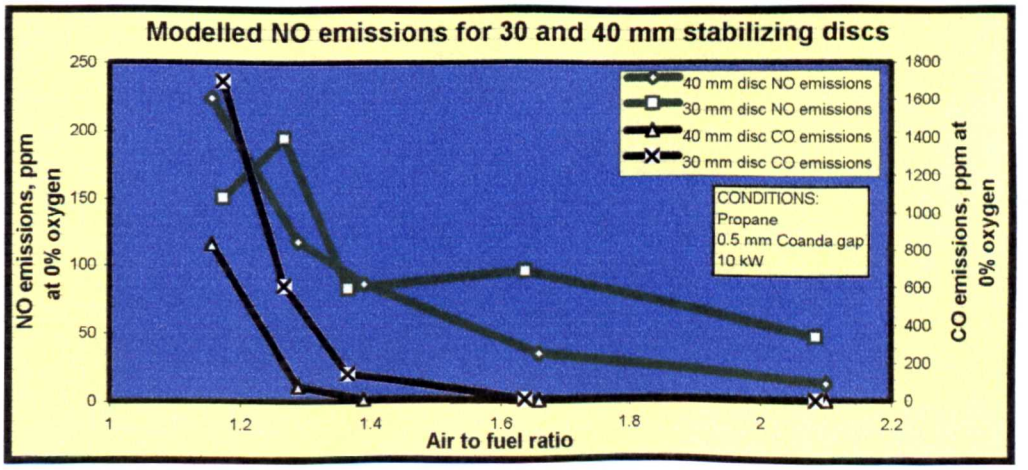

Figure 134. Modelled NOx and CO emissions over a range of air to fuel ratios, operating at 10 kW.

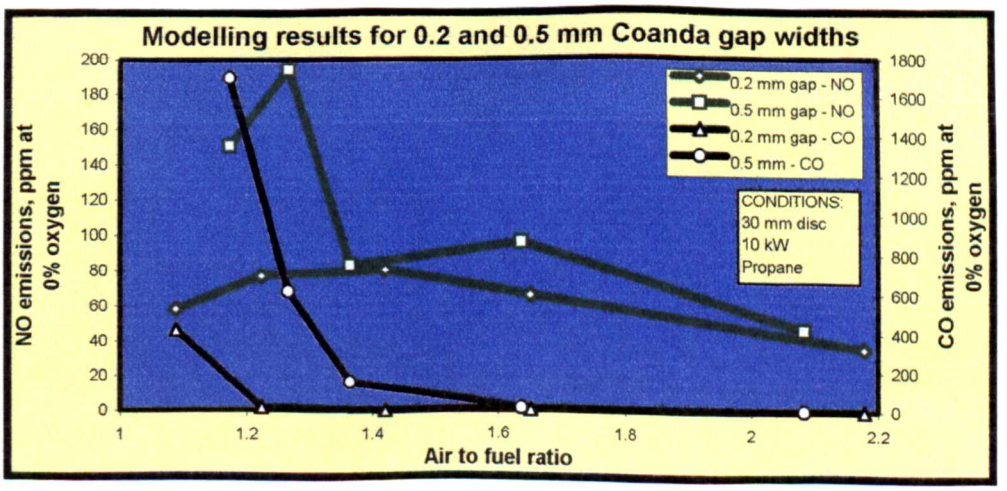

Figure 135. Modelled NO and CO emissions when burning propane with a 30 mm disc flame stabiliser at 10 kW with 0.2 and 0.5 mm Coanda gap widths.

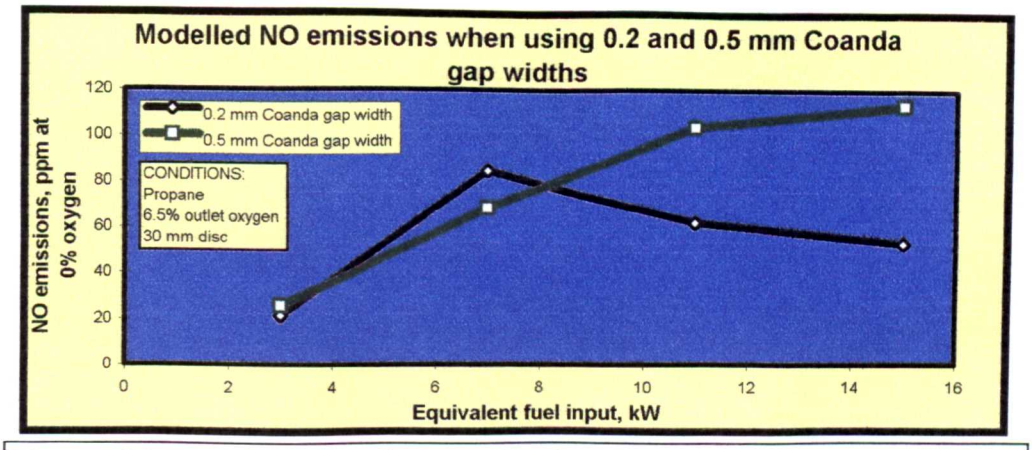

Figure 136. Modelled NO emissions when burning propane over a range of thermal ratings with an oxygen outlet concentration of 6.5% with 0.2 mm and 0.5 mm Coanda gap widths.

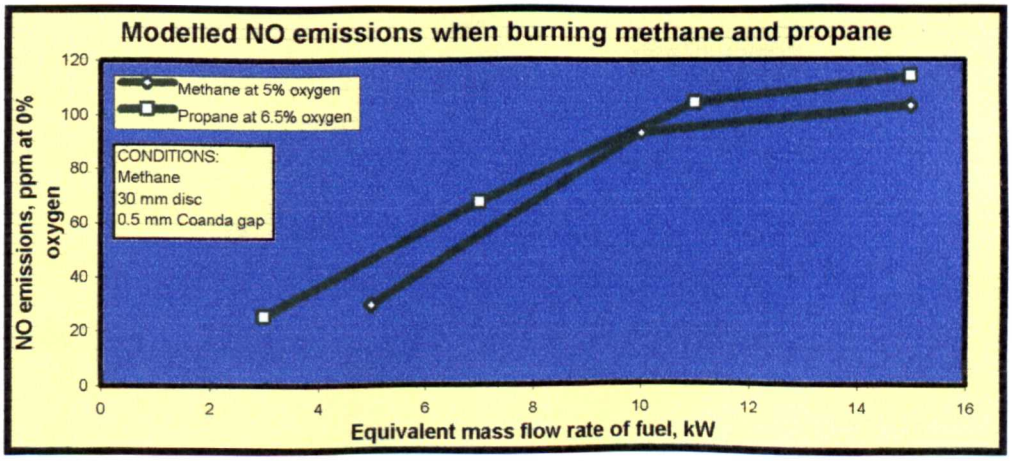

Figure 137. Modelled NO emissions when burning methane and propane with a 30 mm disc and a 0.5 mm Coanda gap width.

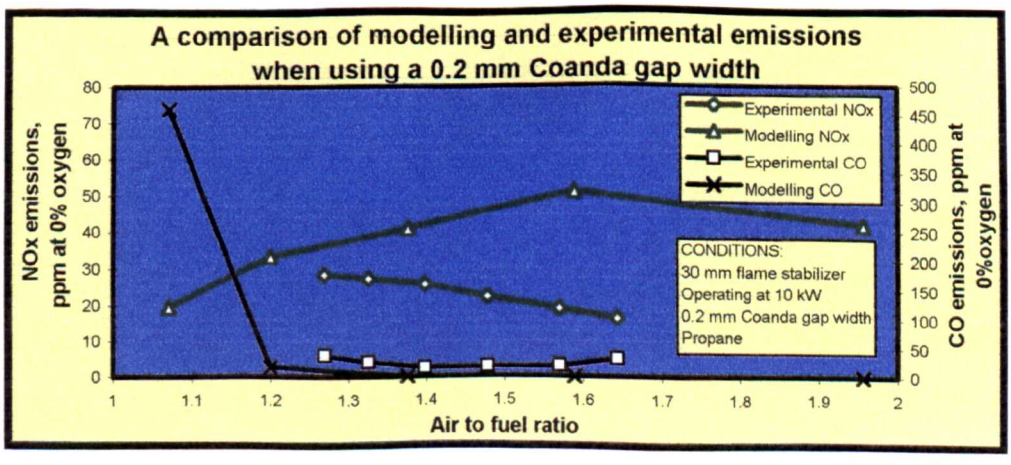

Figure 138. Comparison of modelling and experimental results when burning propane with a 0.2 mm Coanda gap width. A 30 mm disc was used for the modelling results and a five finger flame stabiliser for the experimental results.

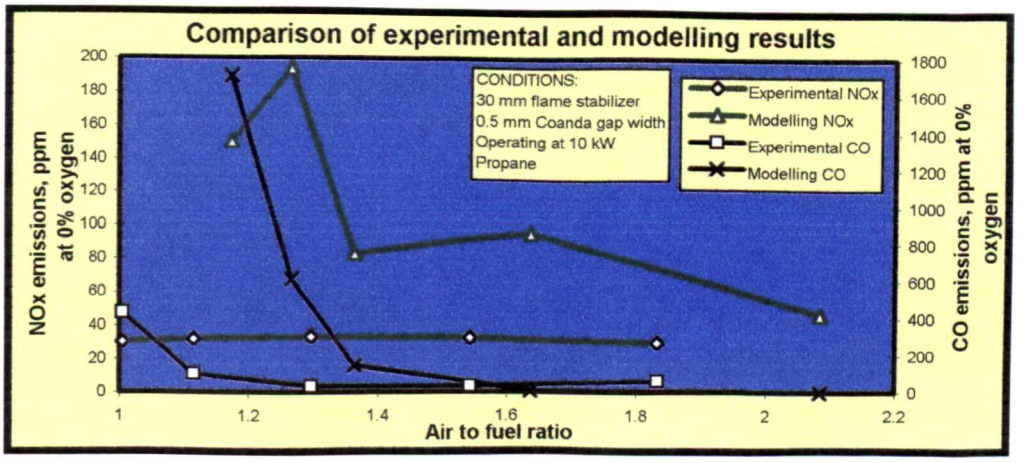

Figure 139. Comparison of modelling and experimental results when burning propane at 10 kW. A 30 mm disc was used for the modelling results and a five finger flame stabiliser for the experimental results.

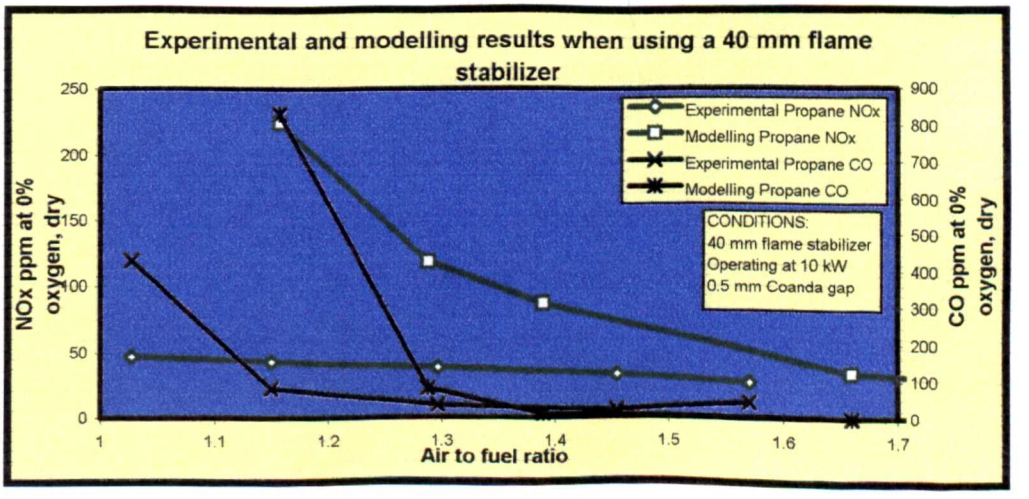

Figure 140. Comparison of experimental and modelling results when burning propane with a 40 mm flame stabiliser and a 0.5 mm Coanda gap width.

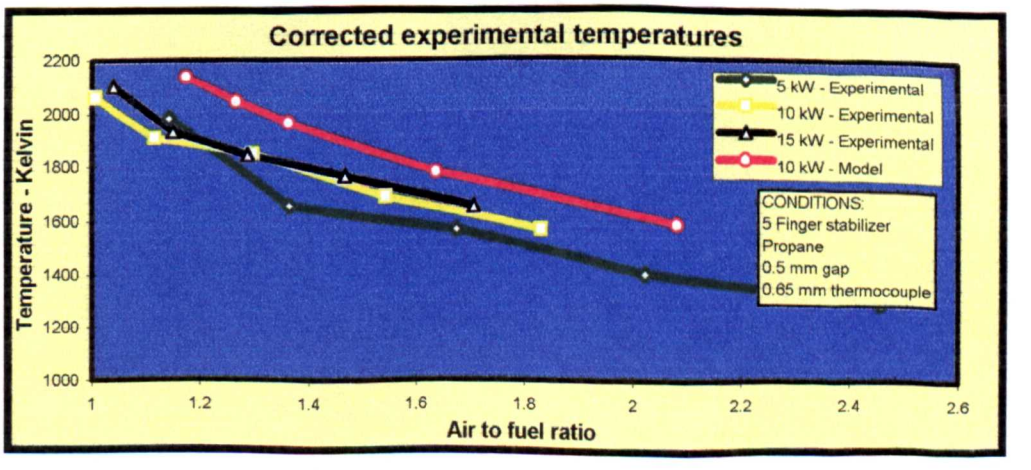

Figure 141. Corrected experimental temperatures when burning propane with a 0.5 mm Coanda gap width and a 0.65 mm diameter thermocouple bead.

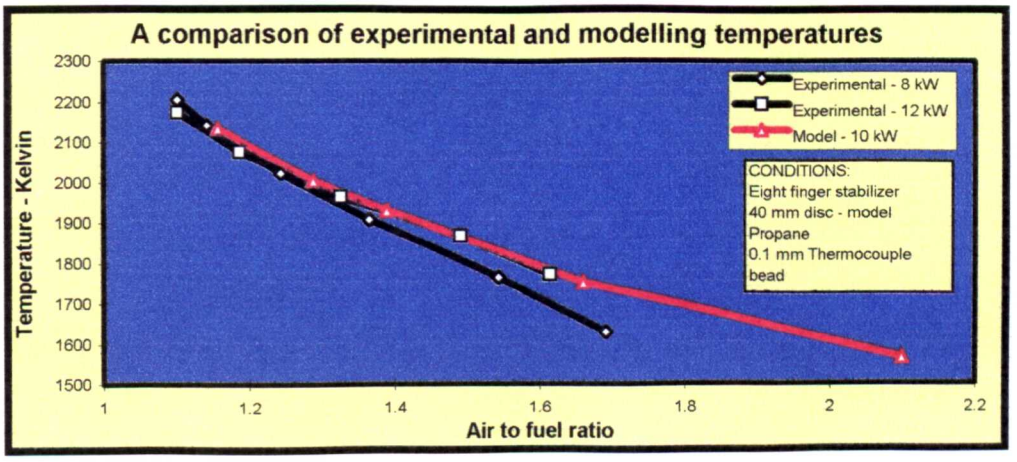

Figure 142. Corrected experimental and modelled temperatures when using a 0.1 mm thermocouple bead diameter.

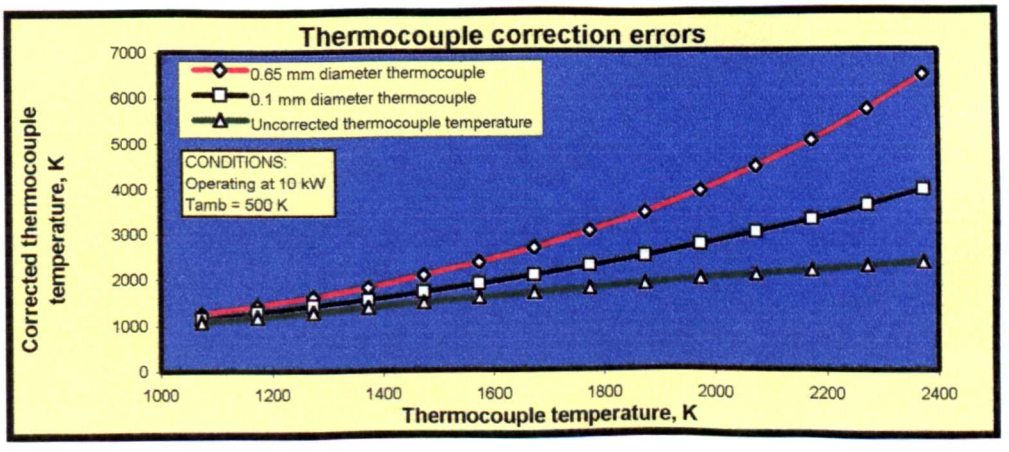

Figure 143. Calculated correction errors for 0.1 mm and 0.65 mm thermocouple bead diameters.

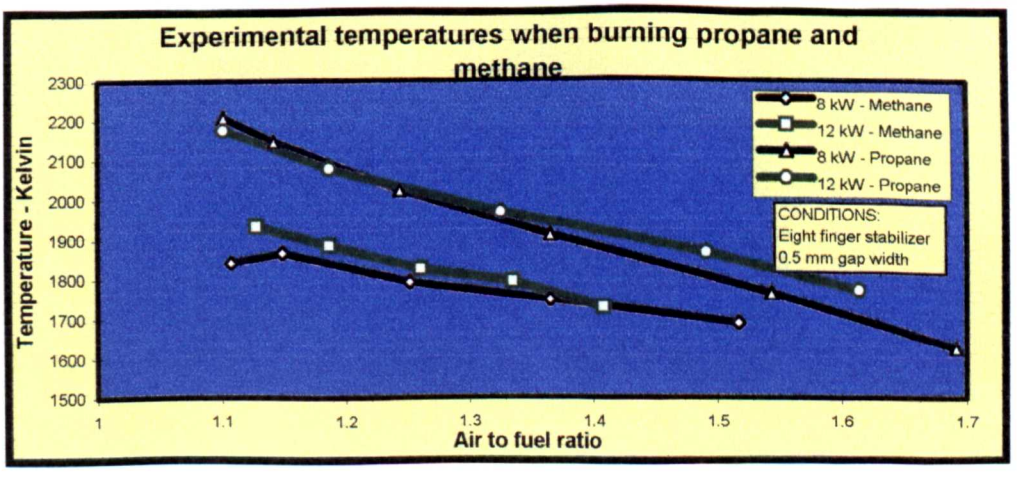

Figure 144. Corrected experimental outlet temperatures when burning propane and methane.

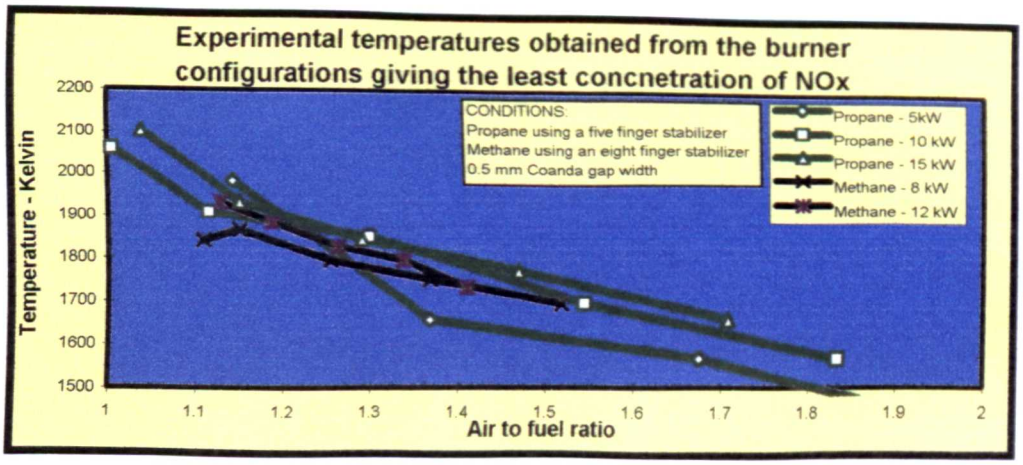

Figure 145. Corrected experimental temperatures for burner configurations burning propane and methane that gave the lowest NOx emissions.

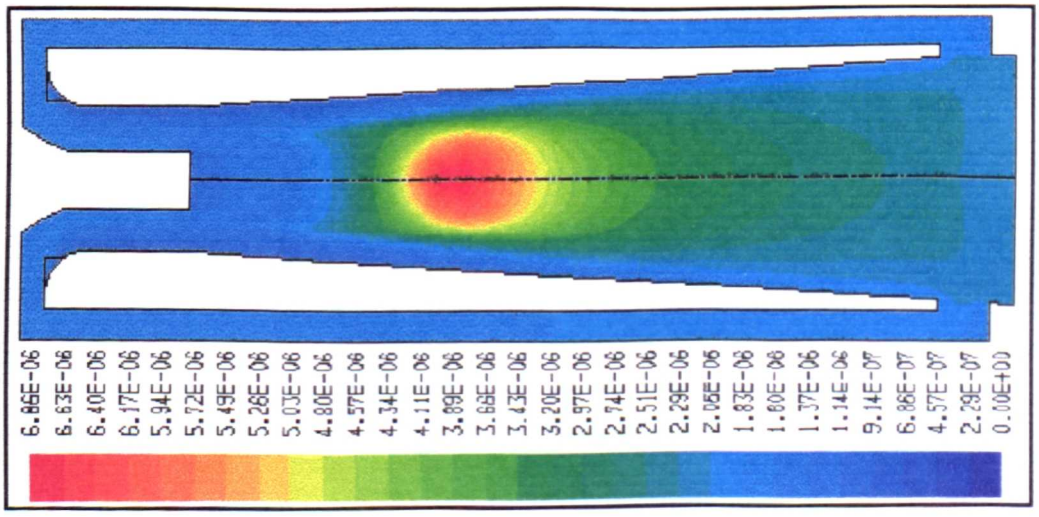

Figure 146. Modelled NOx concentrations without using a flame stabiliser.

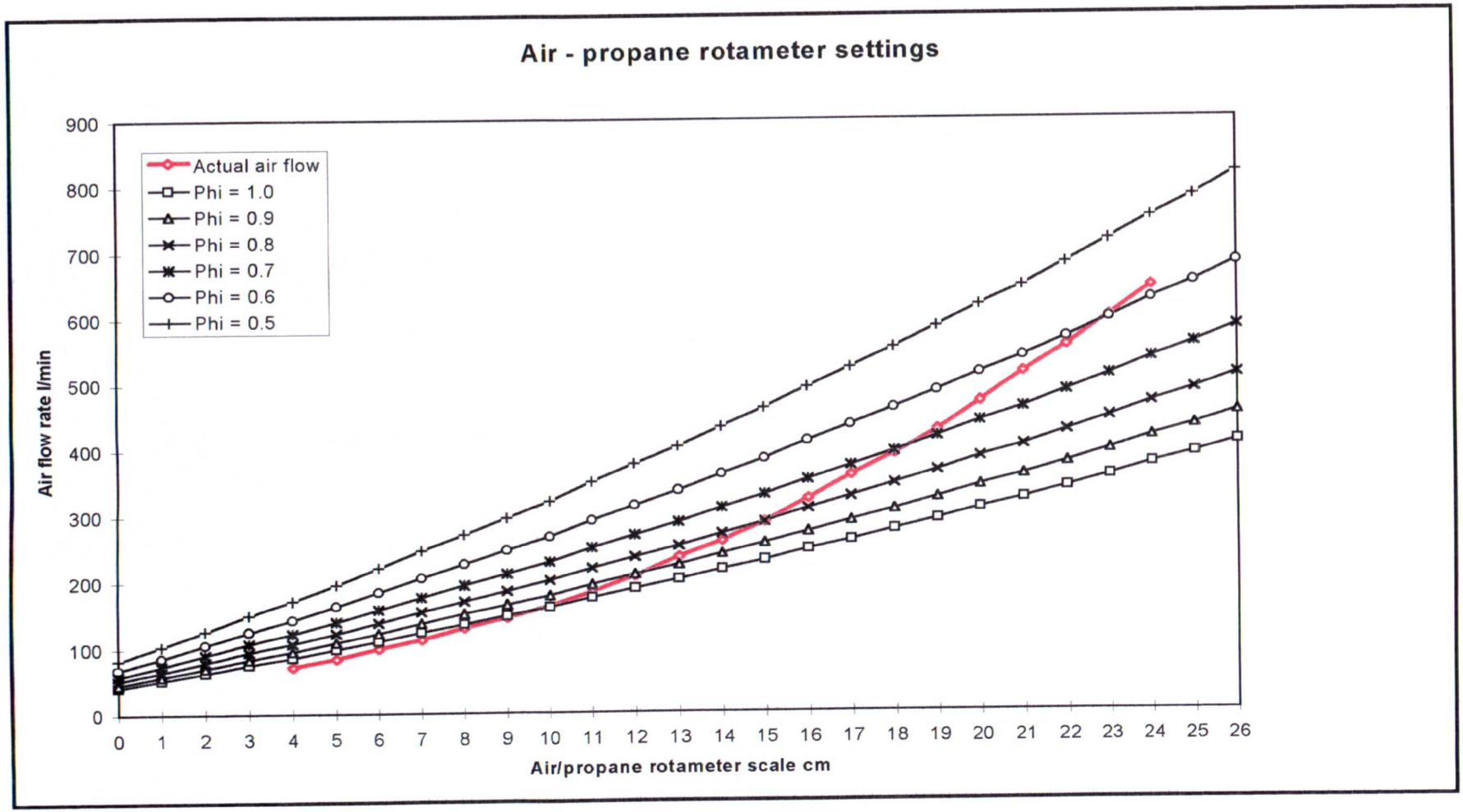

Figure 147. Air-propane rotameter settings.

REFERENCES

1. Harwell combustion centre, Club to monitor burner performance and emissions, volume 1.
2. Clean Coal Technology, "Reducing emissions of nitrogen oxides via low-NOx burner technologies", Topical report number 5, 1996.
3. Twist, T.A and Hargreaves, K.J.A "Emission control and its implications on the domestic gas burner manufacturer", Combustion and Emissions Control 2 1994.
4. Bos, H.G, "Advanced NOx reduction burners", Modern power systems, v.9 p.53-58, 1989.
5. Bowman, C.T. "Control of Combustion Generated Nitrogen Oxide Emissions: Technology Driven by Regulation", Twenty Fourth International Symposium on Combustion 1992 p.859-878.
6. Chigier, N, "Energy, combustion and environment", ISBN 0070107661
7. Chigier, N.A, "Pollution formation and destruction in flames", Prog. Energy Combustion Science, Vol1 p.3-15, 1975.
8. Zeldovich, Y.A, Acta Physiochem, URSS 21, 577 1946.
9. Hayhurst, A.N and Vince, I.M "Nitric Oxide Formation From N_2 In Flames: The Importance Of "Prompt" NO. Prog. Energy Combustion. Science. Vol6 p35 - 51, 1980.
10. Fenimore, C.P. "Formation of nitric oxide in premixed hydrocarbon flames", Thirteenth International Symposium on Combustion, p373 - 397, 1971.
11. Bowman, C.T. "Kinetics of pollutant formation and destruction in combustion", Prog. Energy Combustion Science, Vol1 p.33-45, 1975.
12. V.Dupont, V. Foster, T. Pourkashanian, Williams, A. "Low NOx domestic water heating appliances", Proceedings of the First International Conference on Combustion and Emission Control, Institute of Energy 1993.
13. Francis, W, "Fuel and fuel technology", Pergamon press, 1980.
14. Baltasar, J. Carvalho, M.G. Coelho, P. and Costa, M. "Flue gas recirculation in a gas fired laboratory furnace: Measurements and modelling", Third International Conference on Combustion Technologies for a Clean Environment, 1995.
15. Cooper, P.W and Marek, C.J. "Design of blue flame burners utilising vortex flow or attached-jet entrainment", API Publication 1723-A, 1965.
16. Goodridge, A.M. "Flue gas recirculation in an oil-fired plant", Journal of the Institute of Energy, 1988.
17. Hedley, A.B and Jackson, E.W. "Recirculation and its effects on combustion systems", Journal of the Institute of Fuel, 38, 1965.
18. Lisauskas, R.A, Green, R.W. and Thamaraichelvan, P. "Recent low NOx gas and oil burner applications", Joint Symposium on Stationary Combustion NOx Control, Vol 1, 1993.
19. Reddy, V. and Bell, A. "Retrofit of flue gas recirculation and over-fire air systems for NOx emissions control on a 230 MW gas-fired utility boiler", Joint Symposium on Stationary Combustion NOx Control, Vol 2, 1993.

20. Meier, J.G, and Vollerin, B.L. "The design of an integrated burner-boiler system using flue gas recirculation", Sixteenth International Symposium on Combustion, p.63, 1977.
21. Syska, A. "Low NOx staged air recirculating burner undergoing field trials after excellent test performance", Industrial Heating, September 1993.
22. O'Nions, P and Vahdati, M, "Flue gas recirculation in a Coanda burner", Joint meeting of the Portuguese, British, Spanish and Swedish sections of the combustion institute, 1996.
23. Wuenning, J.A, "Brenner fuer de flammlose oxidation", Gas Waerme International, Vol.41 p.438-444, 1992.
24. Drearden, L.M, Massingham, J.D, "Controlling NOx emissions from high temperature air-preheat burners with air staging", Journal of the Institute of Energy, 69, p.23-30, March 1996.
25. Jong, B.D, "Emission characteristics of the Shell low NOx burner", Combustion Science and Technology, 1993
26. Drearden, L.M, Pourkashanian, M, Williams, A. and Wills, B.J, "Performance and influence of air staging on a direct fired integral bed regenerative burner", Journal of the Institute of Energy, March 1996.
27. Kaplan, N. "NOx control costs in the IAPCS model", Joint Symposium on Stationary Combustion NOx Control, vol.2, 1993.
28. Seu, S.W.H and Castaldini, C. "Retrofit NOx controls for existing industrial, commercial, and institutional boilers: status of technologies and cost effectiveness", Joint Symposium on Stationary Combustion NOx Control, vol.2, 1993.
29. Ashworth, B and Sommer, T, "Reburning for utility boiler NOx control - a comparison of theory and practice", Joint power generation conference, v.1, ASME 1996.
30. Jodal, M and Nielsen, C. "Pilot-scale experiments with ammonia and urea as reductants in selective non-catalytic reduction of nitric oxide", Twenty Third International Symposium on Combustion, p.237-243, 1990.
31. Wenli, D, Dam-Johansen, K and Ostergaard, K. "Widening the temperature range of the thermal de-NOx process, an experimental investigation", Twenty Third International Symposium on Combustion, p.297-303, 1990.
32. Hoffmann, J.E and Johnson, R.A. "Post combustion NOx control for coal-fired utility boilers", Joint Symposium on Stationary Combustion NOx Control, vol.2, 1993.
33. Heck, R.M, Chen, J.M and Speronello, B.K, "Operating characteristics and commercial operating experience with a high temperature SCR NOx catalyst", Environmental progress, vol.13, No.4, 1994.
34. Fewel, K.J and Conroy, J.H, "Design guidelines for NH3 injection grids optimize SCR NOx removal", Oil and Gas Journal, 29, 1993.
35. Mazzi, E.A and Bell, A.W, "Demonstration of flue gas recirculation for NOx control on a natural gas-fired 320 MW tangential boiler", Joint Symposium on Stationary Combustion NOx Control, vol. 1, 1993.
36. Fiveland, W.A and Latham, C.E. "Use of numerical modelling in the design of a low-NOx burner for utility boilers", Combustion Science and Technology, vol.93, p.53-72, 1993.

37. Schefer, R.W and Sawyer, R.F, "Lean premixed recirculating flow combustion for control of oxides of nitrogen", Sixteenth International Symposium on Combustion, p.119-134, 1976.
38. Prior, D.S. "Pollutant minimisation by blue flame staged combustion", PhD Thesis, Sheffield University, 1976.
39. Dagaut, P. Cathonnet, M and Boettner, J.C, "Kinetic modelling of propane oxidation and pyrolysis", International Journal of Chemical Kinetics, vol.24 p813-837, 1992.
40. Kennel, C. Gottgens, J and Peters, N. "The basic structure of lean propane flames", Twenty Third International Symposium on Combustion, p. 479-485, 1990.
41. Peters, N and Williams, F.A, "The asymptotic structure of stoichiometric methane-air flames", Combustion and Flame 68, p. 185-207, 1987.
42. Peters, N and Kee, R.J, "The computation of stretched laminar methane-air diffusion flames using a reduced four-step reaction mechanism", Combustion and flame, 68, 1987.
43. Dryer, F.L and Glassman, I, "High temperature oxidation of CO and CH_4", Sixteenth International Symposium on Combustion, p. 987-1002, 1977.
44. Vandooren, J. Peeters, J and Van Tiggelen, P.J, "Rate constant of the elementary reaction of carbon monoxide with hydroxyl radical", Sixteenth International Symposium on Combustion, p. 745-751, 1977.
45. Howard, J.B, Williams, G.C and Fine, D.H, "Kinetics of carbon monoxide oxidation in postflame gases", Sixteenth International Symposium on Combustion, p. 975-985, 1977.
46. Hampartsoumian, E, Nimmo, W, Pourkashanian, M, and Williams, A, "The prediction of NOx emissions from spray combustion", Combustion Science and Technology, 1992.
47. Williams, G.C, Hottel, H.C and Scurlock, A.C, "Flame stabilization and propagation in high velocity gas streams", Third International Symposium on Combustion, p. 21-39, 1949.
48. Winterfield, G, "On process of turbulent exchange behind flame holders", Tenth International Symposium on Combustion, p. 1265-1275, 1965.
49. Wright, F.H and Zukoski, E.E, "Flame spreading from bluff-body flameholders", Eighth International Symposium on Combustion, p.933-942, 1960.
50. Syred, N, Chigier, N.A and Beer, J.M, "Flame stabilization in recirculation zones of jets with swirl", Thirteenth International Symposium on Combustion, p. 617-624, 1971.
51. ESDU (Ejectors and jet pump design and performance for compressible air flow) Data item no. 84029, ESDU International Ltd. 1984.
52. Hoggarth, M.L. "The design and performance of high-pressure injectors as gas jet boosters", Proceedings of the Institution of Mechanical Engineers, vol.185 56/71, 1970-71.
53. Fricker, N, Cullander, R.H, O'Brien, K and Sutton, J.A, "Coanda jet pumps - facts and fallacies", International gas research conference, 1986.
54. Swithenbank, J. "Ecological aspects of combustion devices (with reference to hydrocarbon flaring)", AIChE Journal, vol.18,no.3, p.553-560, 1972.
55. Reba, I. "Applications of the Coanda effect", Scientific American, June 1966.

56. Ameri, M and Dybbs, A, "Theoretical modelling of Coanda ejectors", Proceedings of the Fluids Engineering Conference, p. 43-48, 1993.
57. Swithenbank, J, "Coanda burner - a technical note", HIC report 140, Department of Fuel Technology and Chemical Engineering, University of Sheffield, 1969.
58. Massey, B.S, Mechanics of fluids, ISBN 0-278-00047-9.
59. Magnussen, B.F and Hjertager, B.H. "On mathematical models of turbulent combustion with special emphasis on soot formation and combustion", Sixteenth International Symposium on Combustion, 1976.
60. Spalding, D.B, "Development of the eddy-break-up model of turbulent combustion", Sixteenth International Symposium on Combustion, p.1657-1663, 1976.
61. Spalding, D.B, Mixing and chemical reaction in steady confined turbulent flames", Thirteenth International Symposium on Combustion, p. 649-657, 1971.
62. Hancock, J.D, "Practical refractories", ISBN 075989.
63. Lixing, Z, "Theory and numerical modelling of turbulent gas particle flows and combustion", Science press, 1993, ISBN 0849377218.
64. Ross, R.B, Metallic materials specification handbook, ISBN 0412369400.
65. Personal communication - Hepworth refractories.
66. De, D.S. "Measurement of flame temperature with a multi element thermocouple", Journal of the Institute of Energy, [113], June 1981.
67. Horio, M, "Nitrogen dioxide formation by the mixing of hot combustion gas with cold air", Twenty Second International Symposium on Combustion, p1175, 1988.
68. Perry, R.H, Green, D. "Perry's chemical engineering handbook", sixth edition, McGraw Hill.